STATIC AND FATIGUE BEHAVIOUR OF INTERNAL REPLACEMENT PIPE SYSTEMS SUBJECTED TO SURFACE LOAD FROM VEHICULAR TRAFFIC

A Thesis submitted by

Shanika Madhumali Kiriella
MEngSci (Structural), BEng (Hons) (Civil)

For the award of

Doctor of Philosophy (PhD) in Structural Engineering

2024

ABSTRACT

Internal replacement pipe (IRP) systems are a new and emerging trenchless technology utilised for rehabilitating legacy gas and oil pipes with circumferential cracks or discontinuities. IRP systems necessitate a design and development approach that ensures their reliable performance and durability against various types of loads throughout their service life. This thesis systematically investigated the static and fatigue behaviour of IRP systems in discontinuous host pipes under vehicular traffic loading to ensure their effective design and implementation. The first investigation involved the numerical analysis of the static bending behaviour of legacy pipes repaired with IRP systems, specifically focusing on those with full circumferential cracks or discontinuities. The influence of critical design parameters, such as width of host pipe discontinuity, thickness and elastic modulus of IRP, on the bending behaviour of pipe repair systems was investigated. A simplified and robust analytical model that can effectively capture the nonlinear lateral deformation behaviour of different IRP systems, including stand-alone IRP, IRP installed within a continuous host pipe and IRP installed within host pipes with discontinuities was also developed. In the second study, the flexural fatigue performance of IRP systems completely bonded to discontinuous host pipe segments was analysed numerically under repeated traffic loading. A comprehensive parametric study was conducted to assess the impact of important design parameters, including discontinuity width, thickness and elastic modulus of IRP, and the magnitude of the traffic loading, on the bending fatigue performance. The combined effect of the internal pressure and traffic load on the flexural fatigue behaviour of IRP systems installed in discontinuous legacy pipes was examined numerically in the third study. The last investigation was undertaken to numerically investigate the influence of bonding level on the flexural fatigue performance of IRP systems. The findings of this research provided a better understanding of the static and fatigue behaviour of IRP systems and the effect of critical design parameters on their lateral deformation behaviour and fatigue life. The numerical results, simplified analytical models, mathematical equations and design charts developed from this study will provide valuable insight for pipeline developers and designers, enabling them to enhance the safety, reliability, and cost efficiency of IRP systems.

CERTIFICATION OF THESIS

I Shanika Madhumali Kiriella declare that the PhD thesis entitled “Static and fatigue behaviour of internal replacement pipe systems subjected to surface load from vehicular traffic” is not more than 100,000 words in length including quotes and exclusive of tables, figures, appendices, bibliography, references, and footnotes.

This thesis is the work of Shanika Madhumali Kiriella except where otherwise acknowledged, with the majority of the contribution to the papers presented as a Thesis by Publication undertaken by the student. The work is original and has not previously been submitted for any other award, except where acknowledged.

Date: 24.01.2024

Endorsed by:

Prof. Allan Manalo
Principal Supervisor

Prof. Karu Karunasena
Associate Supervisor

Dr. Cam Minh Tri Tien
Associate Supervisor

Student and supervisors’ signatures of endorsement are held at the University.

STATEMENT OF CONTRIBUTION

The articles produced from this study were a joint contribution of authors. The details of the scientific contribution of each author are provided below.

Manuscript 1:

Kiriella, S., Manalo, A., Tien, C. M. T., Ahmadi, H., Wham, B. P., Salah, A., Tafsirojjaman, T., Karunasena, W., Dixon, P. and O'Rourke, T. D. (2023), "Lateral deformation behaviour of structural internal replacement pipe repair systems", *Composite Structures*, vol. 319. (Impact factor: 6.3; Cite score: 10.9)

DOI: https://doi.org/10.1016/j.compstruct.2023.117144

The overall contribution of Shanika Kiriella was 70% to the critical review of literature, concept development, numerical and analytical modelling and analysis, interpretation of data, drafting and revising the final submission. Allan Manalo, Cam Minh Tri Tien, Hamid Ahmadi, Brad P. Wham, Ahmad Salah, T. Tafsirojjaman, Warna Karunasena, Patrick Dixon, and Thomas D. O'Rourke contributed to concept development, the structuring of the manuscript, analysis, interpretation of data, editing and providing important technical inputs.

Manuscript 2:

Kiriella, S., Manalo, A., Tien, C. M. T., Ahmadi, H., Dixon, P., Karunasena, W., Salah, A., and Wham, B. P. (2024), "Bending fatigue behaviour of internal replacement pipe systems", *Composite Structures*, vol. 331 (Impact factor: 6.3; Cite score: 10.9)

DOI: https://doi.org/10.1016/j.compstruct.2024.117910

The overall contribution of Shanika Kiriella was 70% to the critical review of literature, concept development, numerical modelling and analysis, interpretation of data, drafting and revising the submission. Allan Manalo, Cam Minh Tri Tien, Hamid Ahmadi, Patrick G. Dixon, Warna Karunasena, Ahmad Salah, and Brad P. Wham contributed to concept development, the structuring of the manuscript, analysis, interpretation of data, editing and providing important technical inputs.

Manuscript 3:

Manuscript 3: Kiriella, S., Manalo, A., Tien, C. M. T., Ahmadi, H., Karunasena, W., Dixon, P., Salah, A., and Wham, B. P., "Effect of internal pressure on the flexural fatigue behaviour

of internal replacement pipe systems", *Composite Structures* (Under review, COMSTR-D-24-00347). (Impact factor: 6.3; Cite score: 10.9)

The overall contribution of Shanika Kiriella was 70% to the critical review of literature, concept development, numerical modelling and analysis, interpretation of data, drafting and revising the submission. Allan Manalo, Cam Minh Tri Tien, Hamid Ahmadi, Warna Karunasena, Patrick G. Dixon, Ahmad Salah, and Brad P. Wham contributed to concept development, the structuring of the manuscript, analysis, interpretation of data, editing and providing important technical inputs.

Manuscript 4:

Kiriella, S., Manalo, A., Tien, C. M. T., Ahmadi, H., Karunasena, W., Dixon, P., Salah, A., and Wham, B. P., "Influence of bonding level on the bending fatigue behaviour of internal replacement pipe systems", *Steel and Composite Structures* (Under review, SCS30015U). (Impact factor: 4.6; Cite score: 9.6)

The overall contribution of Shanika Kiriella was 70% to the critical review of literature, concept development, numerical modelling and analysis, interpretation of data, drafting and revising the submission. Allan C. Manalo, Cam M. T. Tien, Hamid Ahmadi, Warna Karunasena, Patrick G. Dixon, Ahmad Salah, and Brad P. Wham contributed to concept development, the structuring of the manuscript, analysis, interpretation of data, editing and providing important technical inputs.

ACKNOWLEDGEMENTS

First and foremost, I would like to express my utmost gratitude to my principal supervisor, Prof. Allan Manalo, for providing me with an invaluable opportunity to pursue a PhD under his mentorship. I consider myself incredibly fortunate to have had the opportunity to meet him and work under his supervision. His continuous support, extensive knowledge, dedicative guidance and encouragement have played a crucial role in shaping both the direction and quality of this research.

I extend my heartfelt appreciation to Dr. Tri Tien, my associate supervisor, for his support, guidance and encouragement throughout my study. Having discussions with him has significantly improved my knowledge of numerical modelling. I am also grateful to my associate supervisor Prof. Karu Karunasena for providing valuable comments and suggestions which were essential in enhancing the quality of this study. I sincerely appreciate Dr. Hamid Ahmadi for his support and very useful advice that helped me in this research study.

A special thanks go to the technical staff, Brian Lenske, Wayne Crowell, and Adrian Blokland for providing me with huge support for conducting fatigue testing during my study.

I am grateful to the Advance Research Project Agency- Department of Energy in the United States for funding my PhD study and providing me with financial support. I would like to express my gratitude to the CUB team, specifically Patrick Dixon and Brad Wham for their support, comments and suggestions. My appreciation also goes to the co-authors of my paper(s) including Thomas O'Rouke, Ahmad Salah and Tafsirojjaman for their contributions.

I would also like to acknowledge the CFM staff and postgraduate students for their support and friendship during this period.

Most importantly my biggest thanks go to my dearest husband, Kasun Gopallawa for his love, care, encouragement, endless patience and, all of his sacrifices throughout my academic journey. I feel very lucky to have such a wonderful and caring husband who always has my back. I am also extremely grateful to my late father, my mother, my mother-in-law, my younger sister and my younger brother for their support and encouragement throughout this journey.

Thank you very much to those whom I forgot to mention, but who have contributed to this research study.

TABLE OF CONTENTS

LIST OF TABLES

LIST OF FIGURES

CHAPTER 1: INTRODUCTION

1.1. Background and motivation

Gas and oil are regarded as the primary sources of energy on a global scale. Based on the data from the International Energy Agency, natural gas and oil together account for 64.6% of the total energy supply (IEA 2021). Pipelines have been widely employed for transporting natural gas and oil over long distances, primarily due to their high transportation capacity and cost efficiency (Manan et al. 2021; Zang et al. 2023). The majority of these pipelines, composed primarily of legacy cast iron and bare steel, are over 50 years old and have degraded, resulting in leakage and failure (Howarth 2014; Song et al. 2021; Yang et al. 2021; Saeed et al. 2022; Lu et al. 2023). Due to the presence of flammable, explosive and toxic materials, failure in gas and oil pipelines can cause catastrophic damage to humans, properties, and infrastructure (Cunha 2016; Belvederesi et al. 2018; Biezma et al. 2020; Zakikhani et al. 2020a; Zhang et al. 2022; Song et al. 2023). Consequently, these existing pipeline systems that have either reached or surpassed their intended service life need cost-effective repair techniques to restore original operating capacity, maintain structural integrity and extend their safe operating life.

Rehabilitation of existing pipe networks is considered a more favourable solution compared to the replacement primarily due to the limited financial resources (Karbhari 2014). The trenchless technique has gained significant popularity as a globally preferred method for pipe repair due to its unique advantages including shorter construction period, minimal disturbance and surface damage, less disruption to traffic, and lower pollution levels (Tetreault et al. 2018; Li et al. 2023a). In recent years, there has been notable advancement in trenchless technology, specifically with the introduction of a novel approach known as internal replacement repair systems employing different materials including thermoplastics, polymeric coatings, fibre composites and metallic coatings (Tafsirojjaman et al. 2022; Dixon et al. 2023). This rehabilitation method involves the installation of a novel structural pipe within the existing legacy pipes that exhibit defects and discontinuities. The implementation of IRP enhances the strength, structural integrity and durability of the legacy pipes.

To optimise the design of the IRP system for pipeline rehabilitation while in operation, it is critical to consider different performance objectives and associated failure mechanisms. Based on the available literature, the most common failure mechanisms related to IRPs in host pipe systems are as follows: lateral deformation due to surface loads (Jeon et al. 2004; Vazouras et al. 2012; Melissianos et al. 2017; Alzabeebee et al. 2018; Argyrou et al. 2019; Liu et al.

2019; Vasseghi et al. 2021; Tafsirojjaman et al. 2022), fatigue failure caused by repetitive traffic loading (Guo et al. 2005; Tafsirojjaman et al. 2022), localised fracture and leakage due to internal pressure (Mattos et al. 2016; Budhe et al. 2020; Tafsirojjaman et al. 2022) and axial deformation resulting from thermal stresses (Bokaian 2004; Zhong et al. 2018; Tafsirojjaman et al. 2022). Among these failure modes, bending deformation and fatigue failure respectively resulting from static and high cyclic/repetitive surface loads from vehicular traffic are regarded as the most severe conditions for the host pipes and IRP system (Tafsirojjaman et al. 2022; Dixon et al. 2023). The effects of static and cyclic surface loads encountered by the pipelines are often attributable to the surface load exerted by vehicular traffic (Ng 1994). The wheel loads that are positioned directly above the pipes and move parallel to their longitudinal axis (Fig. 1) are transmitted to underground pipes through the soil, leading to stresses and deformations that reflect the worst conditions (Jeon et al. 2004; Stewart et al. 2015).

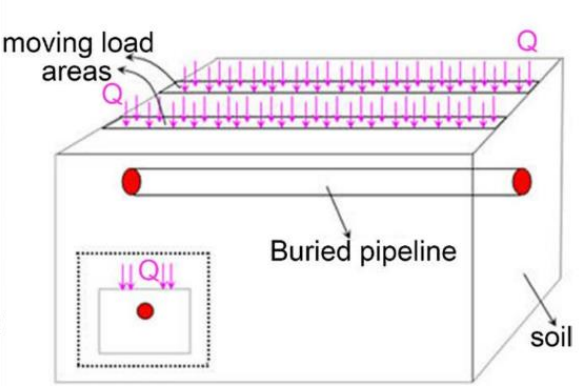

Fig. 1. Moving load parallel to the longitudinal axis of the buried pipeline (Neya et al. 2017)

A complete circumferential fracture, also known as a round crack or can be also represented by the joint, is considered the worst discontinuity along the host pipe (Stewart et al. 2015). Based on the investigation of Makar et al. (2001), it has been determined circumferential cracking is the predominant failure mode of legacy cast iron pipe with a diameter of less than 380 mm (14.96 in). In the presence of such a crack on the host pipe, the IRP can potentially be susceptible to stresses, relative displacements and rotations generated by the traffic loading (Jeon et al. 2004; Stewart et al. 2015). This form of repetitive loading characterises upper bound limits (extreme cases) on vertical distortion (movement or displacement of the pipe in the vertical direction), and rotational distortion (rotation or twisting of the pipe around its axis) that can be anticipated in the field even under extremely heavy traffic circumstances (Jeon et al. 2004).

At present, there is a lack of comparable standards or regulations pertaining to internal composite pipe repair systems (Tafsirojjaman et al. 2022). In addition, there are only a few

studies on static bending (Jeon et al. 2004; Allouche et al. 2012; Stewart et al. 2015; Shou et al. 2018; Yang et al. 2021) and flexural fatigue (Jeon et al. 2004; Stewart et al. 2015; Ha et al. 2016) behaviour of circumferentially cracked pipes repaired with internal composite repair systems. Much of the existing literature on static and fatigue behaviour has primarily focused on pipes containing surface defects exposed to internal pressure changes (Ghaffari et al. 2013; Valadi et al. 2018; Elhady et al. 2020; Chen et al. 2021). These studies indicated that the static bending and flexural fatigue phenomenon creates a bottleneck in the design of a new IRP repair system due to a lack of literature and design standards. Consequently, the behaviour of IRP systems installed in host pipes with circumferential cracks or discontinuities under static and cyclic loads caused by vehicular traffic, along with the selection of the most appropriate material and geometric properties must be thoroughly examined.

A comprehensive evaluation of the effect of various design parameters on static bending deformation or flexural fatigue performance of IRPs is challenging to accomplish exclusively through full-scale laboratory experiments because they are costly and time-consuming. On the other hand, numerical and analytical models require less time, as well as lower costs but require validation from physical tests (Sousa et al. 2013). Once properly calibrated and validated using full-scale laboratory experimental results, numerical and analytical models can serve as highly effective tools for simulating physical behaviour and extrapolating them to other conditions. In addition, the combination of numerical and analytical modelling along with physical testing, enables a comprehensive understanding of the actual performance of structures and their optimisation.

This thesis aimed to investigate numerically the behaviour of IRP systems for repairing legacy pipes with full circumferential cracks or discontinuities induced by the presence of joints under static and cyclic surface loads from vehicular traffic. This was accomplished by simulating an experimental four-point bending test implemented by the University of Colorado, Boulder. Additionally, simplified and robust theoretical models and/or mathematical expressions capable of accurately anticipating the static bending and flexural fatigue behaviour of IRP systems were also developed. The FEA numerical simulations were performed using ANSYS/Mechanical software, while the analytical models were implemented using the MATLAB programming platform. The goal of the flexural fatigue simulations was to assess the long-term performance of the IRP system under repetitive deformations generated by traffic loads over a service life of 50 years.

This research study was undertaken in collaboration with an ongoing international project named Rapid Encapsulation of Pipeline Avoiding Intensive Replacement (REPAIR),

which is funded by the Advance Research Project Agency- Department of Energy in the United States.

1.2. Objectives

The aim of this research is to investigate the behaviour of IRP systems installed in legacy host pipelines with full circumferential cracks or discontinuities subject to static and repetitive surface loads from vehicular traffic. The specific objectives of this study are the following:

1. To investigate the static bending behaviour of host pipe with full circumferential cracks or discontinuities repaired with IRP systems, and to develop a simplified and robust analytical model capable of accurately describing the bending behaviour of these repair systems.
2. To assess numerically the flexural fatigue behaviour of discontinuous host pipes repaired with different IRP material systems and to quantify the influence of different design parameters.
3. To analyse numerically the fatigue performance of IRP systems installed in discontinuous host pipe segments under the combined influence of internal pressure and surface loading.
4. To evaluate numerically the effect of the different bonding levels on the bending fatigue behaviour of IRPs installed in host pipes with discontinuities under both pressurised and non-pressurised conditions.

1.3. Study limitation

This study specifically focused on a standard in-service legacy steel natural gas pipeline system located in the United States in need of repair. Hence, the material and geometric properties of the host pipe (with the exception of discontinuity width) remained consistent throughout the study. The input parameters and the material properties required for the numerical and mathematical models were extracted from the literature and by conducting laboratory testing. These tests included tensile tests and tension-tension fatigue tests using coupon specimens. The numerical and analytical models were calibrated and validated by comparing the results obtained from full-scale laboratory tests performed by the University of Colorado in Boulder. During the experimental test at the University of Colorado Boulder, pressure was exerted inside the IRP using water. As a result, the ends of the pipe were sealed by attaching end caps. However, the choice of pipe length (3048 mm or 120 inches) for the bending test was determined based on a series of prior experiments conducted by Jeon et al.

2004 and Stewart et al. 2015. These studies have demonstrated that the use of end caps has a negligible effect on the IRP under internal pressure, particularly when this specific length of pipe is utilized. Parametric studies were also conducted to examine the influence of various design parameters on the flexural behaviour of discontinuous legacy pipe segments rehabilitated with IRP systems subjected to repeated traffic loading. These design parameters included material properties, geometric properties (such as repair thickness and discontinuity width of the host pipes), magnitude of surface loading, magnitude of internal pressure and bonding condition. The knowledge and data to be gained from this study will be useful in developing design specifications for IRP systems that are exposed to static bending loading and flexural fatigue loads.

The evaluation of the load imposed on IRP systems resulting from overhead vehicular traffic, while considering the effect of the surrounding soil, was conducted by the University of Colorado Boulder (CUB), a key partner in this international project. Their extensive analysis relied on the procedure recommended by Petersen et al. (2010) for assessing the live load distribution to buried concrete culverts. Detailed information can be found in (Klingaman et al. 2022). Therefore, the models implemented in this study do not incorporate the surrounding soil, which is regarded as the most critical condition. However, the impact of soil above the system is integrated into the models by applying the imposed traffic load level as determined by CUB.

The finite element model employed in this study is validated exclusively based on a full-scale experimental behaviour of a discontinuous steel host pipe rehabilitated with an IRP made from a GFRP material with a MOE of 3.7 GPa (536.7 ksi). This choice of validation is due to the limitations posed by cost, time and complexity associated with conducting fully scaled laboratory experiments.

The fatigue life analysis, considering the combined influence of traffic load and internal pressure, relied on stress life behaviours derived from uniaxial fatigue testing conducted in both longitudinal and transverse directions. This approach was chosen due to the high cost and complexity associated with conducting multiaxial fatigue tests.

1.4. Thesis organisation

This study is presented as a thesis by publication. It consists of seven chapters, which are organised as follows:

- **Chapter 1** is the introductory chapter, providing background and motivation, objectives, and limitations of this research.

- **Chapter 2** provides an extensive literature review emphasising the current state of the art within the field, identifying existing research gaps and challenges, which aided in determining the objectives and methodology of this work.
- **Chapter 3** is the first technical chapter in which a simplified theoretical model for the prediction of lateral deformation behaviour of structural pipe repair systems was developed. This chapter addressed the first research gap identified in Chapter 2.
- **Chapter 4** is the second technical chapter in which the bending fatigue behaviour of internal replacement pipe systems was analysed which addressed the second research gap identified in Chapter 2.
- **Chapter 5** is the third technical chapter in which the effect of internal pressure on the flexural fatigue behaviour of internal replacement pipe systems was studied. This chapter addressed the third research gap identified in Chapter 2.
- **Chapter 6** is the last technical chapter in which the influence of bonding level on the bending fatigue behaviour of internal replacement pipe systems was analysed. This chapter addressed the fourth research gap identified in Chapter 2.
- **Chapter 7** presents the conclusion, which highlights the key findings and contribution of this research work. This chapter also provides an overview of new opportunities and recommendations for future studies.

From this research work, four journal papers were published or are currently under review in high-quality international journals, which rank within the top 10%. Additionally, the significant findings and outcome of this study were also presented at a relevant national conference, along with a conference paper that can be found in APPENDIX A. Contributions have been made as a co-author to a few additional papers that have resulted from the REPAIR project. A list of these publications is included in APPENDIX B. APPENDIX The following is an overview of the four journal papers associated with this research work.

Manuscript 1: Kiriella, S., Manalo, A., Tien, C. M. T., Ahmadi, H., Wham, B. P., Salah, A., Tafsirojjaman, T., Karunasena, W., Dixon, P. and O'Rourke, T. D. (2023), "Lateral deformation behaviour of structural internal replacement pipe repair systems", *Composite Structures*, vol. 319. (Impact factor: 6.3; Cite score: 10.9)

This manuscript focuses on the first objective of the study, which involves investigating the static bending behaviour of legacy pipes with full circumferential cracks or discontinuities

repaired using IRP systems. The investigation was conducted through FE numerical four-point bending simulations based on experimental load configuration. The FE model was calibrated and validated using full-scale experimental results. A detailed evaluation of the effect of different design parameters, such as the width of host pipe discontinuity, repair thickness, MOE of repair material and level of loading on the bending behaviour of repair systems was also conducted. Utilising fibre model analysis, a simplified and reliable analytical model that can effectively replicate the lateral deformation behaviour of different IRP systems was developed. The findings of this study demonstrated that the impact of the thickness and the MOE of IRP on the overall lateral deformation behaviour relies on the width of the host pipe discontinuity. The analytical model that was developed demonstrated the ability to accurately capture the flexural behaviour of different IRP systems up to the ultimate loading in a significantly shorter time period and showed a strong correlation with outcomes obtained from FEA and full-scale experimental testing.

Kiriella, S., Manalo, A., Tien, C. M. T., Ahmadi, H., Dixon, P., Karunasena, W., Salah, A., and Wham, B. P. (2024), "Bending fatigue behaviour of internal replacement pipe systems", *Composite Structures,* vol. 331 (Impact factor: 6.3; Cite score: 10.9)

This manuscript investigated the bending fatigue behaviour of IRP systems installed in legacy gas pipes with discontinuities, subjected to repetitive traffic loading, using 3D FEA. Considering that the anticipated lifespan for the investigation is one million loading cycles, which corresponds to a duration of 50 years, the study used the stress life approach for obtaining the fatigue life. A parametric study was undertaken to evaluate the influence of key design parameters, as identified in Manuscript 1, on the bending fatigue response of IRP systems with discontinuous host pipe segments. Using multiple regression analysis, the relative contribution of the investigated parameters on the maximum stress and fatigue life of IRP systems was then determined. The results demonstrated that the concentration of tensile stress at the discontinuity edge governs the bending fatigue behaviour of fully bonded IRP systems. However, the impact of the width of host pipe discontinuity on the fatigue life of IRP systems was shown to be insignificant. Based on the outcomes obtained from multiple regression analysis, it was concluded that the level of traffic load contributes the most to the critical stress while MOE of repair material was found to have the greatest contribution to the fatigue life.

Manuscript 3: Kiriella, S., Manalo, A., Tien, C. M. T., Ahmadi, H., Karunasena, W., Dixon, P., Salah, A., and Wham, B. P., "Effect of internal pressure on the flexural fatigue behaviour

of internal replacement pipe systems", *Composite Structures* (Under review, COMSTR-D-24-00347). (Impact factor: 6.3; Cite score: 10.9)

This manuscript investigated the influence of operating internal pressure on the bending fatigue behaviour of IRP-repaired discontinuous host pipes under repeated traffic loading. By varying the critical design parameters identified in the second manuscript, the combined impact of traffic load and internal pressure on the fatigue performance of IRP was studied. The findings from this study indicated that the level of internal pressure during operation significantly influences the concentration of longitudinal stress in IRP near the edges of host pipe discontinuities when subjected to bending. The failure behaviour of IRP during bending fatigue varies depending on the level of internal pressure. Mathematical formulae that can reliably predict the fatigue life of IRP systems under the combined effect of internal pressure and repeated traffic load were established using the results gathered from comprehensive parametric investigations. The obtained equations were then used to produce design charts for a variety of internal pressure and traffic load combinations.

Manuscript 4: Kiriella, S., Manalo, A., Tien, C. M. T., Ahmadi, H., Karunasena, W., Dixon, P., Salah, A., and Wham, B. P., "Influence of bonding level on the bending fatigue behaviour of internal replacement pipe systems", *Steel and Composite Structures* (Under review, SCS30015U). (Impact factor: 4.6; Cite score: 9.6)

Manuscript 4 undertook a numerical investigation to examine the impact of varying bonding levels, defined by the unbonded length of IRP to the host pipe, on the flexural fatigue performance of the repair pipe under both pressurised and non-pressurised conditions. At various bonding levels, the effect of the repair thickness, material properties, magnitude of the traffic loadings and level of internal pressure on the fatigue life was also investigated. The findings of the analysis indicated that the fatigue life of IRP systems in unbonded circumstances, regardless of whether they are pressurised or non-pressurized, exhibits a significant enhancement when compared to their completely bonded states. This improvement is attributed to a reduction in the maximal longitudinal tensile stress experienced by the systems. The paper also revealed that extending the unbonded length between the IRP and each host pipe segment to a length from the discontinuity edge that is equivalent to the diameter of the IRP leads to the longest fatigue life in non-pressurised IRP systems. Conversely, the longest fatigue life for all pressurised systems can be achieved by detaching IRP from each host pipe segment to a length from the edges of pipe discontinuity that is equivalent to a minimum of twice the diameter of the IRP.

1.5. Summary

The internal replacement pipe (IRP) system is a novel trenchless technique that has been recently introduced for rehabilitating legacy natural gas pipelines with circumferential cracks or discontinuities. However, current knowledge on the static and fatigue behaviour and failure mechanism of IRP systems under surface loading from vehicular traffic is lacking, thereby limiting their application in legacy pipeline rehabilitation projects. This research conducted a numerical evaluation of the static and fatigue behaviour of different IRP material systems subjected to bending loads. The technical chapters of four journal papers investigated and reported on lateral deformation behaviour under surface loading, fatigue behaviour resulting from vehicular traffic loading, the combined effect of traffic load and internal pressure on the fatigue behaviour and the influence of different bonding levels on the bending fatigue behaviour of IRP systems. The findings of this study will provide valuable guidance to pipeline developers and designers in the implementation of IRP systems that prioritise safety, reliability and cost-effectiveness.

CHAPTER 2: LITERATURE REVIEW

2.1. Introduction

This chapter presents a state-of-the-art review of the literature to identify both short-term and long-term behaviours of internal pipe repair systems under surface loading from vehicular traffic, as well as the critical design parameters that influence their effectiveness. The review is commenced by examining the failure characteristics exhibited by buried legacy gas and oil pipelines throughout their operational life span. Following that, an overview of trenchless technologies that are currently available for rehabilitating damaged legacy gas and oil pipelines is provided. Subsequently, a review of various performance objectives and failure mechanisms linked to rehabilitated pipelines was conducted. The review also encompasses an examination of the existing understanding of lateral deformation of pipe repair systems, the bending fatigue performance of such systems, the impact of the internal pressure on fatigue during bending, and the influence of various bonding conditions on fatigue during bending. Through this literature review, current knowledge gaps were identified to justify the novelty of the implemented research works.

2.2. Failure of legacy pipelines

Underground pipelines have been used globally due to their cost effectiveness and high level of safety in transporting crude oil and natural gas across long distances, in comparison to alternative modes of transportation such as road and rail (Kishawy et al. 2010; Lim et al. 2015; Deng et al. 2022; Mao et al. 2022). Despite these advantages, failure of pipelines can have severe negative consequences, including personal injuries, financial losses, and environmental damage due to the explosive, toxic and flammable characteristics of the substance being transported (Soomro et al. 2022; Wang et al. 2022; Al-Sabaeei et al. 2023; Shehata et al. 2023; Woldesellasse et al. 2023). While steel and cast-iron pipes have historically been widely used, a significant portion of these pipe networks is now approaching the end of their operating lifespan, necessitating frequent repairs or replacements (Günaydın et al. 2013; Robert et al. 2016). The buried pipe, unlike exposed structures, has the potential to deteriorate without being noticed for a long period, until a catastrophic failure eventually takes place (Almahakeri et al. 2013). The primary factors contributing to the failure of legacy cast iron and bare steel pipelines are corrosion, natural hazards such as landslides, earthquakes and erosion, construction defects, operational errors and third-party activities (Senouci et al. 2014; Chen et al. 2019; Zakikhani et al. 2020b; Arifin et al. 2021; Wasim et al. 2022; Yao et al. 2022; Li et al. 2023b).

Different types of pipe breakage in literature have been categorised as circumferential cracking, longitudinal cracking, bell splitting, bell shearing, spiral cracking and blow-out hole (Makar et al. 2001; Uslu et al. 2015; Kumar et al. 2020; Parka et al. 2020). Circumferential cracking (Fig. 2a) is the most prevalent failure in pipes with a smaller diameter (< 380 mm or 14.96in) (Makar et al. 2001; Kumar et al. 2020). However, pipes with a large diameter possess a moment of inertia that is too high, thereby preventing the occurrence of circumferential cracking. This type of crack is primarily caused by stresses induced by ground deformation during trench construction (Makar et al. 2001; Jeon et al. 2004). Metal loss due to excessive corrosion can also cause circumferential cracks and discontinuities in buried legacy pipelines (Akhi et al. 2021; Shirazi et al. 2023). On the other hand, longitudinal cracking (Fig. 2b) seems to be limited to pipes with a larger diameter (Uslu et al. 2015). This failure type could potentially arise from internal pressure, external crushing forces exerted on the pipe, or compressive forces acting along the pipe (Makar et al. 2001). Once the crack is initiated, it has the potential to propagate along the entire length of the pipe.

According to Makar et al. (2001), it seems that a bell split (Fig. 2c) is mostly seen in pipes with smaller diameters. The occurrence of this failure mode is often attributed to thermal expansion that takes place between the bell and the leadite seal at the pipe joint (Uslu et al. 2015). The phenomenon of bell shearing (Fig. 2d) is primarily observed in pipes with a large diameter. One possible factor contributing to this failure mode is the application of compressive forces that push the spigot of a pipe into the bell of the adjacent pipe in the pipeline. Additionally, bending forces can also be a potential cause of this failure (Makar et al. 2001). Some pipes with medium diameters ranging from 380 mm (14.96 in) to 500 mm (19.69 in) exhibit a distinct failure mode characterised by the initiation of a crack in a circumferential manner, followed by their propagation in a spiral manner (Fig. 2e) (Uslu et al. 2015). The development of this fracture may be attributed to pressure surges as well as the combination of bending forces and internal pressure (Makar et al. 2001).

Corrosion is often the underlying cause of blow-out holes. The presence of a corrosion pit leads to a reduction in both the thickness and the mechanical strength of the pipe wall. As the wall thickness is reduced to a certain level, the internal pressure may cause a blowout, resulting in the formation of a hole in the pipe (Fig. 2f) (Uslu et al. 2015). In addition to the aforementioned types of failure, it is important to note that segmented pipelines that are connected through joints are prone to pull-out failure (Fig. 3), which can be caused by permanent ground deformation (Shi 2015; Wham et al. 2016; Qin et al. 2022; Chen et al. 2023). This joint pull-out phenomenon can ultimately lead to the occurrence of discontinuities in the

pipeline system (Zhong et al. 2014). According to Jeon et al. (2004) and Stewart et al. (2015), pulled-out joint and full circumferential fracture (also referred to as a round crack), are both regarded as the worst type of discontinuities that can occur in legacy pipelines. Pipelines with these types of failures need to be repaired for their continuous service and safe operation.

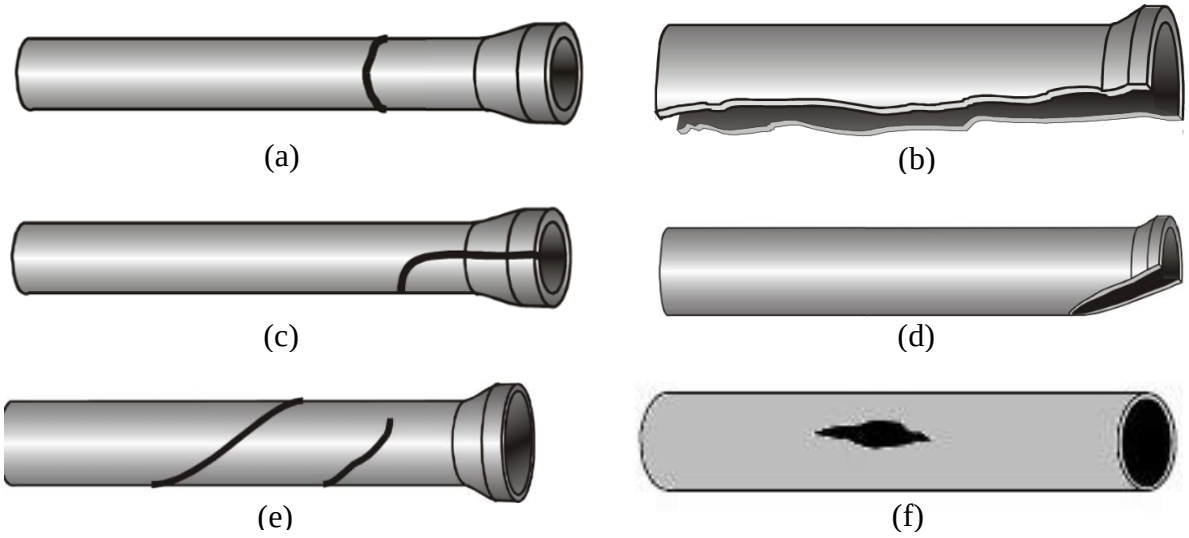

Fig. 2. Pipe breakage types (a) circumferential cracking, (b) longitudinal cracking, (c) bell splitting, (d) bell shearing, (e) spiral cracking (Makar et al. 2001), (f) blow-out hole (Uslu et al. 2015)

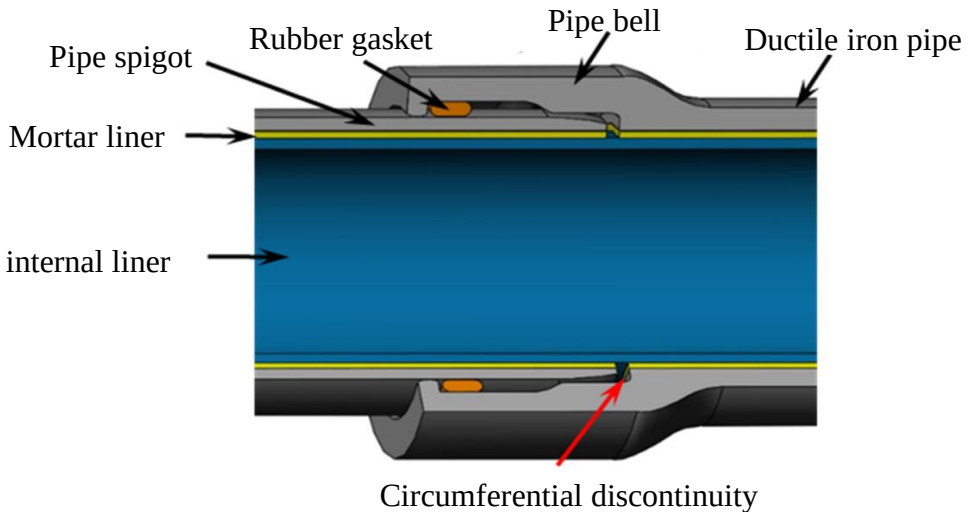

Fig. 3. Cross section of a pull-out joint in ductile iron (DI) pipe rehabilitated with internal liner (Zhong et al. 2018)

2.3. Trenchless rehabilitation technologies for legacy pipelines

Rehabilitation of existing damaged pipe networks and infrastructure systems is a more favourable approach compared to replacement due to the constraints posed by limited financial resources (Karbhari 2014). Currently, the rehabilitation of buried pipelines is accomplished through the use of either open-cut methods or trenchless technologies (Yu et al. 2008; Matthews et al. 2015; Moeini et al. 2021). The trenchless rehabilitation approach holds significant advantages over the traditional open-cut method, including reduced disturbance and surface damage, shorter construction time, less pollution, minimal traffic disruption and lower comprehensive cost (Tetreault et al. 2018; Li et al. 2023a). Moreover, this technology is frequently applied for rehabilitating pipelines in areas that are challenging to reach or have limited access (Chin et al. 2005).

Trenchless rehabilitation can be categorized into three distinct classifications: nonstructural, semi-structural and structural (Zhu et al. 2021). Nonstructural liners do not enhance the structural performance of the host pipe and cannot withstand external and internal loads. As a result, it is necessary for the host pipe to possess a certain level of structural integrity. In practice, their primary function is to protect the host pipe against corrosion and prevent any potential leakage (Li et al. 2023a). In addition to providing corrosion protection and leakage control, semi-structural liners have the ability to partially withstand both external and internal loading but still rely on the residual structural support provided by the host pipe (Gras-Travesset et al. 2023). Finally, structural liners are specifically designed to endure all internal and external loads. Therefore, structural liners are employed in cases where the host pipe has undergone significant damage and compromised its structural capacity (Gras-Travesset et al. 2023). The selection of appropriate pipeline rehabilitation method is dependent upon the failure mechanism, and condition of the legacy pipe including the extent of corrosion, structural degradation, and reduction in pressure capacity (Zhu et al. 2021). The most commonly employed trenchless techniques for rehabilitating gas or oil pipelines encompass cured-in-place pipe lining, spray-applied pipe lining, slip lining and fold and form lining (Lu et al. 2020b; Lu et al. 2020a).

Cured in-place pipe lining

The cured-in-place pipe (CIPP) lining (Fig. 4) was first developed in 1970 and has emerged as the leading and widely utilized trenchless rehabilitation method within the pipeline industry (Alam et al. 2015; Mogielski et al. 2017). The CIPP method involves the insertion of a liner saturated with thermoset resin into a legacy pipe by means of either air, water inversion

or mechanical pulling which is subsequently expanded through the application of either air or water pressure (Matthews et al. 2013). The inflated liner with resin is then subjected to a curing process using either heat or ultraviolet (UV) light in order to facilitate the formation of a thin layer of pipe that tightly adheres to the host pipe (Ji et al. 2020). Upon completion of the rehabilitation process, the flow area of the pipe will undergo a reduction. However, this reduction will result in an increase in the transportation capacity due to a decrease in the roughness of the inner wall. The thermoset resins that are frequently utilized include polyester, vinyl ester and epoxy (Nuruddin et al. 2020). The latest CIPP products designed for pressure applications can now be categorized as either semi-structural or structural (Lu et al. 2020b). However, this approach necessitates the use of advanced construction equipment and demands a high level of expertise from operators (Lu et al. 2020a).

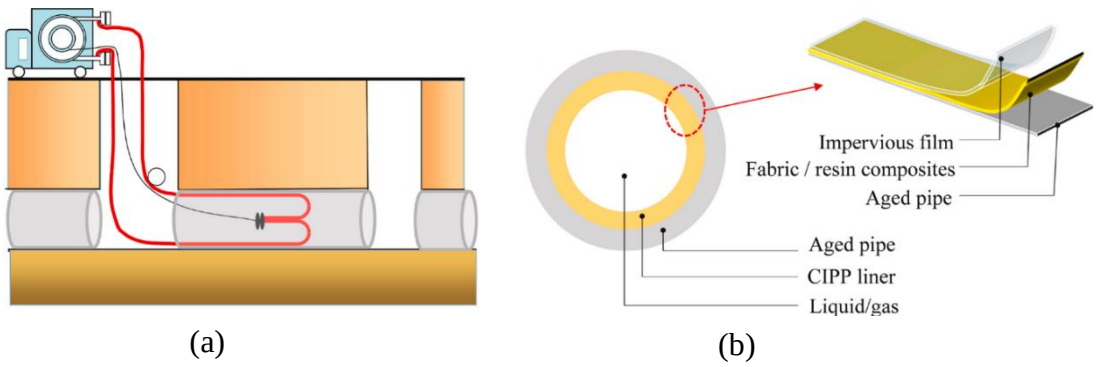

Fig. 4. Schematic of CIPP lining method (a) Installation process and (b) Structure of the lined pipe (Jing et al. 2023)

Spray-applied pipe lining

The spray-applied pipe lining (SAPL) is a nonstructural rehabilitation technology used to prolong the lifespan of legacy pipes. This method involves the spraying of coating material onto the inner surface of the host pipe, resulting in the formation of a liner (Zhu et al. 2021). In general, the coating material utilized for SAPL can be divided into two categories: cement-based materials which consist of mixtures of Portland cement or geopolymer mortar, and polymeric material, which include polyurethane, polyurea and epoxy (Kohankar Kouchesfehani et al. 2020). Before the application of SAPL, it is necessary to perform a thorough cleaning of the internal surface of the host pipe. SAPL installations are often accomplished by the use of either a hand spay method or the use of a spin casting machine

(Kohankar Kouchesfehani et al. 2020). One of the significant constraints of this approach is that the host pipe must have a certain level of structural integrity (Lu et al. 2020a).

Slip-lining

Slip-lining is a structural rehabilitation solution that is extensively employed in underground pipe networks (Li et al. 2023a). This technique involves the insertion of a new structural pipe into the host pipe by means of pushing or pulling. A working pit is required for layout purposes (Selvakumar et al. 2011). The annular gap between the liner and the host pipe must be filled with grout. Polyethylene (PE), polyvinyl chloride (PVC), and glass fiber-reinforced plastic are the most common materials utilized in the slip-lining technique (Li et al. 2020). The repaired pipes form a "pipe-in-pipe" structure, combining the corrosion-resistant characteristics of the internal liner pipe with the mechanical properties of the metallic host pipe (Lu et al. 2020b).

Fold and form lining

The fold and form approach involves modifying the geometry of the liner in order to reduce its cross-sectional area before implementation. Once the liner is inserted into the host pipe, it undergoes expansion by either heating or pressing in order to regain its initial dimensions and shape. The most common shapes for prefabricated liner pipes are U, C and H (Lu et al. 2020b). According to Selvakumar et al. (2002) fold and form liners can be made of PVC or PE materials. However, one of the limitations associated with this approach is the potential for structural damage arising during the construction phase (Lu et al. 2020a).

Internal replacement pipe (IRP)

Internal replacement pipe (IRP) systems are a new and emerging trenchless technology utilised for rehabilitating cast iron, wrought iron, and bare steel natural gas distribution pipes that have circumferential cracks or discontinuities (Fu et al. 2022b; Tafsirojjaman et al. 2022; Dixon et al. 2023). This novel approach involves the fabrication of new structural pipes inside the old pipes using robotics and new inspection tools. IRP systems can be made from a wide range of materials, including thermoplastics, polymeric coatings, fibre composites and metallic coatings (Tafsirojjaman et al. 2022; Dixon et al. 2023). The bonding configuration between IRP and host pipe could be either full bonding, partial bonding or complete unbonding (Tien et al. 2023). The integration of IRP systems yields significant enhancements in the structural integrity and restores the service life of legacy pipelines. However, the IRP systems are specifically designed to function and withstand both internal and external loading throughout

their service life, without relying on the structural support provided by the host pipe (Tafsirojjaman et al. 2022).

2.4. Failure mechanism associated with rehabilitated pipelines

When designing an effective internal repair system for pipeline rehabilitation, it is crucial to consider various performance objectives and the failure mechanism associated with them. The failure modes of the host pipes and IRP systems are significantly affected by the loading conditions. The comprehensive review study undertaken by Tafsirojjaman et al. (2022) and Dixon et al. (2023) within the REPAIR project has highlighted nine primary performance objectives that should be addressed for the optimal design of IRP systems for the rehabilitation of gas pipes. These performance objectives are as follows:

- Lateral deformation: An IPR-repaired host pipe is required to account for lateral deformation in longitudinal bending, caused by a variety of sources, including surface load from vehicular traffic, nearby excavation, earth movement (subsidence), undermining and frost heave (Jeon et al. 2004; Vazouras et al. 2012; Trickey et al. 2016; Melissianos et al. 2017; Neya et al. 2017; Alzabeebee et al. 2018; Argyrou et al. 2019; Liu et al. 2019; Kozman 2020; Vasseghi et al. 2021). Lateral deformation may lead to failure due to bending, axial stresses, buckling and cross-section ovalization.
- Cyclic in-service surface loads: Repetitive surface loads primarily arise from overhead vehicular traffic (Jeon et al. 2004; Guo et al. 2005; Sheldon et al. 2015; Stewart et al. 2015; Ha et al. 2016; Wang et al. 2019). These loads can impose lateral or circumferential deformations of repair systems and have the potential to induce fatigue failure in bending.
- Hoop (circumferential) stress: This is induced by internal pressure and pressure variations (Mattos et al. 2016; Budhe et al. 2020). Bursting failure can occur when there is excessive tensile stress and stretching of the material, leading to a loss of containment (Allouche et al. 2005; Brown et al. 2020).
- Axial deformation: The deformation of rehabilitated IRP systems in the longitudinal direction typically occurs as a result of thermal loading (expansion or contraction) induced by the seasonal temperature changes or seismic loading (Jeon et al. 2004; Stewart et al. 2015; Argyrou et al. 2018; Zhong et al. 2018). The potential failure modes that may occur are stress limit failure caused by axial stresses, pinching, buckling, detachment of IRP from the host pipe and fracture of the IRP.

- Impact/puncture: The IRP systems may be subject to impingement from the fragments of the host pipe that undergo brittle fracture or puncture caused by a foreign object in an area where the host pipe has significantly deteriorated (Gao et al. 2022). It has the potential to cause damage such as dents, cracks, and material loss, which can ultimately reduce the pressure-caring capacity of the repair system.
- Cross-section ovalization: Ovalization of an IRP can be caused by external pressure, surface load, and bending of the pipeline. The potential failure mechanism associated with this loading condition includes ring collapse and excessive ovalization (Hilberink et al. 2011; Vasilikis et al. 2012; Becerril García et al. 2015). Ring collapse refers to the deformation of a pipeline, where its circular cross-section becomes distorted or collapses inward. On the other hand, excessive ovalization occurs when the circular cross-section of a pipeline undergoes significant elongation, resulting in the formation of an oval shape.
- Compatibility with current and future gas compositions: The sources that contribute to this particular scenario involve natural gas and mixtures of hydrogen and methane (Nuruddin et al. 2020). The possible failure modes that may occur are chemical degradation and excessive permeation.
- Debonding at IRP-host pipe interface: The occurrence of debonding at the interface between the IRP and host pipe may be attributed to thermal expansion and mechanical loads (Kozman 2020; O'Rourke et al. 2021). Debonding can lead to several consequences, including backtracking between internal repair and host pipe at service line connections and termination points, loss of containment and compromised delivery, and potential ring collapse.
- Service connections: This refers to sources that are either abandoned or in-service connections(Allouche et al. 2005; Jaganathan et al. 2007). Failure may arise due to stress concentration (Adebola et al. 2021). Additionally, the possibility of differential movement can contribute to failures at connections and leakage at the service line connection and the IRP end joints.

Based on the analytical hierarchy process conducted by Tafsirojjaman et al. (2022), the aforementioned first six performance objectives and associated failure mechanisms were ranked. The results of this ranking can be found in APPENDIX C. It was identified that lateral deformation and fatigue failure caused by traffic loading are the worst conditions for IRP

systems. Regardless of the significance of ensuring the safe design to prevent the failure of IRP systems caused by traffic loading, there is a scarcity of research in this area.

2.5. Lateral deformation of pipe repair systems

Underground legacy pipelines that have been damaged and rehabilitated with IRP systems are typically exposed to surface live loads because of vehicular traffic loading (Tarar 2008; Alam et al. 2019; Li et al. 2019). The load exerted by the wheels, which are located directly above the pipe and move in parallel to their longitudinal axis, are transferred to the buried pipe through the surrounding soil. This transfer of loads results in stresses and deformations that represent the most severe conditions, as documented by Jeon et al. (2004) and Stewart et al. (2015). Several factors influence the extent of lateral deformation of pipelines such as applied load, relative stiffness of the pipeline in relation to supporting soil, the burial depth and the stiffness of the joints connecting the individual pipe sections (Stewart et al. 2015). Under the application of traffic loads, the IRP system experiences its maximum deformation, which includes relative displacement and rotation, at the weakest discontinuity present along the host pipe (Fig. 5). There is a limited number of studies in the open literature that have examined the lateral deformation behaviour of legacy pipes with circumferential cracks or discontinuities repaired with liners (Jeon et al. 2004; Allouche et al. 2012; Stewart et al. 2015). The liners used in these studies were CIPP liners with a lower modulus of elasticity (MOE) and thickness compared to the host pipe.

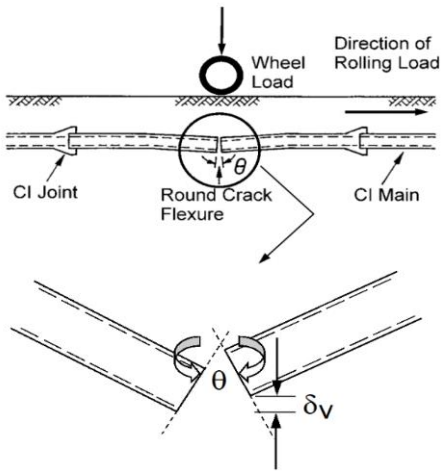

Fig. 5. Relative vertical displacement (δ_v) and rotation (θ) at a round crack imposed by traffic loading (Netravali et al. 2000)

Jeon et al. (2004) investigated the behaviour of 101.6 mm (4 in), 152.4 mm (6 in), and 203.2 mm (8 in) diameter cast iron (CI) pipes with circumferential cracks repaired with

polyurethane (PU) CIPP linear under a heavy traffic loading of 133 kN (30 kips). In addition, a simplified analytical model was formulated to assess the maximum relative displacements and rotations experienced by the legacy pipes due to the circumferential cracks under traffic loading using the loading configuration as shown in Fig. 6(a) and (b), respectively. However, in the analytical model developed by Jeon et al. (2004), they made a conservative assumption that the liner does not contribute any stiffness to the system due to its considerably lower MOE in comparison to the CI host pipe. In their study, Stewart et al. (2015) examined the lateral deformation characteristics of CI host pipe with diameters of 152.4 mm (6 in) and 304.8 mm (12 in) that were repaired using 2.54 mm (0.1 in) thick CIPP liners. Field samples obtained from previously lined CI host pipes with joint openings ranging from 6.4 mm (0.25 in) to 10.9 mm (0.43 in) were utilised in this investigation. The pipes were subjected to a traffic load of 178 kN (40 kips) in four-point bending tests. The finding of this study indicated that the crack openings significantly affect the overall load-deformation behaviour of the repaired pipes. However, it is important to note that the analysis employed for testing did not consider the structural contribution of the liner, which is comparable to the approach taken by Jeon et al. (2004). This is a significant simplification that is no longer valid in structural repair projects due to the relatively higher stiffness of new IRP materials compared to that of CIPP lining.

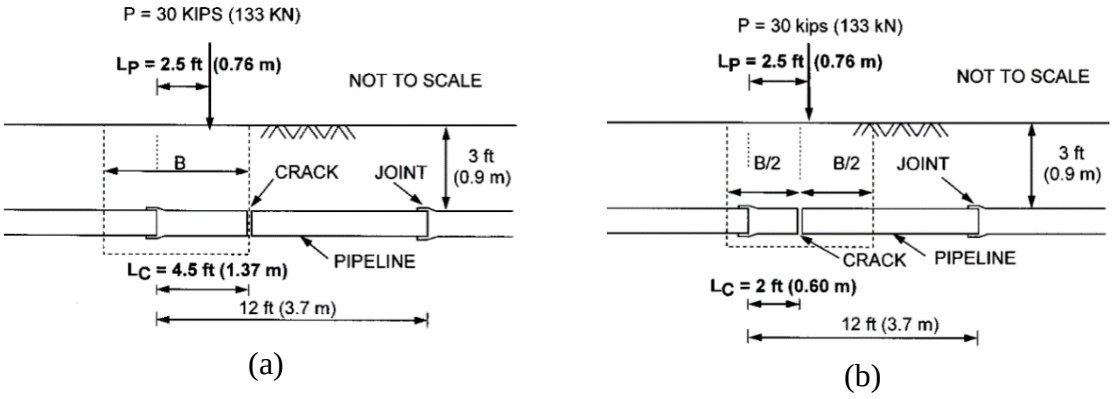

Fig. 6. Loading configuration and geometry of cracked CI pipe employed in the analytical modelling of (a) maximum deformation, (b) maximum rotation (Jeon et al. 2004)

Allouche et al. (2012) performed three-point bending tests to assess the bending behaviour of 152.4 mm (6 in) diameter CI pipes that were cut into two halves and linked together with fibre-reinforced CIPP liners. The pipe tests were conducted under both pressurised and non-pressurised conditions, specifically focusing on the joint area of the pipes. The maximum applied deflection was 127 mm (5 in) while the maximum pressure applied was 827. 4 kPa (120 psi). Based on the findings, it has been determined that the liner successfully

maintained its structural integrity following the failure of the host pipe, with no visible indications of leakage. However, during the bending test, it was observed that the liner buckled at the invert due to the lack of internal pressure in the lined pipe. However, none of these studies on CIPP-lined discontinuous metallic host pipe systems has conducted an in-depth study to clearly demonstrate the effect of various design parameters on the lateral deformation behaviour of pipe liners. This is because these studies rely on costly and time-consuming full-scale experimental testing.

One of the preliminary studies conducted by Tafsirojjaman et al. (2022) in relation to the REPAIR project focused on the influence of several design parameters, including MOE and thickness, on the lateral deformation behaviour of standalone IRPs with a nominal outer diameter of 307.8 mm (12.12 in). The investigation was conducted under a design load of 178 kN (40 kips) using linear FEA. In this study, a wide range of potential IRP materials including unreinforced polymers, glass fibre-reinforced polymers, fibre-reinforced thermosets, steel and cast iron were examined. The materials were evaluated based on their MOE which ranged from 1 GPa (145 ksi) to 200 GPa (29,008 ksi). Additionally, the thickness of the IRP materials considered varied from 3.175 mm (0.125 in) and 25.4 mm (1 in). The findings of this study indicated that the load-carrying capacity of the IRP alone increases as the thickness and MOE increase. Additionally, it was also found that IRP with a thickness of 9.525 mm (0.375 in) or less underwent compressive buckling prior to reaching a tensile strain of 0.02. However, the occurrence of buckling failure was effectively eliminated by increasing the thickness of IRP to a minimum of 12.7 mm (0.5 in). However, it is important to note that this preliminary study did not account for the existence of discontinuous host pipe segments, which may potentially impact the overall bending deformation of the repair system.

There are a few other studies in the literature that investigated the effect of the size of external corrosion defects on the lateral deformation behaviour of pipes. Chegeni et al. (2019) employed FEA to investigate the effect of corrosion depth and defect length in longitudinal and circumferential directions on the performance of corroded thin-walled steel pipes when subjected to four-point bending. These pipes had an external diameter of 203.2 mm (8 in) and a wall thickness of 6 mm (0.236 in). The findings showed that as the corrosion depth increased from 0% to 80% of the wall thickness, there was a significant reduction (34%) in the ultimate load-carrying capacity of the damaged pipe. Additionally, an increase in the length of the defect in both longitudinal and circumferential directions from 0 to 180 mm (7.087 in) also led to a reduction in the ultimate load-carrying capacity of the pipe by 19% and 40%, respectively. These results suggest that an increase in defect length in the circumferential direction has a

more pronounced detrimental effect on the bending performance of the pipe compared to an increase in defect length along the longitudinal direction.

Shuai et al. (2021) utilised nonlinear FEA to investigate the effect of depth, width and length of a corrosion defect on the local buckling behaviour of 1016 mm (40 in) diameter corroded steel pipes with a thickness of 15.3 mm (0.602 in) subjected to four-point bending tests (Fig. 7). The study found that the buckling resistance is significantly influenced by the defect depth and the defect length in the circumferential direction. Specifically, the critical buckling moment decreased as the defect depth and width increased. Although the effect of defect length along the longitudinal axis of the pipe was negligible, when it exceeded 360 mm (14.173 in), the buckling mode changed from a single buckling wave to two waves (Fig. 8). However, the aforementioned studies have exclusively focused on surface defects and their impact on the legacy pipe without any repair systems.

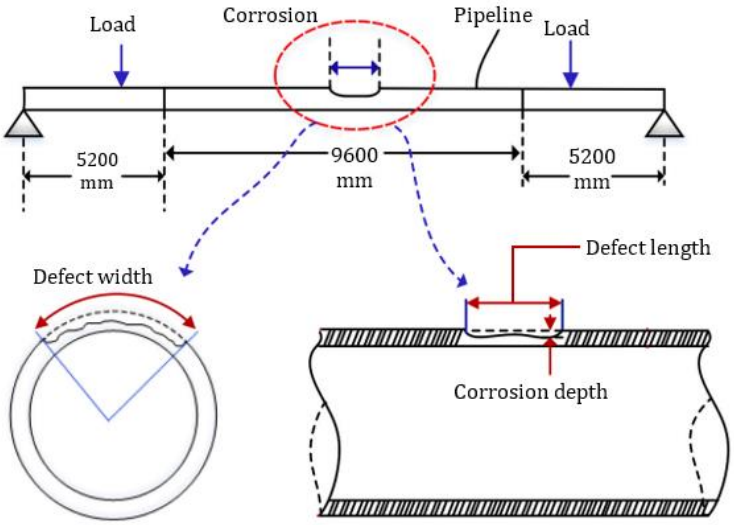

Fig. 7. Schematic diagram of a four-point bending test on a steel pipe with a corrosion defect where L is the length of the corrosion defect (Shuai et al. 2021)

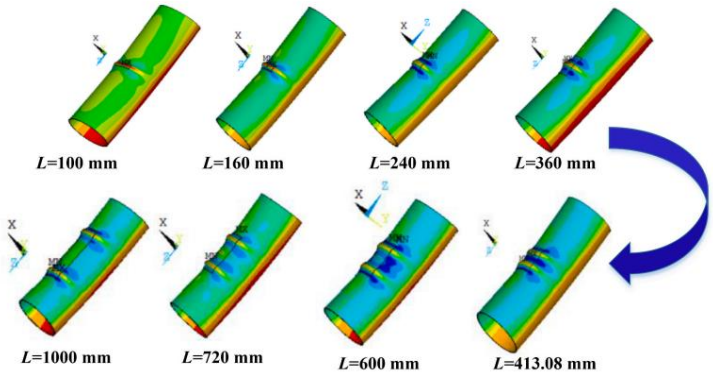

Fig. 8. Buckling modes of the corroded steel pipe with various defect lengths, *L* (Shuai et al. 2021)

2.6. Bending fatigue behaviour of pipe repair systems

High cyclic bending loads are frequently applied to the critical fatigue zones of repaired pipelines, making them one of the dominant loading scenarios (Tarar 2008; Alam et al. 2019; Li et al. 2019). Having an in-depth understanding of fatigue behaviour and precise life estimation of IRP systems is an essential aspect in the design and development of new and emerging IRP systems. As previously stated, IRP repair systems are now being developed using various materials including thermoplastic, composites, or metallic (Tafsirojjaman et al. 2022; Dixon et al. 2023; Tien et al. 2023). Results of several experimental studies demonstrated that the static and fatigue behaviour of these materials are different.

Metallic materials exhibit nonlinear stress-strain behaviour and have a higher elastic modulus than polymeric composites. A predominant single crack is the most typical failure mechanism of metals, as a significant portion of the fatigue process is spent on propagating a single crack (Risicato et al. 2014). Unlike metals, the fatigue behaviour of polymers is governed by the viscoelastic effect (Chandran 2016). Softening and melting occur at higher frequencies, and fatigue failure is primarily determined by the test frequency. Thermoplastic materials have a lower modulus of elasticity, lower tensile strength and a narrow operating temperature range than metals and composites (Mellott 2012), and failure occurs under fatigue loading as a result of either conventional crack initiation and propagation mechanisms or material softening due to self-heating (Crawford et al. 1974). On the other hand, the fatigue failure mechanism of FRP composites includes matrix cracking, fibre debonding, delamination, and fibre fraction, in addition, to crack initiation and crack propagation (Samanci et al. 2008; Shanmugam et al. 2021). Unlike metal fatigue, the stiffness loss of composites is visible from the early stage of fatigue loading and may possibly lead to significant stiffness degradation over the succeeding fatigue process (Lian et al. 2010; Colombi et al. 2012) A detailed review of fatigue characteristics of potential IRP materials is available in APPENDIX D. Therefore, understanding the fatigue behaviour of legacy pipes rehabilitated with IRP made from different material systems is necessary.

The existing literature on the bending fatigue performance of repair systems installed in host pipes with full circumferential cracks or discontinuities is limited, mostly focusing on low-modulus CIPP liners or SAPL materials (Jeon et al. 2004; Stewart et al. 2015; Ha et al. 2016). In their experimental study, Jeon et al. (2004) examined the bending fatigue behaviour of CIPP-lined circumferentially cracked CI legacy pipe. The system was exposed to one million cycles of either a relative displacement of 2.54 mm (0.1 in) or a rotation of 0.23 degrees at the location of the circumferential crack. Throughout the testing, a low internal pressure of nitrogen

gas was maintained. This experimental setup aimed to replicate the heavy traffic load that the repair system would typically experience throughout a 50-year operational period. During the testing process, the liner demonstrated its ability to withstand relative displacement and rotation resulting from heavy traffic load without experiencing any failure. However, after undergoing one million cycles of deformation, it was observed that the internal vertical stiffness of the CIPP liner experienced a reduction of approximately 75%. Additionally, a localised debonding phenomenon was observed at the interface between the host pipe and the liner near the crack edge. Based on their findings, the process of debonding provides benefits to the liner by enhancing the flexibility of the system and minimising the stress concentration at the crack edge. However, this study did not explicitly state the extent of debonding, the amount of the stress concentration reduction, and the level of improvement in fatigue life.

The study conducted by Stewart et al. (2015) involved laboratory experiments of four-point cyclic bending testing of legacy CIPP repaired CI pipe with a joint. The pipe was subjected to one million cycles of deflection, with a magnitude of 1.524 mm (0.06 in) and 1.778 mm (0.07 in), respectively, while maintaining an operational internal pressure of 102 kPa (14.8 psi). During the testing, the liner exhibited the highest level of deformation at the weakest discontinuity along the legacy CI pipe i.e., the joint. Consequently, the overall stiffness of the system was reduced, but the liner remained intact without any fracture. According to Stewart et al. (2015), the observed stiffness reduction in the repair system is primarily attributed to the debonding of the liner from the host pipe. In an investigation conducted by Ha et al. (2016), a three-point cyclic bending test was performed on a 150 mm (5.91 in) diameter steel host pipe containing a circumferential crack of 25 mm (0.98 in) in width, which was repaired using polyurea-polyurethane SAPL. The repair system was subjected to 10^5 bending cycles at a frequency of 1 Hz, with a maximum vertical displacement of 6.1 mm (0.24 in) and an internal pressure of 12 kPa (1.74 psi). In line with the findings of Jeon et al. (2004) and Stewart et al. (2015), Ha et al. (2016) also observed a decrease in stiffness during the experiment, as shown in Fig. 9, without any leakage or failure. However, Ha et al. (2016) did not clearly indicate the motivation for their investigation was the traffic load.

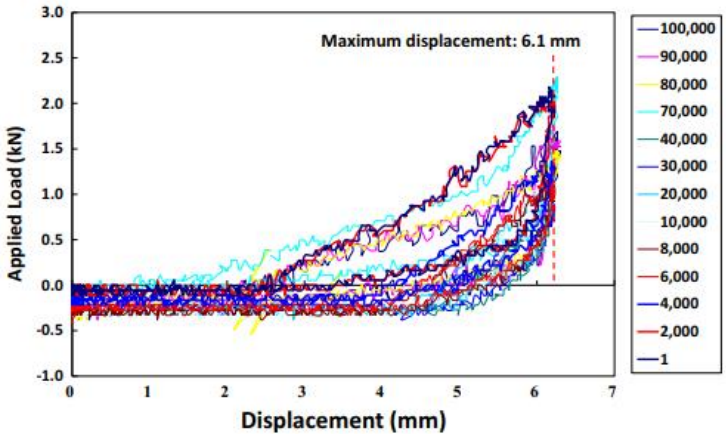

Fig. 9. Load-deformation behaviour of circumferentially cracked steel host pipe repaired with SAPL obtained from cyclic bending test (Ha et al. 2016)

The initial investigation conducted by Tafsirojjaman et al. (2022) using a standalone IRP, has shown that the bending fatigue behaviour of an IRP can be substantially influenced by both its wall thickness and MOE. The range of MOE and thickness utilised in this analysis was identical to those employed in static bending analysis detailed in Section 2.5; however, the repetitive traffic load applied was only 17.35 kN (3.9 kips). The results of this study indicated that an increase in both MOE and the thickness of IRP can result in a significant prolongation of the fatigue life. Further, it has been determined that the IRP with a MOE of 1 GPa (145 ksi) and 3 GPa (435 ksi) necessitates a minimum wall thickness of 9.525 mm (0.375 in) and 3.175 mm (0.125 in), respectively, to attain a design life of one million loading cycles maintaining a design strain limit of 0.02. However, investigating how these design parameters affect the bending fatigue behaviour of IRP systems is crucial with consideration given to the potential impact of discontinuous host pipe segments.

2.7. Effect of internal pressure on fatigue in bending

Based on the specification provided by the Advanced Research Project Agency-Energy (ARPA-E 2020), the legacy steel pipes have a maximum operating internal pressure of 413.7 kPa (60 psi) and a maximum allowable internal pressure of 1379 kPa (200 psi). However, existing studies have primarily focused on investigating the bending fatigue performance of repaired steel pipes under low internal pressure. Consequently, there is no research exploring the influence of varying internal pressure levels on the bending fatigue behaviour of steel host pipes containing circumferential cracks or discontinuities that have undergone rehabilitation employing IRP systems. Available studies on the behaviour of damaged pipes with a repair

system, either under internal pressure alone or in combination with static bending revealed that internal pressure can contribute to stress concentrations in the damaged area (Brown et al. 2014; Shou et al. 2018; Shou et al. 2020; Tien et al. 2023). The study, carried out by Tien et al. (2023) as part of the REPAIR project assessed how the presence of crack edges on steel host pipes with a diameter of 323.85 mm (12.75 in) and a discontinuity (opening) width of 914.4 mm (36 in) affected the performance of a thermoplastic IRP under an internal pressure of 1379 kPa (200 psi). The IRP utilised in the study had a thickness of 3.175 mm (0.125 in) and an MOE of 5 GPa (725 ksi). The study discovered that when subjected to internal pressure alone, the IRP experienced bending as it curved around the edge of the host pipe discontinuity. This bending resulted in a concentration of longitudinal stresses in the IRP near the edge of host pipe discontinuity as depicted in Fig. 10.

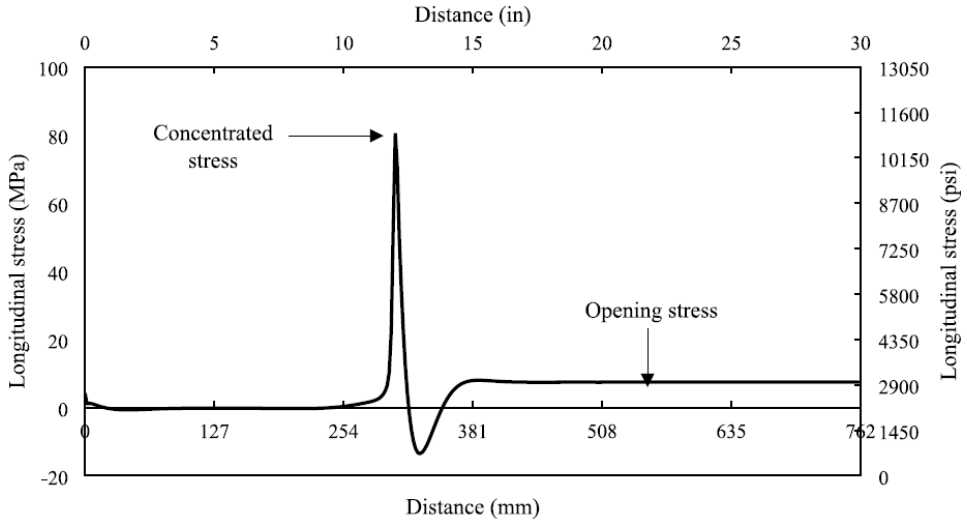

Fig. 10. Internal pressure-induced longitudinal stress concentration at the discontinuity edge (Tien et al. 2023)

In a study conducted by Brown et al. (2014), the behaviour of discontinuous CI host pipe repaired with CIPP liner with a thickness of 5 mm (0.197 in) was investigated under an internal pressure of 700 kPa (101.53 psi) using 3D FEA. The analysis has indicated that when subjected to internal pressure, the axial stress in the liner becomes concentrated at the edge of the host pipe discontinuity where its structural integrity has been compromised. The influence of internal pressure on the static bending performance of steel host pipe with circular corrosion defects repaired with CIPP liners was investigated numerically by Shou et al. (2018) and Shou et al. (2020) in two separate studies. The CIPP liner under consideration had an MOE of 13 GPa (1886 ksi) and was subjected to a traffic load of 350 kN (78.68 kips). The identified corrosion defect had a maximum diameter of 100 mm (3.937 in) and was located on either the

top or lateral surface of the host pipe surface. The findings of these studies demonstrated that an increase in the internal pressure from zero to 588.4 kPa (85.34 psi) leads to a nonlinear increase in von Mises stress at the corrosion defect. Additionally, it was shown that during static bending, the presence of internal pressure contributed to increasing the concentration of longitudinal stress at the defect.

A few investigations on the behaviour of repair systems under internal pressure have shown that the discontinuity widths that exist in host pipes may have an influence on the overall performance of the repair system. Fu et al. (2022a) investigated numerically the effect of varying widths of circumferential discontinuities in 150 mm (5.906 in) diameter CI host pipes on the performance of a polymeric liner with a thickness of 3 mm (0.118 in) and MOE of 2.6 GPa (377 ksi) under an internal pressure of 600 kPa (87.02 psi). The widths of discontinuities ranged from 0 to 80 mm (3.15 in). Based on the findings, it was observed that the maximum tensile stress in the liner exhibited a nonlinear increase as the discontinuity width was increased from 0 to 50 mm (1.969 in), but then remained relatively constant until the discontinuity width reached 80 mm (3.15 in) (Fig. 11). In a recent study, Zhai et al. (2023) conducted a numerical analysis to examine the impact of different widths of existing discontinuities ranging from 4 mm (0.157 in) to 40 (1.575 in) in a 300 mm (11.811 in) diameter host pipe on the mechanical response of the pipe liner under internal pressure of 600 kPa (87.02 psi). The host pipe had a thickness of 15 mm (0.591 in) and MOE of 100 GPa (14,504 ksi), while the liner had a thickness of 3 mm (0.118 in) and a MOE of 3.0 GPa (435 ksi). The results indicated that there is a direct relationship between the discontinuity width and the maximum stress experienced by the liner when subjected to longitudinal bending caused by the internal pressure. As the width of the host pipe discontinuity increases, the maximum stress in the liner also increases.

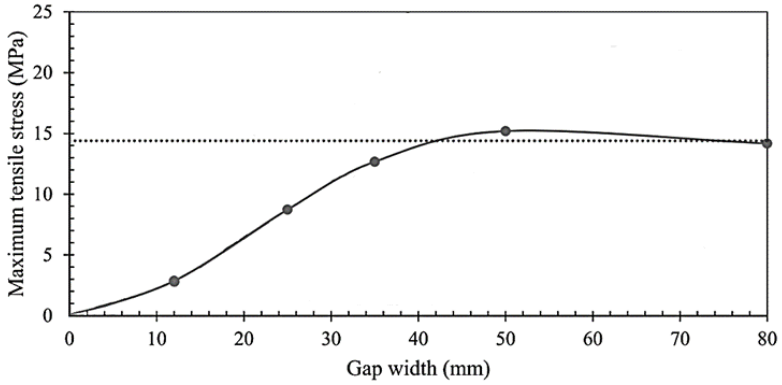

Fig. 11. Effect of discontinuity width on the maximum stress experienced by the liner when subjected to internal pressure (Fu et al. 2022a)

2.8. Effect of different bonding conditions on fatigue in bending

In the repair process of damaged legacy pipelines, it is feasible to employ either partially bonded or completely unbonded connections between the host pipe and IRP (Zhong et al. 2018; Kozman 2020; Hsu et al. 2022). However, there is a lack of studies investigating the potential effect of bonding level on the flexural fatigue life of IRP-repaired legacy pipes, in both pressurised and non-pressurised conditions. As a result, pipeline developers and designers are currently facing a knowledge gap regarding the optimal bonding level that should be implemented between the host pipe and the IRP to enhance the service life of repair systems. However, the existing research on internal pressure alone and static bending has demonstrated that avoiding bonding the repair pipe to the host pipe up to a certain length from the edge of the host pipe discontinuity can effectively reduce potential stress concentrations and enhance the structural capacity of the repair pipes (Kozman 2020; Hsu et al. 2022; Tien et al. 2023).

The experimental investigation conducted by Kozman (2020) examined the longitudinal static bending behaviour of low-density polyethylene CIPP liners, both bonded and unbonded to ductile iron (DI) pipes of 6096 mm (240 in) in length and 304.8 mm (12 in) in diameter with joints positions at the midspan. The liners had a thickness of 6.7 mm (0.264 in) and a flexural modulus of 4.96 GPa (719.4 ksi). According to their findings, the unbonded liner exhibited a joint rotation of 4^{o}, which is four times higher than the joint rotation experienced by the completely bonded liner, before reaching its ultimate failure point. Additionally, the study also concluded that when a CIPP-lined pipe experiences bending, it can result in either cracking of the liner at the joints that are not restrained or minimal retraction into the host pipe if there is no bonding between them.

Hsu et al. (2022) used 3D FEA to replicate the static bending behaviour of CIPP liners installed in concrete pipes with circumferential discontinuities under different bonding conditions: fully, partially bonded or completely unbonded. The concrete pipe had a nominal diameter of 300 mm (11.811 in) and a thickness of 57 mm (2.244 in). The liner, on the other hand, had a thickness of 7.5 mm (0.295 in) and a MOE of 2.88 GPa (418 ksi). The analysis employed a contact pressure of 830 kPa (120.38 psi) for a vehicular tyre, which was applied to an area that was 600 mm (23.622 in) wide. The findings revealed that a significant stress concentration was generated in the liner when it was fully bonded, particularly at the discontinuity edge of the invert due to the constraint of the host pipe (Fig. 12). On the other hand, in the unbonded scenario, while there was a minor stress concentration in the liner at the discontinuity edge of the crown, the stress is significantly diminished at the discontinuity edge of the invert and sidewalls. According to the authors, this is attributed to the fact that in the

unbonded condition, the liner is not constrained by the host pipe, allowing for unrestricted retraction during the bending process. In addition, owing to the decreased stress concentration, the unbonded liner was able to withstand deflection more effectively than the bonded liner (Fig. 13). However, the crown of the liner was compressed between the discontinuity edges to produce a bulge in the unbonded scenario, while the invert was indented due to stress concentration stretching in the bonded scenario (Fig. 13).

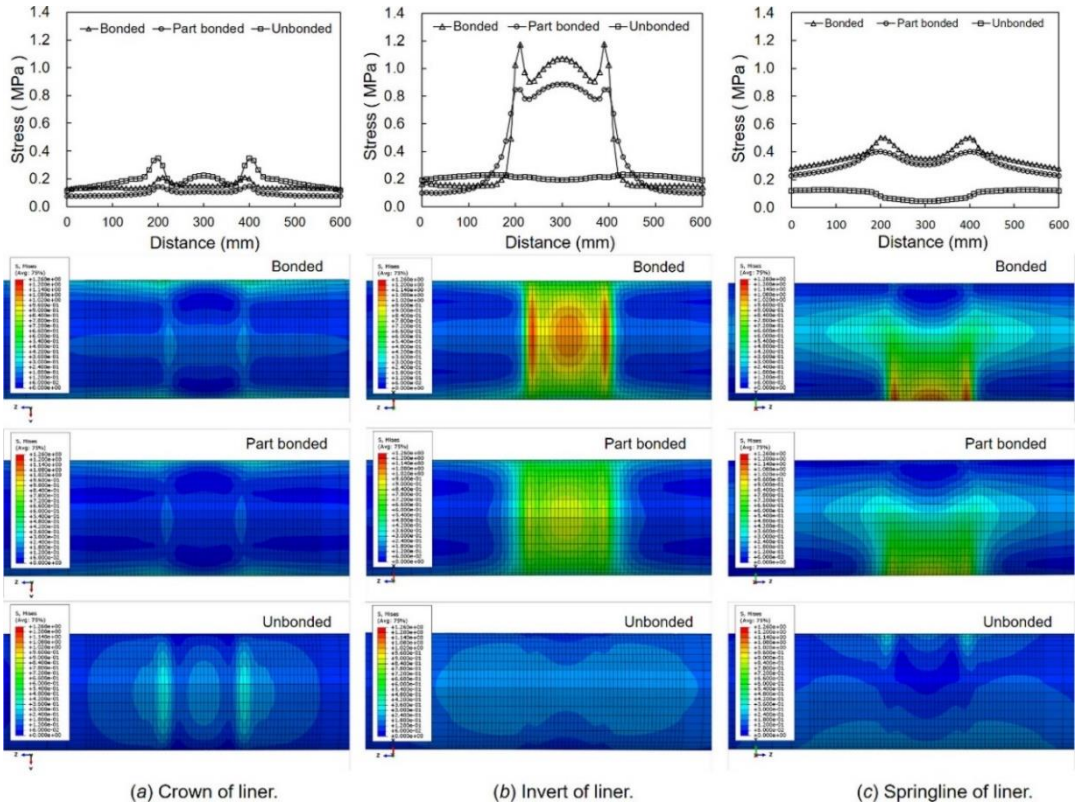

Fig. 12. Stress distribution of the discontinuous concrete pipes repaired with CIPP liner with different bonding levels during bending (Hsu et al. 2022)

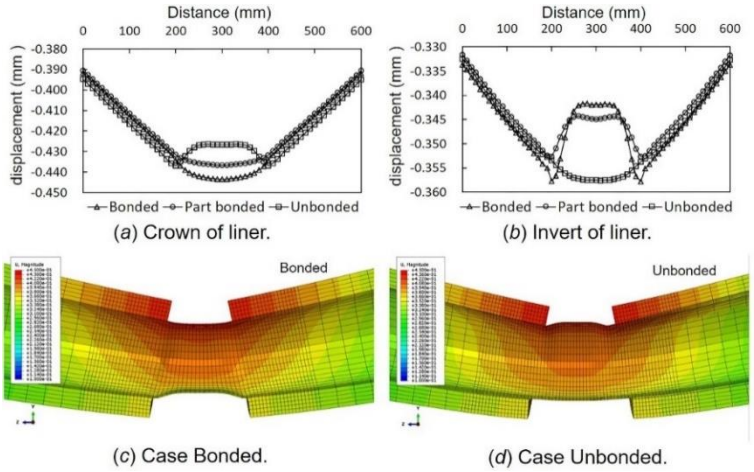

Fig. 13. Vertical displacement distribution of the discontinuous concrete pipes repaired with CIPP liner with different bonding levels during bending (Hsu et al. 2022)

In the study conducted by Tien et al. (2023), the effect of bonding between the IRP and the discontinuous host pipe on the stress concentration caused by an internal pressure of 1379 kPa (200 psi) was also examined. For this, a wide range of IRP materials with MOE between 1 GPa (145.0 ksi) and 200 GPa (29,008 ksi) was utilised. The bonding conditions that were taken into consideration were either fully bonded or unbonded at the pipe ends (Fig. 14). The findings of this study indicated that, in contrast to a fully bonded system, the unbonded system allowed for the sliding of the IRP relative to the host pipe. This sliding resulted in a reduction of the internal pressure-induced stress concentration in IRP at the edges of host pipe discontinuity, with a potential decrease of up to 15%, depending on the materials used (Fig. 15). Additionally, when taking into account the unbonded condition, it has been observed that the impact of the edges of host pipe is limited to materials with a MOE of 15 GPa (2176 ksi) or below (Fig. 15). However, under the fully bonded condition, even with MOE of 25 GPa (3626 ksi), the performance of IRP was affected by the edges of host pipe discontinuities. However, depending on the type of loading, the impact of the bonding level on the behaviour of IRP systems and the ideal bonding condition needed to reduce the potential stress concentration and prolong the service life might differ significantly. For example, a bonding level that enhances the capacity of the IRP system under static bending or internal pressure alone may not be appropriate for flexural fatigue.

Fig. 14. A Schematic of the bonded and unbonded portions considered in the IRP system (Tien et al. 2023)

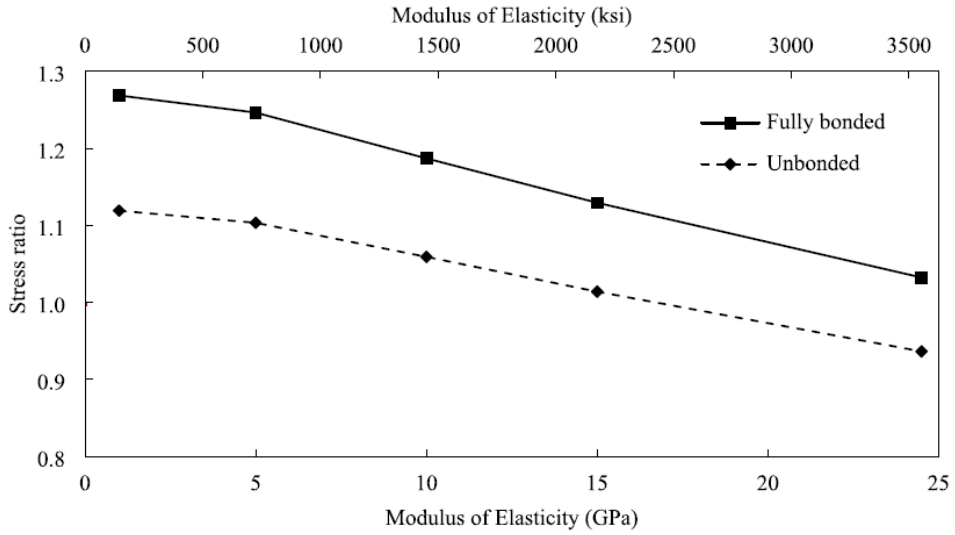

Fig. 15. Ratio between stress at the discontinuity edge and the stress at the midspan in both bonded and unbonded scenarios (Tien et al. 2023)

2.9. Research gap

Static and cyclic surface loads from vehicular traffic are regarded as the most critical loading conditions for host pipes and IRP systems. To ensure the safety and reliability of these repair systems, it is crucial to have an in-depth understanding of their behaviour under critical loading conditions before initiating the design process. Unfortunately, there is a lack of knowledge regarding the behaviour of IRP systems installed in legacy pipes with fully circumferential cracks or discontinuities under static bending and flexural fatigue conditions. Although there are few experimental investigations available, they focused on different repair systems and have practical limitations due to significant time consumption and the high cost involved. As a result, it would be desirable to establish numerical and analytical models or mathematical expressions for evaluating the performance of a wide range of IRP material systems. In addition, most of the available models have been developed for either single materials or host pipe systems with surface defects. In real-life scenarios, legacy pipes requiring

repair systems may also have the worst damages such as circumferential cracks or discontinuities. The existence of these discontinuities in the host pipe might potentially impact the overall performance of the IRP system. Therefore, it is necessary to conduct a thorough investigation to understand their effect. In particular, the following are the main research gaps identified from the literature review.

- There are limited studies available in the literature on the lateral deformation behaviour of IRP systems installed in host pipes with fully circumferential cracks or discontinuities. More importantly, a simplified and reliable analytical model capable of accurately anticipating the flexural behaviour of IRP systems in host pipes with circumferential cracks or discontinuities is not available. Although there are a few analytical models available, none of them have considered the structural contribution of the repair system in their analysis. Additionally, the effect of the important design parameters on the lateral deformation of the IRP in the presence of damaged legacy pipe segments is not well understood.
- The current understanding of the flexural fatigue performance of IRP systems in discontinuous host pipe pipes subjected to repeated traffic loads is extremely limited, and research on the remaining life and residual strength estimation for host pipes that have been rehabilitated using IRP systems is lacking. Existing experimental research on circumferential cracks or joint repair is limited to low-modulus repair systems. Additionally, the influence of various design parameters on the flexural fatigue performance of IRP systems in the presence of damaged host pipes, as well as their relative contributions, have not been properly determined.
- There is a lack of understanding of the fatigue behaviour of IRP systems installed in discontinuous host pipes under the combined influence of repetitive traffic loading and internal pressure. Available studies on the bending fatigue behaviour of repaired pipes focus on low internal pressure and the contribution of the internal pressure to the fatigue performance was not considered. Additionally, the combined influence of the internal pressure and traffic load on fatigue behaviour has not been explored. Most significantly, simplified mathematical expressions or design charts that can predict the remaining flexural fatigue life of IRP systems are unavailable.
- Research into the impact of the bonding level on the bending fatigue behaviour of the pressurised and non-pressurised IRP-repaired damaged host pipes is lacking. There is no study on the influence of design parameters on the flexural fatigue behaviour of IRP-

repaired discontinuous legacy pipes at varying bonding levels. Consequently, the pipeline developers and designers are now confronted with a knowledge gap about the optimum bonding level that should be applied between the IRP and host pipe to extend the service life of various IRP systems.

The research gaps mentioned above are the primary motivations of this study, and they are addressed in Chapters 3 to 6.

CHAPTER 3: PAPER 1 – LATERAL DEFORMATION BEHAVIOUR OF STRUCTURAL INTERNAL REPLACEMENT PIPE REPAIR SYSTEMS

3.1. Introduction

The extensive review of related literature in Chapter 2 revealed that circumferential crack or discontinuity is one of the most critical damages in legacy gas pipes requiring repair systems. A detailed understanding of the effect of the presence of discontinuous legacy pipe segments on the performance of different IRP systems under bending is therefore required. Numerical and analytical simulation are preferred over full-scale laboratory testing due to their advantages in terms of time consumption and cost. However, the existing numerical models do not account for the complete circumferential discontinuities present in legacy pipelines, while the available analytical models do not incorporate the mechanical contribution of the repair pipe.

This chapter addressed the first objective and focused on the evaluation of the lateral deformation behaviour of IRP systems installed in host pipes with discontinuities subjected to surface load from vehicular traffic. The performance evaluation was conducted through FE numerical four-point bending simulations that were validated using full-scale laboratory test results. Various IRP systems were examined, including standalone IRP, IRP installed in continuous host pipe systems and IRP installed in host pipe systems with discontinuities. The systematic evaluation also included the implication of key design parameters, including discontinuity width, repair thickness, repair material and level of traffic load. A simplified and robust analytical model based on fibre model analysis (FMA), was developed to accurately capture the lateral deformation behaviour of IRP systems with discontinuous host pipe systems. A detailed presentation of the analysis and the results can be found in Section 3.2.

It is important to note that the term “crack” used in Section 3.2 refers to a full circumferential discontinuity found in legacy host pipes.

Composite Structures 319 (2023) 117144

Contents lists available at ScienceDirect

Composite Structures

journal homepage: www.elsevier.com/locate/compstruct

Lateral deformation behaviour of structural internal replacement pipe repair systems

Shanika Kiriella [a], Allan Manalo [a], Cam Minh Tri Tien [a], Hamid Ahmadi [a,*], Brad P. Wham [b], Ahmad Salah [a], T. Tafsirojjaman [a], Warna Karunasena [a], Patrick Dixon [b], Thomas D. O'Rourke [c]

[a] Centre for Future Materials (CFM), University of Southern Queensland (UniSQ), Toowoomba, QLD 4350, Australia
[b] Center for Infrastructure, Energy, and Space Testing, University of Colorado Boulder, Boulder, CO 80309, US
[c] School of Civil and Environmental Engineering, Cornell University, Ithaca, NY 14853, US

ARTICLE INFO

Keywords:
Structural internal replacement pipe (SIRP)
Gas pipelines
Composites
Traffic loading
Finite element analysis (FEA)
Fibre model analysis (FMA)

ABSTRACT

Structural internal replacement pipe (SIRP) systems are emerging composite technologies for the repair of circumferentially cracked host pipes or pipes with joints subject to lateral deformation caused by the surface loads from vehicular traffic. However, laboratory experiments to investigate the suitability of different SIRP systems in repairing full-scale pipes are a very costly and time-consuming process. This paper investigated numerically the behaviour of SIRP repair systems under lateral deformation using the three-dimensional finite element analysis (FEA). The FEA model was validated from the results of the full-scale experimental test. The effect of the crack width of the host pipe, thickness, and material properties of the SIRP, on the bending behaviour of the pipe repair system, was evaluated. The results of the analyses show that the effect of the thickness and elastic modulus of the SIRP on the lateral deformation behaviour is dependent on the width of the circumferential crack in the host pipe. A simplified analytical model based on Fibre model analysis (FMA) and incorporating an average stress factor for host pipes with a narrow crack width was developed to reliably describe the lateral deformation behaviour of the SIRP systems.

1. Introduction

A network of 3.2 million kilometres of utility pipes provides critical natural gas service to approximately 80 million people in the United States [1]. However, corrosion of these pipelines which are primarily comprised of legacy cast iron and bare steel is a serious concern for the industry [2–8]. Due to the highly combustible material contained inside, failure in oil and gas pipelines distributed in urban areas can cause catastrophic damage to people, properties, and infrastructure [9–12]. As a result, these critical distribution systems which are nearing or have already exceeded their expected service life require cost-effective repair techniques to restore their original operating capacity, maintain structural integrity, and extend their safe operational life. Rehabilitation of existing pipeline systems is an ideal solution over replacement due to the limited financial resources of asset owners and government institutions [13–15], as well as the complexity of underground structures, buildings and road congestion [16]. This situation has resulted in the investigation and development of various pipe repair technologies [1] suitable for either open trench or trenchless methods [17,18]. In many countries, such as the United States and Canada, the trenchless approach has become the preferred pipe repair method since it reduces environmental damage and excavation operations, making it more reliable and cost-effective [12,19–21]. In recent years, this repair technology has made significant advancements, utilising structural internal replacement pipe (SIRP) systems made from various materials such as thermoplastics, fibre composites [6], polymers and metals [1]. A few recent studies highlighted that while many trenchless repair and installation technologies have grown recently matured, their applicability to oil and gas pipelines is still quite restricted due to their limited technological flexibility and high installation costs [1,22]. Moreover, design procedures and standards for these types of technologies are also unavailable [22]. Consequently, it is essential to assess the suitability of new and emerging SIRP systems to effectively design and utilise them as internal repair systems for pipeline rehabilitation.

* Corresponding author.
E-mail addresses: shanika.kiriella@usq.edu.au (S. Kiriella), allan.manalo@usq.edu.au (A. Manalo), camminhtri.tien@usq.edu.au (C.M.T. Tien), hamid.ahmadi@usq.edu.au (H. Ahmadi), brad.wham@colorado.edu (B.P. Wham), ahmad.salah@usq.edu.au (A. Salah), tafsirojjaman@adelaide.edu.au (T. Tafsirojjaman), karu.karunasena@usq.edu.au (W. Karunasena), padi9036@colorado.edu (P. Dixon), tdo1@cornell.edu (T.D. O'Rourke).

https://doi.org/10.1016/j.compstruct.2023.117144
Received 23 January 2023; Received in revised form 19 April 2023; Accepted 8 May 2023
Available online 12 May 2023

The loading conditions have a substantial impact on the failure modes of the host pipes and the SIRP repair systems. Some of the most common failure mechanisms for the SIRP in a host pipe system include lateral deformation [1,23–28], fatigue failure due to repetitive traffic loading [1,23,29], localized fracture and leakage due to internal pressure [1,30,31] and axial deformation due to thermal stresses [1,23,32,33]. Among these, bending deformation due to surface load is considered to be the worst condition for the host pipes and SIRP system [1,23]. The effects of surface loads experienced by the pipelines are normally caused by vehicular traffic [34]. When wheel loads are located directly above the pipe and moving parallel to the longitudinal axis of a pipeline (Fig. 1), the SIRP system undergoes maximum deformation (relative displacement and rotation) at the weakest discontinuity along the underground pipeline [23,35] such as a complete circumferential fracture/round crack and joints [35]. According to Makar et al [36], circumferential cracking is the most typical failure mode for host pipe with a diameter smaller than 380 mm. These cracks on host pipes might occur because of excessive stress generated by ground deformation during trench construction. When such a crack exists on the host pipe, the SIRP may be vulnerable to stresses, relative displacements and rotations caused by the traffic loading [23,35].

With the development of novel pipeline repair systems, the use of fibre composites as a repair material is continuously growing in the oil and gas industry [6,37–42]. This is due to the inherent advantages of fibre composite repair including lightweight, high tensile strength, flexibility in design, versatility in application, and corrosion resistance [38,39,43–45]. However, available studies on the lateral deformation behaviour of circumferentially cracked pipes with an internal composite repair system are limited [23,35,46–48]. Moreover, no comparable standards or regulations for internal composite pipe repair systems currently exist [1]. Because of this, Jeon et al [23] investigated the performance of circumferentially cracked cast iron (CI) pipes with 4 in (101.6 mm), 6 in (152.4 mm) and 8 in (203.2 mm) diameter and repaired them with a Cured-in-Place Pipe (CIPP) liner subject to traffic loading of 133 kN (30 kips). Additionally, an analytical model was developed to evaluate the maximum relative displacements, rotations and stresses induced on the pipeline at the circumferential crack under the traffic loading. However, in their models, it was conservatively assumed that the liner provides zero stiffness because of its significantly lower elastic modulus (E) compared to the CI host pipe. Stewart et al. [35] studied the lateral deformation behaviour of 6 in (152.4 mm) and 12 in (304.8 mm) diameter CI host pipe repaired with CIPP liners having openings ranging from 0.25 in (6.35) to 0.43 in (10. 922 mm) under a lateral loading of 178 kN (40 kips). This study employed field samples from previously lined CI pipes and found that the crack opening affected the overall behaviour of the repaired pipes. Interestingly, the structural contribution of the repair system was not taken into account in their analysis.

Shou and Chen [47] used three-dimensional (3D) finite element analysis (FEA) to investigate the bending response of buried steel pipe with corroded pipe barrels repaired with CIPP liner (using E of 13 GPa and wall thicknesses of 5 mm and 10 mm) under lateral loading. The study revealed that a repair system can enhance the load-carrying capacity of a damaged pipeline. Allouche et al [46] conducted laboratory experimental three-point bending tests to evaluate the bending behaviour of cast iron pipe that was cut into two halves and linked together with a fibre-reinforced polymer (FRP) CIPP subject to both pressurised and non-pressurised circumstances at the location of the pipe joint. They noted that the FRP liner was able to preserve the structural integrity of the system even after the host pipe failed. There was also no visible evidence of leaking observed. In the absence of internal pressure during the bending test, the liner buckled at the invert. In order to establish a range of material properties and thickness of SIRP repair systems appropriate for natural gas pipelines to avoid such types of failure modes, Tafsirojjaman et al [1] studied the lateral deformation behaviour of these technologies under a design load of 178 kN (40 kips) using linear elastic FEA. In their investigation, a wide range of SIRP materials with E ranging from 1 GPa (145 ksi) to 200 GPa (29,008 ksi) and thicknesses between 3.175 mm (0.125 in.) and 25.4 mm (1 in.) were analysed. This study demonstrated that the lateral deformation behaviour is greatly influenced by the thickness and E of the SIRP. In addition, a system must also have an E and thickness of at least 5 GPa and 12.7 mm (12 in.), respectively, to safely bear a lateral load of 178 kN (40 kips), when the strain is limited to 0.02. A few studies that conducted bending analysis on damaged pipes revealed that defect length influences the overall performance of the pipe. Chegeni et al [36] studied the impact of the length of corrosion defects in the longitudinal and circumferential directions of steel pipe on the ultimate load-carrying capacity using FEA. The results indicated that increasing the length of the defect in longitudinal and circumferential directions reduces the ultimate load-carrying capacity of the pipe by 19% and 40%, respectively. This indicated that an increase in defect length along the circumferential direction of the pipe had a greater negative influence on the bending performance of the pipe than an increase in defect length along the longitudinal direction. Shuai et al [37] investigated numerically the effect of corrosion defect length (along the axial direction) on the buckling of the steel pipe under a four-point bending test. The investigators found that the buckling moment of the pipe is a function of the defect length, where a short defect length will fail in single wrinkle buckling, while a long defect length will exhibit two buckling waves. Similarly, Zheng et al [38] highlighted that the maximum axial strain of the pipeline increases with the increase of corrosion defect width. However, it is important to note that most of these studies have analysed the behaviour of the SIRP system either using single material or a continuous pipe system. In actual situations, however, pipes that need a repair system have existing damage like circumferential cracks or discontinuity, e.g., due to the presence of joints. These discontinuities in the host pipe may affect the performance of the SIRP repair system and require detailed investigation.

The thorough evaluation of the effect of different design parameters of SIRP repair systems under flexural loading from laboratory experiments is a very costly and time-consuming process. In contrast, numerical and analytical models need less time, as well as lower costs, however, require validation from physical tests [49]. Once calibrated

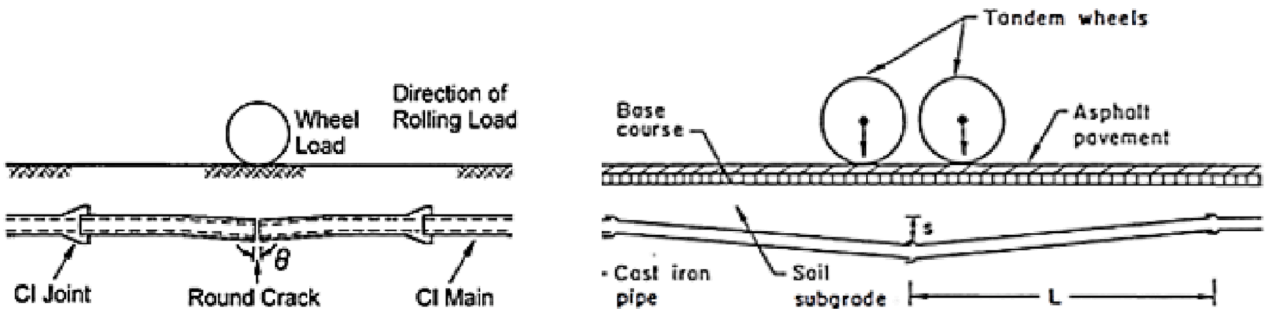

Fig. 1. Representation of the deformation of the underground pipeline subjected to traffic loading [35].

and validated from experimental results, numerical and analytical models can be very powerful tools for simulating experimental behaviour and extrapolating them to other conditions. Additionally, numerical and analytical modelling together with experiments, allow a detailed understanding of the actual behaviour of structures which can be used for structural optimization. Therefore, the primary goal of this study is to numerically investigate the performance of SIRP systems for the repair of circumferentially cracked host pipes subject to surface loads and to investigate the effects of important design parameters such as the crack width of the host pipe, thickness and elastic modulus of SIRP on their lateral deformation behaviour. The reliability of the numerical model to evaluate the effect of traffic loads on the SIRP system is validated from the physical four-point bending tests. The findings of this study will provide the research community, product developers and pipeline engineers with a better understanding of the lateral deformation behaviour of circumferentially cracked gas pipelines repaired with SIRP systems.

2. Finite element analysis (FEA)

2.1. Finite element modelling

A FEA numerical model is created by using ANSYS/Mechanical software [50] to evaluate the behaviour of various SIRP systems including the repair system alone, SIRP in a continuous host pipe (without circumferential crack), and the host pipe with different circumferential crack widths (i.e the host pipe completely fractured into two halves) repaired by a SIRP system under lateral loading. This was accomplished by modelling the experimental four-point bending test at the University of Colorado Boulder with setup dimensions of 762-1016-762 mm (30-40-30 in.), as shown in Fig. 2. This loading configuration represents the wheel loads located directly and moving parallel to the longitudinal axis of a pipeline as reported in [19,31]. A bilinear stress–strain behaviour is used to model the host pipe (Fig. 3a) whereas the SIRP is modelled as a nonlinear material (Fig. 3b). The material properties of ASTM A36 steel host pipe was obtained from [51], whereas that of SIRP was defined by performing tensile tests of the ALTRA10 material in the laboratory in accordance with ASTM D638-10 [52]. The outer diameter and the thickness of the host pipe are 323.85 mm (12.75 in.) and 6.35 mm (0.25 in.) respectively. Based on the inside diameter of the host pipe, the outside diameter of the SIRP is set to 311.15 mm (12.25 in.) and its thickness is 4.1148 mm (0.162 in.). The circumferential crack widths of the host pipe under consideration range from 12.7 to 152.4 mm (0.5 in.–6 in.).

In the parametric study, the effect of different geometrical and material properties such as the repair thickness, crack width of the host pipe, and E of SIRP materials on the lateral deformation of circumferentially cracked host pipes is investigated. Accordingly, SIRP thickness is changed from 3.175 mm (0.125 in.) to 12.7 mm (0.5 in), and the E is varied from 1 GPa (145 ksi) to 200 GPa (29,008 ksi). The SIRP materials that are considered in the parametric study represent polymers, thermoplastics, glass fibre-reinforced polymer (GFRP) composites, and metallic (cast iron and steel) materials. These ranges of thickness and E of the SIRP repair systems are selected based on a previous study by Tafsirojjaman et al. [1]. It was also evaluated whether these systems could provide the structural capacity to withstand a lateral load of 178 kN (40 kips) as suggested by previous studies [1,35,53].

A typical repair scenario in which a steel host pipe having a 50.8 mm (2 in.) circumferential crack repaired by a SIRP material with nonlinear stress–strain behaviour (Fig. 3(b)) and has an elastic modulus and poisons ratio of 3.739 GPa (542.3 ksi) and 0.23 respectively is shown in Fig. 4. For simplification, a quarter model is utilized by applying quarter symmetric boundary conditions in longitudinal and transverse directions. The system is modelled using the standard SOLID186, higher order 3D 20-node solid elements that allow quadratic displacement behaviours and support plasticity, hyper-elasticity, large strain and large deflection capabilities, stress stiffening and creep. The ends of the system are capped by steel blind flanges with properties similar to those of the host pipe. To represent the experimental test setup, pinned supports are used at both ends while the loading head is connected with the pipe clamps via the pin-lug system as shown in Fig. 4. The SIRP repair system is fully bonded to the host pipe. A frictionless connection type is used for the contacts between the host pipe and the supports. Contact pairs include clamp-pipe and lug-pin. Due to the quarter symmetry of the model, only one-fourth of the force is applied to the loading head of the setup vertically in the downward direction. In this study, nonlinear static structural FEA with a full Newton-Raphson solution approach is used to simulate the nonlinearity of both SIRP and host pipe materials. This analysis also allows large deformation and plasticity. The FEA model is validated by comparing numerical results to full-scale experimental data.

2.2. Mesh convergence study and mesh refinement

A mesh convergence study is carried out to determine the optimum mesh sizing required for generating reliable and accurate FEA results. This is accomplished by comparing the maximum midspan deflection of the system under lateral loading obtained by FEA with the theoretical results. A single pipe, representing the SIRP, is modelled for this purpose with an E of 200 GPa (29,008 ksi) and subjected to a load of 178 kN (40 kips). The pipe used for mesh convergence analysis has the same

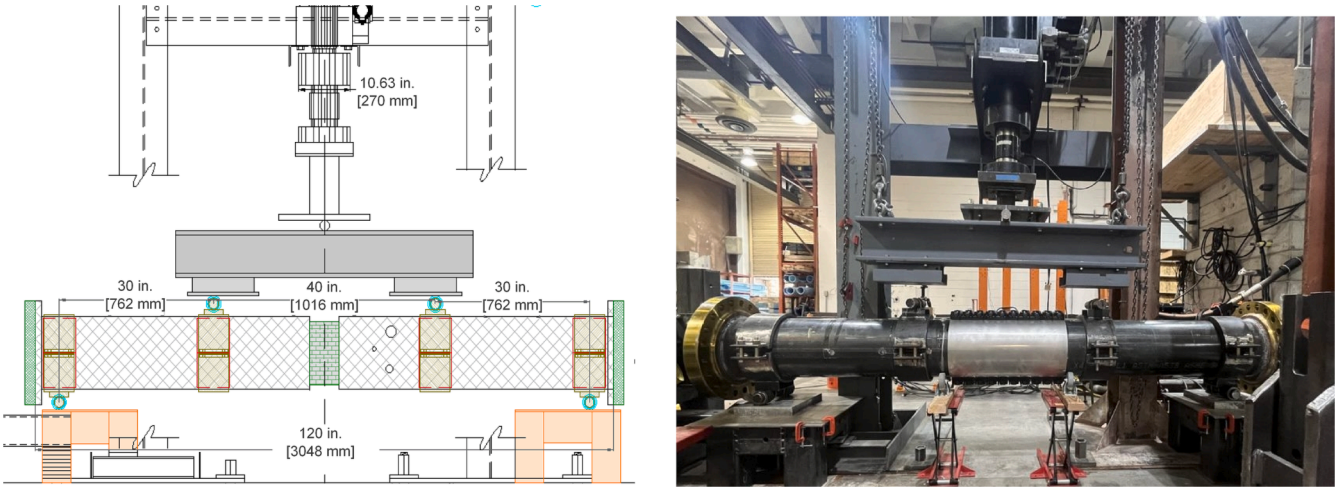

Fig. 2. Schematic view (left) and actual set-up (right) for lateral deflection test of SIRP systems (CUB).

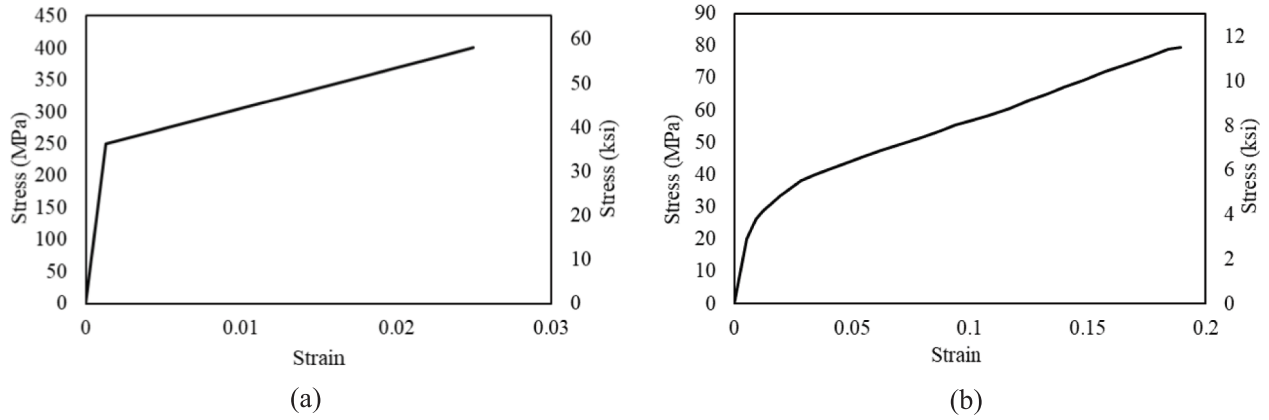

Fig. 3. Stress–strain behaviour: (a) Steel host pipe [42], (b) ALTRA10 SIRP.

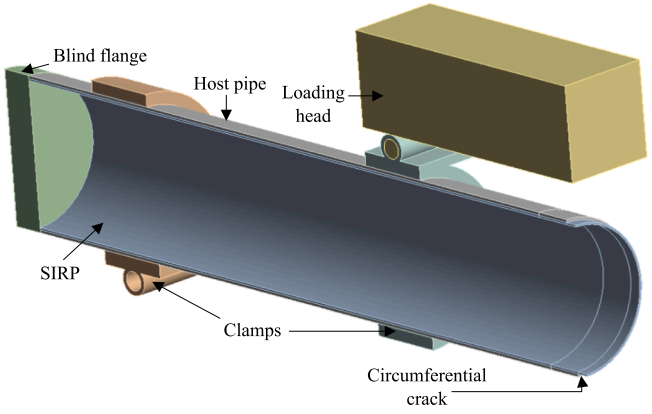

Fig. 4. Geometry, boundary conditions and loading of FEA quarter model of SIRP in host pipe with 50.8 mm (2 in.) crack width.

dimensions as the SIRP system described in Section 2.1. In the thickness direction, a mesh size of three elements is utilised, while the surface element sizing is varied from coarse (30 × 30 mm) to very fine (2 × 2 mm). The FEA outcomes are plotted against the total number of elements and compared to the theoretical result of 3.02 mm. According to this mesh convergence study (Fig. 5), as the mesh size decreases, the solutions tend to converge. The solution starts to converge with an accuracy of at least 5.67% when the mesh size is 5 mm or smaller.

A mesh refinement is conducted in order to increase the accuracy of FEA solutions. Refinement is performed by reducing the element size of the mesh in the region of high stresses. Especially a finer mesh is used around the crack edge and midspan. The refined mesh was designed with a surface element size of 2 × 2 mm along the crack and along a distance of 76.2 mm from the crack edge towards the loading point. An optimum surface element size of 5 mm is utilised for the host pipe and SIRP outside the mesh refinement region. Three elements are used in the thickness direction of both the host pipe and the SIRP over their entire lengths.

2.3. Validation of FEA model

The FEA model of 4.1148 mm thick SIRP in steel host pipe with 12.7 mm (0.5 in.) crack width is validated in Fig. 6 by comparing it to full-scale laboratory experimental results from the University of Colorado Boulder. The comparison demonstrates that the load–deflection behaviour predicted by the FEA is in good agreement with the experimental outcomes. Under a loading of 14.86 kN (3.34 kips), the maximum discrepancies between the FEA and laboratory experimental deflections at the crack edge (43.35 mm or 1.71 in from midspan) and loading point

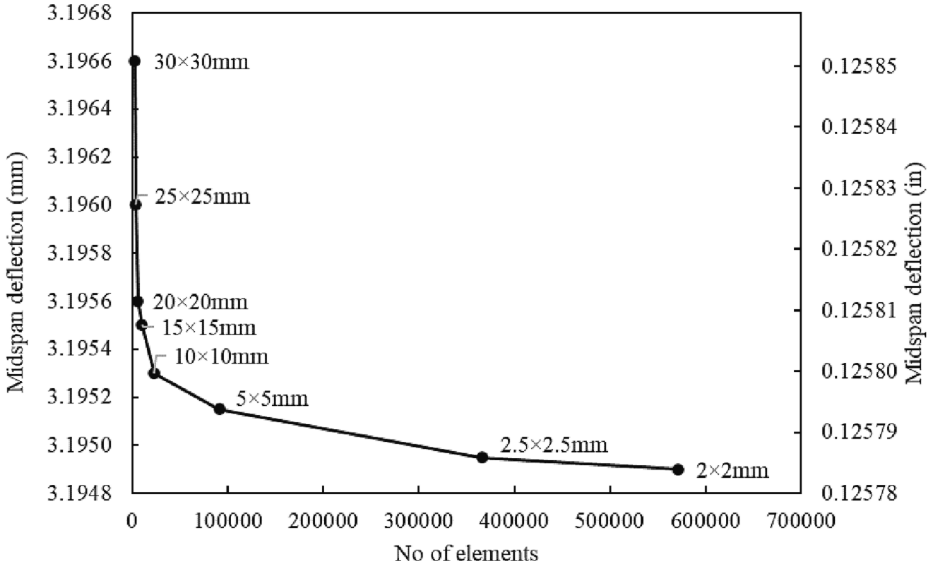

Fig. 5. Mesh convergence study.

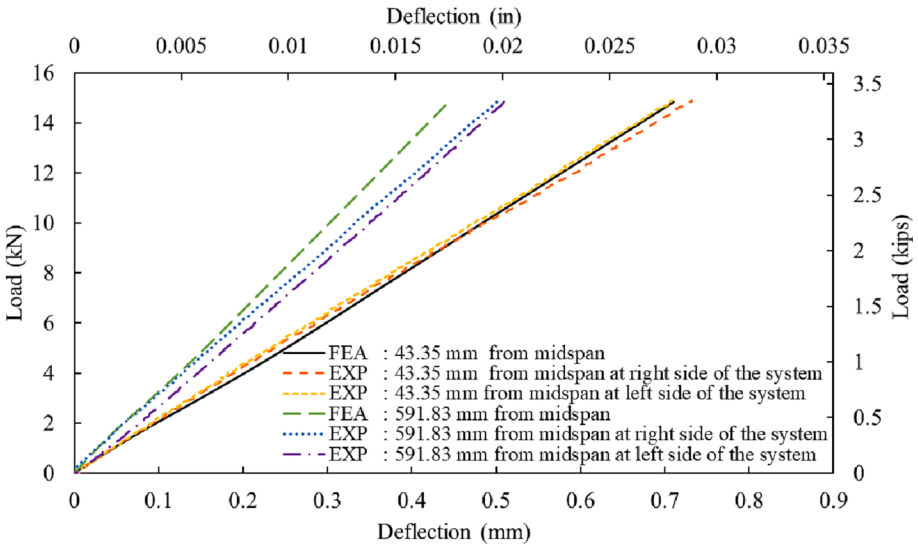

Fig. 6. Comparison of FEA and experimental load–displacement behaviours of SIRP in host pipe with 12.7 mm opening.

(591.83 mm or 23.3 in from midspan) are roughly 2.7% and 12.9%, respectively, indicating high accuracy.

3. Results and discussions

3.1. Behaviour of SIRP repair systems

The nonlinear load-midspan deflection behaviour of a SIRP alone is shown in Fig. 7a. The results showed that the deflection increases linearly with the load up to 18 kN (4.05 kips), after which there is a slight nonlinearity because of the decrease in stiffness until failure at a load of 24.5 kN (5.51 kips). At this level of loading, the compressive strain of SIRP is around 0.8%. This reduction in stiffness is caused by the nonlinearity of SIRP material at higher strain. Fig. 7b illustrates the deflection over the length of SIRP from the left support to the midspan. Due to the quarter symmetry of the FEA model, the deflection along the length of SIRP is only provided for the left-hand side of the model. Under the ultimate load, the deflection along the length of SIRP exhibits a linear relationship up to the loading point followed by a nonlinearly decreasing response up to the midspan. The FEA model shows that compressive buckling of the crown between the loading points governs the failure mechanism of SIRP alone under four-point bending (Fig. 8). This phenomenon is also consistent with the findings in the recent research reported by Tafsirojjaman et al [1] which concluded that SIRP systems with a thickness of 9.5 mm or less are susceptible to compressive buckling.

3.2. Behaviour of SIRP repair systems in the continuous steel host pipe

The load-midspan deflection relation of a continuous steel host pipe with the SIRP system is shown in Fig. 9a. The deflection increases linearly with load up to 400 kN (89.9 kips), beyond which there is a significant drop in stiffness due to the yielding of the steel host pipe. At this level of load, it is noted that the SIRP is in the elastic region with a compressive strain of only 0.19%, which is almost 76% lower than that of the SIRP alone. Therefore, it is evident that the host pipe can stabilize the strain that develops in the SIRP at a higher load and prevents buckling failure. The SIRP in a continuous host pipe system fails at a load of 642.3 kN (144.4 kips) owing to buckling of the crown of the combined pipe section at midspan. This investigation reveals that the overall load–deflection behaviour of SIRP in an undamaged host pipe will be highly influenced by the host pipe. Fig. 9a compares the load against the midspan deflection behaviour of the continuous steel host pipe with SIRP to that of a continuous host pipe alone. It can be seen from the figure that the load at the yielding of the continuous host pipe is almost identical to that of the continuous steel host pipe with the SIRP system. This indicates that the presence of the SIRP does not increase the load at the yielding of the host pipe. This is because, up to the yielding point, the

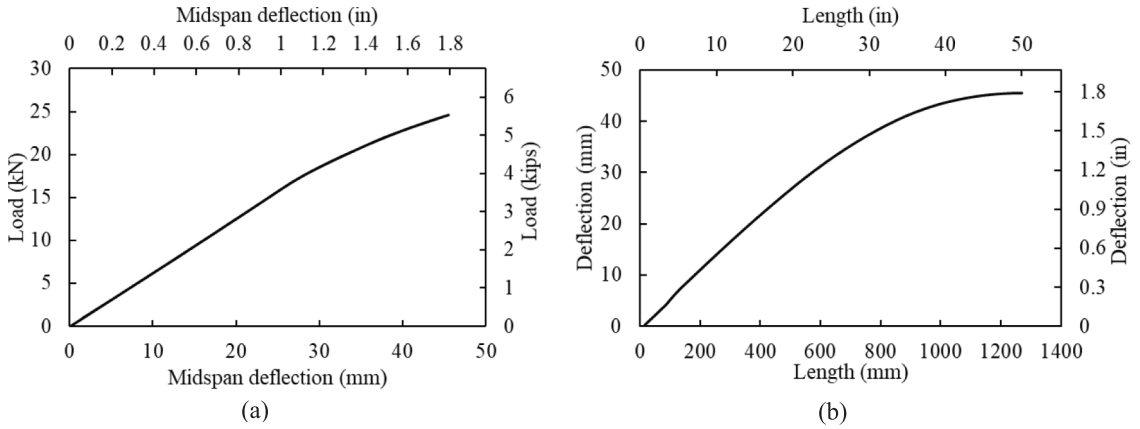

Fig. 7. (a) Load vs. maximum deflection behaviour, (b) deflection (at ultimate load) along the half-length (from left support to midspan) of SIRP alone.

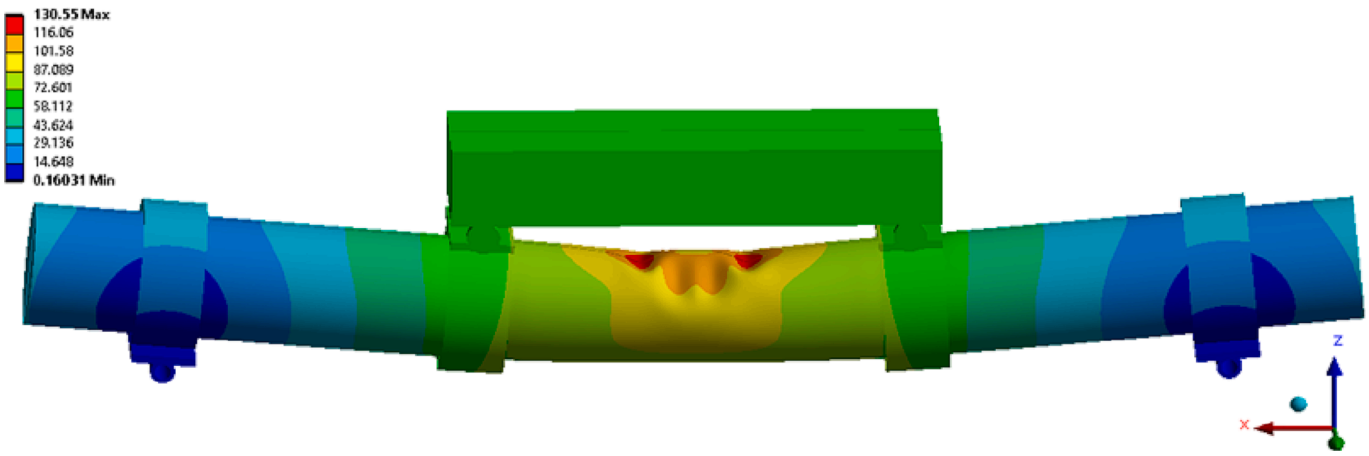

Fig. 8. Compressive buckling of the SIRP alone under a four-point bending test.

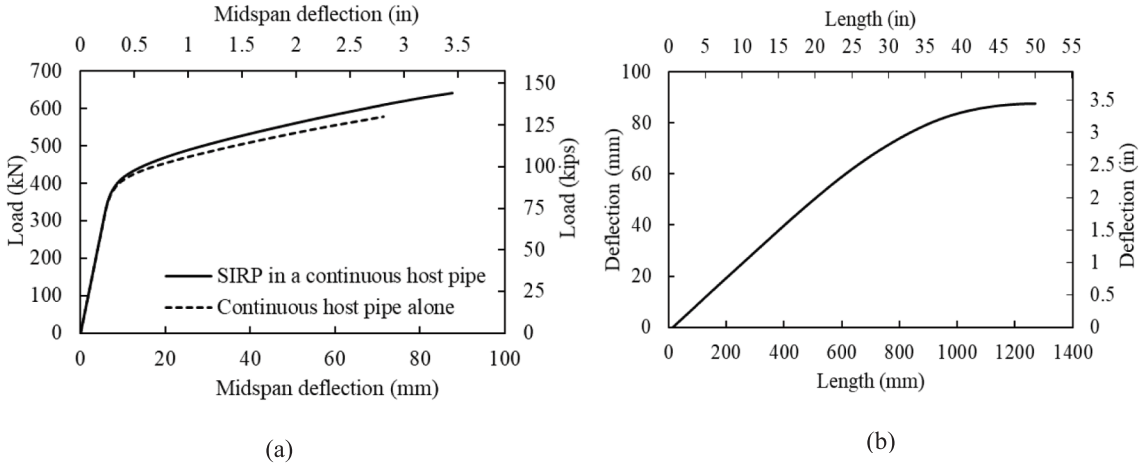

Fig. 9. (a) Load vs. maximum deflection behaviours of SIRP in continuous host pipe and continuous host pipe alone (b) deflection (at ultimate load) along the half-length of SIRP in the continuous host pipe.

steel host pipe has a significantly higher modulus of elasticity and stiffness than the SIRP. Thus, with lower modulus and stiffness, the contribution of SIRP to the overall strength of the continuous host pipe system before yielding can be neglected. However, the ultimate load capacity and the maximum midspan deflection of this continuous host pipe alone are respectively around 578.1 kN (130 kips) and 71.35 mm (2.81 in.), which is less than that of the continuous host pipe with SIRP. At the ultimate load of the host pipe alone, the deflection of the host pipe with the SIRP repair system is only 57.19 mm (2.25 in.), which is approximately 20% less than that of the host pipe alone. Furthermore, the failure mechanism of the continuous host pipe alone is local inward buckling of the pipe crown between loading points, which is quite similar to that of SIRP with the continuous host pipe. This indicates that the failure mode of the SIRP-repaired continuous host pipe is controlled by the host pipe. Despite the fact that the host pipe has a greater influence on the load–deflection behaviours than the SIRP, neglecting the mechanical contribution of the thinner SIRP in deflection calculations after the yielding of steel host pipe underestimates the ultimate load-carrying capacity of the system by 11% and its maximum deflection by 23%. Therefore, the frameworks developed in previous studies [23,35] assessing deflection by neglecting the contribution of the repair materials are not applicable to SIRP systems. The deflection along a half-length of the above-mentioned SIRP in a continuous host pipe at its ultimate load, on the other hand, is depicted in Fig. 9b. The figure indicates that at ultimate load, the deflection along the length of the SIRP in the continuous host pipe increases linearly up to the load point, after which it increases nonlinearly and gradually until the midspan.

3.3. Behaviour of SIRP repair systems in host pipe with a circumferential crack

3.3.1. Effect of crack width in the host pipe

The load versus midspan deflection behaviour of a SIRP repair system in a steel host pipe with different crack widths (l) under lateral loading is displayed in Fig. 10. The results show a linear load–deflection relationship for crack widths of 12.7 mm (0.5 in.), 25.4 mm (1 in.), 50.8 mm (2 in.), 101.6 mm (4 in.) and 152.4 mm (6 in.), respectively, up to a loading of 23.0 kN (5.17 kips), 20.0 kN (4.5 kips), 16.9 kN (3.8), 16.6 kN (3.73 kips) and 16.1 kN (3.62 kips), followed by a slight nonlinear decrease in stiffness until the systems finally fail at a loading of 83.7 kN (18.82 kips), 61.7 kN (13.87 kips), 35.6 kN (8.0 kips), 29.4 kN (6.61 kips) and 27.9 kN (6.27 kips), respectively. The ultimate failure of these circumferentially cracked host pipes repaired with SIRP systems under bending is governed by outward buckling at the crown of the SIRP (compressive zone) between the crack edges. Fig. 11a, b and c display the compressive buckling of SIRP in host pipe with 50.8 mm (2 in.), 101.6 mm (4 in.) and 152.4 mm (6 in.) crack widths, respectively. A similar failure behaviour was reported in a previous study [46], wherein it was concluded that the absence of internal pressure can cause the liner to buckle during the laboratory experiment of the three-point bending

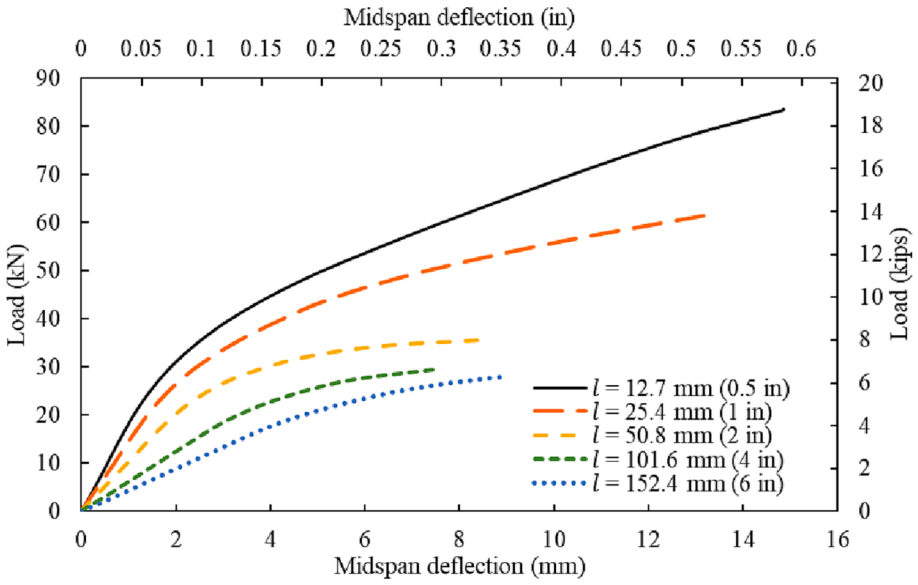

Fig. 10. Load- midspan deflection behaviour of SIRP in host pipe with different crack widths.

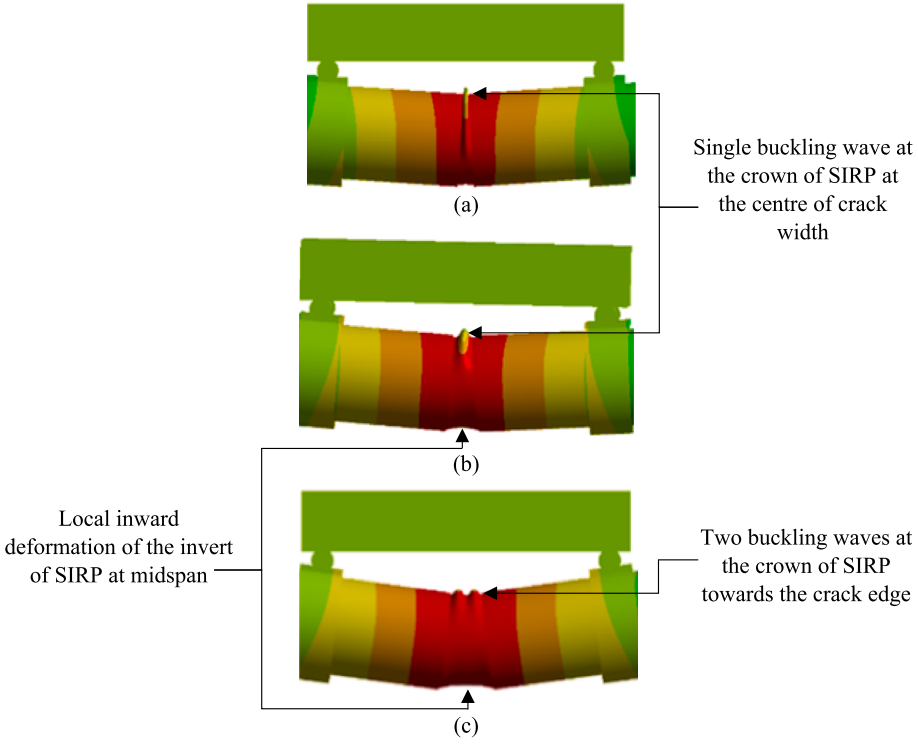

Fig. 11. Failure modes of SIRP in a host pipe with wider crack widths, i.e. (a) 50.8, (b) 101.6 mm and (c) 152.4 mm.

test. Fig. 11 shows that only one buckling wave is visible in the middle of the crack width when the width of the opening is 101.4 mm (4 in.) or less, while there are two buckling waves towards the crack edge when the crack width is greater than 101.4 mm (4 in.). These failure behaviours are consistent with the observations of Shuai et al [37]. This failure behaviour indicates that, unlike a continuous host pipe, the failure mechanism of the SIRP in a host pipe with a circumferential crack will be controlled by the SIRP. It is interesting to note that the analysis of the SIRP alone showed similar failure behaviour. However, the buckling load in which the SIRP system failed is higher for narrow crack width, but it converges to the level of the buckling load of SIRP alone with a significantly lower midspan deflection due to the relatively high stiffness of the host pipe.

The influence of crack widths on the ultimate load-carrying capacity of the above-mentioned circumferentially cracked host pipe repaired with SIRP is illustrated in Fig. 12a. It is clear from the results that the lateral load-carrying capacity of SIRP in host pipe systems with very narrow crack widths is considerably higher than those with wide crack widths. When the crack width increases from 12.7 mm (0.5 in.) to about 50.8 mm (2 in.), the ultimate load capacity of the system exhibits a dramatic nonlinear reduction, after which it shows a slight linear decline until the crack widens to 152.4 mm (6 in.). This behaviour may be

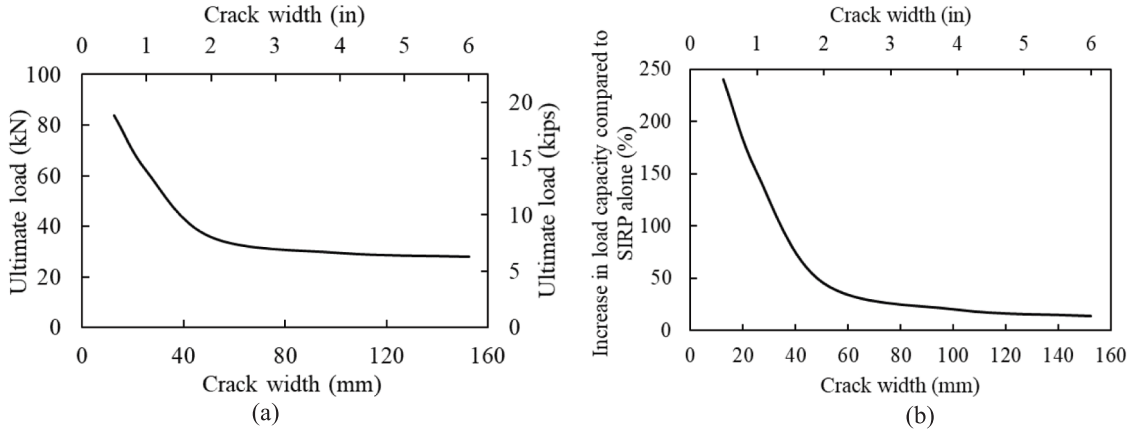

Fig. 12. (a) Effect of crack width of host pipe on the ultimate load capacity of ALTRA10 SIRP system (b) Percentage increase in load capacity compared to SIRP alone.

caused by the considerable reduction in the contribution of the host pipe to the overall strength of the SIRP system when the crack widens from 12.7 mm (0.5 in.) to 50.8 mm (2 in.). The overall decrease in ultimate lateral load capacity is approximately 66.7%. Furthermore, none of these SIRP repair systems with 4.1148 mm thickness can provide structural capacity to circumferentially cracked host pipes to safely carry a design load of 178 kN (40 kips). The increase in lateral load capacity relative to SIRP alone for these repair systems with varying crack widths is shown in Fig. 12b as a percentage. It is seen from the graph that the load capacity of the SIRP in a host pipe with a 12.7 mm (0.5 in.) crack width is about 240% higher than that of SIRP alone. On the other hand, the load capacity of the SIRP system with 152.4 mm (6 in.) crack width is only 13.4% greater than that of SIRP alone. As a result, unlike SIRP systems with very narrow crack widths, the ultimate load-carrying capacity of those with wider crack widths is primarily controlled by the SIRP. Additionally, when the crack width is 152.4 mm (6 in.) or longer, the ultimate loading capacity of the SIRP with the host pipe will approach that of the SIRP alone.

The effect of crack width on midspan deformations of the SIRP system (at invert) under loading of nearly 27.9 kN (ultimate loading of the system with 6 in crack width) is shown in Fig. 13. The results reveal that under the same loading level, the SIRP repair system exhibits a slight nonlinear increase in deflection from 12.7 mm (0.5 in.) to 50.8 mm (2 in.) crack widths followed by an almost a linear increment until 152.4 mm (6 in.) crack width. Overall, when the crack width widens from 12.7 mm (0.5 in.) to 152.4 mm (6 in.), the midspan deflection increases by 415.5%. This is because, unlike the SIRP systems with wider crack widths, the overall load–deflection behaviour of those with narrow crack widths is mostly governed by the host pipe, which has almost 53.5 times higher stiffness than SIRP alone and hence results in significantly lower deformations at the same loading. Fig. 14 displays the deflection behaviour of a host pipe with varying crack widths, obtained from the left support to the midspan under loading of 27.9 kN (6.27 kips). Accordingly, the deflection of SIRP increases linearly from support to crack edge for all crack widths. However, from crack edge to midspan, deflection of the systems with 12.7 mm (0.5 in.) and 25.4 mm (1 in.) crack widths rises nonlinearly, whereas those of the systems with 50.8 mm (2 in.), 101.6 mm (4 in.), and 152.4 (6 in.) crack widths decline nonlinearly. This behaviour of SIRP with narrow crack width is related to the high stresses that develop over the crack width as a result of stress concentration at the crack edge. The nonlinear reduction in deflection of SIRP with wider crack widths from crack edge to midspan, on the other hand, is caused by a slight local inward deformation of the SIRP at the midspan at invert (Fig. 11b and c).

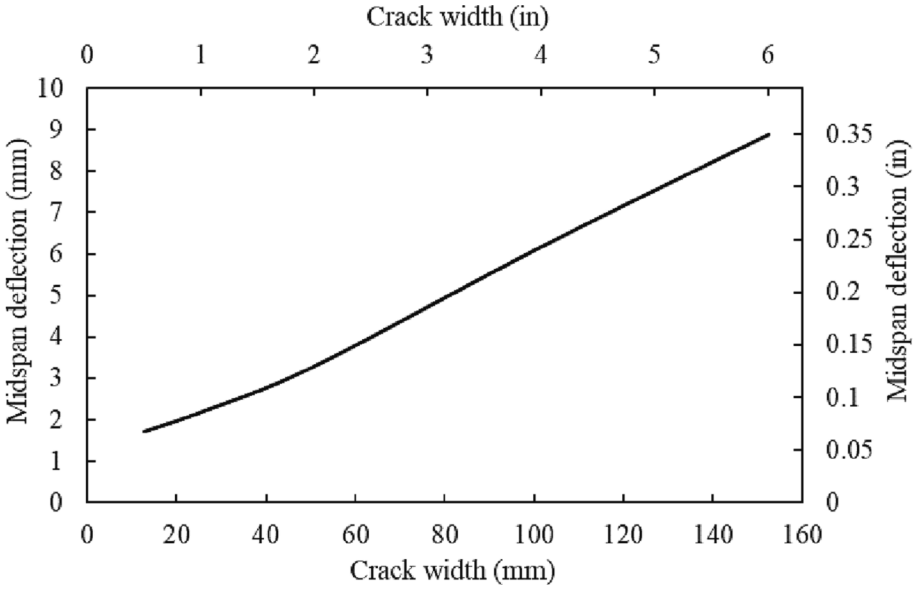

Fig. 13. Effect of crack width of host pipe on midspan deflection of SIRP system.

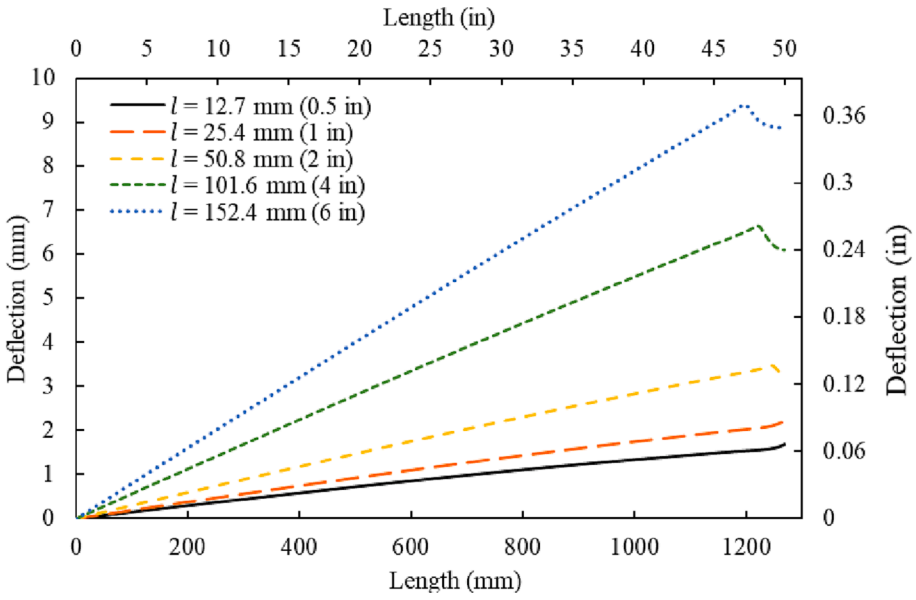

Fig. 14. Deflection along the half-length of SIRP in host pipe with different crack widths.

3.3.2. Effect of the thickness of the SIRP system

Fig. 15 demonstrates how the thickness of the SIRP affects the ultimate lateral load-carrying capacity of the repaired steel pipe with a narrow (12.7 mm) and a wide (152.4 mm) circumferential crack. The results show that when SIRP thickness is increased from 3.175 mm (0.125 in.) to 12.7 mm (0.5 in.), the ultimate load capacity of the system with the wide crack width increases nonlinearly with an overall increment of 773.9% while that of the system with the narrow crack width increases almost linearly with an overall increment of 257.8%. This is because increasing SIRP thickness causes the outer diameter to thickness ratio of SIRP to reduce, making the system less prone to local buckling. The results also reveal that the SIRP system with a narrow crack width requires a repair thickness of at least 9.345 mm (0.368 in.) to be able to safely carry the design load of 178 kN (40 kips). In contrast, even with a maximum thickness of 12.7 mm, the SIRP system with a wider crack width is unable to withstand the design load requirement. Extrapolating the data in Fig. 15, it is evident that the SIRP repair thickness for steel host pipe with a 152.4 mm (6 in.) crack width must be at least 13.854 mm (0.545 in.) to resist the design load. Fig. 16 depicts the influence of the repair thickness on midspan deflection of SIRP in host pipe with varying crack widths under a loading of about 18.08 kN (4.06 kips) (ultimate loading of the SIRP system with 6 in crack width and 3.175 mm repair thickness). According to that, the level of midspan deformation of SIRP systems with 12.7 mm (0.5 in.), 25.4 mm (1 in.), 50.8 mm (2 in.), 101.6 mm (4 in.), and 152.4 mm (6 in.) crack widths appears to decrease nonlinearly by 36.9%, 44.3%, 53.6%, and 63.7%, respectively, as the repair thickness increases from 3.175 mm (0.125 in.) to 12.7 mm (0.5 in.). The reduction in midspan deflection is attributed to the rise in stiffness of the SIRP. Among all crack widths, the SIRP system with the widest opening (152.4 mm or 6 in.) has the highest overall drop in midspan deflection, while the narrowest crack (12.7 mm or 0.5 in.) has the least. This is because the lower flexural stiffness of the SIRP than the host pipe has a greater impact on systems with wide crack widths compared to those with narrow crack widths.

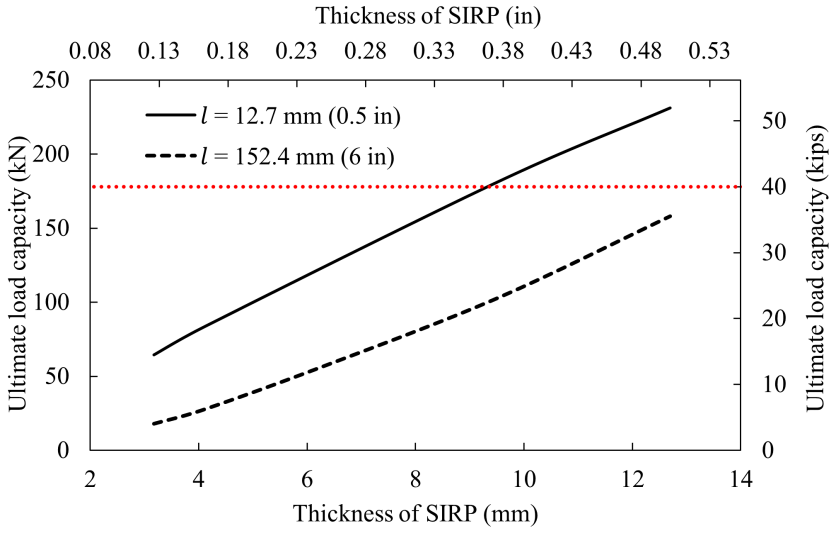

Fig. 15. Effect of SIRP thickness on the ultimate load capacity of the pipelines with 12.7 mm (0.5 in.) and 152.4 mm (6 in.) crack widths.

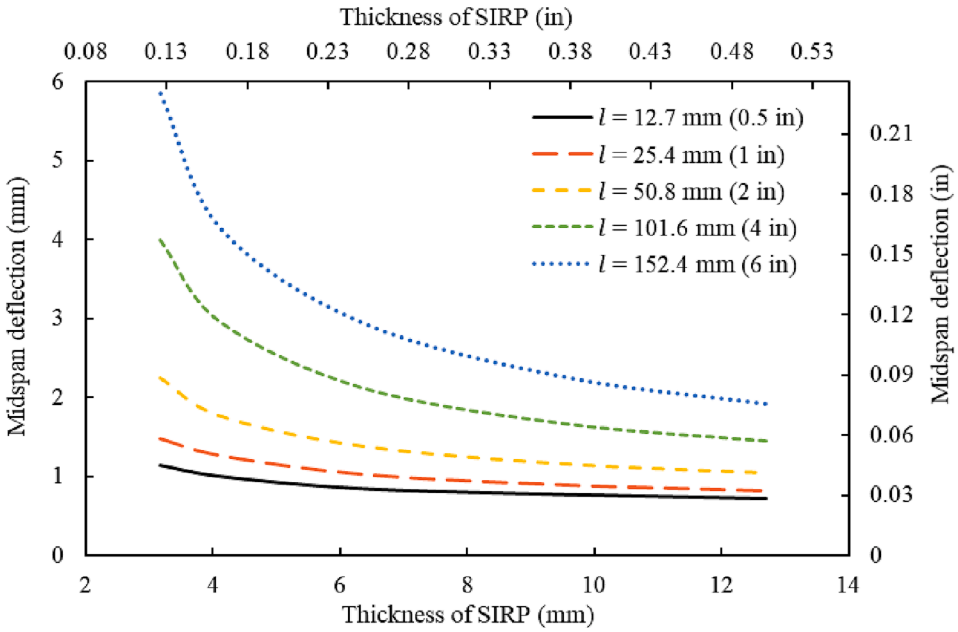

Fig. 16. Effect of repair thickness on midspan deflection for different crack widths at a loading of 18.08 kN.

3.3.3. Effect of the elastic modulus of the SIRP system

The load–strain behaviour of SIRP material systems with different elastic modulus and with 152.4 mm (6 in.) crack widths at 0.002 and 0.02 strain limitations at the midspan, respectively, is summarised in Fig. 17. The analysis is performed with the same repair thickness of 4.1148 mm (0.162 in.). The load capacities of SIRP made from polymeric materials (1–2 GPa), thermoplastics (3 GPa) and GFRP composites (5–24.5) are investigated at an elastic strain of 0.02, while those of metallic systems including CI (70 GPa) and steel (200 GPa) is evaluated at 0.002 strain. These strain constraints followed the approach implemented by Tafsirojjaman et al [1] that divides the design strain of SIRP materials systems into two categories: 0.02 for composites, polymers, and thermoplastic systems, and 0.002 for metallic systems. It is observed that the load capacity of the SIRP repair system with an E of 24.5 GPa (3,553ksi) or lower is controlled by the compressive buckling at the midspan. The results show that the compressive strain in the SIRP system with an E of 1.744 GPa (252.9 ksi) does not reach the design strain of 0.02 due to geometric nonlinearity at the crown of the SIRP between the crack edges. SIRP materials with E ranging from 2 GPa (290 ksi) to 24.5 GPa (3,553 ksi), on the other hand, approach the design strain of 0.02, exhibiting a nonlinear behaviour at higher strains. Fig. 18 displays the load capacity against E of the SIRP systems. Accordingly, the SIRP system with 152.4 mm (6 in.) crack width and 4.1148 mm (0.162 in.) repair thickness should have an E of at least 13.28 GPa (1,926 ksi) to safely carry the design load of 178 kN. (40 kips).

Fig. 19 illustrates the effect of the *E* of SIRP on the midspan deformation of systems with varying crack widths at the same SIRP thickness under a loading of 13.536 kN (3.043 kips) which is the ultimate load capacity of the SIRP system with 152.4 mm (6 in.) crack and *E* of 1 GPa (145 ksi). The results demonstrate that under the same loading when the

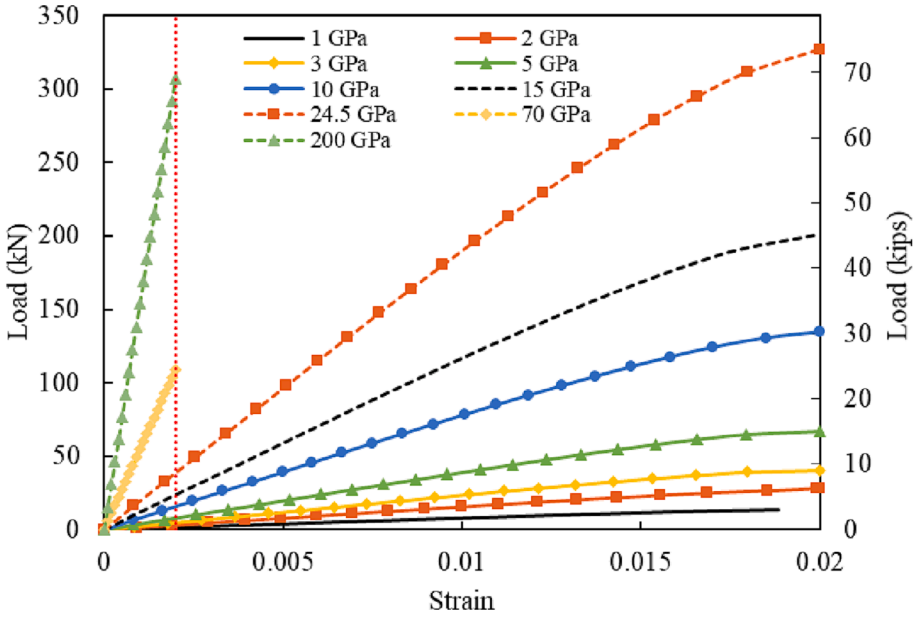

Fig. 17. The load-compressive strain behaviour of SIRP systems with 152.4 mm (6 in.) wide cracks repaired using different materials.

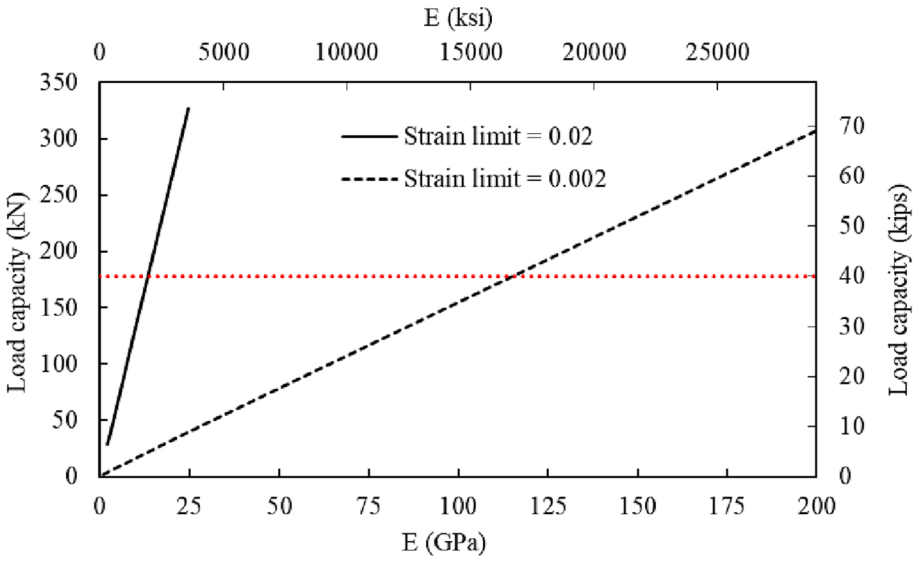

Fig. 18. Effect of the E of SIRP on the ultimate load capacity of host pipe with 152.4 mm (6 in.) crack width.

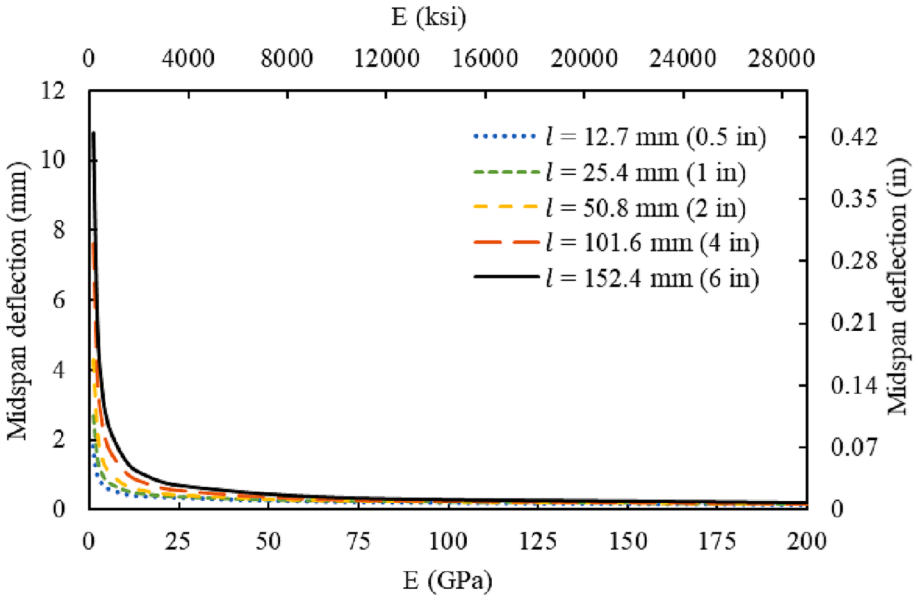

Fig. 19. Effect of E of SIRP on midspan deflection for different crack widths.

E of SIRP increases from 1 GPa (145 ksi) to 24.5 GPa (3,553 ksi), the midspan deflection drops dramatically in all systems, followed by a slight decrease until the *E* reaches 200 GPa (29,008 ksi). As a result, it is obvious that under the same load levels, the SIRP systems with different stiffnesses in circumferentially cracked host pipes experience different levels of midspan deflection, and the mechanical contribution of the internal replacement pipe is an important aspect in the analysis of SIRP systems. The overall reduction in deflection of the SIRP systems with 12.7 mm (0.5 in.), 25.4 mm (1 in.), 50.8 mm (2 in.), 101.6 mm (4 in.) and 152.4 (6 in.) crack widths, respectively, are 90.6%, 93.6%, 95.9%, 97.6% and 98.2%. Thus, a change in *E* of SIRP has a greater impact on the lateral deformation of the system with wider crack widths than it does with narrower crack widths. The largest difference in deflection (88.1%) between systems with 12.7 mm (0.5 in.) and 152.4 mm (6 in.) occurs when the *E* of the repair material is the lowest, while the least difference (11.4%) arises when the E is the greatest.

4. Simplified theoretical prediction of the lateral deformation

While FEA can accurately simulate the bending behaviour of SIRP systems, the process is quite extensive, complex, and requires a longer execution time. This becomes a limitation if material developers in the industry desire to understand how their SIRP system behaves under lateral loading. Thus, the development of a more efficient and simplified analytical model that can still accurately reflect the bending behaviour would be highly beneficial. Considering this requirement, the applicability of the fibre model analysis (FMA) [54] used in the analysis of the layered composite section is investigated to generate simple theoretical predictions of the behaviour of the SIRP system under lateral loading. While this calculation approach can be developed in a Microsoft Excel spreadsheet, the analysis conducted in the current study is implemented using MATLAB [55]. The analysis considers the constitutive nonlinear material behaviour of the host pipe and SIRP as shown in Fig. 3a and b, respectively. In this analysis, it is assumed that the strain in the SIRP and the host pipe is directly proportional to their distance from the neutral

axis and that there is a perfect bond between the SIRP and the host pipe. These assumptions are based on the Euler-Bernoulli theorem of strain compatibility, which states that the plain sections remain plane before and after bending which requires perfect bonding between the SIRP and the host pipe materials and no-slip [56]. The fundamental assumptions of FMA are shown in Fig. 20. In the figure, $D_{p(out)}$ is the outer diameter of SIRP, $D_{p(in)}$ is the inner diameter of SIRP, $\sigma_{h(t)}$ and $\varepsilon_{h(t)}$ characterise the tensile strength and tensile strain of the host pipe material, respectively, whereas $\sigma_{h(c)}$ and $\varepsilon_{h(c)}$ represent the compressive strength and corresponding compressive strain of the host pipe. Similarly, $\sigma_{p(t)}$ and $\varepsilon_{p(t)}$ indicate the failure strength and strain of the SIRP material in tension, respectively, while $\sigma_{p(c)}$ and $\varepsilon_{p(c)}$ reflect the compressive strength and corresponding compressive strain of the SIRP material.

Due to the nonlinearity of the materials, when the load increases, variations in stiffness (EI) within the layers of cross-section and sections along the longitudinal axis of the SIRP system may occur. To account for this behaviour, the varying EI values are predicted, and the deflections are calculated as follows: Firstly, a compressive strain value at the topmost layer of the SIRP alone (at the middle crack) is assumed and the corresponding moment capacity and the applied load are calculated. In addition, the corresponding equivalent effective secant stiffness of SIRP ($(EI)_{SIRP}$) is determined by taking the summation of the secant stiffness of all the layers of the SIRP section as shown in Eq. (1). A separate FMA is then performed by increasing the maximum bending strain value at the topmost layer of the host pipe with SIRP section from a lower value to a higher value to determine moment capacities and corresponding equivalent effective secant stiffnesses (Eq.(2)). The moment capacities against the equivalent effective secant stiffness of the cross-section of SIRP with the host pipe ($(EI)_{EFF}$) is then plotted. Thirdly, the loading length of the beam is divided into small segments and the moment capacity at each segment is calculated using the applied load obtained from the previous analysis of the SIRP section alone. The $(EI)_{EFF}$ values corresponding to these moments over the loading length are obtained using $(EI)_{EFF}$ versus moment capacity plot of the host pipe with SIRP section via interpolation curve fit.

$$(EI)_{SIRP} = \sum_{i=1}^{n_{p(c)}} E_{p(c)i} I_{p(c)i} + \sum_{i=1}^{n_{p(t)}} E_{p(t)i} I_{p(t)i} \tag{1}$$

$$(EI)_{EFF} = \sum_{i=1}^{n_{h(c)}} E_{h(c)i} I_{h(c)i} + \sum_{i=1}^{n_{p(c)}} E_{p(c)i} I_{p(c)i} + \sum_{i=1}^{n_{h(t)}} E_{h(t)i} I_{h(t)i} + \sum_{i=1}^{n_{p(t)}} E_{p(t)i} I_{p(t)i} \tag{2}$$

where $E_{h(c)i}$, $E_{p(c)i}$, $E_{h(t)i}$ and $E_{p(t)i}$ are the secant modulus of each layer of host pipe in compression, SIRP in compression, host pipe in tension and SIRP in tension, respectively, while $I_{h(c)i}$, $I_{p(c)i}$, $I_{h(t)i}$ and $I_{p(t)i}$ are the corresponding moment of inertia of each layer of host pipe in compression, SIRP in compression, host pipe in tension and SIRP in tension, respectively.

The maximum midspan deflection of SIRP in a circumferentially cracked host pipe with nonlinear stress–strain behaviour is then determined using Eq. (3). A schematic diagram of SIRP in a host pipe with a middle crack is shown in Fig. 21 where Δ_{max} is the maximum mid-span deflection, L corresponds to the length of the SIRP between supports, $\frac{(L-l)}{2}$ is the length of one of the cracked host pipe sections, l is the crack width, P is half of the applied load n is the total number of segments into which the loading length, a is subdivided, w_i is the length to the right boundary of each segment from the left support, $(EI)_{eff_i}$ is the equivalent effective secant stiffness of the cross-section of each segment SIRP segment with host pipe over the length a (on the left side of the system) from the support to the loading point. Finally, by increasing the compressive strain value at the mid-span of SIRP alone from a very lower value to a higher value, a series of corresponding applied loads, $(EI)_{SIRP}$ and $(EI)_{EFF}$ values over the length and the corresponding maximum midspan deflection of SIRP in a host pipe with a middle crack with

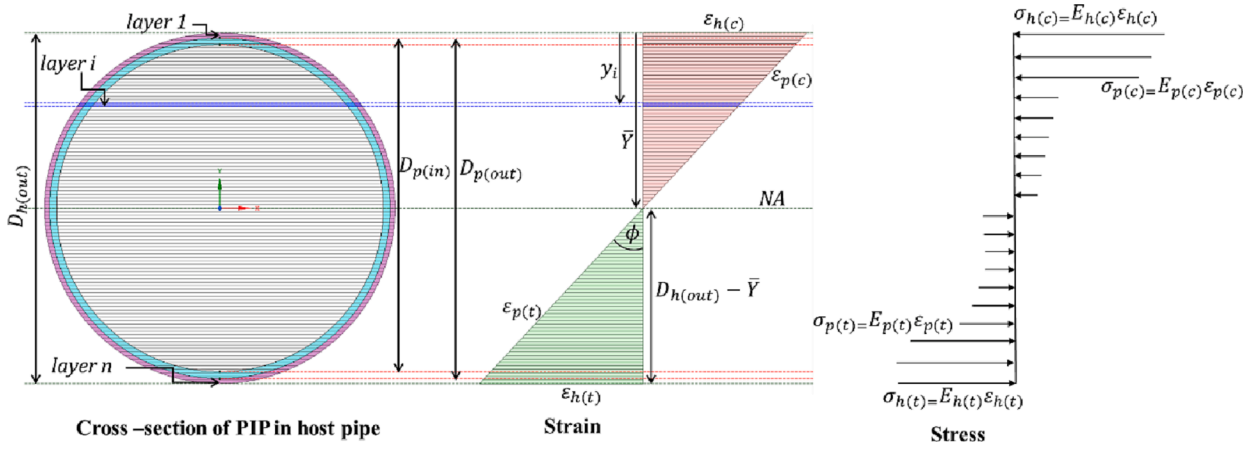

Fig. 20. Fundamental assumptions of FMA.

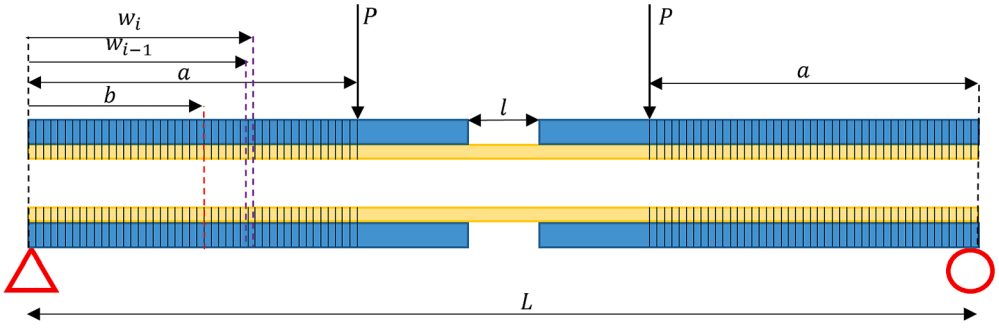

Fig. 21. Schematic illustration of SIRP in host pipe with a circumferential middle crack.

nonlinear stress–strain behaviour is computed. The deflection along $0 \le b \le a$, $a \le b \le \frac{(L-l)}{2}$ and $\frac{(L-l)}{2} \le b \le \frac{L}{2}$ of SIRP is predicted using Eqs. (4)–(6) respectively, where b is the length from the left support to the point where the deflection requires to be computed (Fig. 21).

$$\Delta_{\max} = 2\left\{ \sum_{i=1}^{n} \left[\frac{P({w_i}^3 - {w_{i-1}}^3)}{6(EI)_{effi}} \right] + \frac{Pa}{16(EI)_{EFF}} \left((L-l)^2 - 4a^2 \right) + \frac{Pa}{16(EI)_{SIRP}} \left(2Ll - l^2 \right) \right\} \quad (3)$$

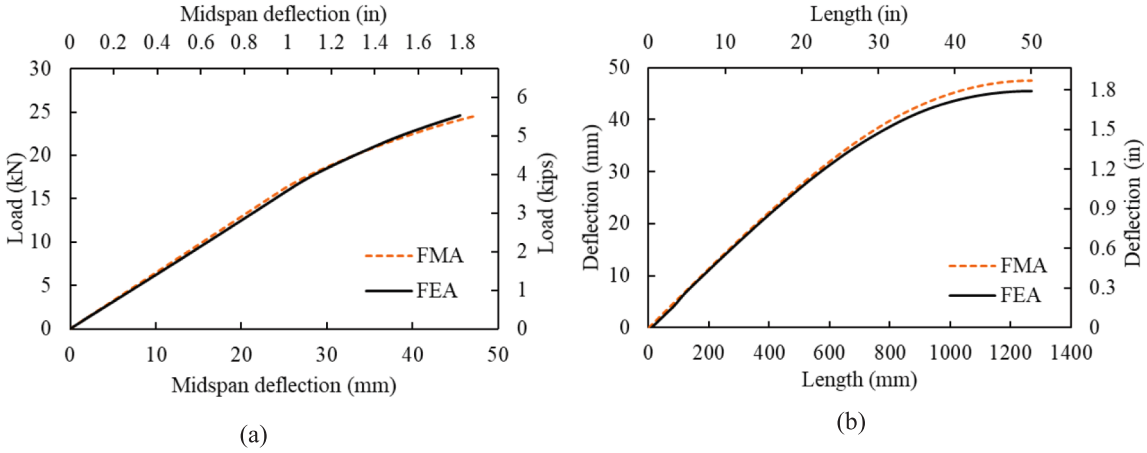

Fig. 22. Comparison of FMA and FEA (a) load- midspan deflection behaviour, (b) deflection (at ultimate load) over the half-length (from left support to midspan) of SIRP alone.

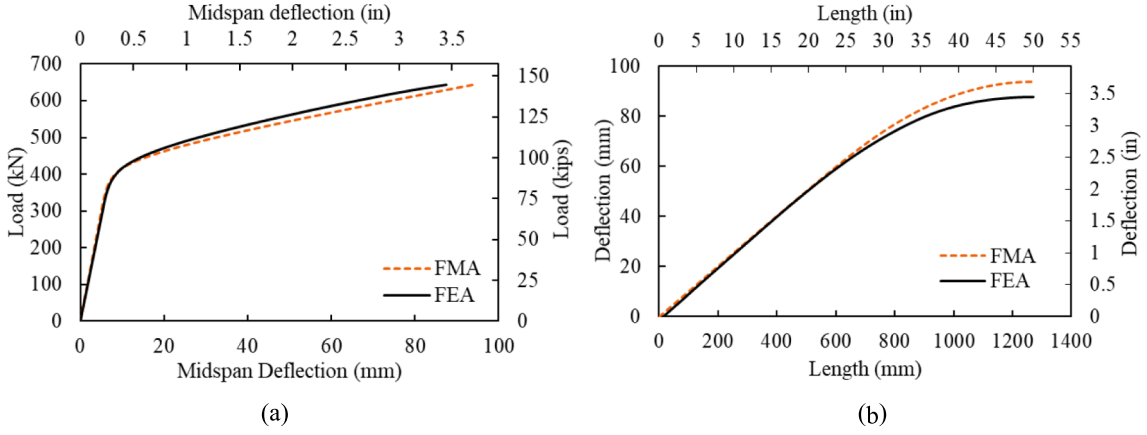

Fig. 23. Comparison of FMA and FEA (a) load- midspan deflection behaviour, (b) deflection (at ultimate load) over the half-length of SIRP in a continuous host pipe.

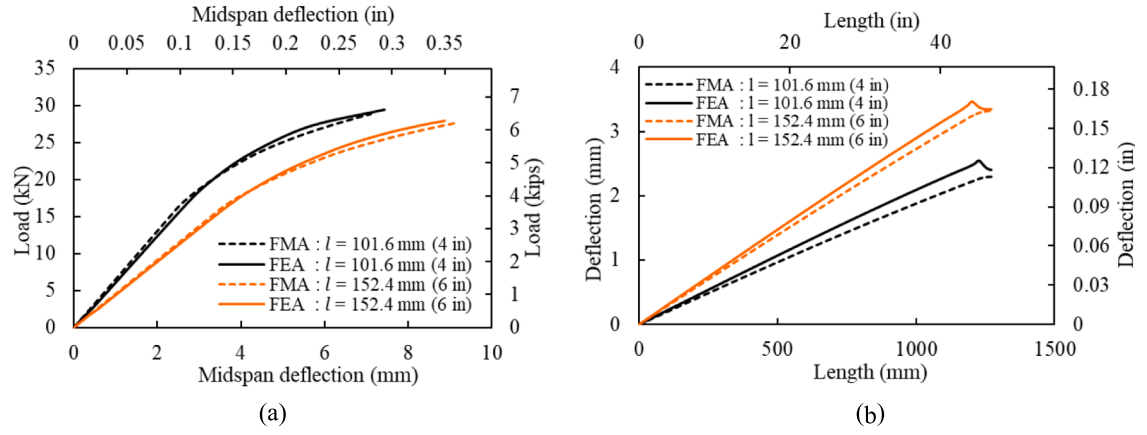

Fig. 24. Comparison of FMA and FEA (a) load- midspan deflection behaviour and (b) deflection along half-length of SIRP in host pipe with wider crack widths.

The deflection at any point along $0 \le b \le a$:

$$\begin{aligned}\Delta_{(0\le b\le a)} &= \sum_{i=1}^{n_b}\left\{\frac{P\left(1-\frac{b}{L}\right)\left({w_i}^3-{w_{i-1}}^3\right)}{3(EI)_{effi}}\right\} \\ &+ \sum_{i=1}^{(n-n_b)}\left\{\frac{Pb}{(EI)_{eff_{(a-b)i}}}\left[\left(\frac{{w_i}^2-{w_{i-1}}^2}{2}\right)-\left(\frac{{w_i}^3-{w_{i-1}}^3}{3L}\right)\right]\right\} \\ &+ \frac{Pab}{(EI)_{EFF}}\left\{\frac{L-l}{2}-a-\frac{(L-l)^2}{8L}+\frac{a^2}{2L}\right\}+\frac{Pabl}{2(EI)_{PIP}} \\ &+ \frac{Pab}{(EI)_{EFF}}\left\{\left(\frac{L}{2}-a-\frac{l}{2}\right)-\frac{1}{2L}\left[(L-a)^2-\frac{(L+l)^2}{4}\right]\right\} \\ &+ \sum_{i=1}^{n}\left\{\frac{Pb}{\left((EI)_{eff}\right)'_i}\left[L(w_i-w_{i-1})-\left({w_i}^2-{w_{i-1}}^2\right)\right.\right. \\ &\left.\left.+\frac{1}{3L}\left({w_i}^3-{w_{i-1}}^3\right)\right]\right\}\end{aligned} \tag{4}$$

The deflection at any point along $a \le b \le \frac{(L-l)}{2}$:

$$\begin{aligned}\Delta_{\left(a\le b\le\frac{L-l}{2}\right)} &= \sum_{i=1}^{n}\left\{\frac{P\left(1-\frac{b}{L}\right)\left({w_i}^3-{w_{i-1}}^3\right)}{3(EI)_{effi}}\right\} \\ &+ \frac{Pa\left(1-\frac{b}{L}\right)\left(b^2-a^2\right)}{2(EI)_{EFF}} \\ &+ \frac{Pab}{8L(EI)_{EFF}}\left(3L^2-2Ll-8bL-l^2+4b^2\right)+\frac{Pabl}{2(EI)_{SIRP}} \\ &+ \frac{Pab}{(EI)_{EFF}}\left\{\left(\frac{L}{2}-a-\frac{l}{2}\right)-\frac{1}{2L}\left[(L-a)^2-\frac{(L+l)^2}{4}\right]\right\} \\ &+ \sum_{i=1}^{n}\left\{\frac{Pb}{\left((EI)_{eff}\right)'_i}\left[L(w_i-w_{i-1})-\left({w_i}^2-{w_{i-1}}^2\right)\right.\right. \\ &\left.\left.+\frac{1}{3L}\left({w_i}^3-{w_{i-1}}^3\right)\right]\right\}\end{aligned} \tag{5}$$

The deflection at any point along $\frac{(L-l)}{2} \le b \le \frac{L}{2}$:

$$\begin{aligned}\Delta_{\left(\frac{L-l}{2}\le b\le\frac{L}{2}\right)} &= \sum_{i=1}^{n}\left\{\frac{P\left(1-\frac{b}{L}\right)\left({w_i}^3-{w_{i-1}}^3\right)}{3(EI)_{effi}}\right\}+\frac{Pa}{8(EI)_{EFF}}\left[(L-l)^2-4a^2\right] \\ &+ \frac{Pa\left(1-\frac{b}{L}\right)\left[4b^2-(L-l)^2\right]}{8(EI)_{SIRP}}+\frac{Pab\left\{\frac{L+l}{2}-b-\frac{(L+l)^2}{8L}+\frac{b^2}{2L}\right\}}{(EI)_{PIP}} \\ &+ \frac{Pab}{(EI)_{EFF}}\left\{\left(\frac{L}{2}-a-\frac{l}{2}\right)-\frac{1}{2L}\left[(L-a)^2-\frac{(L+l)^2}{4}\right]\right\} \\ &+ \sum_{i=1}^{n}\left\{\frac{Pb}{\left((EI)_{eff}\right)'_i}\left[L(w_i-w_{i-1})-\left({w_i}^2-{w_{i-1}}^2\right)\right.\right. \\ &\left.\left.+\frac{1}{3L}\left({w_i}^3-{w_{i-1}}^3\right)\right]\right\}\end{aligned} \tag{6}$$

where $\Delta_{(0\le b\le a)}$, $\Delta_{\left(a\le b\le\frac{L-l}{2}\right)}$ and $\Delta_{\left(\frac{L-l}{2}\le b\le\frac{L}{2}\right)}$ are the deflection at any point along $0 \le b \le a$, $a \le b \le \frac{(L-l)}{2}$ and $\frac{(L-l)}{2} \le b \le \frac{L}{2}$ of SIRP, respectively, n_b and $(n-n_b)$ are respectively the number of segments over length b and length $(a-b)$-, $(EI)_{eff_{(a-b)i}}$ is the equivalent effective secant stiffness of the cross-section of each segment of SIRP with host pipe over length $(a-b)$ from length b to the loading point and $\left((EI)_{eff}\right)'_i$ is the equivalent effective secant stiffness of the cross-section of each segment of SIRP with host pipe over the length a (on the right side of the system) from the loading point to support.

4.1. Comparison with FEA results

4.1.1. SIRP repair systems only

The load-midspan deflection behaviour and the deflection (at ultimate load) over a half-length of a SIRP alone obtained from FMA and FEA are compared in Fig. 22a and b respectively. Fig. 22a demonstrates that the nonlinear load-midspan deflection response of SIRP predicted by FMA correlates well with FEA, with a maximum discrepancy of only about 4.1%. This minor deviation can be attributed to geometric nonlinearity considered by the FEA due to the local buckling of SIRP at the midspan. FMA, on the other hand, is a simplified approach that does not capture every single change in 3D geometry including local bucking during bending. As shown in Fig. 22b, the FMA deflection prediction along the half length of SIRP at ultimate load exhibits a linear response up to the loading point followed by a nonlinear response. These FMA results are also found to be in close agreement with FEA ones.

4.1.2. SIRP repair systems in a continuous host pipe

A comparison between the FMA and FEA load-midspan deflection relation and the deflection (at ultimate load) along the half-length of a continuous steel host pipe with SIRP is shown in Fig. 23a and b, respectively. The load-midspan deflection response of SIRP in continuous steel host pipe under bending predicted by FMA is very similar to that of FEA, with a maximum deviation in deflection of only about 12.7% at a load of 546 kN, as shown in Fig. 23a. This difference is because, unlike FMA, which only considers material nonlinearity, 3D FEA nonlinear analysis incorporates geometric nonlinearity, which causes the stiffness of the beam to rise when deformations are large. Enabling large deflection ensures that the program accounts for the change in stiffness caused by geometric changes. Since curved beams have a greater stiffness than straight beams, when a straight beam is turned into a curved beam, its stiffness increases, resulting in less vertical downward deflection than FMA at the same loading level. This increase in stiffness is also called stress stiffening. Fig. 23b indicates that the deflection along the length of the SIRP in continuous host pipe at the ultimate load predicted using FMA, which exhibits a linear response up to the loading point followed by a nonlinear response until midspan, correlates well with the FEA behaviour, with the maximum deviation being only 6.6% at midspan.

4.1.3. SIRP repair systems in a host pipe with wide circumferential cracks

The load versus midspan deflection behaviour of SIRP repair systems in host pipe with wide circumferential crack widths predicted by FMA is compared to FEA results in Fig. 24a. The FMA findings for crack widths of 101.6 mm (4 in.) and 152.4 mm (6 in.) show a linear load–deflection relationship up to 16.8 kN (3.78 kips) and 16.6 kN (3.73 kips), respectively. Thereafter, a slightly nonlinear decrease in stiffness occurs until it finally fails at loadings of 29.4 kN (6.61 kips) and 27.9 kN (6.27 kips), respectively. This overall behaviour of FMA is in good agreement with FEA, with a maximum deviation of less than 6%. Fig. 24b compares the FMA and FEA predictions of deflection along the half-length of the SIRP systems under a load of 15 kN (3.37 kips). Accordingly, it is confirmed that FMA can capture a linear deflection response along the pipe length up to the crack edge, which is similar to the behaviour predicted by FEA. However, the deviation of the FMA prediction from the FEA results rises gradually from the support to the crack edge, and it can be as high as 9.3% at the crack edge of the SIRP system with a crack width of 101.6 mm (4 in.), which is more than twice that at the midspan under the same load. The difference between FMA and FEA prediction is that when the crack width narrows, stress concentration at the crack edge causes an

increase in stresses along the crack width in 3D FEA models. This results in higher average stress over the narrow crack width, which the simplified FMA model cannot account for. However, for crack widths narrower than 101.6 mm (4 in.), the average stress along them further increases, resulting in considerable differences between the initial FMA and FEA deflection predictions. To overcome this limitation of the initial FMA, a factor termed the average stress factor (K) is established and incorporated into the simplified FMA models to be applied in the deflection computation of SIRP systems with narrow crack widths.

4.2. Average stress factor

The average stress factor (K) is computed by dividing the average of FEA normal stress along the crack width (at the invert of SIRP) by the corresponding average FMA stresses. The initial FMA deflection prediction is then multiplied by K, to obtain the factored FMA deflection, which accounts for the effect of stress concentration on average stresses over crack width. Then, a parametric study is carried out using both FMA and FEA to produce an equation that can accurately estimate the average stress factor. For this, a range of SIRP thicknesses between 3.175 mm (0.125 in.) and 9.525 mm (0.375 in.), crack widths from 12.7 mm (0.5 in.) to 152.4 mm (6 in.) and elastic moduli of materials from 1 GPa (145 ksi) to 200 GPa (29008 ksi) are considered. The parametric analysis shows that the average stress factor is mostly governed by the geometry of the fracture, i.e. the width of the crack and the thickness of SIRP, whereas the E of the material has almost no effect. This is because, under the same load, the stress is determined primarily by the applied load and geometry and does not depend on the E in the elastic region. Fig. 25a compares the effect of crack width on the average stress factor of a repaired host pipe with varied SIRP thicknesses. Accordingly, the average stress factor for a given SIRP thickness reduces with increasing crack width and reaches a constant value once the crack width exceeds 101.6 mm (4 in.). This is due to the fact that when the crack width widens, the local stresses produced by the host pipe discontinuities stabilise along the crack width, resulting in a reduction in average stress. In contrast, when the crack width narrows, the average stress factor increases dramatically. This is because the crack width is insufficient to stabilise the higher stresses leading to an increase in average FEA stress over it. The influence of relative SIRP thickness on the average stress factor of SIRP in host pipes with varied crack widths is shown in Fig. 25. For a given crack width, the average stress factor rises linearly as the relative SIRP thickness increases.

By considering the K as a function of two governing dimensionless parameters, crack width to the thickness of SIRP and the total wall thicknesses of SIRP and host pipe thickness to the thickness of SIRP, a mathematical formulation (Eq. (7)) is developed. This was performed by nonlinear-least squares regression analysis in MATLAB to achieve the best surface fit (Fig. 26). The model equation used in this analysis is Eq. (8), where t_T is the total wall thickness, t_p is the thickness of SIRP, p, q, r and s are the unknown parameters, and x and y are the total wall thicknesses to SIRP thickness and crack widths to SIRP wall thickness, respectively.

$$K = 1.097e^{-0.01529\left(\frac{t_T}{t_p}\right)} + 1.461e^{-0.3368\left(\frac{l}{t_p}\right)} \tag{7}$$

$$K = pe^{q(x)} + re^{-s(y)} \tag{8}$$

4.3. Factored FMA for deflection prediction of SIRP systems with narrow crack widths

The factored FMA deflection of a very narrow crack width (12.7 mm) is compared to both FEA and full-scale laboratory experimental results from the University of Colorado Boulder in Fig. 27. The comparison demonstrates that the load–deflection behaviour predicted by the factored FMA for SIRP with narrow crack widths is in good agreement with the FEA and experimental outcomes. At a loading of 14.9 kN (3.35 kips), the differences between factored FMA and FEA deflection

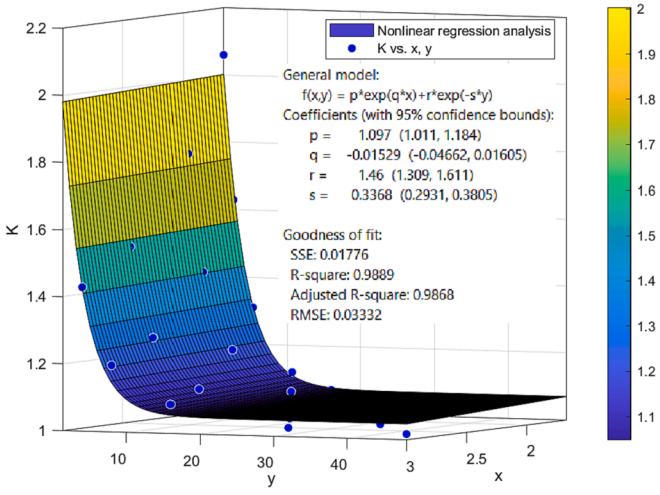

Fig. 26. 3D surface fitting in MATLAB.

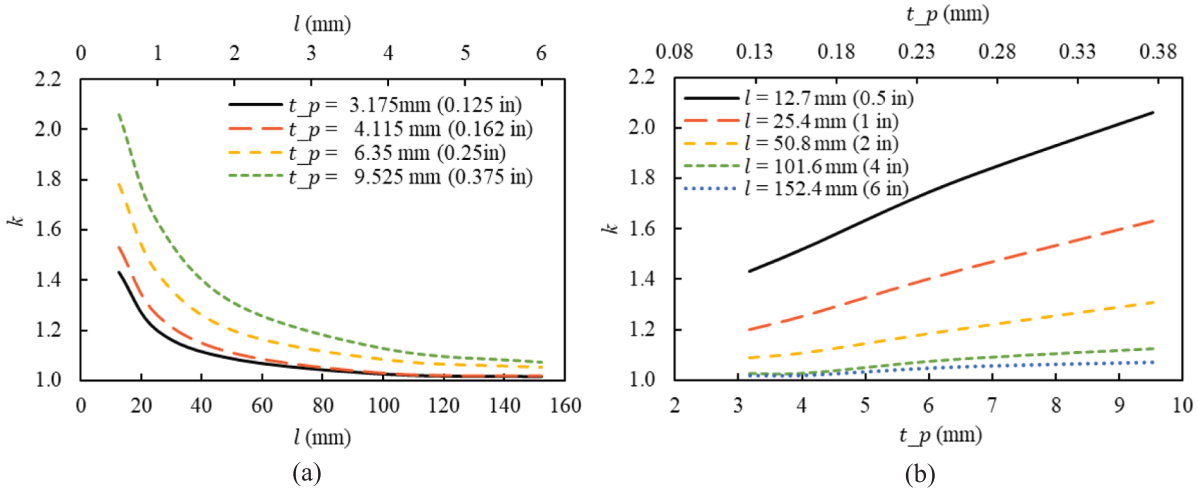

Fig. 25. Average stress factor against (a) crack widths with varying SIRP thickness and (b) SIRP thickness for different crack widths.

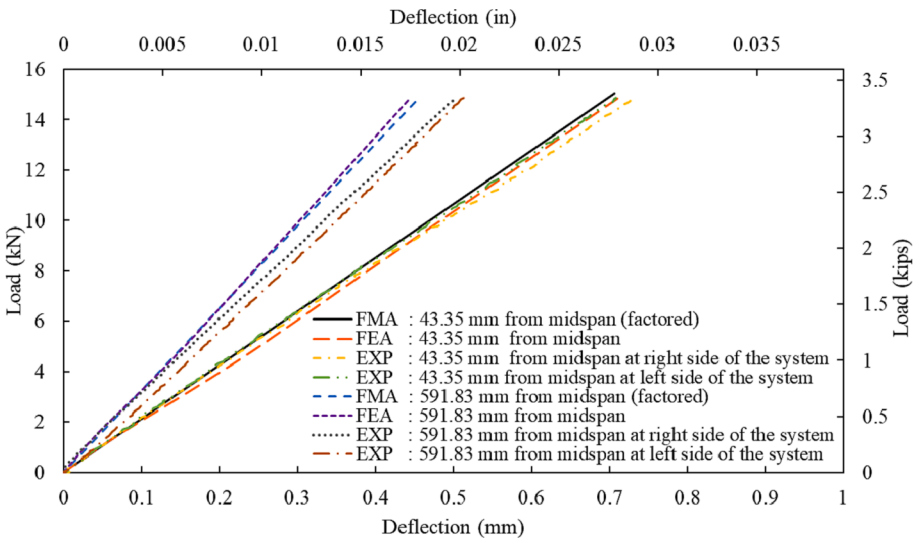

Fig. 27. Comparison of FMA, 3D FEA and experimental load–displacement behaviours of SIRP in host pipe with 12.7 mm opening.

prediction are approximately 1.9% and 2.2%, respectively. Furthermore, under the same loading, the highest discrepancies between the deflections predicted by the factored FMA and the laboratory experiment at the crack edge and loading point, respectively, are around 4.7% and 10.8%.

It should be noted that the developed FMA can reliably predict the load–deflection behaviour of fully bonded SIRP repair systems under lateral loading until the ultimate strain of repair material is reached. This model can be extended to account to predict the capacity of the repair system against local failure modes such as buckling as well as the influence of the combination loading cases and the effect of the unbonded length during bending. Further analyses and verification can be implemented to extend the developed FMA to predict such complex behaviour.

5. Conclusions

The flexural behaviour of structural internal replacement pipe (SIRP) system alone, SIRP in a continuous host pipe, and SIRP in a host pipe with narrow and wide crack widths under the effect of wheel loads located directly and moving parallel to the longitudinal axis of a pipeline have been investigated numerically in this study. The effect of the crack width of the host pipe, thickness, and material properties of the SIRP, on the bending behaviour of the composite pipe repair system, was systematically evaluated. From the results of these analyses and investigations, the following conclusions can be drawn:

- The lateral deformation of SIRP alone increases nonlinearly with the applied load and their failure mechanism is governed by local buckling of the crown.
- The lateral deformation behaviour of a continuous steel pipe system with SIRP is mostly influenced by the host pipe. The failure of the system is initiated by the yielding of the host pipe followed by local inward buckling of the SIRP. While the inclusion of the SIRP does not improve the load at yielding of the host pipe, it increases the ultimate load and maximum deflection capacity of the system by 11% and 23%, respectively.
- The lateral deformation behaviour of the repair system with a narrow circumferentially crack host pipe is governed by the host pipe while that of the system with wide cracks is governed by the SIRP systems. The strength and stiffness of the system decrease with the increase in crack width. Regardless of the crack width, the mode of failure is due to local outward buckling of the crown of SIRP between the crack edges.
- The increase in the SIRP thickness increases the flexural capacity of the system, with a nonlinear increase for the systems with a wide crack but a linear increase for the system with narrow crack widths. The thickness of the SIRP has a more substantial impact on the lateral deformation of the system with wider than narrower crack widths. The SIRP system with crack widths of 12.7 mm (0.5 in.) and 152.4 mm (6 in.) respectively require repair thicknesses of at least 9.345 mm (0.368 in.) and 13.854 mm (0.545 in.) to safely carry the design load of 178 kN (40 kips).
- The midspan deflection lowers dramatically as the elastic modulus of SIRP increases from 1 GPa (145 ksi) to 24.5 GPa (3,553 ksi). The change in E of SIRP has a greater effect on the lateral deformation of the system with wider than narrower crack widths.
- The mechanical contribution of the inner liner pipe is an important consideration in the analysis of SIRP systems because, at the same loading levels, SIRP systems in circumferentially cracked host pipes with different stiffness undergo varying levels of deformation.
- The simplified FMA can reliably predict the lateral deformation behaviour of SIRP systems in host pipes with wide circumferential cracks. The factored FMA considering the ratio of the average normal stress along the crack width from the FEA to that of the corresponding average FMA stresses can accurately predict of load-midspan deflection behaviour of the system with narrow circumferential cracks.

Declaration of Competing Interest

The authors declare that they have no known competing financial interests or personal relationships that could have appeared to influence the work reported in this paper.

Data availability

Data will be made available on request.

Acknowledgement

The information, data, or work presented herein was funded in part by the Advanced Research Projects Agency-Energy (ARPA-E), US Department of Energy, under Award Number DE-AR0001327. The views and opinions of authors expressed herein do not necessarily state or reflect those of the United States Government or any agency thereof.

References

[1] Tafsirojjaman T, Manalo A, Tien CMT, Wham BP, Salah A, Kiriella S, et al. Analysis of failure modes in pipe-in-pipe repair systems for water and gas pipelines. Eng Fail Anal 2022;140:106510.
[2] Zhang S, Zhou W. Cost-based optimal maintenance decisions for corroding natural gas pipelines based on stochastic degradation models. Eng Struct 2014;74:74–85.
[3] Ossai CI, Boswell B, Davies IJ. Pipeline failures in corrosive environments A conceptual analysis of trends and effects. Eng Fail Anal 2015;53:36–58.
[4] Sun J, Cheng YF. Assessment by finite element modeling of the interaction of multiple corrosion defects and the effect on failure pressure of corroded pipelines. Eng Struct 2018;165:278–86.
[5] Pimentel JT, et al. New procedure of automatic modeling of pipelines with realistic shaped corrosion defects. Eng Struct 2020;221:111030.
[6] Shamsuddoha Md, Islam MM, Aravinthan T, Manalo A, Lau K-T. Effectiveness of using fibre-reinforced polymer composites for underwater steel pipeline repairs. Compos Struct 2013;100:40–54.
[7] Rohem NRF, Pacheco LJ, Budhe S, Banea MD, Sampaio EM, de Barros S. Development and qualification of a new polymeric matrix laminated composite for pipe repair. Compos Struct 2016;152:737–45.
[8] Al-Abtah FG, Mahdi E, Eliyan FF. The use of fiber reinforced polymeric composites in pipelines: A review. Compos Struct 2021;276:114595.
[9] Yang H-N, Chen J-H, Chiu H-J, Kao T-J, Tsai H-Y, Chen J-R. Confined vapor explosion in Kaohsiung City – A detailed analysis of the tragedy in the harbor city. J Loss Prev Process Ind 2016;41:107–20.
[10] Witek M, Batura A, Orynyak I, Borodii M. An integrated risk assessment of onshore gas transmission pipelines based on defect population. Eng Struct 2018;173:150–65.
[11] Biezma MV, et al. Most fatal oil & gas pipeline accidents through history: A lessons learned approach. Eng Fail Anal 2020;110.
[12] Chin WS, Lee DG. Development of the trenchless rehabilitation process for underground pipes based on RTM. Compos Struct 2005;68(3):267–83.
[13] Karbhari VM. Rehabilitation of Pipelines Using Fiber-reinforced Polymer (FRP) Composites. 2014. Cambridge, United Kingdom: Elsevier Science; 2015.
[14] Pesinis K, Tee KF. Bayesian analysis of small probability incidents for corroding energy pipelines. Eng Struct 2018;165:264–77.
[15] Li Z, Tang F, Chen Y, Zou X. Stability of the pipe-liner system with a grouting void surrounded by the saturated soil. Eng Struct 2019;196:109284.
[16] Selvakumar A, et al. State of technology for rehabilitation of water distribution system. Edison, NJ, USA: US Environmental Protection Agency (EPA); 2013.
[17] Rahmaninezhad SM, et al. Field evaluation of performance of corroded corrugated steel pipe before and after sliplining rehabilitation. Tunn Undergr Space Technol 2020;102:103442.
[18] Wu Y, Kang C, Nojumi MM, Bayat A, Bontus G. Current water main rehabilitation practice using trenchless technology. Water Pract Technol 2021;16(3):707–23.
[19] Jung YJ, Sinha SK. Evaluation of trenchless technology methods for municipal infrastructure system. J Infrastruct Syst 2007;13(2):144–56.
[20] Yu HN, Kim SS, Hwang IU, Lee DG. Application of natural fiber reinforced composites to trenchless rehabilitation of underground pipes. Compos Struct 2008;86(1-3):285–90.
[21] Czél G, Czigány T. Finite element method assisted stiffness design procedure for non-circular profile composite wastewater pipe linings. Compos Struct 2014;112:78–84.
[22] Lu H, Behbahani S, Azimi M, Matthews JC, Han S, Iseley T. Trenchless construction technologies for oil and gas pipelines: State-of-the-art review. J Constr Eng Manag 2020;146(6).
[23] Jeon S-S, O'Rourke TD, Neravali AN. Repetitive loading effects on cast iron pipelines with cast-in-place pipe lining system. J Transport Eng-ASCE 2004;130:692–705.
[24] Argyrou C, O'Rourke TD, Stewart HE, Wham BP. Large-scale fault rupture tests on pipelines reinforced with cured-in-place linings. J Geotech Geoenviron Eng 2019;145(3).
[25] Vasseghi A, Haghshenas E, Soroushian A, Rakhshandeh M. Failure analysis of a natural gas pipeline subjected to landslide. Eng Fail Anal 2021;119:105009.
[26] Vazouras P, Karamanos SA, Dakoulas PC. Mechanical behavior of buried steel pipes crossing active strike-slip faults. Soil Dyn Earthq Eng 2012;41:164–80.
[27] Liu Wu, Guo Q, Qiao C, Hou W. Strain design method of buried pipeline crossing fault. Eng Fail Anal 2019;105:659–71.
[28] Melissianos VE, Vamvatsikos D, Gantes CJ. Performance-based assessment of protection measures for buried pipes at strike-slip fault crossings. Soil Dyn Earthq Eng 2017;101:1–11.
[29] Guo B, et al. Offshore Pipelines. 1 ed. Burlington, MA: Elsevier; 2005.
[30] Costa Mattos HSd, Reis JML, Paim LM, Silva MLd, Lopes Junior R, Perrut VA. Failure analysis of corroded pipelines reinforced with composite repair systems. Eng Fail Anal 2016;59:223–36.
[31] Budhe S, Banea MD, de Barros S. Composite repair system for corroded metallic pipelines: an overview of recent developments and modelling. J Mar Sci Technol 2020;25(4):1308–23.
[32] Bokaian A. Thermal expansion of pipe-in-pipe systems. Mar Struct 2004;17(6):475–500.
[33] Zhong Z, Wang S, Zhao Mi, Du X, Li L. Performance of ductile iron push-on joints rehabilitated with CIPP liner under repetitive and seismic loadings. Soil Dyn Earthq Eng 2018;115:776–86.
[34] Ng PCF. Behaviour of buried pipelines subjected to external loading. In: Department of civil and structural engineering. University of Sheffield; 1994. p. 339.
[35] Stewart HE, Netravali AN, O'Rourke TD. Performance testing of field-aged cured-in-place liners (CIPL) for cast iron piping. School of Civil and Environmental Engineering, Cornell University; 2015. p. 1–128.
[36] Makar JM, Desnoyers R, McDonald SE. Failure modes and mechanisms in gray cast iron pipe. ttawa, Ontario, Canada: Institute for Research in Construction, National Research Council Canada; 2001. p. 1–10.
[37] Farag MH, Mahdi E. New approach of pipelines joining using fiber reinforced plastics composites. Compos Struct 2019;228:111341.
[38] Mahdi E, Eltai EO. Development of cost-effective composite repair system for oil/gas pipelines. Compos Struct 2018;202:802–6.
[39] Sirimanna CS, Banerjee S, Karunasena W, Manalo AC, McGarva L. Analysis of retrofitted corroded steel pipes using internally bonded FRP composite repair systems. Aust J Struct Eng 2015;16(3):187–98.
[40] Lim KS, Azraai SNA, Yahaya N, Md Noor N, Zardasti L, Kim J-H. Behaviour of steel pipelines with composite repairs analysed using experimental and numerical approaches. Thin-Walled Struct 2019;139:321–33.
[41] Yeleswarapu S, Chandra Khan V, P. NK, Gurusamy B, Pandit MK. Performance assessment of polymeric composite wrap to repair damaged pipelines exposed under accelerated environment conditions. J Pipeline Syst Eng Pract 2021;12(3).
[42] Saeed N, Kang W-H, Samali B. Composite overwrap repair of pipelines-reliability based design framework. Structures 2022;40:448–59.
[43] Sever VF, Ehsani M. *Designing an Economical FRP System for Pipeline Rehabilitation*. In: *Pipelines 2019*. 2019.
[44] Fan T, Liu Z, Li M, Zhao Y, Zuo Z, Guo R. Development of cost-effective repair system for locally damaged long-distance oil pipelines. Constr Build Mater 2022;333:127342.
[45] Chen J, et al. Finite element analysis of composite repair for damaged steel pipeline. Coatings 2021;11:301.
[46] Allouche EN, et al. Experimental Examination of selected limit states of structural liners at locations of ring fracture. In: *Pipelines Conference 2012*. 2012. p. 783-794.
[47] Shou KJ, Chen BC. Numerical analysis of the mechanical behaviors of pressurized underground pipelines rehabilitated by cured-in-place-pipe method. Tunn Undergr Space Technol 2018;71:544–54.
[48] Yang K, Xue B, Fang H, Du X, Li B, Chen J. Mechanical sensitivity analysis of pipe-liner composite structure under multi-field coupling. Structures 2021;29:484–93.
[49] Sousa R, Sousa H, Guedes JPM. Diagonal compressive strength of masonry sample" experimental and numerical approach. Mater Struct 2013;46:765–86.
[50] Ansys, Finite Element Analysis (FEA). Software for Structuaral Engineering. ANSYS, Inc.; 2021.
[51] Preedawiphat P, Mahayotsanun N, Sa-ngoen K, Noipitak M, Tuengsook P, Sucharitpwatskul S, et al. Mechanical investigations of ASTM A36 welded steels with stainless steel cladding. Coatings 2020;10(9):844.
[52] ASTM, Standard Test Method for Tensile Properties of Plastics. In: ASTM D638-14. ASTM International; 2015. p. 1-17.
[53] Gereber WS. In: IngVer ZBA (eds.) Calculation of the allowable stresses in iron structures. Vol. 6. P. 101-110. 1874.
[54] Manalo AC, Aravinthan T, Karunasena W, Islam MM. Flexural behaviour of structural fibre composite sandwich beams in flatwise and edgewise positions. Compos Struct 2010;92(4):984–95.
[55] MATLAB. MATLAB version 9.9.0.1524771 (R2020b) Update 2. The Mathworks, Inc.: Natick, Massachusetts; 2020.
[56] Manalo A. Behaviour of fibre composite sandwich structures: A case study on railway sleeper application. In: Centre of excellence in engineered fibre composites, faculty of engineering and surveying. University of Southern Queensland; 2011. p. 305.

3.3. Links and implications

The investigation in Chapter 3 indicated that the lateral deformation behaviour of IRP systems with narrow discontinuity widths is mostly influenced by the host pipe, while that of the systems with wider discontinuity widths is primarily governed by the IRP. The failure mode of the IRP is attributed to the outward buckling of its crown between the edges of the host pipe discontinuity, regardless of its width. The analysis further revealed that the influence of the thickness and MOE of IRP on the lateral deformation behaviour is dependent upon the width of the host pipe discontinuity. Despite the cyclic nature of traffic load and its potential negative impact on the long-term performance of the repair system, Chapter 3 solely focused on the short-term behaviour. Therefore Chapter 4 focuses on the investigation of the bending fatigue behaviour of IRP systems under repeated traffic load.

CHAPTER 4: PAPER 2 – BENDING FATIGUE BEHAVIOUR OF INTERNAL PREPLACEMENT PIPE SYSTEMS

4.1. Introduction

Chapter 3 has demonstrated that the IRP systems in legacy pipes with narrow and wider circumferential discontinuities exhibit distinct structural performance under static bending. To ensure the long-term performance of IRP systems, their fatigue behaviour under the influence of repetitive traffic loading should also be evaluated. However, the available few experimental investigations of circumferentially cracked host pipes with repair systems under repeated traffic loading had exclusively utilised low-modulus CIPP liners or SAPL lining materials. Additionally, the available numerical models that examine the bending fatigue behaviour of repair systems have a certain limitation, as they do not account for the presence of discontinuities in the host pipes.

To ensure the long-term performance of IRP systems and to address Objective 2, the fatigue behaviour under the influence of repetitive traffic loading is evaluated in this Chapter. This study employed FE four-point bending simulations in conjunction with the stress-life approach to examine the flexural fatigue performance of IRP systems used for rehabilitating legacy pipes with discontinuities, under repetitive vehicular traffic loading. The study further assessed the impact of various design parameters, as identified in Chapter 3, on the bending fatigue response of IRP-repaired discontinuous host pipe segments. The investigated parameters were then ranked based on their relative contribution to the fatigue strength through multiple regression analysis. Section 4.2 contains a comprehensive description of the analysis and the outcomes.

Composite Structures 331 (2024) 117910

Contents lists available at ScienceDirect

Composite Structures

journal homepage: www.elsevier.com/locate/compstruct

Bending fatigue behaviour of internal replacement pipe systems

Shanika Kiriella [a], Allan Manalo [a], Cam Minh Tri Tien [a], Hamid Ahmadi [a,*], Patrick G. Dixon [b], Warna Karunasena [a], Ahmad Salah [a], Brad P. Wham [b]

[a] Centre for Future Materials, University of Southern Queensland, Toowoomba, QLD 4350, Australia
[b] Center for Infrastructure, Energy, and Space Testing, University of Colorado Boulder, CO 80309, United States

ARTICLE INFO

Keywords:
Internal replacement pipe (IRP)
Gas pipelines
Repetitive traffic loading
Finite element analysis
Stress-life method
Multiple regression analysis

ABSTRACT

Internal replacement pipe (IRP) systems are becoming an effective rehabilitation technique for legacy oil and gas pipelines with defects and discontinuities. Under repetitive traffic loads, the IRP-repaired pipes are subjected to fatigue. However, existing knowledge on the fatigue behaviour and remaining service life of IRP systems with circumferential discontinuities under cyclic bending is limited. Therefore, this paper investigated numerically the bending fatigue behaviour of legacy pipelines with circumferential discontinuities rehabilitated with IRP made from various material systems. The influence of the discontinuity width of the host pipe, thickness and elastic modulus of IRP, and level of traffic loading on the fatigue behaviour is evaluated. The results show that the tensile stress concentration at the discontinuity edge controls the bending fatigue behaviour of fully bonded IRP. The critical stresses and the minimum fatigue lifetimes are considerably influenced by the thickness and elastic modulus of the IRP systems, and the level of traffic loading while the width of the circumferential discontinuity has an insignificant effect. Multiple regression analyses show that the level of the traffic load has the most significant effect on the critical stress generated in the IRP, while the largest contribution to the minimum fatigue life comes from the elastic modulus of the repair material.

1. Introduction

Hydrocarbons, including crude oil, natural gas, and liquid petroleum products, are the primary sources of global energy and are directly related to economic growth [1]. Despite being the most common method of transporting oil and gas for over a century, pipelines, predominately composed of cast iron and steel, have the potential to fail during their service life for various reasons [2,3]. According to several studies [4–9], corrosion has been identified as the primary cause of pipeline failure, which can result in circumferential cracks and discontinuities in the host pipes [10]. Corrosion can result in a reduction in wall thickness, strength, and structural integrity of the pipes and can lead to accidents caused by leakage [6,11]. Circumferential cracks in buried pipelines can also be produced by external loadings such as earth load, traffic load, and soil movement [12]. The failure of gas and oil pipelines can lead to substantial financial losses for the energy industry and can cause irreversible damage to both human life and the environment [13]. Consequently, the rehabilitation of damaged pipelines is crucial to prevent them from exacerbating into more significant problems.

The traditional pipeline repair techniques mainly involve replacing the pipes via excavation [14,15]. However, due to financial concerns, it is usually preferable to repair damaged pipes using trenchless rehabilitation techniques rather than replacing them [16]. The internal replacement pipe (IRP) system is an advanced and efficient trenchless rehabilitation technology that has recently been integrated into the pipeline industry [17,18]. This repair method entails the installation of a new structural pipe inside existing legacy pipes which contain defects and discontinuities. During the installation process, the outer surface of IRP is bonded to the inside of the cleaned and prepared host pipe [19]. The implementation of IRP contributes to improving the strength, structural integrity and durability of the existing legacy pipes. However, the application of this technology in rehabilitating legacy gas pipelines has been limited due to the absence of established design procedures and design standards. Hence, it is essential to undertake an in-depth investigation of the structural performance of new and emerging IRP systems under different loading conditions.

* Corresponding author.
E-mail addresses: shanika.kiriella@unisq.edu.au (S. Kiriella), allan.manalo@unisq.edu.au (A. Manalo), camminhtri.tien@unisq.edu.au (C.M.T. Tien), hamid.ahmadi@unisq.edu.au (H. Ahmadi), padi9036@colorado.edu (P.G. Dixon), karu.karunasena@unisq.edu.au (W. Karunasena), ahmad.salah@unisq.edu.au (A. Salah), brad.wham@colorado.edu (B.P. Wham).

https://doi.org/10.1016/j.compstruct.2024.117910
Received 21 August 2023; Received in revised form 14 December 2023; Accepted 11 January 2024
Available online 17 January 2024

Dixon et al [20] have identified nine potential performance objectives that should be taken into consideration for the effective design of IRP systems for rehabilitating legacy gas pipelines. These objectives include cyclic in-service surface loads, lateral deformation, hoop stress, axial deformation, cross-sectional ovalization, puncture, debonding, service connections and compatibility with current and future gas compositions. According to the study conducted by Tafsirojjaman et al [17], cyclic in-service surface loads have been identified as a significant factor that impacts the performance of IRP systems. Repetitive surface loads often arise from overhead vehicular traffic [21] and might induce dynamic fatigue stresses, potentially resulting in the failure of the repair system [17,19,20,22–24]. Additionally, offshore pipelines are vulnerable to fluctuating loads initiated by waves and currents, resulting in catastrophic damage [25–30]. Fatigue can cause a material to accumulate damage, leading to cracking or complete failure at a stress lower than its ultimate strength [31,32]. A detailed understanding of fatigue behaviour and accurate life estimation of IRP systems, therefore, is an important aspect of IRP design and development.

Despite the significance of implementing safe design practices to prevent bending fatigue failure of IRP caused by repetitive surface loading, there is a lack of extensive research in this area. The existing experimental studies on the bending fatigue behaviour of circumferential discontinuities or joint repairs are restricted to a few repair systems, specifically those utilizing low-modulus CIPP liners or SAPL [19,22,23]. Jeon et al [22] studied the behaviour of a cured-in-place pipe (CIPP) lining system in cast iron (CI) host pipe with a complete circumferential crack subjected to repetitive heavy traffic loading over 50 years of design life. The test results showed that the internal vertical stiffness of the pipe lining decreased by approximately 75 % after 1 million cycles of deformation. Throughout the testing, the liner was able to endure relative displacement and rotation caused by heavy traffic loads at circumferential cracks without breaking. However, localized debonding between the interfaces of the CI host pipe and liner near the circumferential crack was observed. According to Jeon et al [22], this localised debonding right near the crack edge benefits the liner by improving flexibility and decreasing the stress concentration. Under a similar approach, Stewart et al [19] examined the performance of CI pipes with a joint repaired by a CIPP liner subjected to one million cycles of deflections, which was equivalent to traffic loading over 50 years of the service life. During the testing, the liner experienced the greatest relative deformation and rotation at the discontinuity of the CI pipe. However, the rotational stiffness of the system remained almost constant over one million cycles. Additionally, the level of deflection applied in these two studies [19,22] was estimated from an analytical model developed by Jeon et al [22] and O'Rourke et al [33], respectively under the assumption that the stiffness of the liner is negligible. Recent studies [17,20] have indicated that this simplification can lead to the underutilisation of relatively stiffer new and emerging IRP materials. Ha et al [23] performed a three-point cyclic bending test on a steel host pipe with a circumferential crack repaired using a polyurea-polyurethane spray-applied pipe lining (SAPL). During testing, the liner demonstrated a stiffness reduction but no indication of leakage or failure. However, the motivation behind the investigation conducted by Ha et al [23] was not explicitly stated as the traffic load. It can be noted that these previous works rely on expensive and time-consuming full-scale experiments and cover very limited parameters that can influence the fatigue behaviour of pipe liners in bending.

IRP repair systems are currently being developed employing a variety of materials such as polymers (both thermosets and thermoplastics), composites, and metallic materials [17,18]. Many investigations have demonstrated that the fatigue performance of these materials varies substantially due to the differences in their strength, stiffness, toughness and resistance to cracking and fracture [34–39]. As compared to composites and metals, most polymeric materials have lower tensile strength, modulus of elasticity (MOE), and toughness, which can have a major impact on their fatigue resistance [40–44]. FRP composites, on the other hand, can exhibit outstanding fatigue performance because of their high strength, and stiffness. [36,45]. In contrast to metal fatigue, the loss of stiffness in composite materials can be observed from the early stage of the fatigue loading process [46,47]. Further, compared to polymers, metallic materials have higher MOE and toughness, which contributes to their excellent fatigue performance [48]. However, metallic materials, are prone to corrosion, which may diminish their fatigue resistance over time [49]. Therefore, a detailed evaluation of the structural performance of IRP systems made from different materials is required to ensure that they will be in operation throughout their design life.

There are some attempts in doing numerical simulations of internal repair systems in the literature. Tafsirojjaman et al [17] conducted finite element analyses (FEA) to investigate the fatigue behaviour of an IRP alone subjected to repetitive vehicular traffic loads by utilising the stress-life approach. This study evaluated IRP materials with MOE ranging from 1 GPa (145 ksi) to 200 GPa (29,008 ksi) and repair thicknesses varying from 3.175 mm (0.125 in) to 25.4 mm (1 in), assuming a design life of one million cycles. The findings of this study showed that an increase in thickness and MOE of IRP can lead to a significant extension of the fatigue life. The influence of repair thickness, repair material, and discontinuity width on the static bending behaviour of IRP-repaired discontinuous legacy steel pipes exposed to surface load from vehicular traffic was studied by Kiriella et al [50]. The results of this initial study showed that when the discontinuity is narrow, the host pipe has the most effect on the lateral deformation behaviour of the system, while IRP has a larger influence when the discontinuity is wider. Additionally, the impact of the repair thickness and repair material on the lateral deformation behaviour is dependent upon the width of the host pipe discontinuity. Therefore, the findings of this study highlight the importance of conducting a numerical investigation to understand how different parameters affect the bending fatigue behaviour in the presence of host pipes with circumferential discontinuities.

Shou and Chen [51] and Yang et al [52] conducted numerical studies on CIPP-rehabilitated pipe subjected to bending caused by vehicular traffic loading, which was validated through full-scale experimental testing [53]. These studies developed three-dimensional FE models that incorporated surrounding soil. However, they did not account for the cyclic nature of the traffic loading and solely considered surface corrosion defects on the host pipe rather than full circumferential discontinuities. According to Yang et al [52], the thickness of the CIPP liner was identified as the most critical parameter affecting the stress development in the liner. In their respective studies, Brown et al [54] and Tien et al [18] investigated numerically the effect of the discontinuity edge of CI host pipe on the performance of a CIPP liner and a thermoplastic IRP, respectively, under internal pressure. These studies revealed that the application of internal pressure results in the concentration of axial stress in the repair pipe at the edge of the host pipe discontinuity. Tien et al [18] has further explained that this phenomenon occurs due to IRP curving around the host pipe discontinuity. However, the effect of discontinuity edge on stress concentration may vary depending on the loading condition. Therefore, it is necessary to investigate these effects under the cyclic bending condition.

The literature review reveals a scarcity of extensive numerical studies on the bending fatigue performance of IRP systems in the presence of legacy pipes with full circumferential discontinuities. Also, there is a lack of understanding of the potential effect of various design parameters on the bending fatigue behaviour of IRP systems, which is crucial for ensuring long-term structural integrity and reliability. Therefore, the present study investigated numerically the fatigue behaviour of IRP systems used for repairing host pipes with circumferential discontinuities at the midspan under repeated traffic loading. The investigation considered both the mechanical contribution of the IRP and the potential impact resulting from the presence of discontinuous legacy pipe segments. Additionally, the study also evaluated the influence of different parameters identified from previous studies, such as the

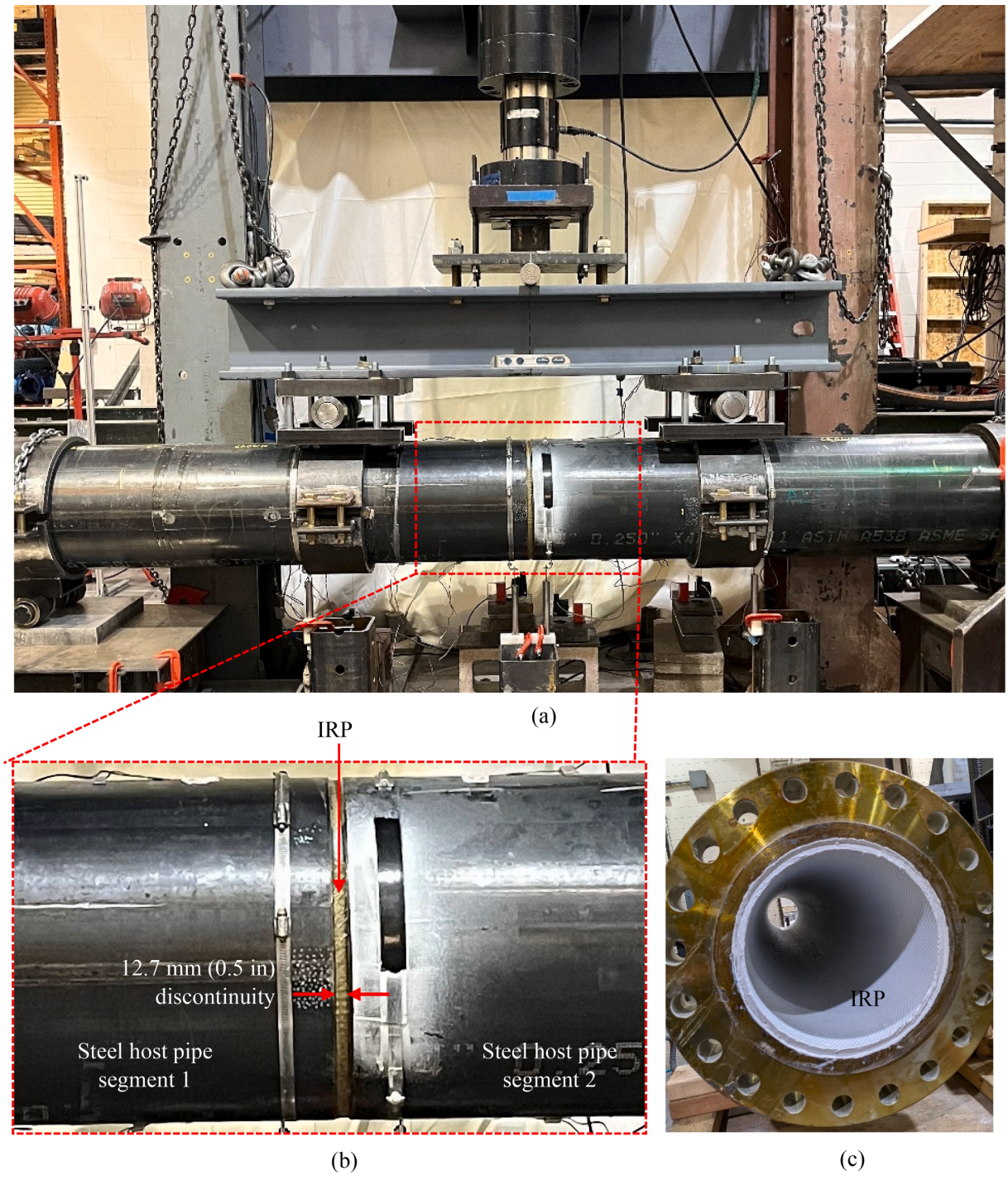

Fig. 1. (a) Actual experimental bending test setup of IRP installed in host pipe with a circumferential discontinuity at the midspan, (b) Longitudinal view of circumferential discontinuity and (c) Interior view of repaired steel pipe with IRP (CUB).

discontinuity width of the host pipe, thickness and MOE of the repair material, and level of loading on the bending fatigue performance of IRP-repaired discontinuous host pipe segments. Furthermore, the relative contribution of the investigated parameters to the critical stress and fatigue life of IRP in discontinuous host pipes during cyclic bending are also assessed using multiple regression analysis. The results of this study provide a detailed understanding of how key design parameters affect the fatigue behaviour of IRP systems, which enables their effective design, development, and field application.

2. Numerical modelling and analysis

2.1. Geometry, contact types and boundary conditions

Three-dimensional FE four-point bending simulations are carried out using ANSYS mechanical [55] to assess the fatigue performance of IRP systems under repetitive surface load from overhead traffic over 50 years of service life. These simulations are based on an experimental load configuration of 762–1016-762 mm (30–40-30 in) implemented at the University of Colorado Boulder (CUB), as illustrated in Fig. 1 and Fig. 2. The FE simulations include scenarios where the IRP is evaluated

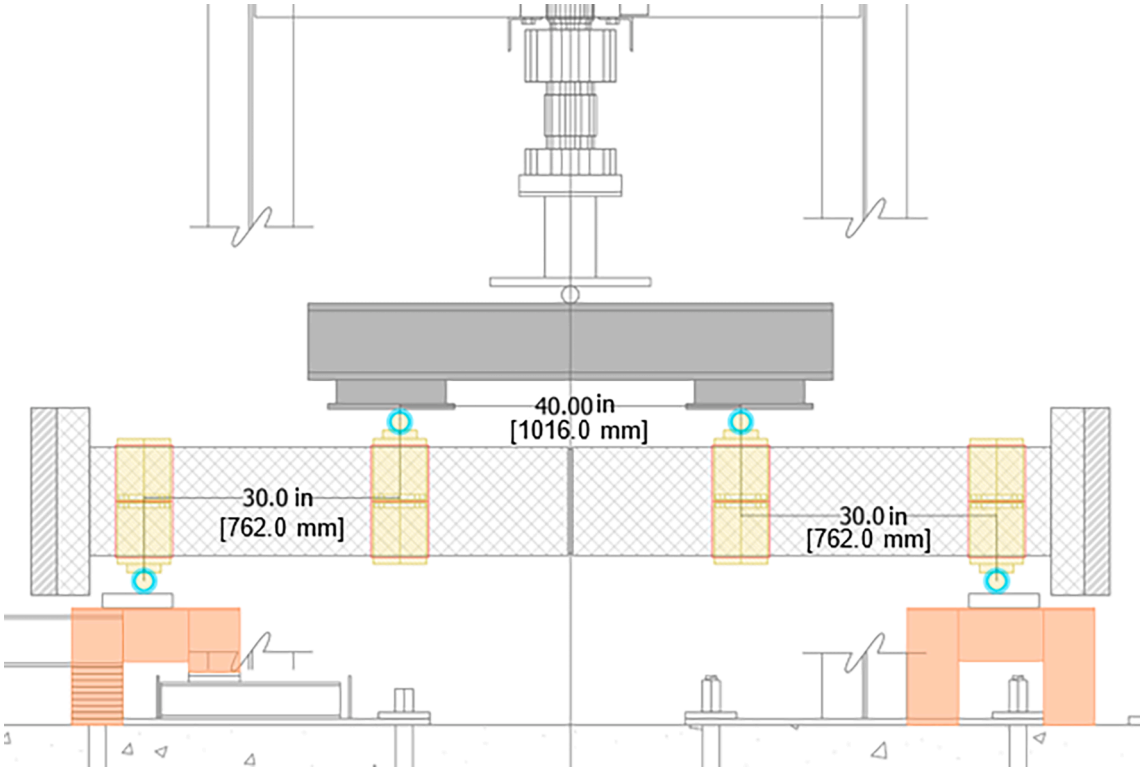

Fig. 2. Instrumentation schematic of bending test setup (CUB) [Units: in].

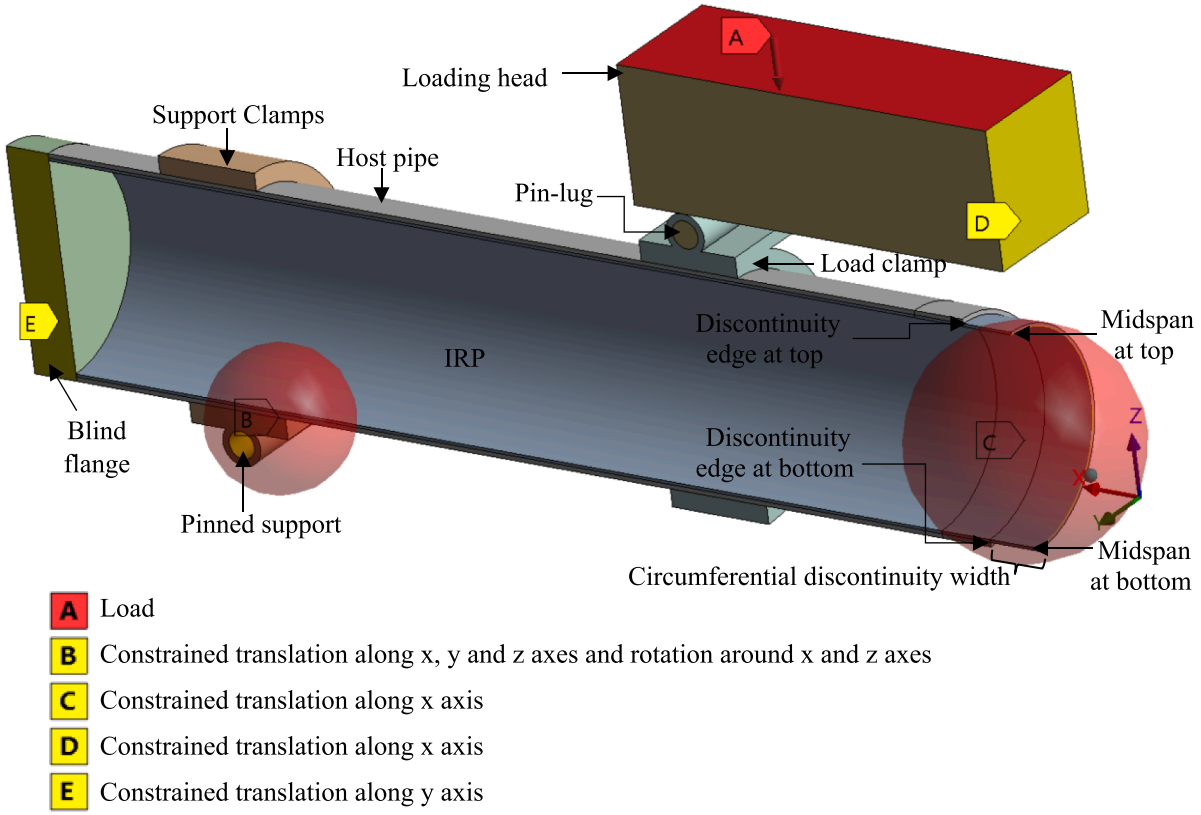

Fig. 3. (a) A quarter of the geometry of the FE model of an IRP installed in a host pipe with 152.4 mm (6 in) discontinuity at the midspan with loading and boundary conditions.

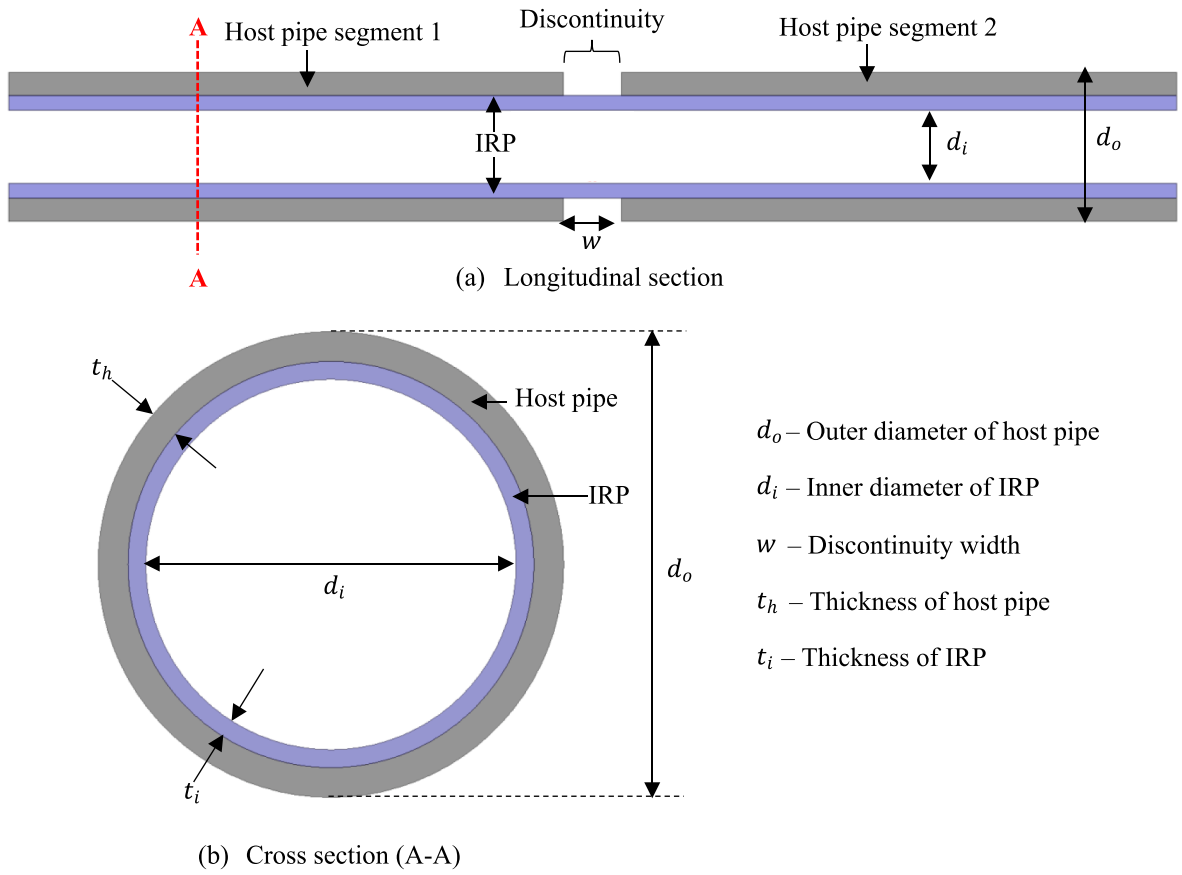

Fig. 4. Schematic diagram of IRP installed in discontinuous host pipe.

when it is alone, as well as when installed in a continuous (undamaged) host pipe and in a host pipe with a circumferential discontinuity at the midspan. To minimise computational time, only a quarter of the system is modelled considering symmetry, with appropriate boundary conditions applied (Fig. 3). Fig. 4 displays a schematic diagram of an IRP installed in a discontinuous host pipe. Throughout the investigation, the outer diameter and thickness of the host pipe are kept constant at 325.85 mm (12.83 in) and 6.35 mm (0.25 in), respectively [50]. The outer diameter of the IRP is defined by the inner diameter of the host pipe, which is 311.15 mm (12.25 in), and the thickness is assumed to be 4.115 mm (0.162 in). However, in the parametric study, the thickness of the IRP varies from 3.175 mm (0.125 in) to 9.525 mm (0.375 in). Further, the discontinuity widths of the host pipe considered are 12.7 mm (0.5 in), 25.4 mm (1 in), 50.8 mm (2 in), 101.6 mm (4 in), and 152.4 mm (6 in). The discontinuity width of 12.7 mm (0.5 in) reflects an axial pulled-out failure of a weak joint in a segmental legacy pipeline. This type of failure can be attributed to earthquake indued transient ground deformation and repetitive axial loading, which is typically induced by thermal expansion and contraction [22,56–58]. A discontinuity width of 152.4 mm (6 in) on the other hand indicates excessive deterioration of legacy pipelines caused by corrosion and ageing [10,59]. These parameters are selected based on a prior study conducted by Kiriella et al [50].

To accurately simulate the mechanical contacts within the experimental test setup, while avoiding any convergence issues, a pinned support with frictionless connection between the outer surface of the host pipe and the support clamp is used. The loading head is connected to another clamp using a pin-lug system. Both clamps have an inner diameter that matches the outer diameter of the host pipe, and their thickness measures 25.7 mm (1.01 in). Frictionless connections are used between the pin-lug and load clamp, as well as between the load clamp and host pipe. Additionally, a blind flange is used to seal the open end of the quarter model of pipe. The thickness of the blind flange is 66.5 mm (2.62 in), and its diameter is equal to the outer diameter of the host pipe. In the FE model, it is assumed that the host pipe and the IRP are adhered to each other along their entire interface using the bonded connection type available in ANSYS Mechanical. This contact type does not allow sliding or separation between faces or edges. The normal and tangential forces are very strong exerting resistance against the forces that may induce relative motion between surfaces. Bonded contact facilitates a linear solution as the contact length/area remains unchanged throughout the load application process. The test involves subjecting the IRP system to 14.8 kN (3.3 kips) of vehicular traffic loading, as determined by Klingaman et al [21] utilising the procedure recommended by Petersen et al [60] for evaluating the live load distribution to buried concrete culverts. This level of loading, which is repeated 1 million times, is equivalent to the traffic load that an IRP system is anticipated to experience over a service life of 50 years. Additionally, the parametric study involves varying levels of surface loads to further examine the effect of the loading magnitude on the repair system.

Table 1
Properties of IRP materials.

Material	MOE GPa	ksi	Poisson's ratio	Reference
Polymer	1.744	253	0.11	Mellott and Fatemi [62]
Thermoplastic	2.762	401	0.11	Mellott and Fatemi [62]
ALTRA10	3.739	542	0.23	Laboratory testing
GFRP-1	7.9	1,146	0.25	Zakaria et al [63]
GFRP-2	14.03	2,035	0.25	Huh et al [64]
GFRP-3	26.43	3,833	0.25	Huh et al [64]
GFRP-4	38.63	5,603	0.25	Huh et al [64]
CI	70	10,153	0.29	Seica and Packer [65]
Steel	200	29,008	0.29	Preedawiphat et al [66]

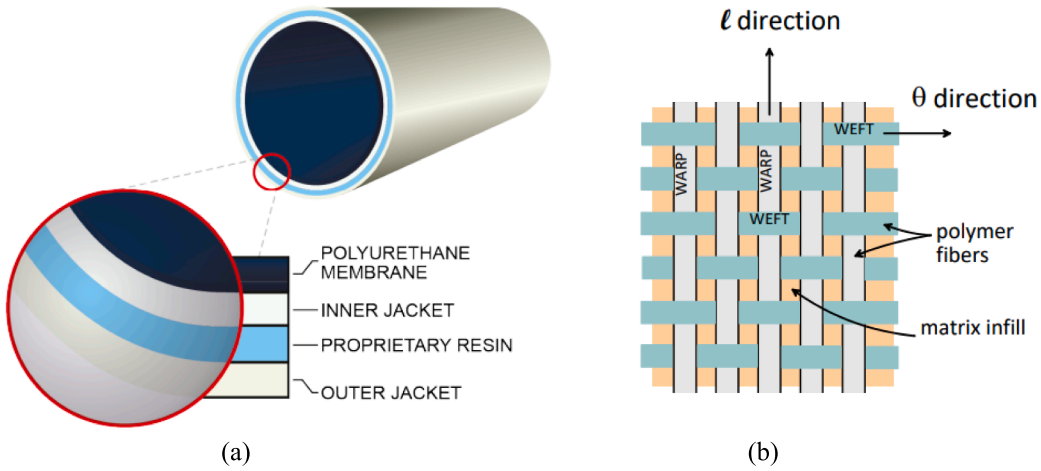

Fig. 5. Schematic of ALTRA10 (a) lining components and [68] warp and weft yarn pattern [67].

2.2. Element types and material properties

The entire system, which includes the IRP, host pipe, clamps and loading head, is modelled using the standard SOLID 186, a higher-order 3D solid element that comprises 20 nodes. Each node has three degrees of freedom, including movement in the x, y and z nodal directions and it also exhibits quadratic displacement behaviour. Additionally, the elements can undergo large deformation and strain, exhibit plasticity, display hyper-elasticity, experience stress stiffening and show creep behaviour [61]. Throughout the analysis, the host pipe is assigned as steel, whereas a variety of potential IRP materials are employed. As shown in Table 1, these IRP materials include polymers, composites and metallic materials. Additionally, steel is employed for all the remaining components of the setup, including clamps, lugs, pins, loading head and blind flange. It should be noted that if not specified, the IRP material used in the analyses is ALTRA10 structural lining supplied by Sanexen Environmental Services Inc. (Quebec, Canada). The analysis is carried out under the assumption of two design strain limits of the IRP material systems, which are 0.02 for polymeric and composites systems (MOE of 38.63 GPa/ 5,603 ksi or less) and 0.002 for metallic systems (MOE of 70 GPa/ 10,1523 ksi or greater). These design strain limits are based on the work of Tafsirojjaman et al [17].

Further information regarding the composition of the aforementioned IRP materials is provided below.

- Polymer – The material under consideration is a pure, unreinforced (neat) form of an impact polypropylene copolymer [62].
- Thermoplastic – The material under investigation is a blend of polypropylene and thermoplastic elastomers. The elastomer component constitutes approximately 25 % of the total weight of the material and contributes to its elasticity [62].
- ALTRA10 – This is formerly known as Aqua-Pipe® which is a commercial lining material developed by Sanexen Environmental Services Inc. (Quebec, Canada). This material is employed in the production of CIPP liners for rehabilitating water mains. As shown in Fig. 5a, ALTRA10 is an epoxy resin-impregnated lining consisting of an inner and outer layer each composed of seamless, circular woven fabric. Each layer of woven fabric consists of polyethylene thermoplastic yarn in the longitudinal (warp) direction and in the circumferential (weft) direction, as shown in the schematic in Fig. 5b. Comprehensive details regarding this lining material can be found in the publications by O'Rourke et al [67] and Matthews et al [68].

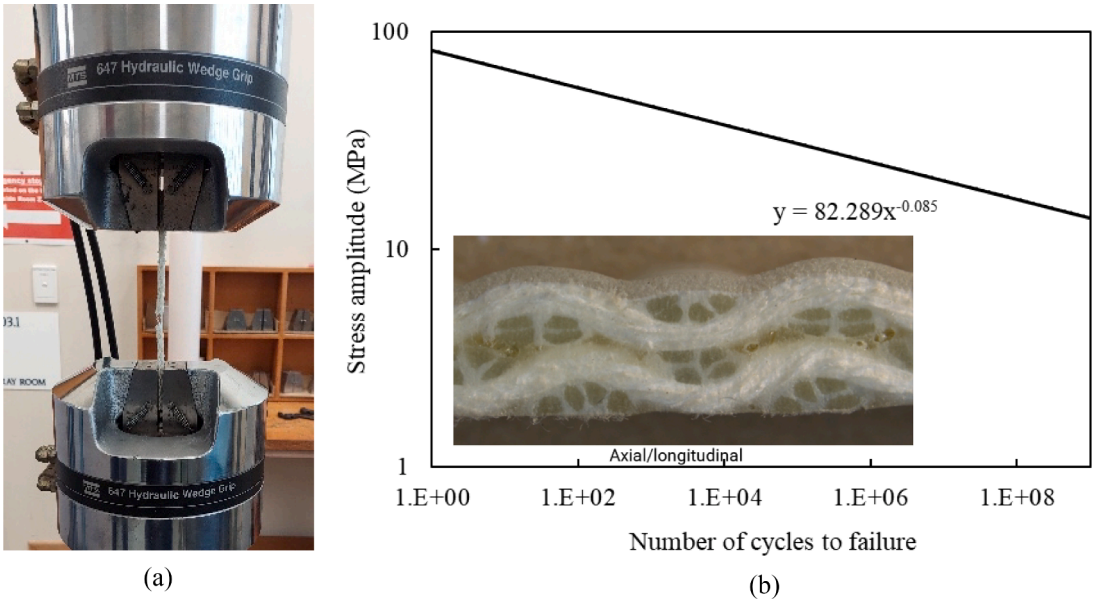

Fig. 6. (a) Tension-tension fatigue test (b) Stress-Life (S-N) curve of ALTRA10 IRP material (with mean stress correction).

Table 2
References that include S-N curves for IRP materials, along with their corresponding stress ratios.

Material	Stress ratio	Reference
Polymer	−1	Mellott and Fatemi [62]
Thermoplastic	−1	Mellott and Fatemi [62]
ALTRA10	0.1	Laboratory testing
GFRP-1	0.1	Zakaria et al [63]
GFRP-2	0.1	Huh et al [64]
GFRP-3	0.1	Huh et al [64]
GFRP-4	0.1	Huh et al [64]
CI	−1	Rausch et al [74]
Steel	−1	Gorash and MacKenzie [75]

- GFRP 1 – The composition of this material consists of unidirectional E-glass fibre and epoxy resin. The fibre orientation is 0/90° [63].
- GFRP 2 – This material is composed of E-glass fibre and epoxy resin, with a fibre orientation of ± 45° (Bidiagonal glass fibre) [64].
- GFRP 3 – This material is fabricated from E-glass fibre and epoxy resin. The fibres are oriented at an angle of 0 ± 45°, forming a triaxial glass fabric [64].
- GFRP 4 – This is a composite material made from E-glass fibre and epoxy resin. The fibres are oriented in a unidirectional manner, with a 0° angle[64].
- CI – The investigation employs a CI of ENGJL-270 grade, a type of cast iron that contains lamellar graphite, commonly referred to as grey iron [65].
- Steel – The type of structural steel utilised in this study is ASTM A36 [66].

2.3. Stress-life approach

There are three fundamental approaches for conducting fatigue analysis, including the stress-life approach, the strain-life method, and the crack growth method [69]. Considering that the projected design life for this investigation is one million cycles, the stress-life approach is utilized. This method is particularly appropriate for scenarios involving high-cycle fatigue, where materials experience cyclic loading primarily within their elastic range [70]. The stress-life approach is based on fatigue data represented by an S-N curve, which is derived from laboratory testing and does not account for crack initiation or growth [71]. By assuming a correlation between stress and expected fatigue life, the stress-life method calculates the life span of a structure or structural component based on its stress history and the S-N curve [72]. In the present study, the S-N curve of ALTRA10 repair material was established by performing laboratory tensile-tension fatigue testing in accordance with ASTM D 3479/D 3479 M [73], as shown in Fig. 6. The stress-life data for polymeric, thermoplastic, GFRP and metallic IRP materials were obtained from previously published journal papers, which are referenced in Table 2. The stress ratios (R) applied during the fatigue testing of these materials can also be found in Table 2.

The stress-life approach starts with calculating the stress values of the components of IRP under static loading. The study focuses on normal stress in the longitudinal direction (x-axis), as it is the dominant stress type during bending. The simulation of the fatigue resulting from cyclic loading is then performed using the fatigue tool, which calculates the effective alternating stress based on the magnitude of the maximum and minimum stresses. The amount of damage resulting from a stress cycle is influenced by the alternating stress and the mean stress [71,76]. As a result, the level of mean stress during a stress cycle is significant for the stress-life approach. In this study, the loading cycle being examined is

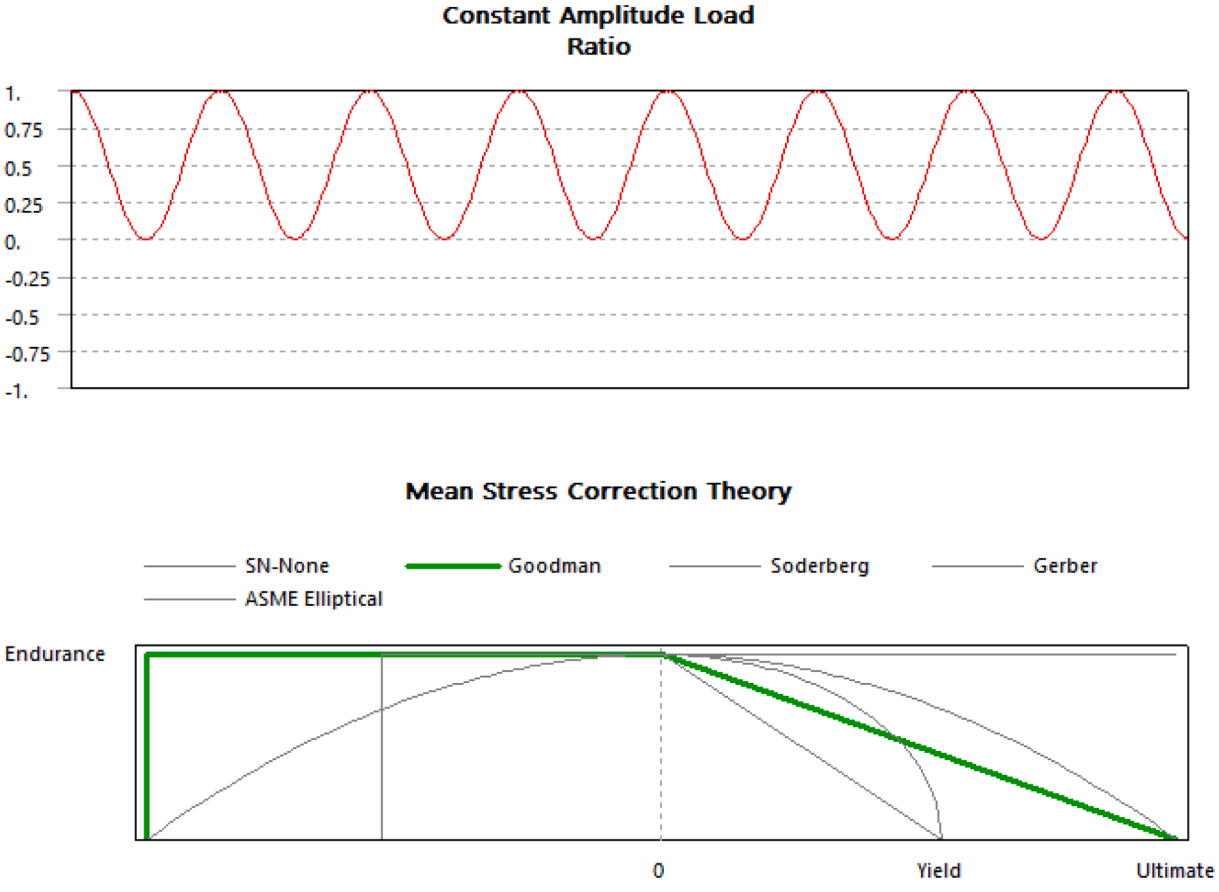

Fig. 7. Constant amplitude load ratio and mean stress correction theory applied in bending fatigue simulations.

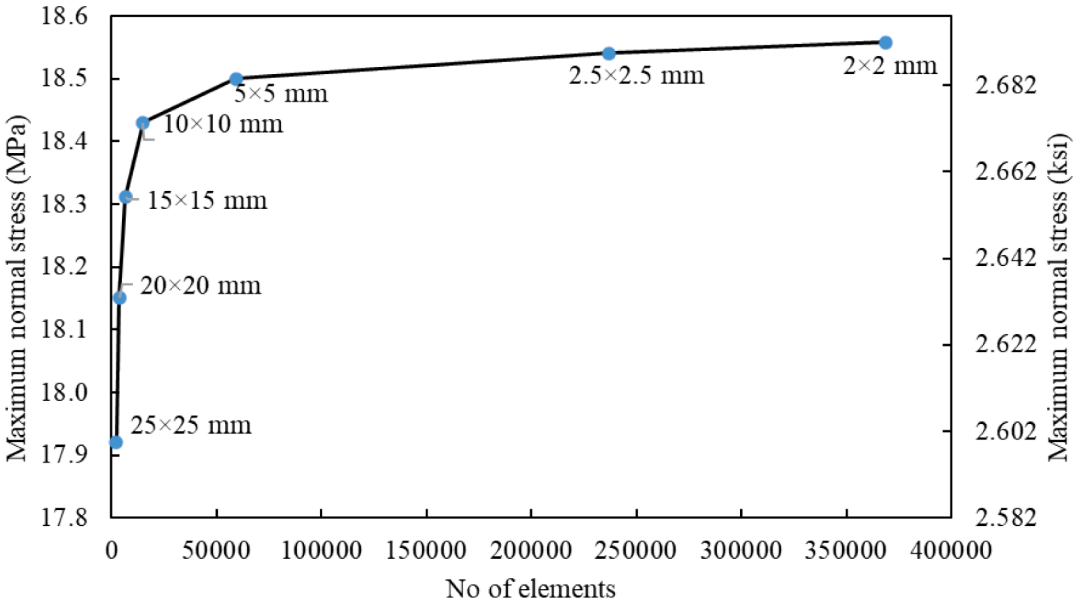

Fig. 8. Mesh convergence.

conducted under nonzero mean stress, and thus, the mean stress that arises is adjusted using a mean stress correction theory (Fig. 7). The Goodman mean stress theory (Eq. (1)) is applied to convert the applied stress cycle into an equivalent stress cycle with zero mean stress [36,71,77–80]. The corrected alternating stress (effective alternating stress) is then projected onto the S-N curve of the material to define the alternating stress at the failure and determine the corresponding life cycles.

$$\frac{S_a}{S_e}+\frac{S_m}{S_u}=1 \tag{1}$$

where S_a is the stress amplitude or alternating stress given by Eq.(2), S_e is the corrected alternating stress or effective alternating stress, S_m is the mean stress given by Eq.(3) and S_u is the ultimate tensile strength

$$S_a=\frac{S_{max}-S_{min}}{2} \tag{2}$$

$$S_m=\frac{S_{max}+S_{min}}{2} \tag{3}$$

where S_{max} is the maximum stress and S_{min} is the minimum stress.

2.4. Mesh convergence study and mesh refinement

A mesh convergence study is conducted to identify the optimal mesh size for producing reliable FEA results. The accuracy of numerical solutions is assessed by comparing the maximum normal stress generated by FEA with the maximum theoretical stress of 18.8 MPa (2.72 ksi) calculated using the bending stress formula (Eq. (4)) This is done by simulating an IRP pipe with a MOE of 3.739 GPa (542 ksi) under a traffic

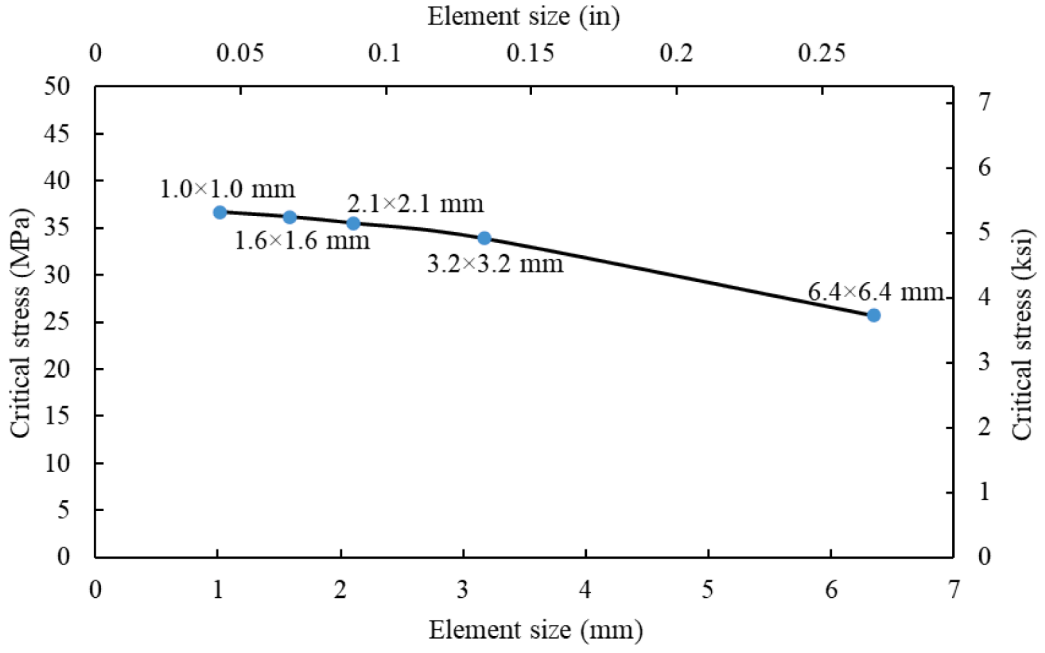

Fig. 9. Mesh sensitivity study for critical stress in refinement region.

Table 3
Number of elements in the compound section of host pipe and IRP with different discontinuity widths after mesh refinement.

Width of host pipe discontinuity		Number of elements in the compound section of the host pipe and IRP
mm	in	
12.7	0.5	209,061
25.4	1	208,761
50.8	2	207,861
101.6	4	206,361
152.4	6	204,861

loading of 14.8 kN (3.3 kips). The pipe used in the mesh convergence study has the same dimensions as the IRP outlined in section 2.1. The mesh size in the direction of thickness is set to three elements, and the surface element size of the pipe varies from coarse (25 × 25 mm or 0.984 × 0.984 in) to very fine (2 × 2 mm or 0.079 × 0.079 in). Fig. 8 displays the relationship between the maximum normal stress and the number of elements in the mesh of FEA models. The figure indicates that the accuracy of the FEA solution is within 1.6 % of the theoretical result when an element size of 5 × 5 mm (0.197 × 0.197 in) or smaller is employed.

$$\sigma = \frac{M}{S} \tag{4}$$

where σ is the bending stress, M is the bending moment, S is the section modulus of IRP.

A mesh sensitivity analysis was performed in order to determine the optimal surface element size for refining the mesh in the vicinity of the discontinuity edge of the host pipe, with the aim of accurately capturing potential stress concentrations (Fig. 9). For this, a steel host pipe with a 12.7 mm (0.5 in) wide discontinuity repaired using the same IRP that was employed for the mesh convergence discussed above is analyzed under traffic loading of 14.8 kN (3.3 kips). Taking into account the computational efficiency, the mesh is refined along a length equal to the width of the host pipe discontinuity and an additional 76.2 mm (3 in) beyond the edge of discontinuity. In sensitivity analysis, the surface

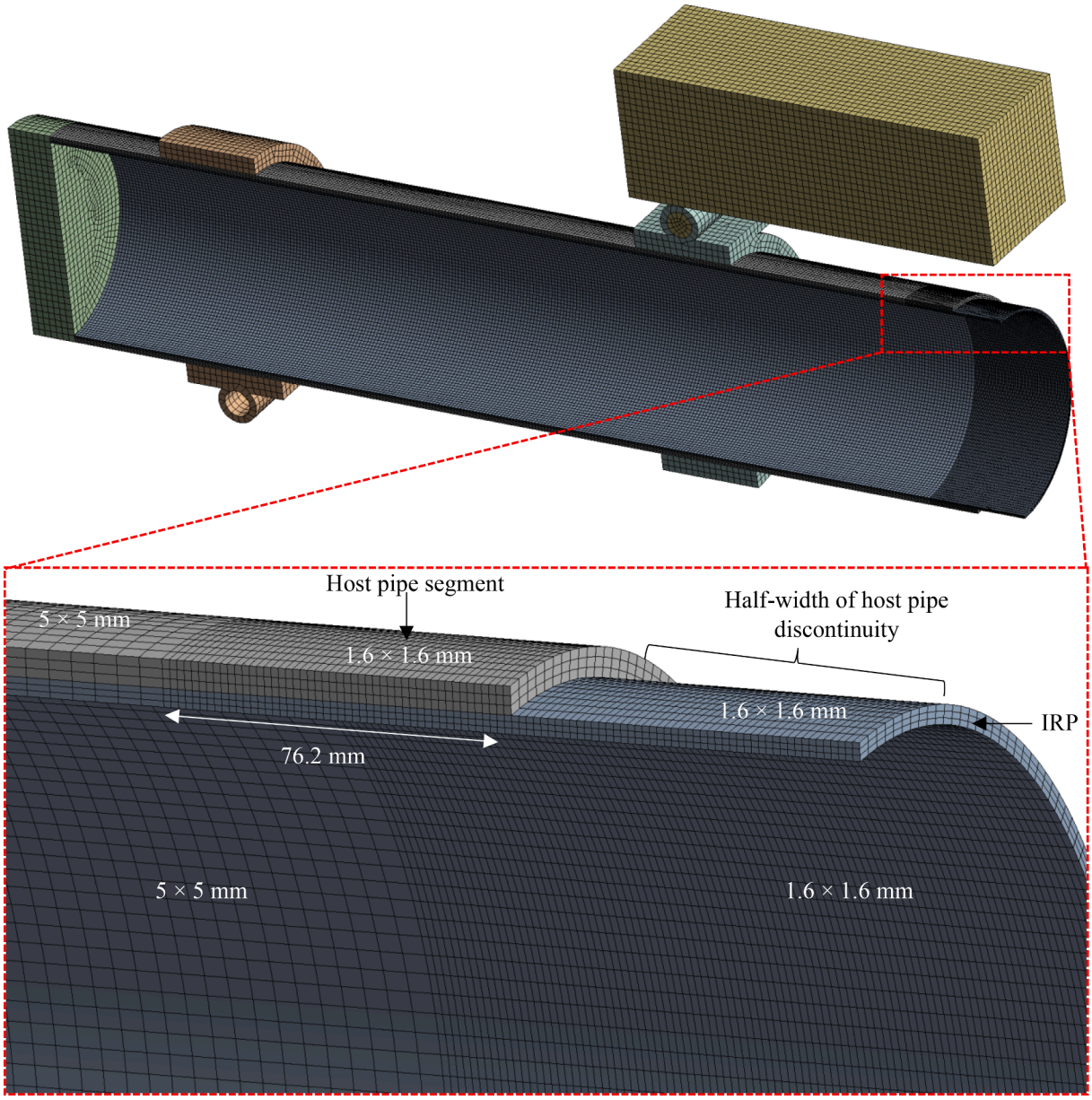

Fig. 10. Mesh refinement of quarter FE model of an IRP installed in host pipe with 152.4 mm (6 in) wide discontinuity.

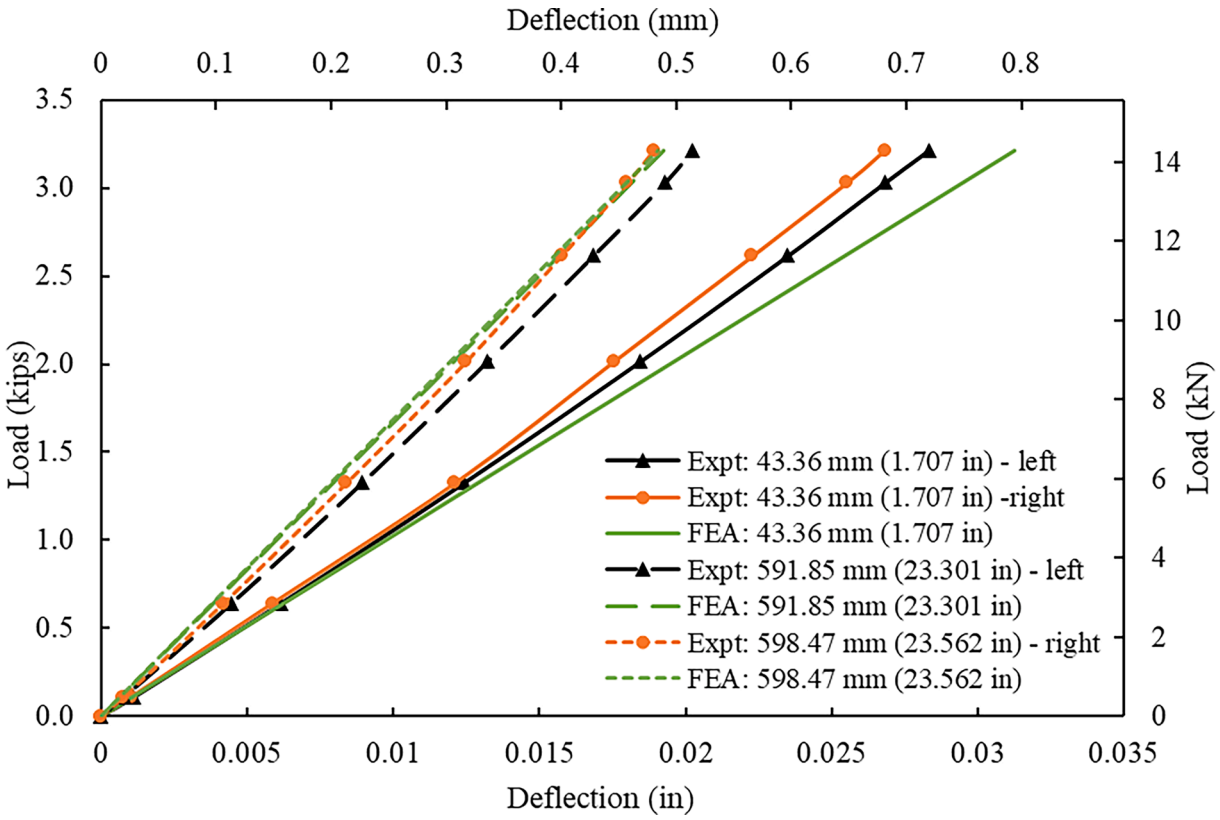

Fig. 11. Comparison between FEA and experimental load–deflection behaviours.

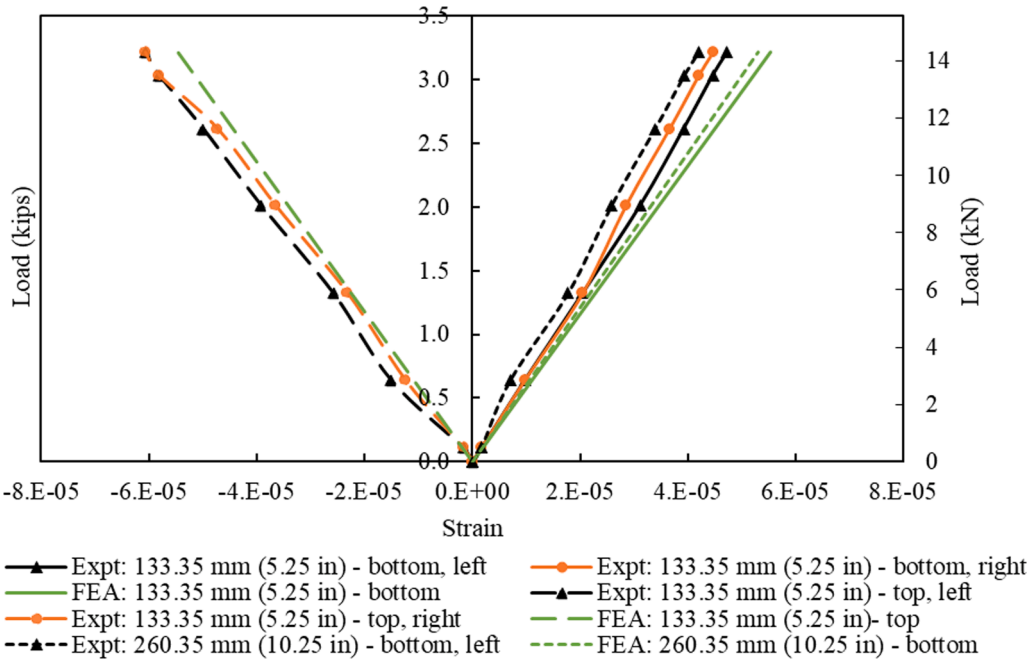

Fig. 12. Comparison between FEA and experimental load - strain behaviours.

element sizes of refined mesh are varied between 6.4 × 6.4 mm (0.252 × 0.252 in) and 1.0 mm × 1.0 mm (0.039 × 0.039 in). In areas outside of these refined regions, a 5 × 5 mm (0.197 × 0.197 in) element size is used. Fig. 9 illustrates the influence of different element sizes used for mesh refinement on the localized stress in the IRP at the edge of host pipe discontinuity. Accordingly, localized stress at the discontinuity edge begins to converge towards a finite value when a surface element size of less than 2.1 × 2.1 mm (0.083 × 0.083 in) is used. After considering the computational cost and the observation that the discrepancy in the local stress at the discontinuity edge between element sizes of 1.0 mm × 1.0 mm (0.039 × 0.039 in) and 1.6 × 1.6 mm (0.063 × 0.063 in) is within 2.0 %, it has been decided to select an element size of a 1.6 × 1.6 mm (0.063 × 0.063 in) for refining mesh. The selected element size is applied for refining the mesh across systems with varying

Table 4
Discrepancies in the maximum deformations observed between experimental data and FEA.

Location	Expt mm	in	FEA mm	in	Difference (%)
43.36 mm (1.707 in) from the midspan on the left-side section	7.19E-01	2.83E-02	7.94E-01	3.12E-02	9.4
43.36 mm (1.707 in) from the midspan on the right-side section	6.81E-01	2.68E-02	7.94E-01	3.12E-02	14.2
591.85 mm (23.301 in) from the midspan on the left-side section	5.14E-01	2.02E-02	4.89E-01	1.92E-02	4.9
598.47 mm (23.562 in) from the midspan on the right-side section	4.80E-01	1.89E-02	4.84E-01	1.91E-02	0.9

Table 5
Discrepancies in the maximum strains observed between experimental data and FEA.

Location	Expt mm	in	FEA mm	in	Difference (%)
133.35 mm (5.25 in) distance from the midspan at the bottom of the left-side section	1.20E-03	4.73E-05	1.41E-03	5.53E-05	14.5
133.35 mm (5.25 in) distance from the midspan at the bottom of the right-side section	1.13E-03	4.46E-05	1.41E-03	5.53E-05	19.3
133.35 mm (5.25 in) distance from the midspan at the top of the left-side section	−1.54E-03	−6.07E-05	−1.39E-03	−5.46E-05	10.1
133.35 mm (5.25 in) distance from the midspan at the top of the right-side section	−1.54E-03	−6.07E-05	−1.39E-03	−5.46E-05	10.1
260.35 mm (10.25 in) distance from the midspan at the bottom of the left-side section	1.07E-03	4.19E-05	1.35E-03	5.30E-05	20.9

discontinuity widths. Table 3 presents the total number of elements found in the compound section of the host pipe and IRP after mesh refinement. The mesh refinement of a quarter symmetry model of an IRP installed in a host with 152.4 mm (6 in) wide discontinuity is shown in Fig. 10.

2.5. Validation of the FE model

The FEA results are validated using the outcomes from a laboratory experiment conducted by CUB to ensure the accuracy of the model. This involves comparing the FE and experimental load–deflection (Fig. 11), and load–strain (Fig. 12) behaviours at different locations at the bottom (tension side) and top (compression side) of an ALTRA10 IRP in a steel host pipe with a discontinuity width of 12.7 mm (0.5 in) under a traffic load of 14.3 kN (3.2 kips). Fig. 11 demonstrates a good correlation between FEA and experimental load–deflection behaviours, with a maximum deviation of 14.2 % at 43.36 mm (1.707 in) from the midspan on the right-side section (Table 4). (It should be noted that the absence of a strain gauge at the midspan is due to the difficulty encountered during installation, primarily resulting from the limited width of discontinuity). As shown in Fig. 12, the FEA load–strain behaviour agrees well with the corresponding experimental results, with maximum variations of 20.8 % at 260.35 mm (10.25 in) distance from the midspan at the bottom of the left-side section (Table 5).

2.6. Hot-spot stress for calculating stress concentration

Hot-spot stress (HSS) is widely recognized as an appropriate measure for the maximum stress at a discontinuity of a segment, which can be applicable for fatigue analysis of IRP systems installed in host pipes with discontinuities. To determine HSS, it is necessary to compute the surface stress field in the immediate vicinity of the edge of the discontinuity [81]. Extrapolation procedures are then applied to specific pre-defined stress evaluation points to obtain HSS [82]. Based on the study conducted by Haghpanahi and Pirali [83], which focuses on acrylic tubular joints without weld fillet, as well as the extrapolation rules proposed by the international institute of welding (IIW), it has been selected that the initial extrapolation point should be positioned at a distance of 0.4 times the thickness of IRP from the edge of discontinuity and the second point is chosen to be located 0.6 times the thickness of IRP beyond the first point [84]. The HSS is determined by performing a linear extrapolation of the geometric stress at these two specified points to the edge of discontinuity. The process is illustrated in Fig. 13 and can be mathematically represented by Eq. (5).

where t_i is the thickness of IRP, σ_{hs} is the HSS, $\sigma_{0.4t_i}$ is the stress at a distance of 0.4 times the thickness of IRP from the edge of discontinuity and $\sigma_{1.0t_i}$ is the stress at a distance of 0.6 times the thickness of IRP beyond the first point.

$$\sigma_{hs} = 1.67\sigma_{0.4t_i} - 0.67\sigma_{1.0t_i} \tag{5}$$

Fig. 14 shows a comparison between the HSS and localized FE stress in the tension side of IRP at the edge of host pipe discontinuity. According to this figure, the HSS and the localized stress at the discontinuity edge follow a similar trend as the discontinuity width increases. It has been observed that the maximum difference between the HSS and the localized FE stress is less than 10 %, which is considered insignificant for this type of problem. While determining fatigue life using the HSS approach is not very time-consuming when analyzing a limited number of cases, it becomes more complex and time-consuming when dealing with a large number of different scenarios in parametric studies. This is because the use of the HSS approach requires manual calculation of the effective alternating stress and the corresponding fatigue life. Alternatively, by utilizing the local stress approach, the ANSYS fatigue tool can provide a direct measurement of the fatigue life, eliminating the need for manual calculations. Although local stress may be slightly over-conservative (within 10 % of HSS), it can still be considered a reasonable estimate. Consequently, the local stress approach is selected over the HSS approach for fatigue analysis of this study as it balances practicality with accuracy, efficiently fulfilling the analysis requirements.

3. Results and discussion

3.1. Effect of discontinuity width

The stress distribution over the length from the loading point to the midspan at the top (compression side) and bottom of IRP (tension side) in the presence of host pipe having a discontinuity width of 12.7 mm (0.5 in) under traffic load of 14.8 kN (3.3 kips) is compared in Fig. 15. The results indicate that a significant stress concentration arises at the edge of circumferential discontinuity at both the top and bottom of the IRP due to the abrupt change in cross-section caused by the presence of damaged host pipe segments (Fig. 16). This stress concentration decreases nonlinearly from the discontinuity edge to the midspan. The stress developed at the discontinuity edge at the tension side and compression side is 24.5 % and 16.3 % higher, respectively, than the

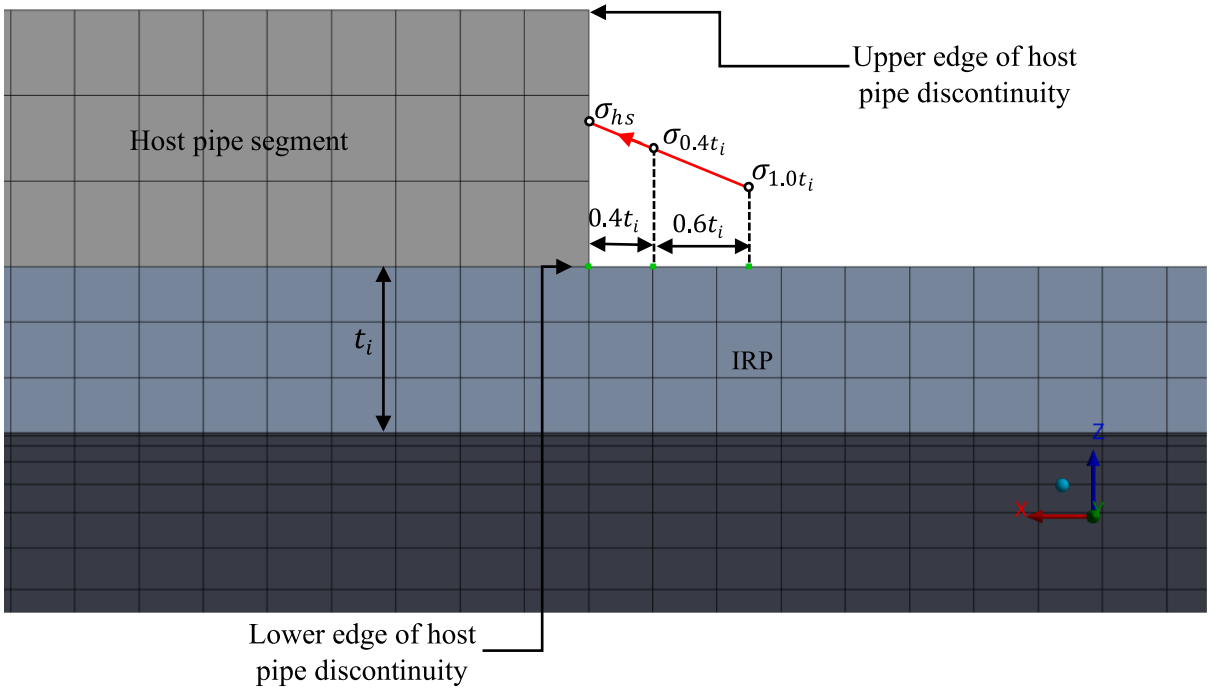

Fig. 13. Extraction of HSS from FE model using the linear extrapolation method.

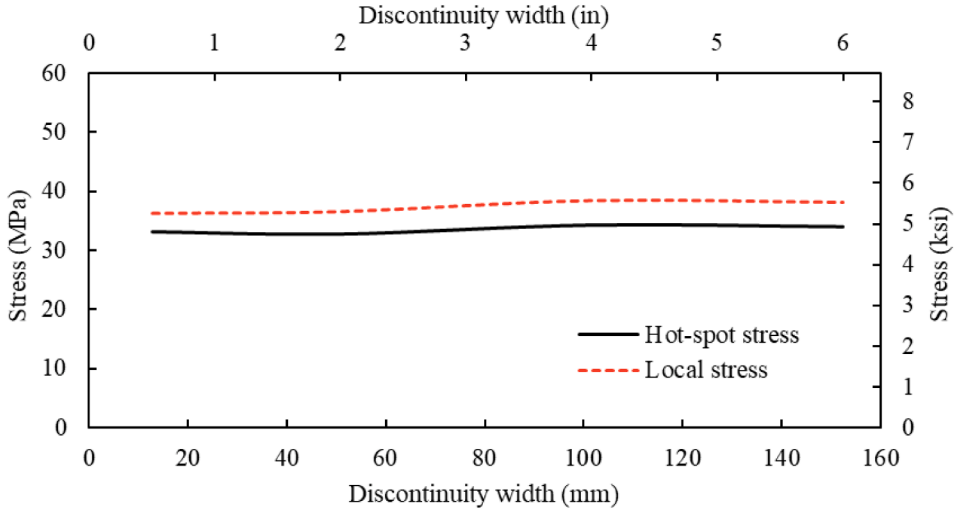

Fig. 14. Comparison of HSS and localized FE stress in the tension side of IRP at the edge of host pipe discontinuity.

stress developed at the midspan at the tension side and compression (Fig. 17). Note that in order to facilitate clear visualisation of stress distribution of IRP in the region of host pipe discontinuity, the host pipe segments have been temporarily hidden in Fig. 17. It can also be observed that the stress at the discontinuity edge at the crown of IRP is 5.6 % lower than that at the bottom. This observation highlights that stress concentration is much higher at the discontinuity edge at the bottom of IRP and can potentially control their fatigue failure/minimum fatigue life. It is desirable therefore to minimise stress concentration to prevent premature fatigue failure under cyclic bending when designing an IRP system for a host pipe with such discontinuities. According to Tien et al [18], the stress concentration issue could be addressed by introducing an appropriate unbonded length at the discontinuity edges. When subjected to bending, the unbonded length may allow the portion of the IRP that is not attached to the host pipe to move relative to the host pipe, thereby reducing stress concentration and extending fatigue life compared to the fully bonded condition.

The fatigue life contour plot of IRP around the midspan is shown in Fig. 18. Table 6 provides a summary of the fatigue life cycles at different locations of IRP. Based on the observations, it is evident that this IRP system has a minimum lifespan exceeding one million cycles. This suggests that even if the discontinuity edges of the host pipe segments cause stress concentration in IRP, the system will not fail before reaching its intended design life. This demonstrates that a thickness of 4.115 mm (0.162 in) and MOE of 3.739 GPa (542 ksi) are sufficient to safely withstand repeated traffic loads of 14.8 kN (3.3 kips) exerted for one million cycles of design fatigue life. In Fig. 19, the percentage of stiffness retained by ALTRA10 repair material is shown against the number of loading cycles at the three different applied alternating stress levels during the laboratory tension–tension fatigue tests of coupons. By extrapolating (linear) this dataset, considering a design life of 1 million cyles and maximum alternating stress obtained through FEA, it is

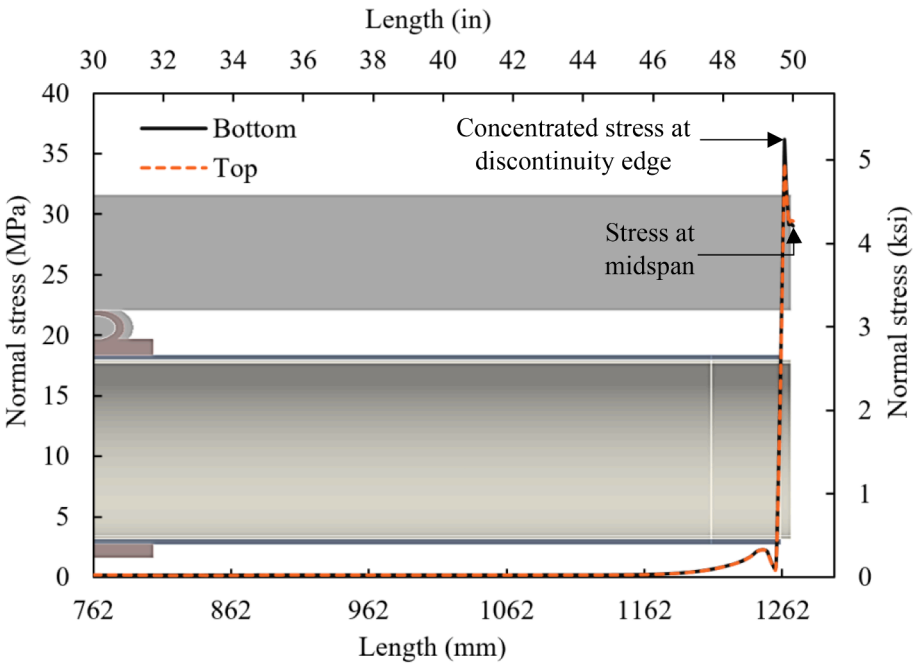

Fig. 15. Stress along the top (compression side) and bottom (tension side) of IRP from loading point to midspan.

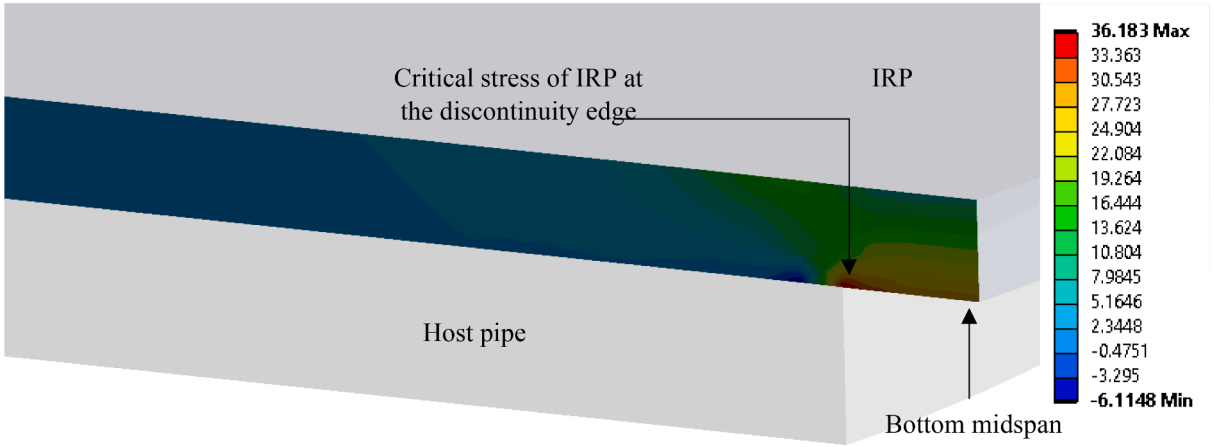

Fig. 16. Normal stress distribution along the x-axis at the bottom of IRP [units: MPa].

evident that even if the repair system would not fail at the design life under the imposed traffic load, its stiffness will degrade by 38.8 %. This finding is consistent with prior research [22,23], which demonstrated that while the CIPP repair system did not fail, stiffness loss could be observed under repetitive traffic loadings. However, this reduction in stiffness is significantly impacted by the stress concentration at the discontinuity edge.

Fig. 20 compares the stress in IRP at the midspan and at the edge of the host pipe discontinuity for different discontinuity widths, including zero (continuous host pipe), 12.7 mm (0.5 in), 25.4 mm (1 in), 50.8 mm (2 in), 101.6 mm (4 in), 152.4 mm (6 in) under the traffic load. Accordingly, when there is no damage in the host pipe, the maximum stress in the IRP is only 0.2 MPa (0.03 ksi) and is developed at the bottom midspan. This maximum stress is 98.1 % lower than the highest stress of the overall undamaged system, which occurs at the bottom midspan of the host pipe (Fig. 21a and b). This means that the presence of the continuous host pipe can stabilise the stresses generated in the IRP under repetitive lateral loading. Moreover, the minimum fatigue life of this IRP in a continuous host pipe system exceeds one billion cycles. When compared to the maximum stress that develops in an IRP installed in a continuous host pipe, the critical stresses generated in IRPs at the edges of host pipe discontinuities are 176.2 times higher. This demonstrates that while the continuous portion of the host pipe stabilises the stresses that develop in the IRP, the circumferential discontinuity induces the stress concentration in the repair pipe, potentially leading to fatigue failure. However, the stress concentration at the discontinuity edge, which controls the minimum fatigue life of the IRP in damaged host pipe systems, is almost the same for all discontinuity widths, with a maximum deviation of 5.0 %. The result indicates that the stress concentration in IRP at the discontinuity edge is independent of the width of the discontinuity. This is because, regardless of the discontinuity widths, the reduction in cross-sectional area at the discontinuity edge remains constant. Therefore, irrespective of the width of the host pipe discontinuity, when the same internal force is transmitted across the cross-sectional area at the discontinuity edge, the stress flow lines become denser (Fig. 22) by the same amount, resulting in constant stress amplification. Due to this, fatigue failure of IRP in fully bonded IRP systems with different discontinuity widths might occur at almost the same service life (Fig. 23). Under the imposed traffic load in the current study, the IRP systems for all discontinuity widths investigated will

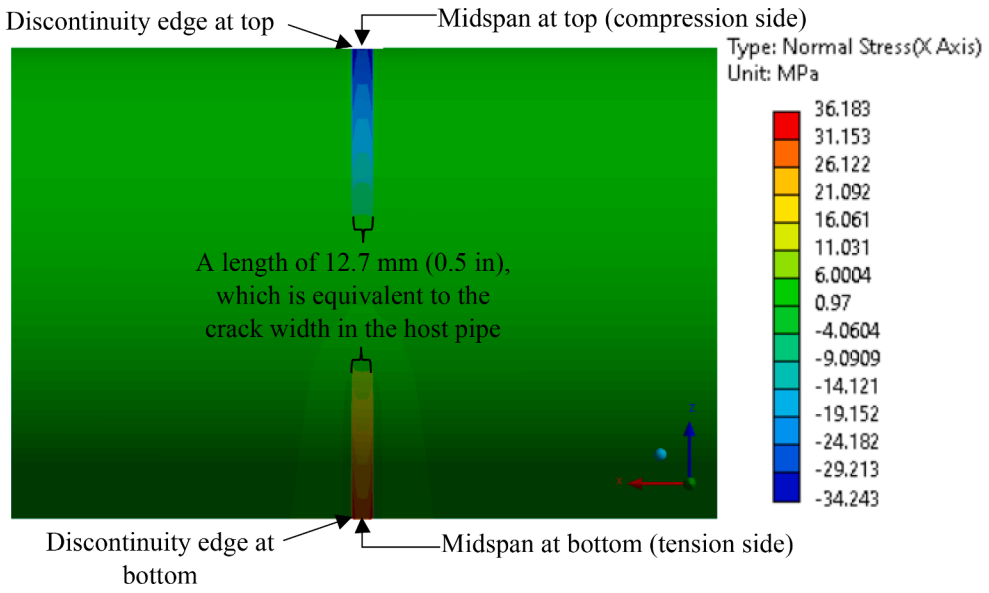

Fig. 17. Stress at the discontinuity edge and midspan at the top and bottom of IRP in host pipe with 0.5 in discontinuity width under bending (host pipe segments are temporarily hidden).

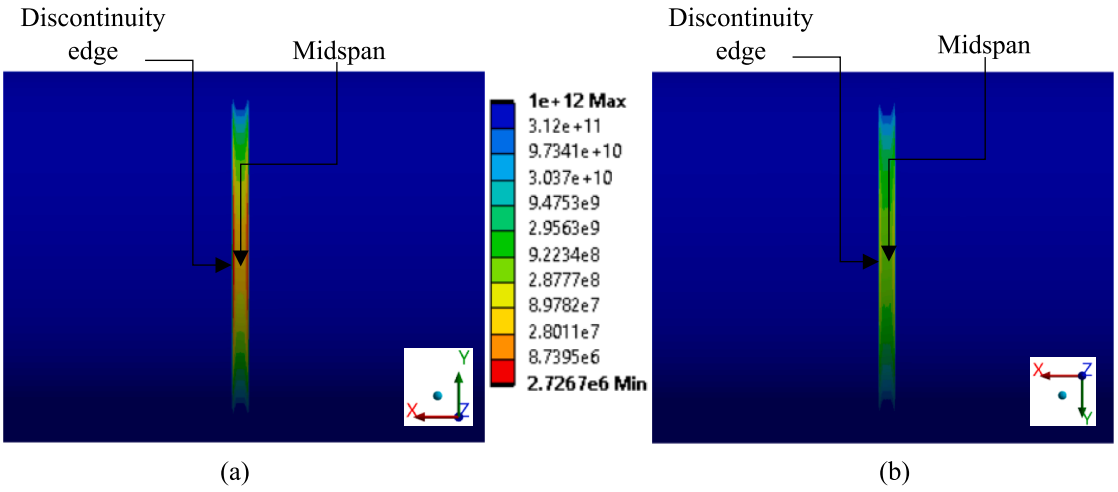

Fig. 18. Fatigue life contour plot (a) bottom (b) top of IRP at midspan (host pipe segments are temporarily hidden).

Table 6
Fatigue life at different locations of IRP.

Location	Fatigue life cycles
Discontinuity edge at the tension side of IRP	2.727e + 006
Discontinuity edge at the compression side of IRP	6.711e + 007
Midspan at the tension side of IRP	9.489e + 007
Midspan edge at the compression side of IRP	5.568e + 008

exceed the design life of one million cycles, according to the Fig. 23. To investigate the influence of other parameters, a discontinuity width of 12.7 mm (0.5 in) is employed since the minimum fatigue life of IRP is not significantly affected by the width of host pipe discontinuity.

Fig. 20 shows that increasing the discontinuity width from zero (continuous host pipe) to 12.7 mm (0.5 in) raises the stress at the midspan of IRP by 137 times. This indicates that stress concentration in IRP caused by a discontinuous host pipe segment leads to a substantial increase in the stress level at the midspan, particularly when the discontinuity width is narrower. However, stress at the midspan exhibits a nonlinear decrease as the discontinuity width increases from 12.7 mm (0.5 in) to 25.4 mm (1 in), followed by a linear reduction until the discontinuity width approaches 152.4 mm (6 in). Also, the midspan of the IRP experiences 41.1 % higher stress when the discontinuity width is 12.7 mm (0.5 in) compared to the system with a discontinuity width of 152.4 mm (6 in). Furthermore, as depicted in Fig. 24, unlike the system with a discontinuity width of 12.7 mm (0.5 in), in the system with a discontinuity width of 152.4 mm (6 in), the concentrated stress in IRP dissipates significantly over a length of 26.2 mm (1 in.) form the discontinuity edge before reaching a stable state that persists until midspan. The observed behaviour may be related to the fact that, as the width of circumferential discontinuity in the host pipe increases, the stress flow lines, which were densely packed together in IRP at the discontinuity edge, become more evenly distributed as they move away from the transition zone towards the midspan. This results in a greater reduction in localised stresses. On the other hand, when the discontinuity widths are relatively small, these widths may not be adequate for the densely packed stress flow lines to be uniformly distributed as they move towards the midspan. Consequently, the reduction in localised stress is diminished. Subsequently, if the discontinuity width reduces, there will be a substantial decline in the associated fatigue life at the

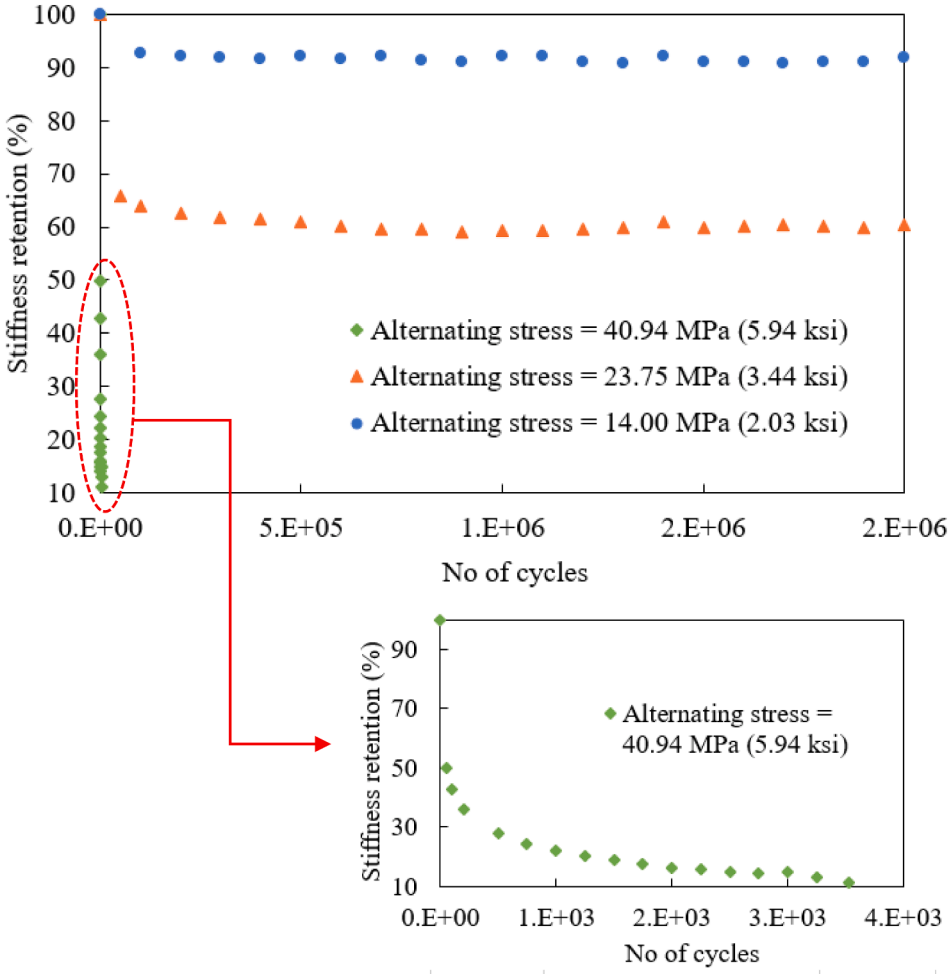

Fig. 19. Percentage stiffness retention of ALTRA10 coupons against the number of loading cycles at the three different applied alternating stress levels during the laboratory tension–tension fatigue tests.

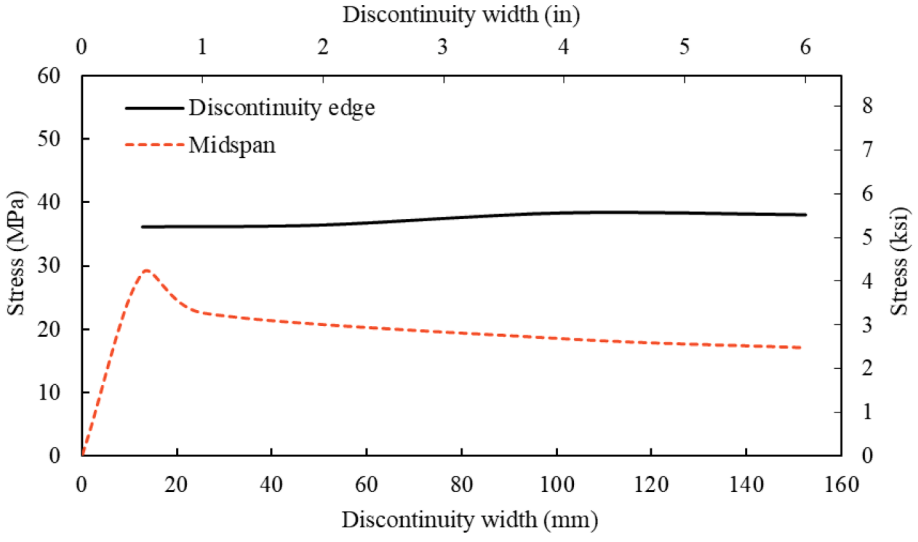

Fig. 20. Stress in IRP at the discontinuity edge and midspan at the bottom under a cyclic load of 14.8 kN (3.3 kips).

midspan (Fig. 23).

Fig. 25 shows the increase in stresses at the discontinuity edge and midspan of the compound IRP systems with varying discontinuity widths, relative to the maximum stress generated in IRP alone. Under the same load, the critical stresses in IRPs installed in discontinuous host pipe segments are around 120 times greater than the maximum stress developed in an IRP alone. The findings indicate that the service life of the IRP can be significantly reduced due to the presence of the host pipe

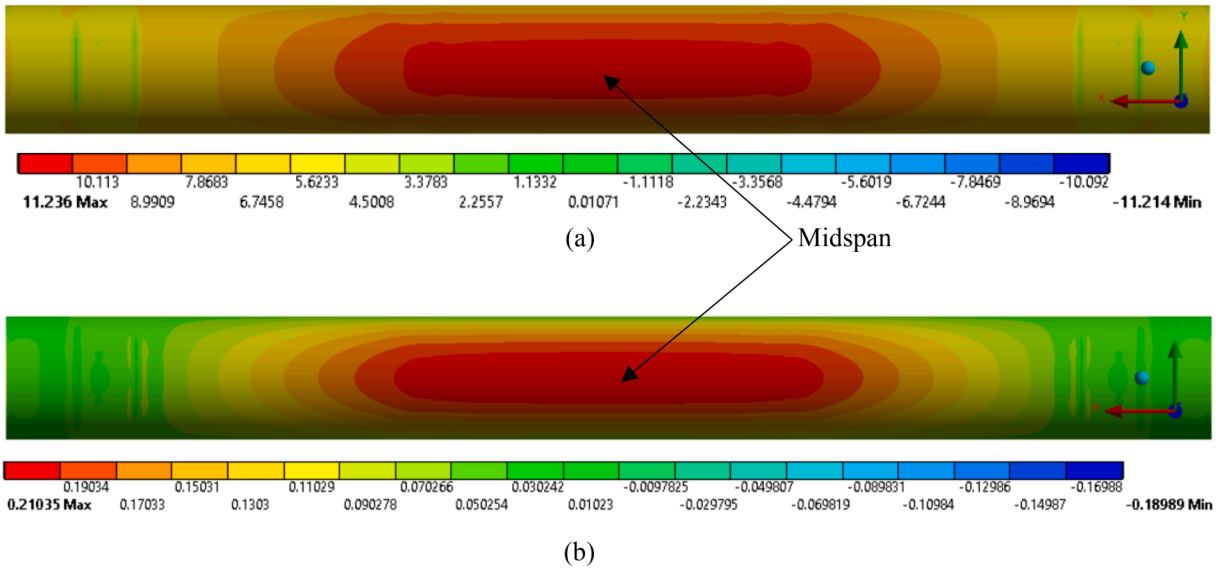

Fig. 21. Normal stress (x-axis) at the bottom of (a) continuous host pipe (b) IRP of the continuous host pipe repaired with IRP system under traffic loading [units: MPa].

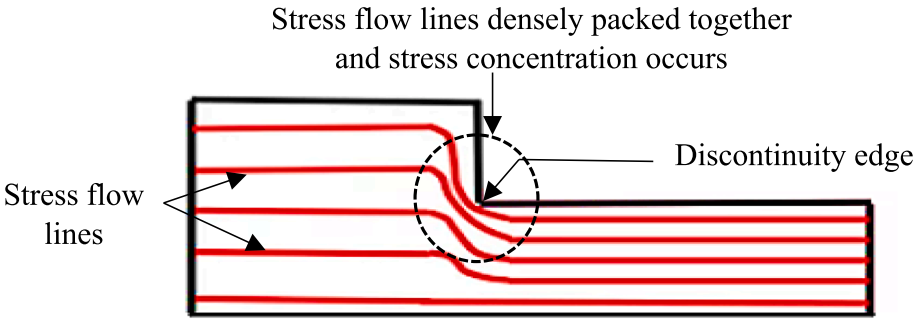

Fig. 22. Stress flow lines and stress concentration.

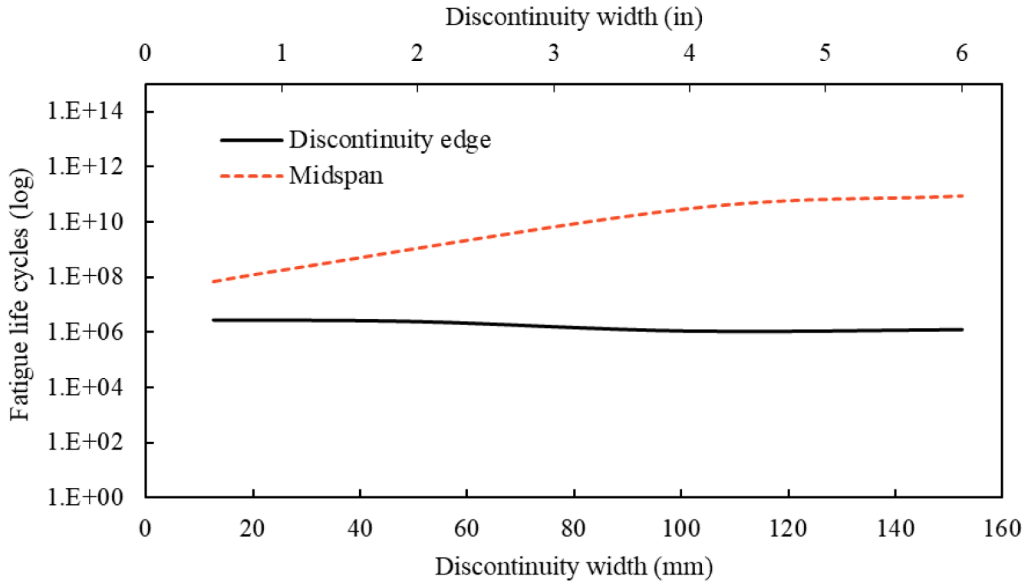

Fig. 23. Fatigue life at the discontinuity edge and midspan at the bottom under a cyclic load of 14.8 kN (3.3 kips).

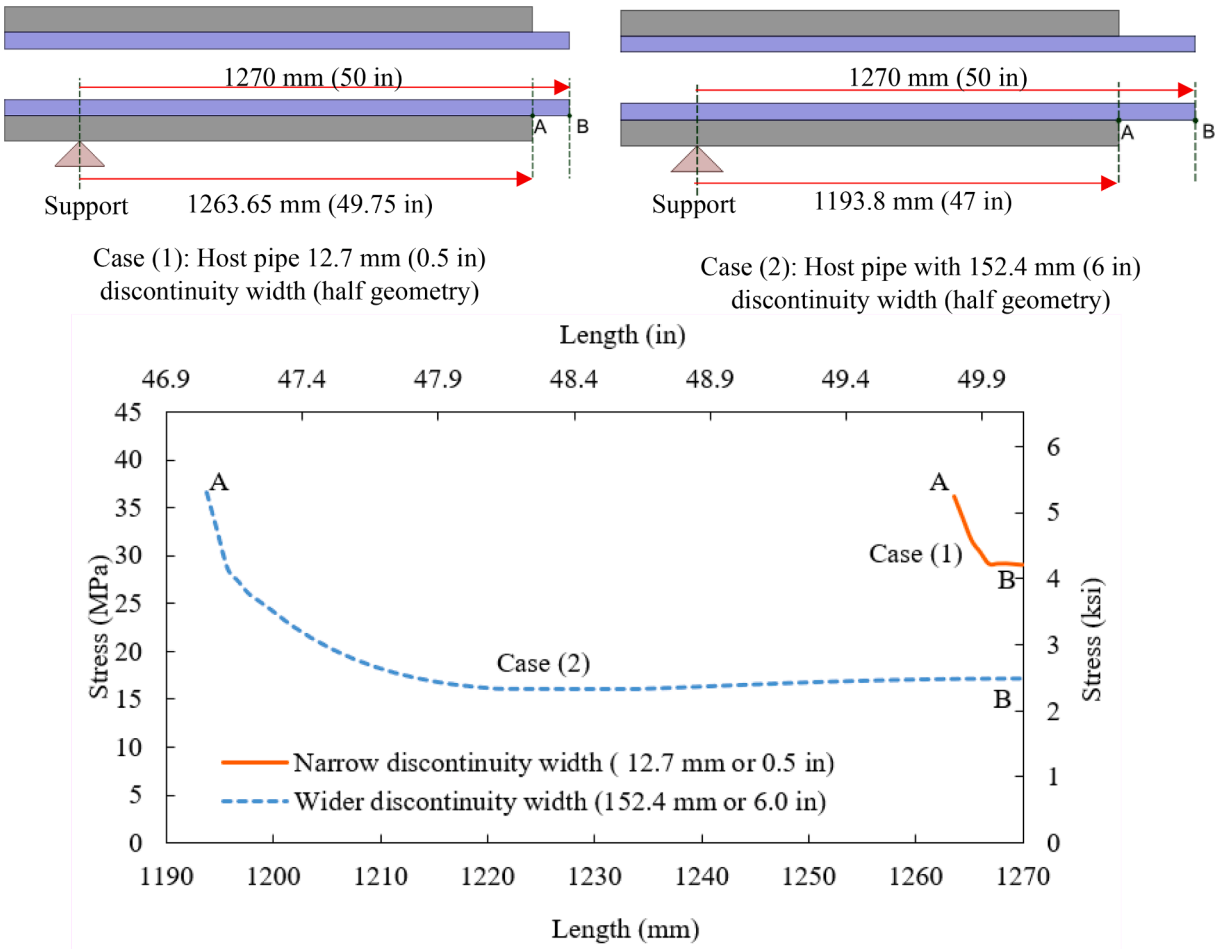

Fig. 24. Stress distribution at the bottom of IRP, from discontinuity edge to midspan for host pipe with narrow and wider discontinuity widths (length is measured from left support).

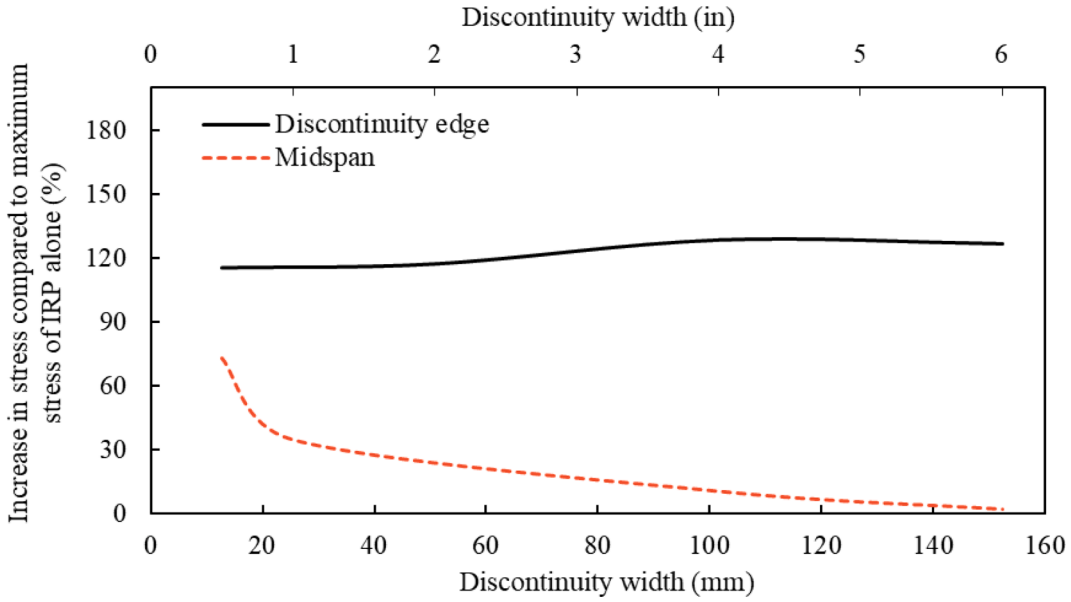

Fig. 25. Percentage increase in stress of IRP in damaged host pipe compared to the maximum stress generated in IRP alone under a cyclic load of 14.8 kN (3.3 kips).

with circumferential discontinuity, and this should be taken into consideration during the design and development of a repair system. It is also seen that the stresses generated at the midspan of IRP with the narrowest discontinuity width and widest discontinuity width under consideration are respectively 72.9 % and 1.8 % greater than that of IRP alone (Table 7). This result shows that, as the discontinuity width

Table 7
Percentage increase midspan stress of IRPs in discontinuous host pipes relative to the maximum stress in IRP alone, subjected to a traffic load of 14.8 kN (3.3 kips).

Width of host pipe discontinuity		% increase in midspan stress compared to maximum stress in IRP alone
mm	in	
12.7	0.5	72.9
25.4	1	34.6
50.8	2	21.5
101.6	4	10.3
152.4	6	1.8

widens the stress at the midspan approaches that of IRP alone. Compared to the IRP in continuous host pipe, the maximum stress produced in IRP alone is 78.8 times higher. However, unlike IRP in discontinuous host pipes, both IRP alone and IRP in continuous host pipes have significantly longer service lifespans exceeding one billion load cycles as they do not experience stress concentrations. In addition, Fig. 26 shows the level of maximum deformation for these systems. Accordingly, the lateral deformation at the discontinuity edge and mid-span of the IRP system increases almost linearly with the widening of discontinuity. Even the maximum deformation level attributed to the system with a discontinuity width of 152.4 mm (6 in) is less than 4 mm (0.157 in), which is quite minimal.

3.2. Effect of IRP thickness and MOE

The effect of repair thickness on the maximum strain of IRP (at the edge of the circumferential discontinuity) made from different material systems is shown in Fig. 27. As can be seen, the maximum strain in IRP decreases nonlinearly as the repair thickness increases. This is because increasing the thickness of the IRP improves its stiffness, which reduces deformation. In addition, IRP systems generate their maximum strain when the repair thickness is minimal. Furthermore, it can also be seen from the graph that the maximum strain in the polymer system exceeds the design strain limit of 0.02 when the repair thickness is less than 4.115 mm (0.162 in) due to its low MOE, i.e. 1.744 GPa (253 ksi). Fig. 28 depicts how the tensile stress concentration at the discontinuity edge varies with increasing IRP thickness. The graph demonstrates that, for all repair materials, the stress concentration at the discontinuity edge diminishes nonlinearly and gradually as the repair thickness increases. IRP will experience high stress when the repair thickness is low. This is because, compared to damaged host pipes with thick IRP, the stress flow lines in those with thin IRP are more densely packed due to a greater reduction in total cross-sectional area at the discontinuity edge. As the repair thickness increases from 3.175 mm (0.125 in) to 9.525 mm (0.375 in), the total reduction in stress concentration in IRP systems with different repair materials varies between 46.6 % and 64.2 %. This variation is related to the fact that stress concentration appears to be influenced by the MOE of repair materials, as explained in subsequent sections.

Fig. 29 illustrates the relationship between the MOE and the strain of the IRP at the edge of the host pipe discontinuity (It is important to note that this figure is derived from an analysis conducted on IRP systems in steel host pipes). At the same thickness, polymeric IRP with the lowest MOE produces the highest strain at the discontinuity edge. When MOE increases from 1.744 GPa (253 ksi) to 7.9 GPa (1,146 ksi), the strain at the discontinuity edge decreases dramatically for all IRP thicknesses. From MOE of 26.43 GPa (2,035 ksi), a slight nonlinear reduction in strain is observed, followed by a linear decline until MOE of 200 GPa (29,008 ksi). This shows that IRP with low MOE deforms easily under low levels of load. A small increase in MOE substantially improves the resistance to deformation. IRP materials with higher elastic moduli, i.e greater than 26.43 GPa (2,035 ksi), on the other hand, are hard to deform under a traffic load of 14.8 kN (3.3 kips) and require a high load to experience significant strain. The overall reduction in the strain at the discontinuity edge as the MOE rises from 1.744 GPa (253 ksi) to 200 GPa (29,008 ksi) is the same for each IRP thickness, which is roughly 99 %. The influence of the MOE of IRP on the stress concentration for various repair thicknesses is shown in Fig. 30. According to that when the MOE rises, the stress concentration exhibits a slight nonlinear drop up to a MOE of 38.63 GPa (5,603 ksi) for repair thicknesses of 3.175 mm (0.125 in) and 4.115 mm (0.162 in) and up to a MOE of 26.43 GPa (2,035 ksi) for thicknesses of 6.35 mm (0.25 in) and 9.525 mm (0.375 in). From that point on, the stress concentration remains steady until the MOE of 200 GPa (29,008 ksi). The highest stress concentration at each repair thickness is observed in the polymeric IRP, which has the lowest MOE among all repair materials. This means that flexible IRP material can experience high stress concentration while stiff repair material can undergo lower stress concentration at the discontinuity edge. This is because stiff repair materials are more resistant to deformation than

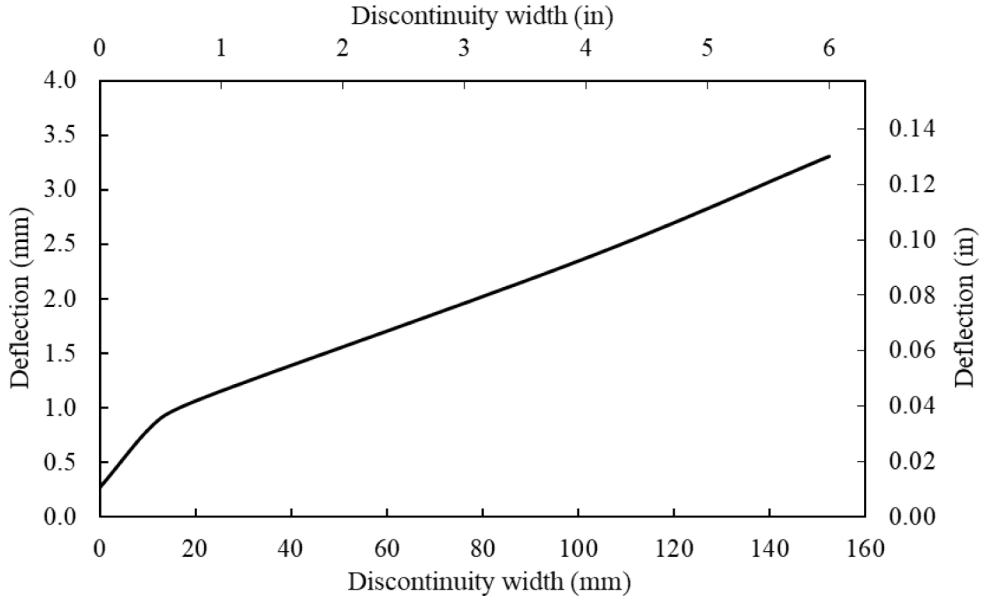

Fig. 26. Level of maximum deflection under a cyclic load of 14.8 kN (3.3 kips).

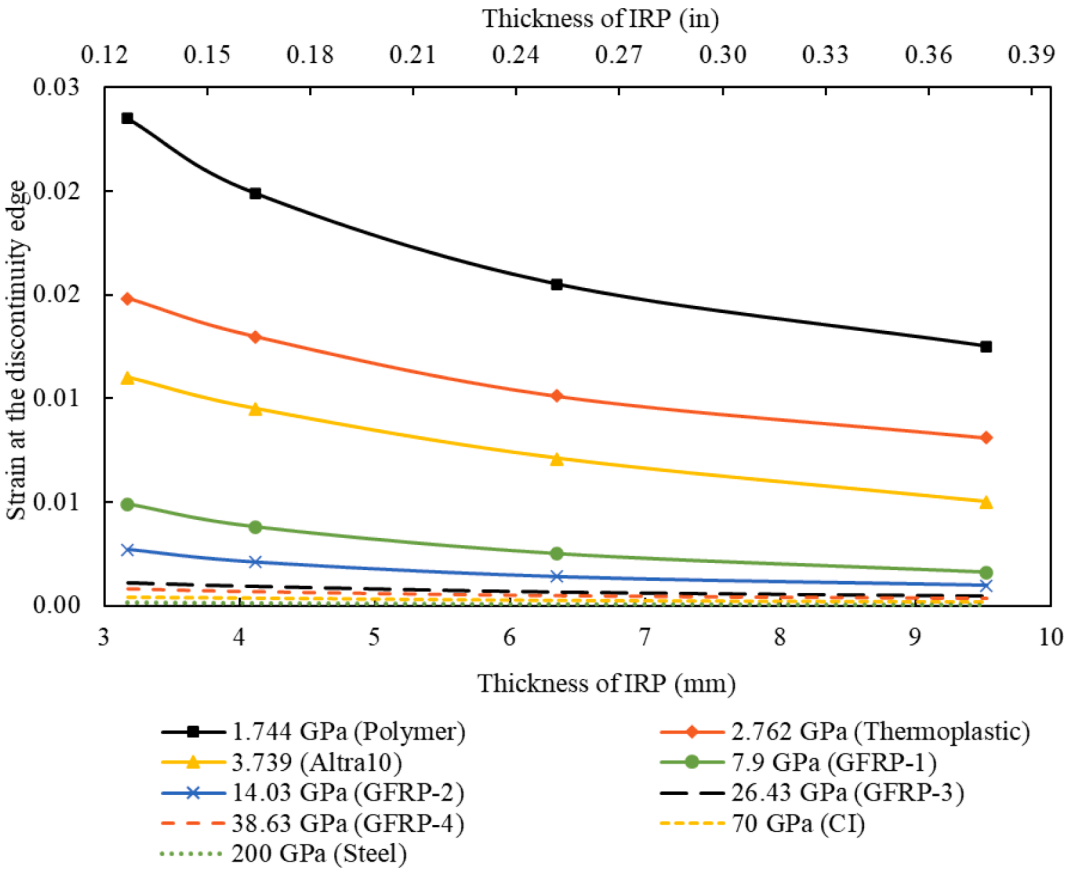

Fig. 27. Relationship of strain at the discontinuity edge and IRP thickness.

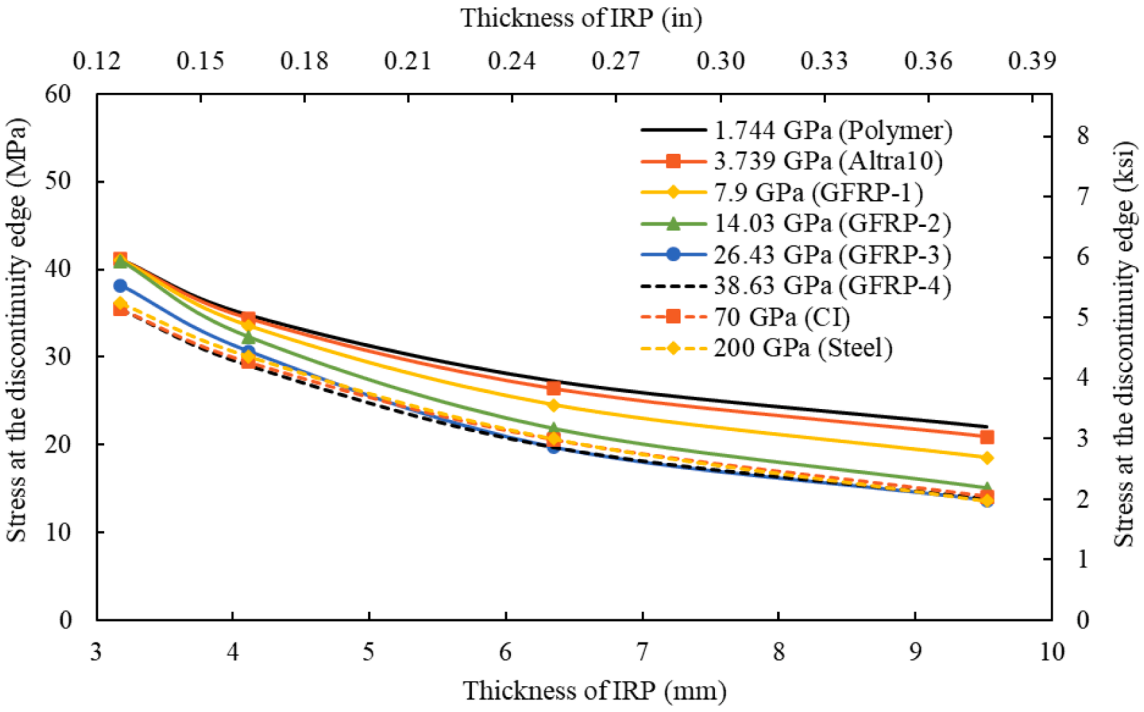

Fig. 28. Relationship of stress at the discontinuity edge and IRP thickness.

flexible repair materials, which undergo greater deformations or strain levels under the same applied load. As a consequence, in stiff IRP, stress is distributed more evenly at the discontinuity edge where the cross-sectional area changes, resulting in lower stress concentration than in flexible repair material systems.

Table 8 summarises the minimum loading cycles to failure of the IRP

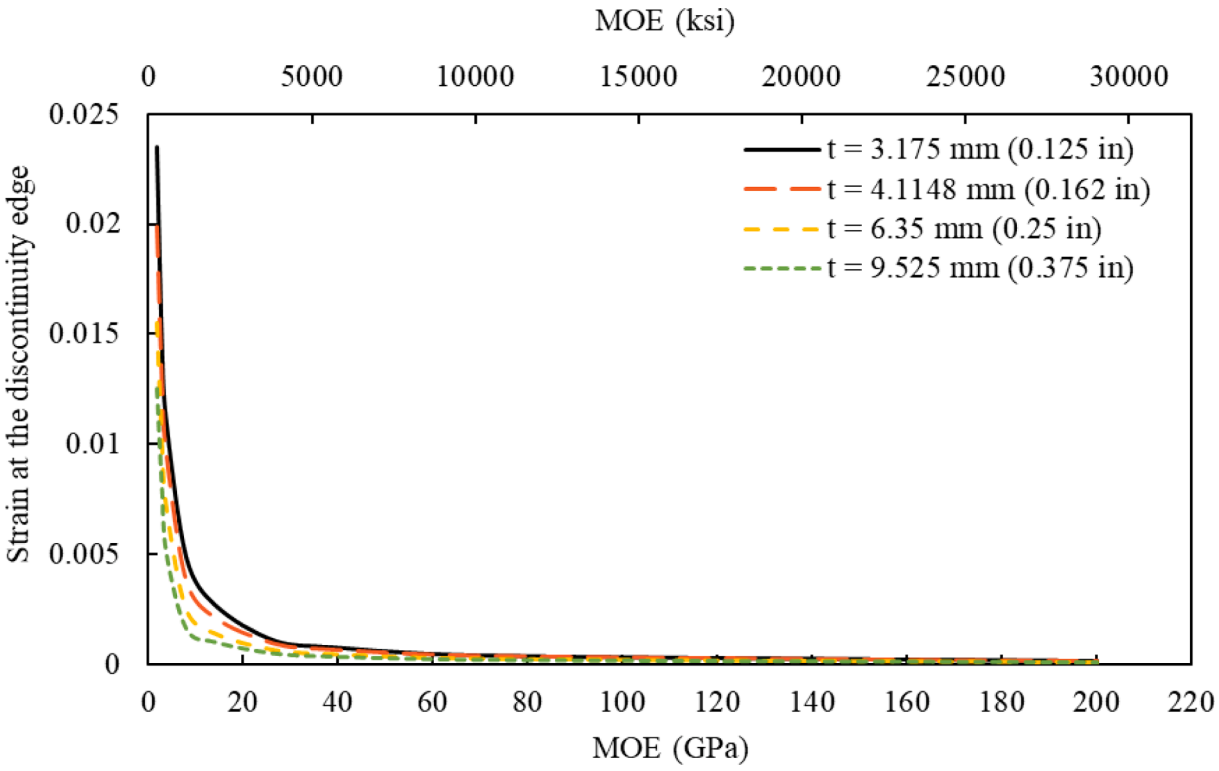

Fig. 29. Relationship of strain at the discontinuity edge and MOE of IRP.

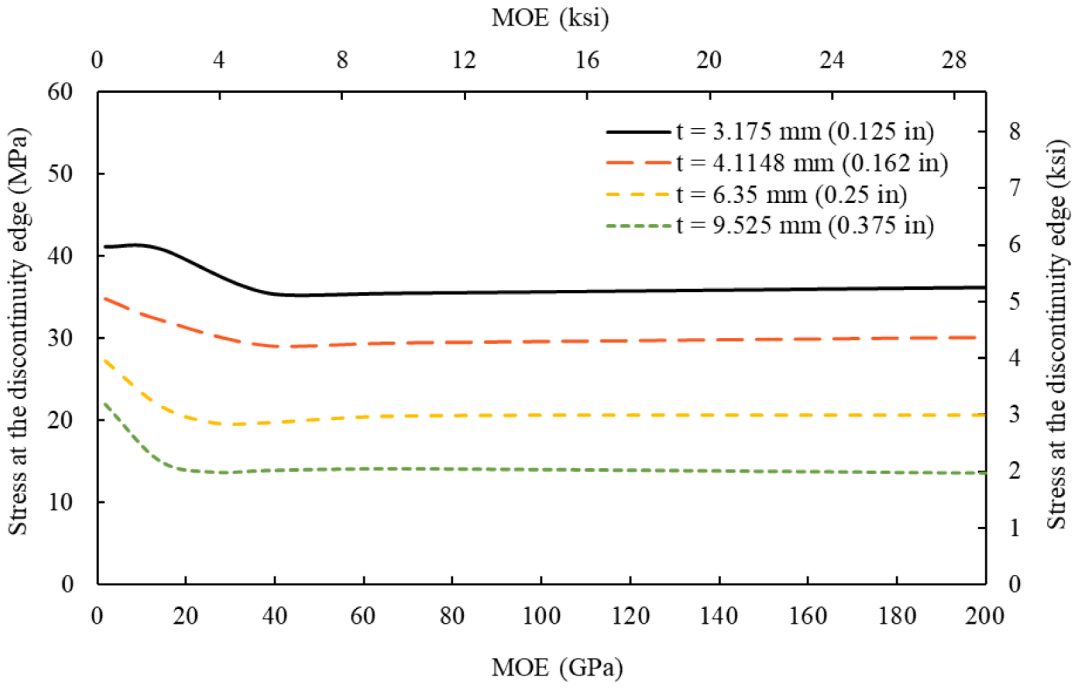

Fig. 30. Relationship of stress at the discontinuity edge and MOE of IRP.

systems installed in host pipes with circumferential discontinuities for various repair thicknesses and MOE based on the S-N curve of corresponding materials. The study found that the minimum fatigue life of IRP significantly extends with greater thickness and high MOE. This observation is in line with Huang et al [85], which concluded that the thickness of the composite pipe significantly increases its fatigue life, and with Tafsirojjaman et al [17], which demonstrated that an increase in both MOE and thickness of IRP leads to a significant improvement in fatigue life under cyclic bending. According to Table 8, among all the materials, the 3.175 mm (0.125 in) thick polymeric system has the lowest fatigue life which is only around 3 cycles during the traffic load under consideration. Based on the contour-plots in Fig. 31 (a), (b) and (c) respectively, in polymeric systems with 3.175 mm (0.125 in) and 4.115 mm (0.162 in) thickness, fatigue damage (at the bottom) would occur at the discontinuity edge and midspan during the service life, but only at the discontinuity edges with 6.35 mm (0.25 in) repair thickness.

Table 8
Minimum fatigue life of the IRP systems with different MOE and repair thicknesses.

Thickness of SIRP	Number of cycles							
	1.744 GPa (253 ksi) [Polymer]	3.739 GPa (542 ksi) [Altra10]	7.9 GPa (1,146 ksi) [GFRP-1]	14.03 GPa (2,035 ksi) [GFRP-2]	26.43 GPa (2,035 ksi) [GFRP-3]	38.63 GPa (5,603 ksi) [GFRP-4]	70 GPa (10,153 ksi) [CI]	200 GPa (29,008 ksi) [Steel]
3.175 mm (0.125 in)	3	2.684e + 005	>1E + 09	>1E + 09	>1E + 09	>1E + 09	>1E + 09	>1E + 09
4.115 mm (0.162 in)	130	2.727E + 06	>1E + 09	>1E + 09	>1E + 09	>1E + 09	>1E + 09	>1E + 09
6.35 mm (0.25 in)	26,209	7.165E + 07	>1E + 09	>1E + 09	>1E + 09	>1E + 09	>1E + 09	>1E + 09
9.525 mm (0.375 in)	2.048e + 006	1.519 + 09	>1E + 09	>1E + 09	>1E + 09	>1E + 09	>1E + 09	>1E + 09

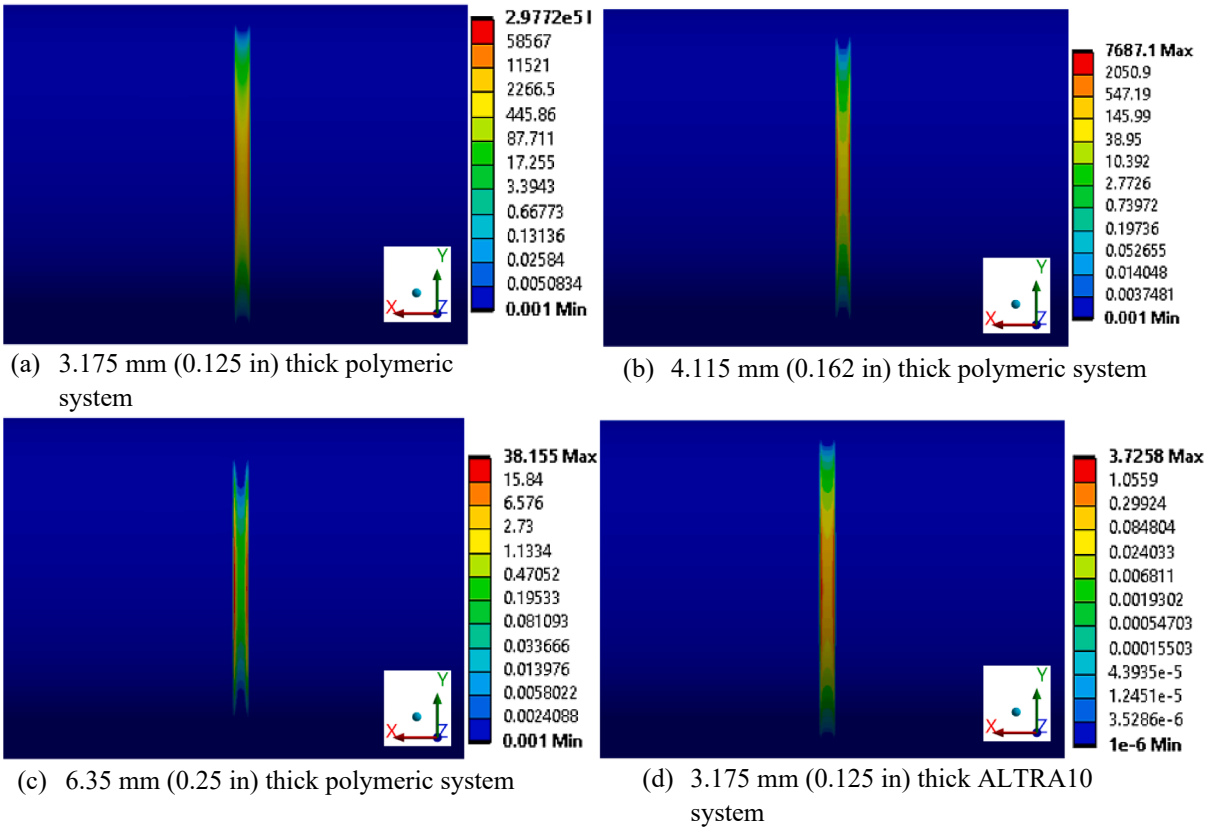

(a) 3.175 mm (0.125 in) thick polymeric system

(b) 4.115 mm (0.162 in) thick polymeric system

(c) 6.35 mm (0.25 in) thick polymeric system

(d) 3.175 mm (0.125 in) thick ALTRA10 system

Fig. 31. Fatigue damage of IRP at the bottom at midspan during the service life of 1 million loading cycles (host pipe segments are temporarily hidden).

Therefore, to achieve the targeted life of one million cycles, the polymeric IRP system with MOE of 1.744 GPa (253 ksi) requires a minimum repair thickness of 8.4 mm (0.331 in).

On the other hand, a 3.175 mm (0.125 in) thick ALTRA10 IRP system will fail after 268,400 fatigue cycles. The fatigue damage contour-plot for the bottom of the ALTRA10 IRP system in Fig. 31(d) shows that during the service life, only the discontinuity edge will experience fatigue damage (damage factor > 1.0) whereas there will be no damage to the midspan. Additionally, in order to use ALTRA10 as the repair material and achieve the intended fatigue life of one million cycles, the repair thickness must be at least 3.7 mm (0.146 in). Additionally, Fig. 32 displays the potential maximum stiffness degradation as a percentage, which IRP with a thickness of 4.115 mm (0.162 in) or greater might experience during its service life. This stiffness degradation is obtained through linear extrapolation of the data set from Fig. 19, based on the maximum alternating stresses obtained from FE simulations and service life of one million cycles. Accordingly, the stiffness degradation decreases nonlinearly and gradually as the repair thickness increases. The overall reduction in stiffness degradation when the IRP thickness increases from 4.115 mm (0.162 in) to 9.525 mm (0.375 in) is around 88 %. Moreover, the findings reveal that when the MOE of the IRP material increases, the thickness required to meet the targeted life reduces. Even with an IRP thickness of 3.175 mm (0.125 in), all other IRP material systems, those with a MOE of 7.9 GPa (1,146 ksi) or higher, will exceed the design fatigue life of one million cycles under the traffic load of 14.8 kN (3.3 kips).

3.3. *Effect of loading level and critical loadings*

The effect of loading level on the fatigue life of an IRP system with different repair thicknesses and MOE representing polymeric, ALTRA10, GFRP, and metallic is shown in Fig. 33 a, b, c and d, respectively. All IRP material systems regardless of their thickness indicate that a slight increase in lateral loading significantly shortens the fatigue life, and the responses are slightly nonlinear, even on semi-log plots. This finding is similar to that of Huang et al [85], who demonstrated that composite pipe had a considerably shorter fatigue life under cyclic bending as the imposed stress level increased. This decrease in fatigue life is caused by the significant rise in tensile stress concentration, which is directly related to the applied load. As a result, the minimum repair thickness that must be utilized for each repair material increases significantly. While increasing repair thickness prolongs the fatigue life, it can also be

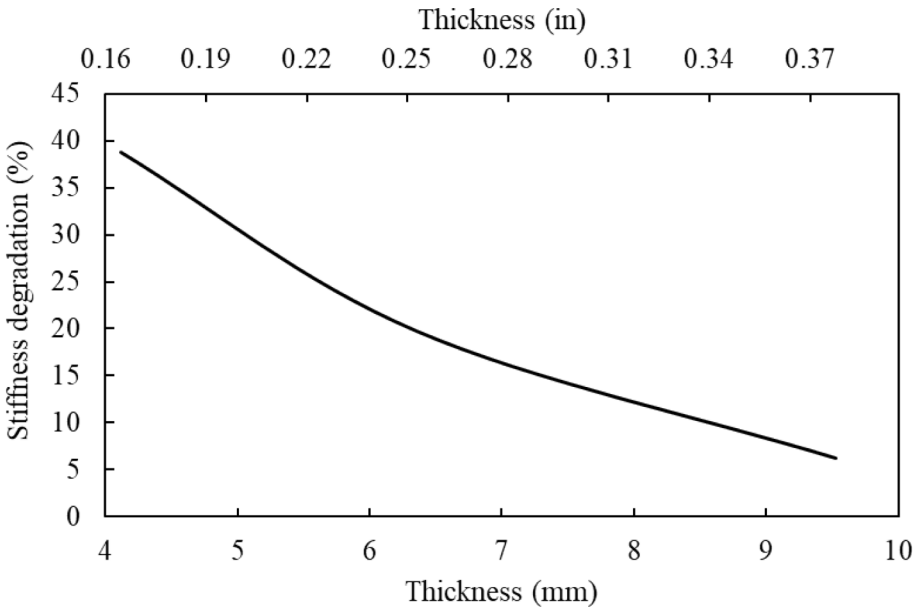

Fig. 32. Stiffness degradation of ALTRA10 IRP systems with different thicknesses at one million cycles.

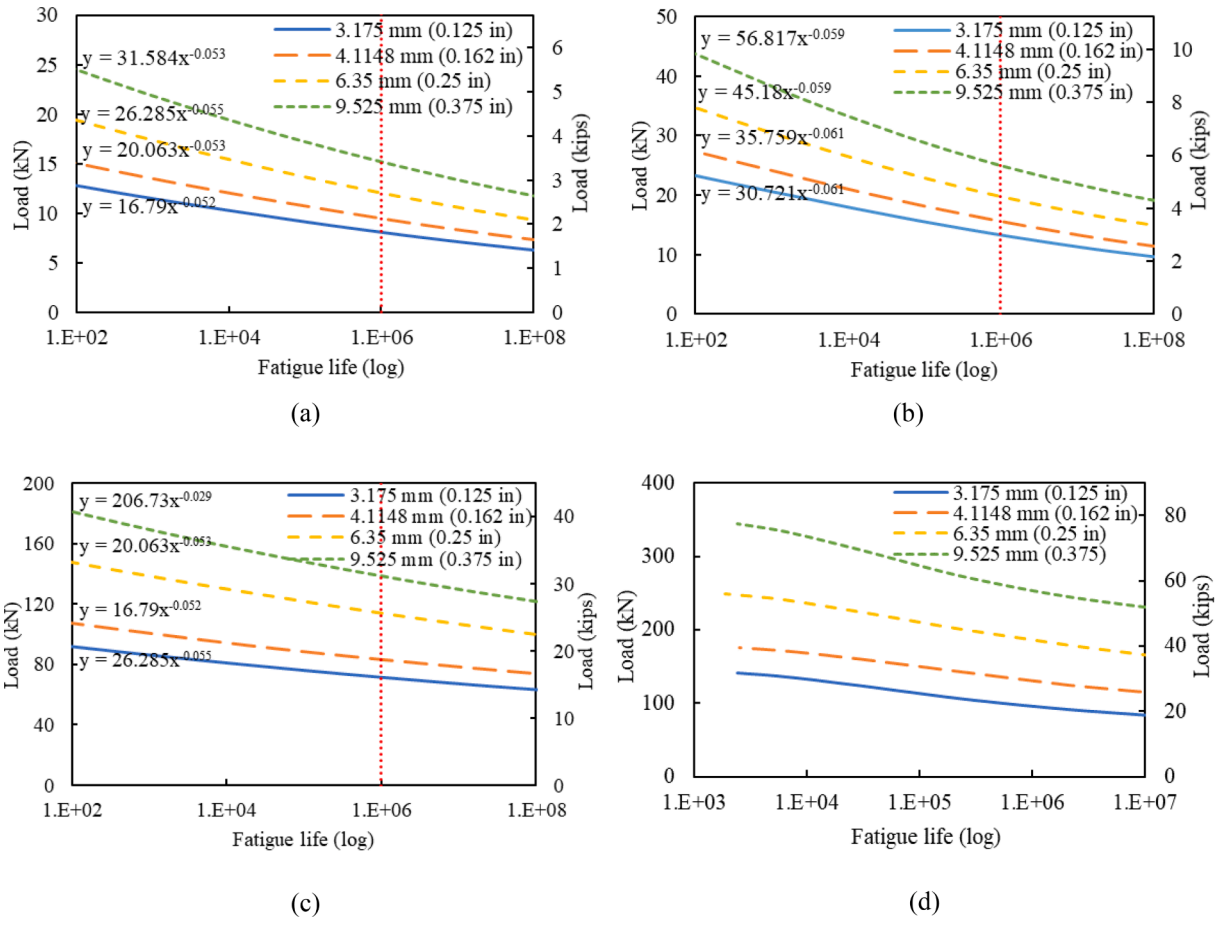

Fig. 33. Effect of loading level on the fatigue life of (a) polymeric (MOE of 1.744 GPa or 253 ksi), (b) ALTRA10 (MOE of 3.739 GPa or 542 ksi), (c) GFRP (MOE of 38.63 GPa or 5,603 ksi) (d) metallic (MOE of 200 GPa or 29,008 ksi) IRP repair systems.

problematic in practice due to potential reduction in flow capacity and increased cost. From these graphs, the maximum load that can be applied to various IRP systems to meet the desired design life of one million cycles are plotted against the MOE and thickness of the IRP, as shown in Fig. 34 and Fig. 35, respectively. According to Fig. 34, the critical load required to achieve the projected design of IRP systems dramatically increases when the MOE rises from 1.744 GPa (253 ksi) to 3.739 GPa (542 ksi) as a result of a substantial drop in the tensile stress

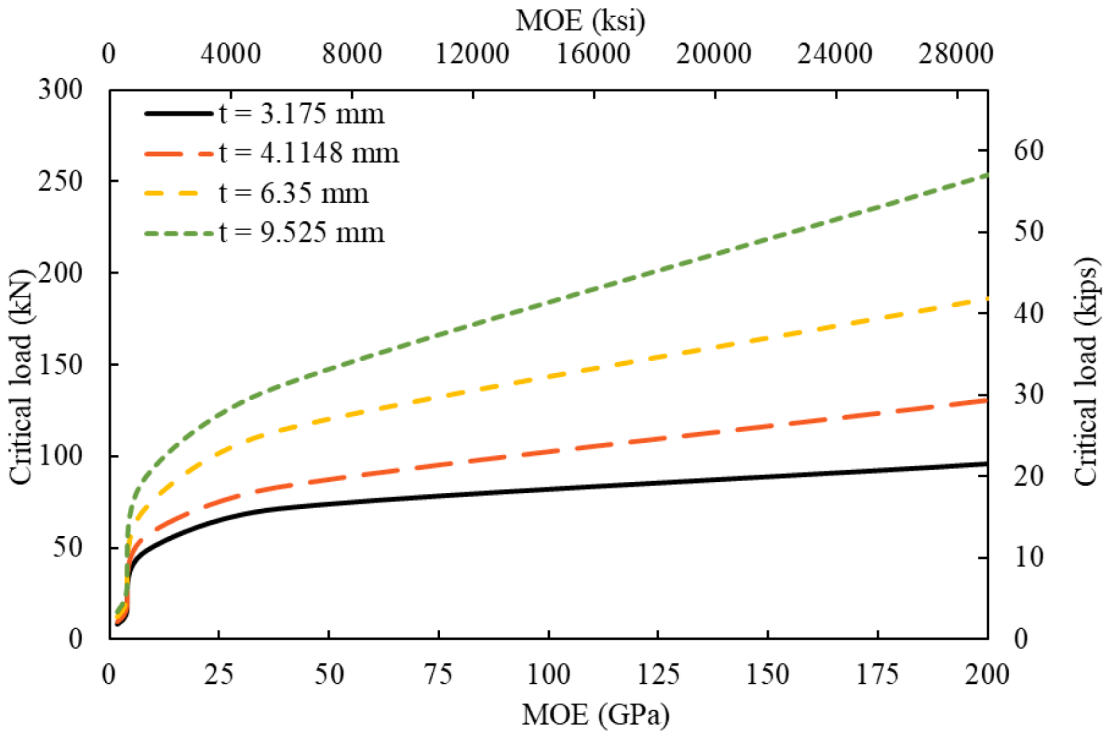

Fig. 34. Effect of the MOE on the critical lateral cyclic loading.

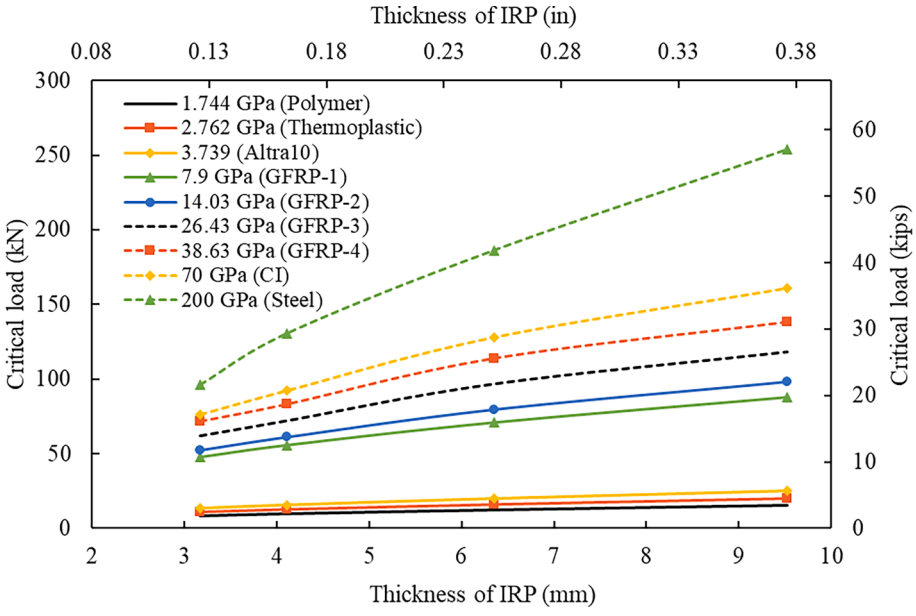

Fig. 35. Effect of the repair thickness on the critical lateral cyclic loading.

concentration, which controls the fatigue failure of IRP systems. Thereafter, it exhibits a nonlinear increase up to 38.63 GPa (5,603 ksi), followed by a linear increase up to 200 GPa (29,008 ksi). The maximum overall increment in critical load as the MOE increases from 1.744 GPa (253 ksi) to 200 GPa (29,008 ksi) is around 99 %. According to Fig. 35, the critical load displays a slightly nonlinear increase with increasing thickness, with an overall growth range between 84 % and 164 %. This is related to a reduction in the maximum stiffness degradation of IRP and the lowering in the density of the stress flow lines at the discontinuity edge as repair thickness increases.

3.4. Quantifying the influence of investigated parameters

Multiple regression analysis is carried out to quantify the influence of investigated parameters in this study using the SPSS (Statistical Package for the Social Sciences) statistical analysis software [86]. The investigated parameters are ranked based on their relative contribution to the fatigue strength of IRPs installed in host pipes with circumferential discontinuities during bending fatigue using the standardized coefficients or beta coefficients obtained from the multiple regression analysis, as suggested by Freedman [87]. Two regression analyses are performed, with the dependent variable being the maximum stress

Table 9
Summary[b] of models.

Model	R	R Square	Adjusted R Square	Std. Error of the Estimate
1	0.940[a]	0.883	0.881	11.096
2	0.935[a]	0.874	0.872	5.211

[a] Predictors: (constant), level of load (kN), MOE of IRP (GPa), thickness of IRP (mm).
[b] Dependent variable: maximum stress (MPa) or minimum fatigue life of IRP (cycles).

Table 10
ANOVA[a] of models.

Model		Sum of Squares	df	Mean Square	F	Sig.
1	Regression	144742.610	3	48247.537	391.851	<0.001[b]
	Residual	19207.831	156	123.127		
	Total	163950.441	159			
2	Regression	33167.352	3	11055.784	407.194	<0.001[b]
	Residual	4778.603	176	27.151		
	Total	37945.955	179			

[a] Dependent variable: maximum stress (MPa) or minimum fatigue life of IRP (cycles).
[b] Predictors: (constant), level of load (kN), MOE of IRP (GPa), thickness of IRP (mm).

(model 1) or the minimum fatigue life (model 2). In both regression models, repair thickness, MOE of the repair material, and level of loading are the independent variables. The reason for using two dependent variables is that changes in repair thickness, MOE of repair material, and loading affect maximum stress and minimal fatigue life differently. Therefore, the relative contribution of these parameters to maximum stress and fatigue life may differ. Since the study already revealed that changing the discontinuity width has almost no noticeable effect on the stress concentration and fatigue life under cyclic bending, it is recognised as the least important parameter and is eliminated from the regression analysis. Table 9 contains a summary of the multiple regression model 1 and 2. According to the statistical results, when taken as a group, the repair thickness, MOE of the repair material, and loading level in model 1 account for 88.3 % ($R^2 = 0.883$) of the variance in the maximum stress of IRP in the damaged host pipe, whereas those in model 2 account for 87.4 % ($R^2 = 0.874$) of the variance in the minimum fatigue life, which is good in practice. The results of the one-way ANOVA global test in Table 10 also indicate that, overall, the regression models 1 and 2 are statistically significant with F (3,156), $p < 0.001$, $R^2 = 0.883$ (tested using a significance level of 0.05) and F (3,176), $p < 0.001$, $R^2 = 0.874$, respectively. Therefore, when considered together, the repair thickness, the MOE of the repair material, and the loading level can predict the maximum stress and the minimum fatigue life of IRP in discontinuous host pipe significantly.

Table 11 shows the coefficient of the regression models. The significance levels reported in this table indicate that, when considered individually, the repair thickness, MOE of the repair material, and loading level all contribute to a significant amount of unique variance in maximum stress and minimum fatigue life of IRP in host pipe with circumferential discontinuity under lateral loading. Table 11 also displays the standardised beta coefficients, which compare the strength of the effect of the individual independent variable on the dependent variable. Accordingly, absolute standardised beta coefficients of the MOE of repair material, repair thickness and level of a load of regression model 1 are, respectively, 0.104, 0.425 and 0.851 while those of model 2 are, respectively, 0.897, 0.155 and 0.703. The findings demonstrate that the level of load, which has the highest standardized beta coefficient in model 1, is the parameter that contributes mostly to maximum stress. However, it is the second-most significant parameter that contributes to minimum fatigue life in model 2. This result can be explained by the fact that the imposed load level dominates the contribution to maximum stress, as it is related to the moment capacity of the cross-section of the system, which is a significant component of normal stress induced during bending. On the other hand, the MOE of the repair material, which has the lowest absolute standardised beta coefficient, is the parameter that has the least effect on the maximum stress generated in the IRP repair system. However, it is discovered to be the most important parameter in model 2, which has the greatest effect on the minimum fatigue life. This is because the maximum stress developed in IRP with the same thickness but different MOE in the elastic region only slightly varies under the same repetitive loading. In contrast, the corresponding fatigue life at the same alternating stress changes greatly when MOE changes. This is due to the fact that repair materials with higher MOE are better able to resist the deformation produced by the loading cycles and therefore have a reduced probability of failure in comparison to repair materials with lower MOE. As in model 1, the repair thickness is the parameter that has the second-largest influence on the maximum stress, but in model 2 it is the parameter that has the least impact on the minimum fatigue life. Due to its relationship to the moment of inertia of the repair cross-section, which is a component of bending stress, repair thickness has a relatively greater impact on maximum stress than it does on fatigue life. It is important to note however that using metallic materials such as cast iron and steel, which have the highest MOE among the repair materials considered, may not be the best choice. Water and gas pipelines are operating in harsh service environmental conditions (temperature, hygrothermal) which can accelerate the corrosion of steel and cast iron and can lead to premature fatigue failure.

4. Conclusion

Numerical simulations through finite element analyses were implemented to investigate the bending fatigue behaviour of a continuous host pipe with IRP, host pipes with circumferential discontinuities repaired with IRPs, and IRP alone (without host pipe). The influence of the discontinuity width of the host pipe, thickness and elastic modulus of the repair material, and level of imposed loading, were thoroughly examined. Multiple regression statistical analysis was utilised to determine which of the investigated parameters has a significant effect on

Table 11
Coefficients[a] of models.

Model		Unstandardized Coefficients		Standardized Coefficients	t	Sig.	Rank
		B	Std. Error	Beta			
1	(Constant)	31.684	2.770		11.440	<0.001	
	Level of load (kN)	1.994	0.065	0.851	30.517	<0.001	1
	MOE of IRP (GPa)	−0.051	0.014	−0.104	−3.721	<0.001	3
	Thickness of IRP (mm)	−5.561	0.359	−0.425	−15.497	<0.001	2
2	(Constant)	9.897	1.277		7.753	<0.001	
	Level of load (kN)	−0.743	0.030	−0.703	−24.720	<0.001	2
	MOE of PIP (GPa)	0.982	0.031	0.897	31.506	<0.001	1
	Thickness of IRP (mm)	0.906	0.157	0.155	5.771	<0.001	3

[a] Dependent variable: maximum stress (MPa) or minimum fatigue life of IRP (cycles).

stress concentration and fatigue life. Based on the findings of this investigation, the following conclusion can be drawn:

- Host pipe segments with circumferential discontinuities repaired with fully bonded IRP systems can be critical in bending fatigue due to the high stress concentration induced in IRP at the discontinuity edge. The stress concentration results in a reduction in the minimum fatigue life or failure before reaching the desired design life. It is essential therefore to minimise stress concentration when designing an IRP system to be installed in host pipe segments with circumferential discontinuity to avoid premature fatigue failure under cyclic bending.
- The continuity of the host pipe stabilises the stress generated in the IRP during bending, thereby extending fatigue life and reducing fatigue failure.
- The stress and the fatigue life at the midspan of the repair system become closer to that of IRP alone for wide discontinuity widths.
- The width of the circumferential discontinuity in the host pipe has no significant effect on the level of stress concentration in IRP at the discontinuity edge indicating that the fatigue failure of fully bonded IRP systems with varying discontinuity widths may occur at around the same service life.
- The minimum fatigue life of IRP systems with discontinuous host pipes significantly extends as the thickness and MOE of repair material increase, under the same loading due to the reduction in stress concentration at the discontinuity edge at the bottom. The polymeric IRP system with a MOE of 1.744 GPa (253 ksi) requires a minimum repair thickness of 8.4 mm (0.331 in), whereas an ALTRA10 IRP with a MOE of 3.739 GPa (542 ksi) requires a repair thickness of at least 3.7 mm (0.146 in) under a repetitive traffic load of 14.8 kN (3.3 kips) to reach the intended life of one million cycles.
- Under the traffic load of 14.8 kN (3.3 kips), the ALTRA10 IRP material system with a thickness of 4.115 mm (0.162 in) will experience a 38 % reduction in stiffness at one million fatigue cycles. This stiffness reduction is heavily influenced by the stress concentration in the IRP at the edge of circumferential host-pipe discontinuity. Increasing the IRP thickness to 9.525 mm (0.375 in) reduced the stiffness loss by 88.0 %.
- The level of loading has a significant effect on fatigue life. A high level of applied load shortens the fatigue life of IRP regardless of repair thickness or MOE of repair material.
- Multiple regression analysis indicated that the maximum stress generated in IRP systems during bending fatigue is significantly affected by the level of load, followed by repair thickness, MOE, and discontinuity width. On the other hand, the MOE of the IRP is identified to have the greatest contribution to fatigue life, followed by the level of load, repair thickness, and discontinuity width.

The results of this study demonstrated that the material and geometrical properties of the IRP and the host pipe can influence the bending fatigue behaviour of the repaired system. Investigating the effects of other important design parameters such as Poisson's ratio of IRP materials and type of host pipes will provide a more detailed understanding of the bending fatigue behaviour of IRP-repaired discontinuous legacy pipe systems.

CRediT authorship contribution statement

Shanika Kiriella: Data curation, Investigation, Methodology, Software, Validation, Visualization, Writing – original draft, Writing – review & editing, Conceptualization. **Allan Manalo:** Conceptualization, Funding acquisition, Investigation, Methodology, Project administration, Supervision, Writing – original draft, Writing – review & editing. **Cam Minh Tri Tien:** . **Hamid Ahmadi:** Conceptualization, Investigation, Writing – review & editing, Methodology, Software, Supervision. **Patrick G. Dixon:** Conceptualization, Data curation, Investigation, Methodology, Writing – review & editing. **Warna Karunasena:** Conceptualization, Investigation, Methodology, Supervision, Writing – review & editing. **Ahmad Salah:** Conceptualization, Investigation, Methodology, Software. **Brad P. Wham:** Conceptualization, Funding acquisition, Methodology, Project administration, Resources, Writing – review & editing.

Declaration of competing interest

The authors declare that they have no known competing financial interests or personal relationships that could have appeared to influence the work reported in this paper.

Data availability

Data will be made available on request.

Acknowledgement

The information, data, or work presented herein was funded in part by the Advanced Research Projects Agency-Energy (ARPA-E), US Department of Energy, under Award Number DE-AR0001327 and Sanexen Environmental Services Inc. (Quebec, Canada). The views and opinions of authors expressed herein do not necessarily state or reflect those of the United States Government or any agency thereof.

References

[1] Dumitrescu A, Minescu M, Dinita A, Lambrescu I. Corrosion Repair of Pipelines Using Modern Composite Materials Systems: A Numerical Performance Evaluation. Energies 2021;14(3):615.
[2] Li X, Han Z, Zhang R, Abbassi R, Chang D. An integrated methodology to manage risk factors of aging urban oil and gas pipelines. J Loss Prev Process Ind 2020;66:104154.
[3] Duell JM, Wilson JM, Kessler MR. Analysis of a carbon composite overwrap pipeline repair system. Int J Press Vessel Pip 2008;85(11):782–8.
[4] Sinha SK, Pandey MD. Probabilistic Neural Network for Reliability Assessment of Oil and Gas Pipelines. Comput Aided Civ Inf Eng 2002;17(5):320–9.
[5] Mahmoodian M, Li C-Q. Structural integrity of corrosion-affected cast iron water pipes using a reliability-based stochastic analysis method. Struct Infrastruct Eng 2016;12(10):1356–63.
[6] Zhao W, Zhang T, Wang Y, Qiao J, Wang Z. Corrosion Failure Mechanism of Associated Gas Transmission Pipeline. Materials 2018;11(10):1935.
[7] Gamboa E, Linton V, Law M. Fatigue of stress corrosion cracks in X65 pipeline steels. Int J Fatigue 2008;30(5):850–60.
[8] Fang J, Cheng X, Gai H, Lin S, Lou H. Development of machine learning algorithms for predicting internal corrosion of crude oil and natural gas pipelines. Comput Chem Eng 2023;177:108358.
[9] Hussein Khalaf A, Xiao Y, Xu N, Wu B, Li H, Lin B, et al. Emerging AI technologies for corrosion monitoring in oil and gas industry: A comprehensive review. Eng Fail Anal 2024;155:107735.
[10] Akhi AH, Dhar AS. Fracture parameters for buried cast iron pipes subjected to internal surface corrosions and cracks. Journal of Pipeline Science and Engineering 2021;1(2):187–97.
[11] Mahmoodian M, Li C-Q. Failure assessment and safe life prediction of corroded oil and gas pipelines. J Pet Sci Eng 2017;151:434–8.
[12] Rajeev, P., J. Kodikara, D. Robert, P. Zeman, and B. Rajani. *Factors contributing to large diameter water pipe failure as evident from failure inspection*. 2013.
[13] Biezma MV, Andrés MA, Agudo D, Briz E. Most fatal oil & gas pipeline accidents through history: A lessons learned approach. Eng Fail Anal 2020;110:104446.
[14] Abd-Elhady AA, Sallam H-E-D-M, Alarifi IM, Malik RA, EL-Bagory TMAA. Investigation of fatigue crack propagation in steel pipeline repaired by glass fiber reinforced polymer. Compos Struct 2020;242:112189.
[15] Li B, Wang F, Fang H, Yang K, Zhang X, Ji Y. Experimental and numerical study on polymer grouting pretreatment technology in void and corroded concrete pipes. Tunn Undergr Space Technol 2021;113:103842.
[16] Shaukat MM, Ashraf F, Asif M, Pashah S, Makawi M. Environmental Impact Analysis of Oil and Gas Pipe Repair Techniques Using Life Cycle Assessment (LCA). Sustainability 2022;14(15):9499.
[17] Tafsirojjaman T, Manalo A, Tien CMT, Wham BP, Salah A, Kiriella S, et al. Analysis of failure modes in pipe-in-pipe repair systems for water and gas pipelines. Eng Fail Anal 2022;140:106510.
[18] Tien CMT, Manalo A, Dixon P, Tafsirojjaman T, Karunasena W, Flood WW, et al. Effects of the legacy pipe ends on the behaviour of pipe-in-pipe repair systems under internal pressure. Eng Fail Anal 2023;144:106957.

[19] Stewart, H.E., A.N. Netravali, and T.D. O'Rourke, *Performance Testing of Field-Aged Cured-in-Place Liners (CIPL) for Cast Iron Piping* 2015: School of Civil and Environmental Engineering, Cornell University p. 1-128.
[20] Dixon PG, Tafsirojjaman T, Klingaman J, Hubler MH, Dashti S, O'rourke TD, et al. State-of-the-Art Review of Performance Objectives for Legacy Gas Pipelines with Pipe-in-Pipe Rehabilitation Technologies. J Pipeline Syst Eng Pract 2023;14(2).
[21] Klingaman, J., P.G. Dixon, B.P. Wham, S. Dashti, and M.H. Hubler. *Traffic Loading Effects on Rehabilitated Cast Iron Distribution Pipelines*. in *Pipelines 2022*. 2022. Indianapolis, Indiana.
[22] Jeon S-S, O'Rourke TD, Neravali AN. Repetitive loading effects on cast iron pipelines with cast-in-place pipe lining system. J Transp Eng 2004;130(6):692–705.
[23] Ha SK, Lee HK, Kang IS. Structural behavior and performance of water pipes rehabilitated with a fast-setting polyurea–urethane lining. Tunn Undergr Space Technol 2016;52:192–201.
[24] Ellison, D., F. Sever, P. Oram, W. Lovins, and A. Romer, *Global review of spray-on structural lining technologies*. 2010, EnvironmentalProtection Agency (USEPA) p. 1–158.
[25] Barros SD, Fadhil BM, Alila F, Diop J, Reis JML, Casari P, et al. Using blister test to predict the failure pressure in bonded composite repaired pipes. Compos Struct 2019;211:125–33.
[26] Beyene AT, Belingardi G. Bending fatigue failure mechanisms of twill fabric E-Glass/Epoxy composite. Compos Struct 2015;122:250–9.
[27] Lee H-G, Kang MG, Park J. Fatigue failure of a composite wind turbine blade at its root end. Compos Struct 2015;133:878–85.
[28] Muc A, Barski M, ChwbB M, Romanowicz PJ, Stawiarski A. Fatigue damage growth monitoring for composite structures with holes. Compos Struct 2018;189:117–26.
[29] Rafiee R. Stochastic fatigue analysis of glass fiber reinforced polymer pipes. Compos Struct 2017;167:96–102.
[30] Olamide A, Bennecer A, Kaczmarczyk S. Finite Element Analysis of Fatigue in Offshore Pipelines with Internal and External Circumferential Cracks. Applied Mechanics 2020;1(4):193–223.
[31] Song S, Zang H, Duan N, Jiang J. Experimental Research and Analysis on Fatigue Life of Carbon Fiber Reinforced Polymer (CFRP) Tendons. Materials 2019;12(20):3383.
[32] Bennani, M., A.E. Akkad, and A. Elkhalfi, *Impact of an internal polymeric liner on the fatigue strength of pressure vessels under internal pressure*. 2016, WSEAS Transactions on Applied and Theoretical Mechanics. p. 1-9.
[33] O'Rourke TD, Netravali AN, Pendharkar SM, Toprak S, Tonkinson A, Chaudhuri D. Evaluating Service Life of Anaerobic Joint Sealant Products and Techniques. Chicago: Gas Research Institute; 1996.
[34] Brunbauer J, Stadler H, Pinter G. Mechanical properties, fatigue damage and microstructure of carbon/epoxy laminates depending on fibre volume content. Int J Fatigue 2015;70:85–92.
[35] Ansari MTA, Singh KK, Azam MS. Fatigue damage analysis of fiber-reinforced polymer composites—A review. J Reinf Plast Compos 2018;37(9):636–54.
[36] Ferdous W, Manalo A, Peauril J, Salih C, Raghava Reddy K, Yu P, et al. *Testing and modelling the fatigue behaviour of GFRP composites@ Effect of stress level, stress concentration and frequency*. Engineering Science and Technology, an. Int J 2020;23(5):1223–32.
[37] Lai J, Huang H, Buising W. Effects of microstructure and surface roughness on the fatigue strength of high-strength steels. Procedia Struct Integrity 2016;2:1213–20.
[38] Brnic J, Turkalj G, Canadija M, Lanc D, Krscanski S, Brcic M, et al. Mechanical Properties, Short Time Creep, and Fatigue of an Austenitic Steel. Materials 2016;9(4):298.
[39] Abdelhaleem AM, Megahed M, Saber D. Fatigue behavior of pure polypropylene and recycled polypropylene reinforced with short glass fiber. J Compos Mater 2018;52(12):1633–40.
[40] Chandran KSR. Mechanical fatigue of polymers: A new approach to characterize the SN behavior on the basis of macroscopic crack growth mechanism. Polymer 2016;91:222–38.
[41] Maiti S, Geubelle PH. A cohesive model for fatigue failure of polymers. Eng Fract Mech 2005;72(5):691–708.
[42] Sauer JA, Chen CC. Deformation modes and fatigue behavior in styrene-acrylonitrile and acrylonitrile-butadiene-styrene copolymers. Polym Eng Sci 1984;24(10):786–97.
[43] Brostow W, Lobland HEH, Khoja S. Brittleness and toughness of polymers and other materials. Mater Lett 2015;159:478–80.
[44] Mellott, S.R., *Tensile, Creep, and Fatigue Behaviors of Thermoplastics Including Thickness, Mold Flow Direction, Mean Stress, Temperature, and Loading Rate Effects*, in *Graduate Faculty*. 2012, The University of Toledo. p. 328.
[45] Guo R, Li C, Niu YB, Xian G. The fatigue performances of carbon fiber reinforced polymer composites – A review. J Mater Res Technol 2022;21:4773–89.
[46] Lian W, Yao W. Fatigue life prediction of composite laminates by FEA simulation method. Int J Fatigue 2010;32(1):123–33.
[47] Colombi P, Fava G. Fatigue behaviour of tensile steel/CFRP joints. Compos Struct 2012;94(8):2407–17.
[48] Yin G-Q, Kang X, Zhao G-P. Fatigue Properties of the Ultra-High Strength Steel TM210A. Materials 2017;10(9):1057.
[49] Jiang R, Rathnayaka S, Shannon B, Zhao XL, Ji J, Kodikara J. Analysis of failure initiation in corroded cast iron pipes under cyclic loading due to formation of through-wall cracks. Eng Fail Anal 2019;103:238–48.
[50] Kiriella S, Manalo A, Tien CMT, Ahmadi H, Wham BP, Salah A, et al. Lateral deformation behaviour of structural internal replacement pipe repair systems. Compos Struct 2023;319:117144.
[51] Shou KJ, Chen BC. Numerical analysis of the mechanical behaviors of pressurized underground pipelines rehabilitated by cured-in-place-pipe method. Tunn Undergr Space Technol 2018;71:544–54.
[52] Yang K, Xue B, Fang H, Du X, Li B, Chen J. Mechanical sensitivity analysis of pipe-liner composite structure under multi-field coupling. Structures 2021;29:484–93.
[53] Yang K, Fang H, Bu J, Zhang X, Li B, Du X, et al. Full-scale experimental investigation of the mechanical characteristics of corroded buried concrete pipes after cured-in-place-pipe rehabilitation. Tunn Undergr Space Technol 2021;117:104153.
[54] Brown MJP, Moore ID, Fam A. Performance of a cured-in-place pressure pipe liner passing through a pipe section without structural integrity. Tunn Undergr Space Technol 2014;42:87–95.
[55] Ansys, Finite Element Analysis (FEA) Software for Structuaral Engineering. 2021, ANSYS, Inc.
[56] Zhong Z, Wang S, Zhao Mi, Du X, Li L. Performance of ductile iron push-on joints rehabilitated with CIPP liner under repetitive and seismic loadings. Soil Dyn Earthq Eng 2018;115:776–86.
[57] Argyrou C, Bouziou D, O'Rourke TD, Stewart HE. Retrofitting pipelines with cured-in-place linings for earthquake-induced ground deformations. Soil Dyn Earthq Eng 2018;115:156–68.
[58] Zhong Z, Bouziou D, Wham B, Filiatrault A, Aref A, O'Rourke TD, et al. Seismic Testing of Critical Lifelines Rehabilitated with Cured in Place Pipeline Lining Technology. J Earthq Eng 2014;18(6):964–85.
[59] Shirazi H, Eadie R, Chen W. A REVIEW ON CURRENT UNDERSTANDING OF PIPELINE CIRCUMFERENTIAL STRESS CORROSION CRACKING IN NEAR-NEUTRAL PH ENVIRONMENT. Eng Fail Anal 2023;148:107215.
[60] Petersen, D.L., C.R. Nelson, G. Li, T.J. McGrath, and Y. Kitane, *Recommended Design Specifications for Live Load Distribution to Buried Structures*. 210, National Research Cooperative Highway Program: Washington, D.C.
[61] Gowtham KL, Srivatsa SR. Study of Convergence of Results in Finite Element Analysis of a Plane Stress Bracket. Journal of Engineering Research and Application 2018:7–12.
[62] Mellott SR, Fatemi A. Fatigue behavior and modeling of thermoplastics including temperature and mean stress effects. Polym Eng Sci 2014;54(3):725–38.
[63] Zakaria KA, Jimit RH, Ramli SNR, Aziz AA, Bapokutty O, Ali MB. Study On Fatigue Life And Fracture Behaviour Of Fibreglass Reinforced Composites. Journal of Mechanical Engineering and Sciences 2016;10(3):2300–10.
[64] Huh Y-H, Lee J-H, Kim D-J, Lee Y-S. Effect of stress ratio on fatigue life of GFRP composites for WT blade. J Mech Sci Technol 2012;26(7):2117–20.
[65] Seica MV, Packer JA. Mechanical Properties and Strength of Aged Cast Iron Water Pipes. J Mater Civ Eng 2004;16(1):69–77.
[66] Preedawiphat P, Mahayotsanun N, Sa-ngoen K, Noipitak M, Tuengsook P, Sucharitpwatskul S, et al. Mechanical Investigations of ASTM A36 Welded Steels with Stainless Steel Cladding. Coatings 2020;10(9):844.
[67] O'Rourke TD, Strait JE, Mottl N, Berger B, Wham B, Stewart HE, et al. Cornell University. NY: Ithaca; 2021.
[68] Matthews, J., W. Condit, R. Wensink, and G. Lewis, *Performance Evaluation of Innovative Water Main Rehabilitation Cured-in-Place Pipe Lining Product in Cleveland*. 2012, U.S. Environmental Protection Agency (EPA).
[69] Babu S, Hosamath M, Gai R. Fatigue Life Calculator for Ansys Workbench using ACT/PYTHON. International Journal of Engineering Research & Technology (IJERT) 2021;10(2):435–7.
[70] Murakami Y, Takagi T, Wada K, Matsunaga H. Essential structure of S-N curve: Prediction of fatigue life and fatigue limit of defective materials and nature of scatter. Int J Fatigue 2021;146:106138.
[71] Fajri A, Prabowo AR, Surojo E, Imaduddin F, Sohn JM, Adiputra R. Validation and Verification of Fatigue Assessment using FE Analysis: A Study Case on the Notched Cantilever Beam. Procedia Struct Integrity 2021;33:11–8.
[72] Hou Y, Lin HT. Fatigue Life Prediction Based on AMPS Stress-Life Approach Fatigue FEA. in *The 8th International Conference on Computational Methods (ICCM2017)*. 2017.
[73] ASTM, *ASTM D3479/D3479M-19*, in *Standard Test Method for Tension-Tension Fatigue of Polymer Matrix Composite Materials*. 2019, ASTM International. p. 1-6.
[74] Rausch T, Beiss P, Broeckmann C, Lindlohr S, Weber R. Application of quantitave image analysis of graphite structures for the fatigue strength estimation of cast iron materials. Procedia Eng 2010;2(1):1283–90.
[75] Gorash Y, MacKenzie D. On cyclic yield strength in definition of limits for characterisation of fatigue and creep behaviour. Open Engineering 2017;7(1):126–40.
[76] Nieslony A, Bohm M. Mean stress effect correction using constant stress ratio S-N curves. Int J Fatigue 2013;52:49–56.
[77] Puigoriol-Forcada JM, Alsina A, Salazar-Martín AG, Gómez-Gras G, Pérez MA. Flexural fatigue properties of polycarbonate fused-deposition modelling specimens. Mater Des 2018;155:414–21.
[78] Zhang C, Chen H, Huang T-L. Fatigue damage assessment of wind turbine composite blades using corrected blade element momentum theory. Measurement 2018;129:102–11.
[79] Zheng T, Zhao C, He J. Research on fatigue performance of offshore wind turbine blade with basalt fiber bionic plate. Structures 2023;47:466–81.
[80] Susmel L, Tovo R, Lazzarin P. The mean stress effect on the high-cycle fatigue strength from a multiaxial fatigue point of view. Int J Fatigue 2005;27(8):928–43.
[81] Mecséri BJ, Kövesdi B. Discussion on the Hot-Spot and Notch Stress Based Fatigue Assessment Methods Based on Test Results. International Journal of Steel Structures 2020;20(4):1100–14.
[82] Lee J-M, Seo J-K, Kim M-H, Shin S-B, Han M-S, Park J-S, et al. and M. Int J Nav Archit Ocean Eng 2010;2(4):200–10.

[83] Haghpanahi M, Pirali H. Hot Spot Stress Determination for a Tubular T-Joint under Combined Axial and Bending Loading. International Journal of Industrial Engineering & Production Research 2006;17:21–8.
[84] Hobbacher A. The new IIW recommendations for fatigue assessment of welded joints and components – A comprehensive code recently updated. Int J Fatigue 2009;31(1):50–8.
[85] Huang Z-Y, Zhang W, Qian X, Su Z, Pham DC, Sridhar N. Fatigue behaviour and life prediction of filament wound CFRP pipes based on coupon tests. Mar Struct 2020; 72:102756.
[86] IBM, *IBM SPSS Statistics for Windows*. 2021, IBM Corp: Armonk, NY.
[87] Freedman, D.A., *Statistical models: theory and practice*. 2009: cambridge university press.

4.3. Links and implications

The findings of the study presented in Chapter 4 showed that the bending fatigue behaviour of fully bonded IRP systems is primarily influenced by the tensile stress concentration occurring at the bottom of IRP specifically at the edge of host pipe discontinuity. According to the multiple regression analysis, the level of loading is the parameter that contributes mostly to the maximum stress generated in IRP during bending fatigue, while MOE of the IRP material, is recognised as having the biggest contribution to the fatigue life. The discontinuity width was identified as the least important parameter due to its negligible effect on both maximum stress and fatigue life. Consequently, only the critical discontinuity width identified in Chapter 3 was used in subsequent chapters. Chapter 4 has primarily focused fatigue behaviour of the IRP system under cyclic traffic load conditions, without considering the impact of internal pressure during operation. Therefore, Chapter 5 focuses on analysing the combined effect of traffic load and internal pressure on the bending fatigue performance of IRP systems in the presence of discontinuous host pipe segments.

CHAPTER 5: PAPER 3 – EFFECT OF INTERNAL PRESSURE ON THE FLEXURAL FATIGUE BEHAVIOUR OF INTERNAL REPLACEMENT PIPE SYSTEM

5.1. Introduction

Chapter 2 highlighted that the maximum operating internal pressure and allowable internal pressure for bare steel gas pipelines are determined to be 413.7 kPa (60.0 psi) and 1379.0 kPa (200.0 psi), respectively. The existing literature on the bending fatigue performance of repaired pipe systems has primarily focused on low internal pressure, with no clear demonstration of how the operating internal pressure applied during cyclic bending could affect the fatigue life of the IRP in the presence of the discontinuous host pipe.

This chapter addressed Objective 3 and numerically investigated the influence of internal pressure on the flexural fatigue behaviour of IRP installed in host pipes with circumferential discontinuities under repetitive traffic loading. The investigation was carried conducted by varying the design parameters that were determined to be critical in Chapter 4. Using results obtained from extensive parametric studies, mathematical formulae that can reliably predict the fatigue life of IRP systems under the combined effect of traffic load and internal pressure were derived. These formulae consider the elastic modulus of repair material, repair thickness, internal pressure level and the magnitude of traffic loading. By incorporating the established equations, a MATLAB function was developed to facilitate user interaction in inputting design parameters and generating design charts for fatigue life. By employing the developed MATLAB function, sample design charts that can be used by IRP developers and pipeline engineers for fatigue life prediction under various combinations of internal pressures and traffic loads were generated. Section 5.2 provides a comprehensive presentation of the analysis and the results.

5.2. Publication

Effect of internal pressure on the flexural fatigue behaviour of internal replacement pipe systems

Shanika Kiriella [a], Allan Manalo [a], Cam Minh Tri Tien [a], Hamid Ahmadi *, [a], Warna Karunasena [a], Patrick G. Dixon [b], Ahmad Salah [a], Brad P. Wham [b]

[a] *Centre for Future Materials, University of Southern Queensland, Toowoomba, QLD 4350, Australia.*
[b] *Center for Infrastructure, Energy, and Space Testing, University of Colorado, Boulder, CO 80309, US.*

* Corresponding Author

E-mail Addresses:

shanika.kiriella@unisq.edu.au (S. Kiriella), allan.manalo@unisq.edu.au (A. Manalo), camminhtri.tien@unisq.edu.au (C. M. T. Tien), hamid.ahmadi@unisq.edu.au (H. Ahmadi), karu.karunasena@unisq.edu.au (W. Karunasena), padi9036@colorado.edu (P. G. Dixon), ahmad.salah@unisq.edu.au (A. Salah), brad.wham@colorado.edu (B. P. Wham)

Abstract

The internal replacement pipe (IRP) systems are a novel trenchless technique that is gaining interest in the rehabilitation of damaged legacy pipelines distributing natural gas. Performance evaluation of IRP systems under repetitive traffic loading is essential to ensure their optimal and safe design. This paper investigated numerically the effect of internal pressure on the bending fatigue performance of IRP used for rehabilitating host pipes with circumferential discontinuities. Other design parameters include the thicknesses and elastic modulus of IRP and the level of traffic loads. The results show that the operating internal pressure has a more significant effect on the longitudinal stresses than the circumferential stresses of the IRP subjected to cyclic bending. The level of internal pressure changes the failure behaviour of IRP under fatigue. Mathematical expressions were developed to predict the fatigue life of the IRP systems through the utilization of FEA results obtained from a comprehensive parametric study. Utilising the derived equations, contour plots which provide a visual representation of fatigue life response under different combinations of internal pressure and traffic loads were generated.

Keywords: Trenchless repair technology; Internal replacement pipe (IRP); Gas pipelines; Repetitive traffic loading; Flexural fatigue behaviour; Finite element analysis (FEA)

1 Introduction

Pipelines have been extensively utilised for transporting gas and oil over long distances, primarily due to their high transportation capacity, cost efficiency and safety [1-5]. Underground pipelines are susceptible to damage and failure during their service life, due to various factors, including but not limited to ageing, corrosion, construction defects, third-party disruption and operational errors [6-11]. Circumferential crack is the most prevalent failure in pipes with a smaller diameter (< 380.0 mm or 15.0 in) [12]. This type of crack is primarily caused by stresses induced by ground deformation during trench construction [12, 13]. Metal loss due to corrosion can also cause circumferential cracks in the legacy pipes [14, 15].

Internal replacement pipe (IRP) systems are a novel and developing trenchless rehabilitation technology that has been introduced for repairing bare steel and cast-iron legacy gas pipelines with circumferential cracks, discontinuities or pulled-out joints [16, 17]. This repair technique involves the insertion of a new structural pipe into legacy pipes that have defects and discontinuities. The integration of IRP systems yields significant enhancements in the structural integrity and restores the service life of legacy pipelines. This type of repair system is cost-effective, environmentally friendly and requires less construction time [18-22]. However, IRPs must be designed and developed in such a way that they can withstand different types of loading over their service life, including fatigue caused by repetitive traffic loads [16, 23].

There have been a limited number of studies on the bending fatigue behaviour of host pipes with circumferential cracks, discontinuities, or joints repaired with liners [13, 24, 25]. These repair systems are either cured-in-place pipe (CIPP) liners [13, 25] or spray-applied pipe liners (SAPL) [24] with low elastic modulus and low thickness in comparison to the host pipe. By conducting experimental three-point cyclic bending tests, Jeon et al [13] examined the fatigue performance of 0.25 mm (0.01 in) thick CIPP lined 152.4 mm (6.0 in) diameter cast iron (CI) pipe with a low internal pressure of nitrogen gas under one million loading cycles with a maximum vertical displacement of 2.5 mm (0.1 in). The liner was fully bonded to the host pipe, and there was 75% stiffness degradation after one million cycles, but no failures were observed.

Stewart et al [25] performed four-point cyclic bending tests of 2.5 mm (0.1 in) thick CIPP liners that were fully bonded to 152.4 mm (6.0 in) and 304.8 mm (12.0 in) diameter CI pipes with a joint under one million loading cycles with maximum deflections of 1.5 mm (0.06 in) and 1.8 mm (0.07 in), respectively while maintaining an operating pressure of 102 kPa (14.8 psi). These systems were subjected to a predetermined number of cycles in accordance with

service life requirements, rather than being cycled until failure, during which a decrease in stiffness was observed. The flexural fatigue behaviour of a 150.0 mm (5.9 in) diameter steel host pipe with a 25.0 mm (1.0 in) wide circumferential crack that was repaired with 3.0 mm (0.1 in) thick SAPL under a cyclic vertical displacement of 0.3 mm (0.01 in) with an internal water pressure of 12.0 kPa (1.7 psi) was studied by Ha et al [24]. Despite the observation of stiffness degradation in the system throughout the testing, Ha et al [21] found no failure or leakage in the liner pipe.

Available studies on the fatigue behaviour of repaired pipes were conducted under low internal pressure levels. However, according to Tien et al [26], the maximum operating internal pressure of the legacy steel pipe can be 413.7 kPa (60.0 psi), and their maximum allowable internal pressure can be 1379.0 kPa (200.0 psi). In their study, Tien et al [26] investigated the effect of crack edges on a steel host pipe with a diameter of 323.9 mm (12.8 in) on the behaviour of a thermoplastic IRP under an internal pressure of 1379.0 kPa (200.0 psi). The IRP had a thickness of 3.2 mm (0.1 in) and a modulus of elasticity (MOE) of 5.0 GPa (725.2 ksi). The width of the crack opening measured 914.4 mm (36.0 in) in width. It was found that under internal pressure alone, the IRP underwent bending as it curved around the crack edge of the host pipe, resulting in a concentration of longitudinal stresses. Unlike the crack edge region, the opening region of IRP is primarily influenced by hoop stress. These findings indicate that the application of internal pressure during cyclic bending could also have a detrimental effect on the fatigue life of the IRP when the circumferentially cracked host pipe exists.

Similarly, in a study conducted by Brown et al [27], the performance of a 5.0 mm (0.2 in) thick CIPP liner installed in circumferentially cracked CI host pipe under internal pressure of 689.5 kPa (100 psi) was investigated using FEA. Upon analysis, it was found that there was a significant concentration of axial stresses in the liner near the edge of the host pipe, where its structural integrity had been compromised. Shou and Chen [28] and Shou and Huang [29] investigated the effect of internal pressure on the static bending behaviour of steel pipes with circular corrosion defects repaired by CIPP liners with a MOE of 13.0 GPa (1885.5 ksi) under a vehicular load of 350.0 kN (78.7 kips). The defects found in the host pipes had a maximum diameter of 100.0 mm (3.9 in) and were located either on the upper or lateral surface. Shou and Chen [28] and Shou and Huang [29] discovered that maximum von Mises stress at the defect increases nonlinearly when the internal pressure is increased from zero to 588.4 kPa (85.3 psi). It was also revealed that under static bending, the internal pressure leads to a localised accumulation of longitudinal stresses at the damaged area.

The fatigue behaviour of an IRP could potentially be influenced by their wall thickness, MOE and the magnitude of the traffic load. In a recent study conducted by Tafsirojjaman et al [30] the behaviour of IRP alone made of various materials with MOE ranging from 1.0 GPa (145.0 ksi) to 200.0 GPa (29,007.5 ksi) and wall thicknesses ranging from 3.2 mm (0.1 in) to 25.4 mm (1.0 in) under repetitive traffic load of 17.4 kN (3.9 kips) was numerically investigated. They found that an increase in both MOE and wall thickness can significantly improve the fatigue life of IRP. Based on the outcomes of an experimental cyclic bending testing on carbon fibre-reinforced polymer (CFRP) pipe with thicknesses of 5.0 mm (0.2 in) and 11.2 mm (4.4 in), Huang et al [31] demonstrated that the CFRP pipes do not exhibit failure even after one million cycles when subjected to a load of 43.6 kN (9.8 kips) whereas those exposed to a relatively higher load (87.0 kN or 19.6 kips) failed before reaching the anticipated design life of one million cycles.

However, these existing studies have focused on the behaviour of non-pressurized IRP alone even though the operating internal pressure may have a detrimental effect on the behaviour of the repair pipe during cyclic bending, particularly in the existence of the damaged host pipe. According to the parametric studies on the effect of internal pressure alone and the combined effect of surface load and internal pressure, Shou and Chen [28] found that reducing the thickness of CIPP liner from 10.0 mm (0.4 in) to 5.0 mm (0.2 in) greatly increased the stress at the circular corrosion defect, while Shou and Huang [29] discovered that, increasing MOE of the liner from 13.0 GPa (1885.5 ksi) to 130.0 GPa (18,854.9 ksi) and thickness from 3.8 mm (0.1 in) to 6.2 mm (0.2 in) led to decrease the concentration of stress at the circular corrosion defect. The effects of these parameters on IRP used for host pipes with circumferential discontinuities require investigation under fatigue loading.

The present study examines numerically the effect of internal pressure on the bending fatigue behaviours of IRPs installed in host pipes with circumferential discontinuities at the midspan subjected to repetitive traffic loading. The investigations were carried out by varying thickness and MOE of the IRP and the levels of the loads caused by the repetitive traffic. By utilising the results obtained from extensive parametric investigations, mathematical equations that can predict the fatigue life of the IRP systems were established. Contour plots were generated by employing the derived equations to graphically represent the fatigue life response under different combinations of internal pressure and traffic loads. The outcomes of this study will assist pipeline developers and designers in delivering safe, reliable and cost-effective IRP repair systems, which are in high demand within the pipeline industry.

2 Methodology

2.1 Finite element modelling and analysis

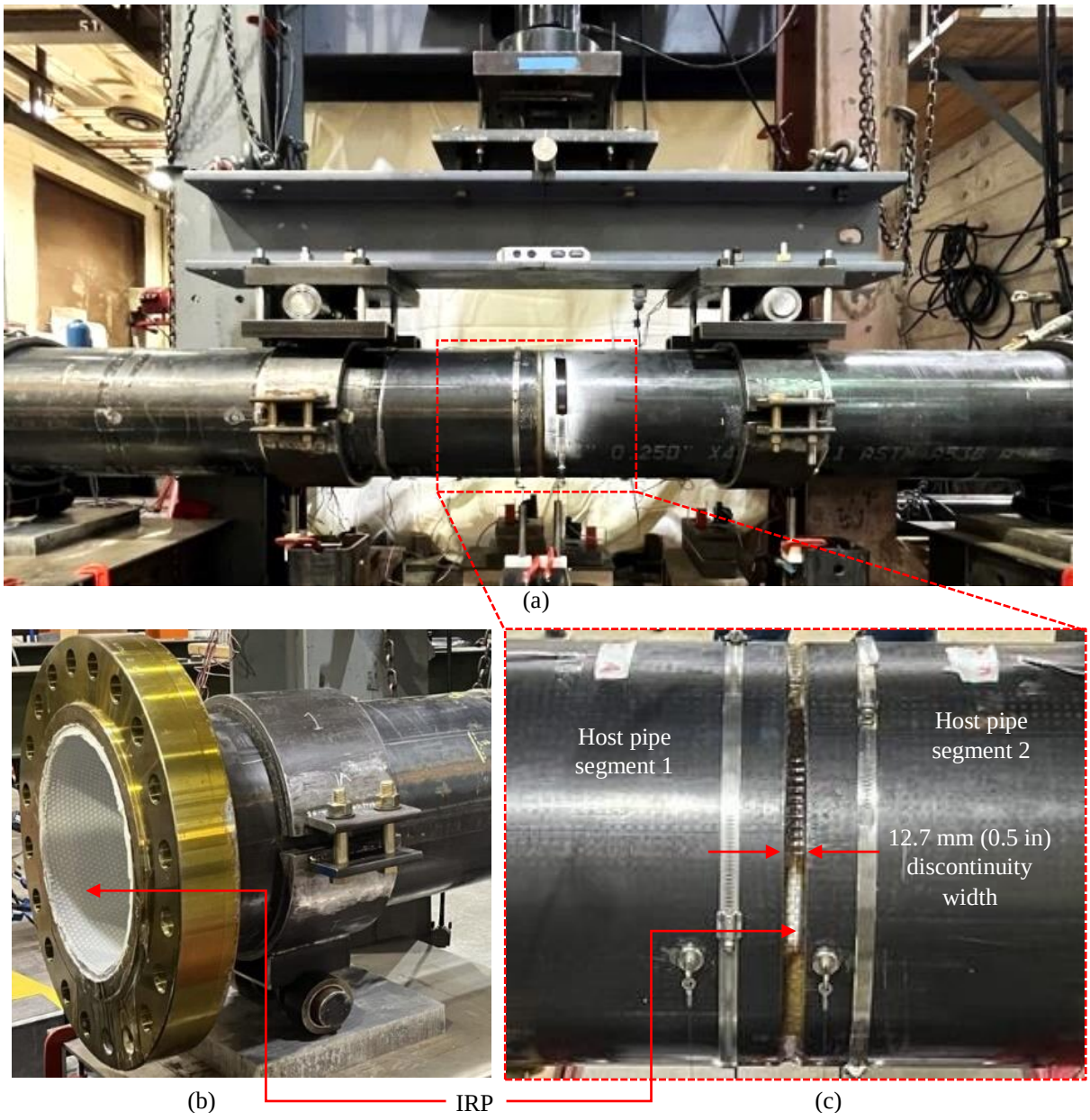

Fig. 1. (a) Actual four-point bending test setup developed by CUB, (b) Interior view of the system (c) circumferential host pipe discontinuity at the midspan

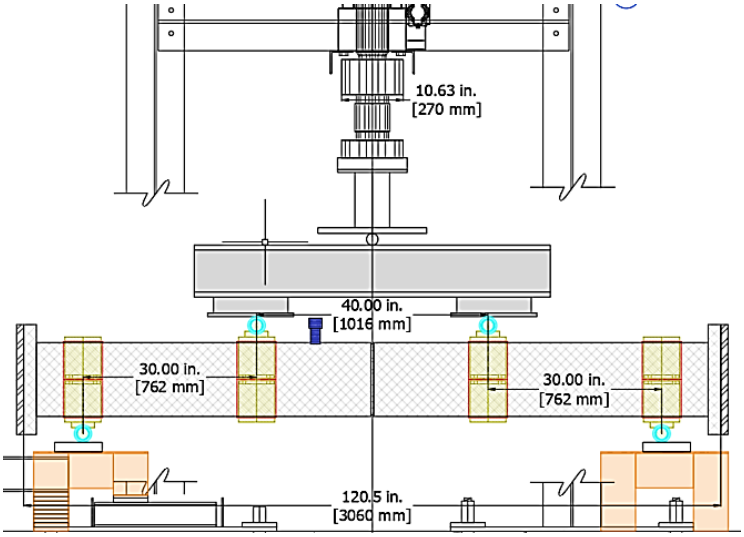

Fig. 2. Schematic diagram of four-point bending test setup (CUB)

Finite element models of four-point bending test in three dimensions (3D) are executed using ANSYS mechanical [32] to replicate the experimental configuration of IRP-repaired host pipe systems with discontinuities under vehicular traffic loading over 50 years of service life. The parameters employed in the simulation are identical to those utilised in the four-point bending test setup developed by the University of Colorado Boulder (CUB), as shown in Fig. 1 and Fig. 2. The host pipe in the FE model has a full circumferential discontinuity at the midspan. The present study employs a 12.7 mm (0.5 in) wide narrow discontinuity (Fig. 1c) that was identified as critical under static bending of IRP systems in an investigation conducted by Kiriella et al [33]. This discontinuity width indicates the presence of a pulled-out but operational joint in legacy pipelines. The host pipe has an outer diameter of 325.9 mm (12.8 in) and a wall thickness of 6.4 mm (0.3 in), both of which are kept at constant values throughout the study. While the outer diameter of the IRP, which is determined by the inner diameter of the host pipe, is held constant at 311.2 mm (12.3 in), the wall thickness is varied during the investigation.

The parameters utilised in this study were taken from a previous investigation, as reported in Tafsirojjaman et al [30], Tien et al [26], Kiriella et al [33] and Kiriella et al [34]. In order to optimise computational efficiency while taking into account the symmetry only one-quarter of the system (Fig. 3) is modelled by applying appropriate boundary conditions. A pinned support containing a frictionless connection between the host pipe and clamp is implemented to ensure a precise representation of experimental test configuration while mitigating potential convergence problems. Additionally, the loading head is attached to another clamp through the employment of a pin-lug mechanism. In most of the simulations,

the repair systems are subjected to an equivalent vehicular traffic load of 14.8 kN (3.3 kips) [35]. Standard SOLID186, a higher-order 3D solid element with 20 nodes, is used in the modelling of IRP systems. Steel is utilised for the host pipe, whereas several materials, including unreinforced polymer, and glass fibre-reinforced polymer (GFRP) composites are employed for IRP (Table 1).

Steel is also used for all other components such as clamps, lugs, pins and loading head. The analyses are conducted employing linear elastic isotropic material behaviour, under the assumption that the IRP material properties are consistent in both longitudinal and hoop direction directions. Additionally, it is assumed that both polymeric and FRP composites have a failure strain limit of 0.02 [30]. The current investigations employ the stress-life approach, considering that the anticipated design life of IRP is one million loading cycles [13, 25]. Stress-life (S-N) data for polymeric, GFRP-2, GFRP-3, GFRP-4 and GFRP-5 repair materials were gathered from the literature [36-38], while the stress-life behaviour of GFRP-1 material in both the longitudinal and transverse directions (as shown in Fig. 4(a) and (b), respectively) was generated by conducting fatigue tests according to ASTM D3479/D 3479M [39]. The stress ratio of the polymeric IRP material is -1, while that of all GFRP materials is 0.1[34]. In this investigation, the applied loading has a constant amplitude and a zero-based loading ratio. The Goodman mean stress correction theory is employed to correct any mean stress that arises during the fatigue analysis process [40-44].

Table 1. Properties of IRP and host pipe materials

Component	Material	MOE		Poisons ratio	Reference
		GPa	ksi		
IRP	Polymer	1.7	246.6	0.11	Mellott and Fatemi [36]
	GFRP-1	3.7	536.6	0.23	Laboratory testing
	GFRP-2	7.9	1145.8	0.25	Zakaria et al [37]
	GFRP-3	14.0	2030.5	0.25	Huh et al [38]
	GFRP-4	26.4	3829.0	0.25	Huh et al [38]
	GFRP-5	38.6	5598.5	0.25	Huh et al [38]
Host pipe	Steel	200	29007.5	0.29	Preedawiphat et al [45]

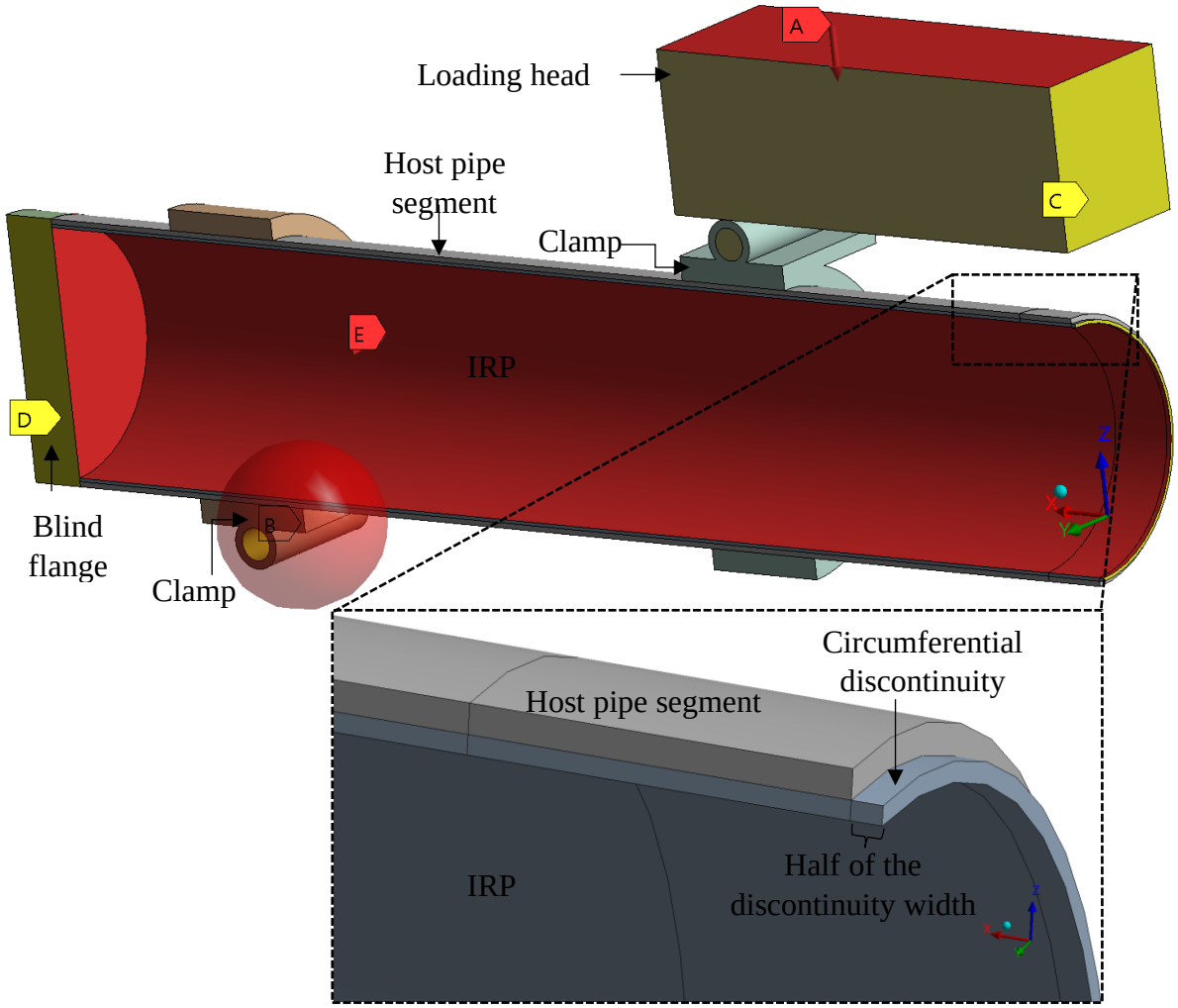

A Load
B Translational constraint along x, y and z axes and rotational constraints about x and z axes
C Translational constrains along x axis
D Translational constrains along y axis
E Internal pressure

Fig. 3. One-quarter of the FE model of an IRP installed within a host pipe that has a circumferential discontinuity at its midspan

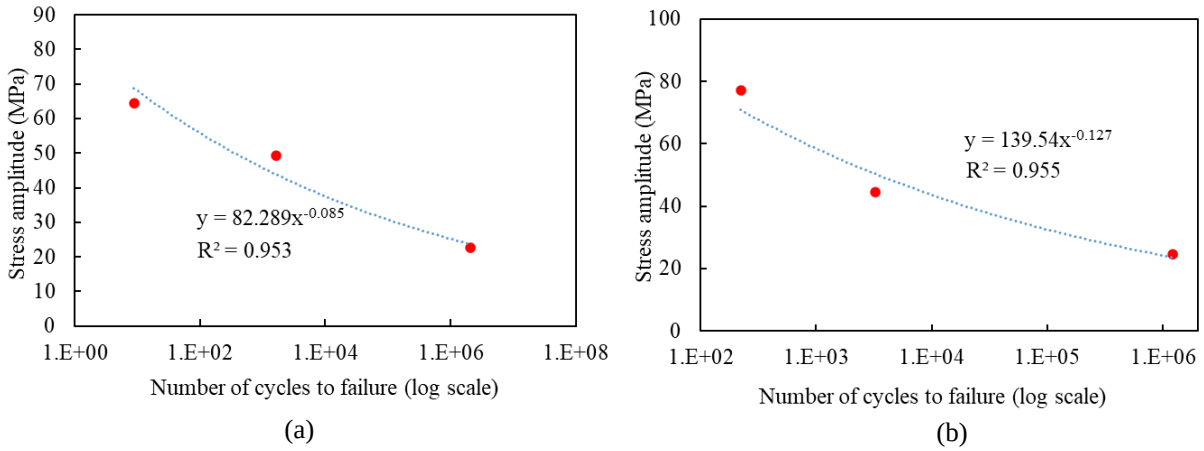

Fig. 4. S-N curve of GFRP-1 obtained from dog bone specimens that were cut in a manner where their lengths aligned with (a) longitudinal direction of IRP (MOE of 3.7 GPa or 536.6 ksi) and (b) circumferential direction of IRP (MOE of 9.7 GPa or 1406.9 ksi)

In the FE model, the IRP and discontinuous host pipe segments are adhered together along their entire interface using the bonded connection type in ANSYS mechanical. This ensures a fully bonded connection between the two components. Additionally, it is assumed that throughout the entire service life, the bond between the host pipe and IRP remains intact, with no debonding or detachment occurring at the interface. In the analysis, the internal pressure is varied from 0 to 620.5 kPa (90.0 psi) in increments of 206.8 kPa (30.0 psi). The selected internal pressure levels cover the maximum operating internal pressure of 413.7 kPa (60.0 psi), as reported by Tien et al [26], as well as pressure levels that are both below and above this threshold by 206.8 kPa (30.0 psi) in addition to the non-pressurised condition. The investigation examines the impact of internal pressure with different thicknesses and MOEs of IRP and levels of traffic loadings. The IRP thicknesses considered are 3.2 mm (0.1 in), 4.1 mm (0.2 in), 6.4 mm (0.3 in) and 9.5 mm (0.4 in). Various MOE of IRP materials used are listed in Table 1. The different levels of traffic loading are 10.0 kN (2.2 kips), 14.8 kN (3.3 kips), 20.0 kN (4.5 kips) and 25.0 kN (5.6 kips). These parameters are based on Kiriella et al [33].

2.2 Mesh convergence study

A mesh convergence study is conducted to identify the optimal mesh size for generating reliable FE results. The accuracy of the numerical model is determined by comparing the maximum bending stress generated by FEA to the maximum theoretical stress of 18.8 MPa (2.7 ksi) obtained from Eq. (1). To accomplish this, an IRP alone with a MOE of 3.7 GPa

(536.6 ksi) and dimensions specified in section 2.1 is simulated under a traffic load of 14.8 kN (3.3 kips). The element size of the pipe surface is varied from 25.0 × 25.0 mm (1.0 × 1.0 in) to 2.0 × 2.0 mm (0.08 × 0.08 in), and the mesh size in the direction of wall thickness is fixed to three elements as found optimal in Kiriella et al [33]. Fig. 5 shows how the number of elements in the mesh of the FE model correlates with the maximum bending stress. The FE solutions are found to be within 1.6% of theoretical results following the bending stress formula (Eq. (1)) when the element size is smaller than 5.0 × 5.0 mm (0.2 × 0.2 in).

$$\sigma = \frac{M}{S} \tag{1}$$

where σ is the bending stress, M is the bending moment applied to the pipe, S is the section modulus of the pipe.

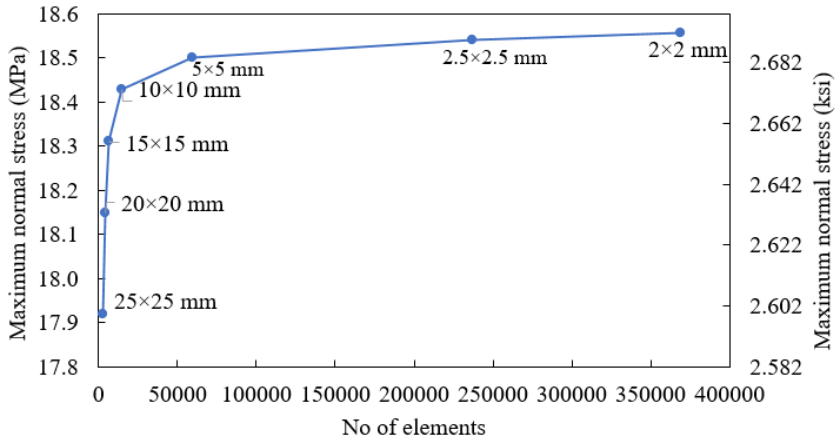

Fig. 5. Mesh convergence study of IRP

A mesh refinement was performed in the region of the discontinuity edge of the host pipe segment to accurately capture potential stress concentration. The optimal surface element size for the refined mesh was determined through the execution of a mesh sensitivity analysis, as illustrated in Fig. 6. This involves analysing a steel host pipe with a discontinuity width of 12.7 mm (0.5 in) repaired using the same IRP that was used for the mesh convergence study outlined above under a traffic load of 14.8 kN (3.3 kips). Considering the computational efficiency, the mesh refinement is performed over a length equivalent to the width of host pipe discontinuity, with an additional 76.2 mm (3.0 in) extending beyond the edge of discontinuity.

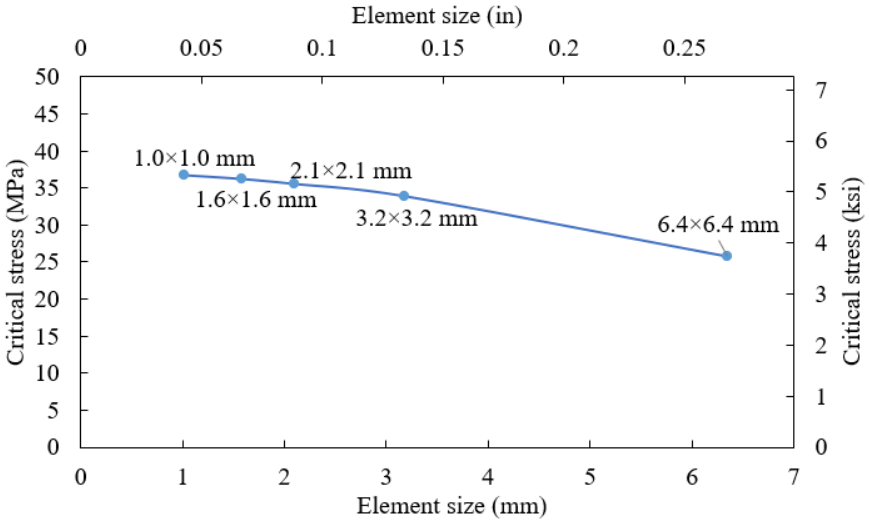

Fig. 6. Mesh sensitivity analysis for critical stress in IRP at the crack edge

During the sensitivity analysis, the surface element sizes of the refined mesh are adjusted within the range of 6.4 × 6.4 mm (0.3 × 0.3 in) and 1.0 mm × 1.0 mm (0.04 × 0.04 in). A size of 5.0 × 5.0 mm (0.2 ×0.2 in) is employed in the region beyond these refined areas. Fig. 6 shows the impact of varying element sizes employed for mesh refinement on the localised stress in the IRP at the edge of the host pipe discontinuity. When the surface element size of the refined mesh is reduced below 2.1× 2.1 mm (0.08× 0.08 in), the localised stress in IRP at the discontinuity edge starts to converge towards a finite value. After taking into account the computational cost and the observation that the difference in the local stress at the discontinuity edge between element sizes of 1.0 mm× 1.0 mm (0.04 × 0.04 in) and 1.6× 1.6 mm (0.06× 0.06 in) is less than 2.0%, a decision has been made to choose an element size of 1.6× 1.6 mm (0.06× 0.06 in) for the mesh refinement. Fig. 7 illustrates the mesh refinement of a quarter symmetry model of an IRP installed within a host pipe containing a 12.7 mm (0.5 in) wide discontinuity. After the mesh refinement, the total number of elements in the compound section of IRP and host pipe is 209,061.

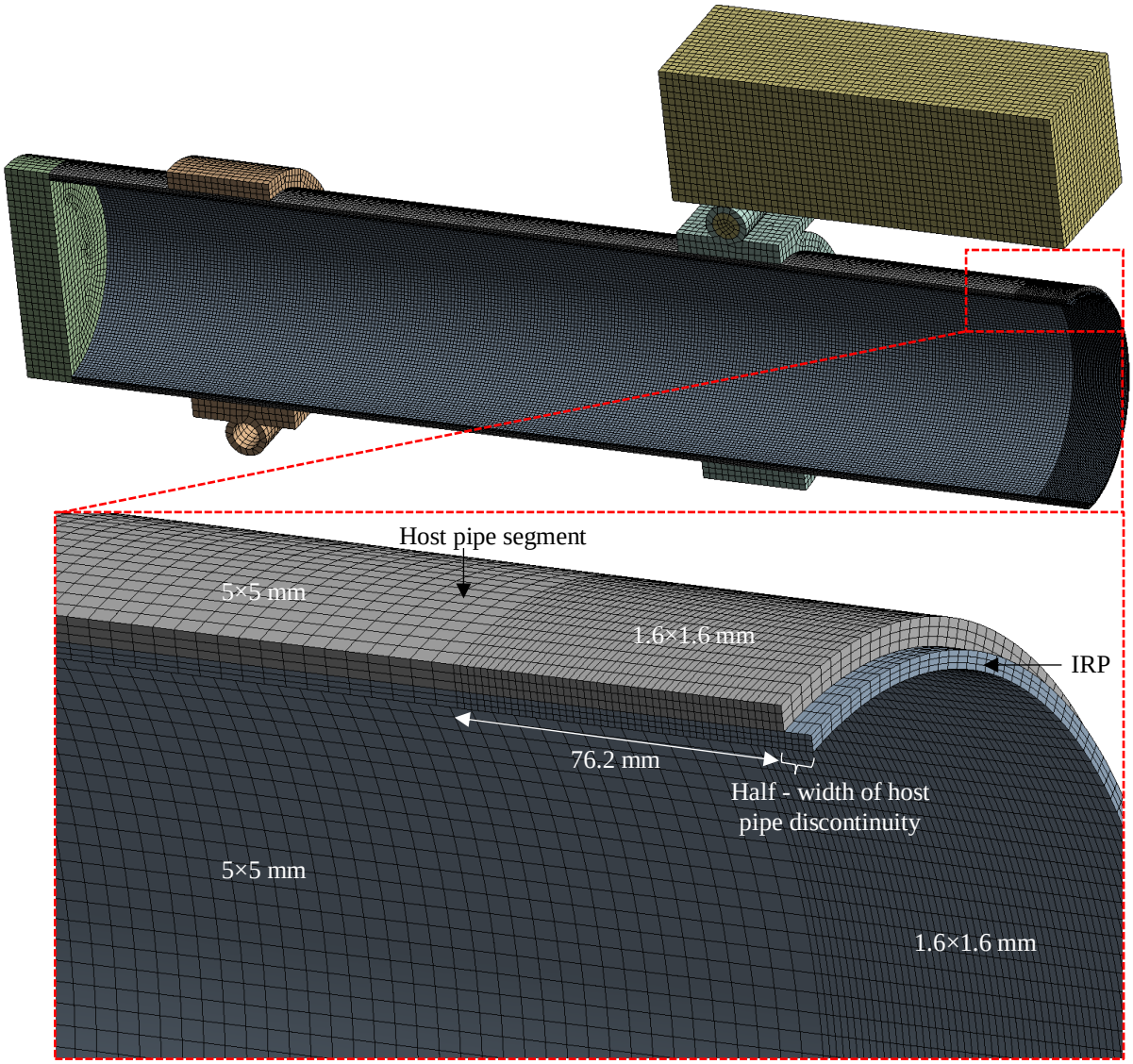

Fig. 7. Mesh refinement of quarter FE model of an IRP inserted in host pipe with 12.7 mm (0.5 in) wide discontinuity

2.3 Hot-spot stress approach for determining stress concentration

Hot-spot stress (HSS) method is often acknowledged as an acceptable approach for determining the highest stress at a discontinuity in a segment, which can be applied for fatigue analysis of IRP systems installed within host pipes containing discontinuities. In order to calculate HSS, it is required to determine the surface stress field in the close vicinity of the discontinuity edge, at which the HSS is computed using extrapolation rules at specific predefined stress evaluation points [46]. According to the extrapolation rules recommended by the International Institute of Welding (IIW) and the study conducted by Haghpanahi and Pirali [47] that focuses on acrylic tubular joints without welding, it has been identified that the first extrapolation point should be set at a distance that is 0.4 times the thickness of the IRP from

the host pipe discontinuity edge and the second should be set at a distance beyond the first point that is equal to the thickness of IRP [48]. The geometric stress at these two specific points is linearly extrapolated to the edge of the host pipe discontinuity to determine the HSS. This process is depicted in Fig. 8 and can be mathematically expressed by Eq.(2).

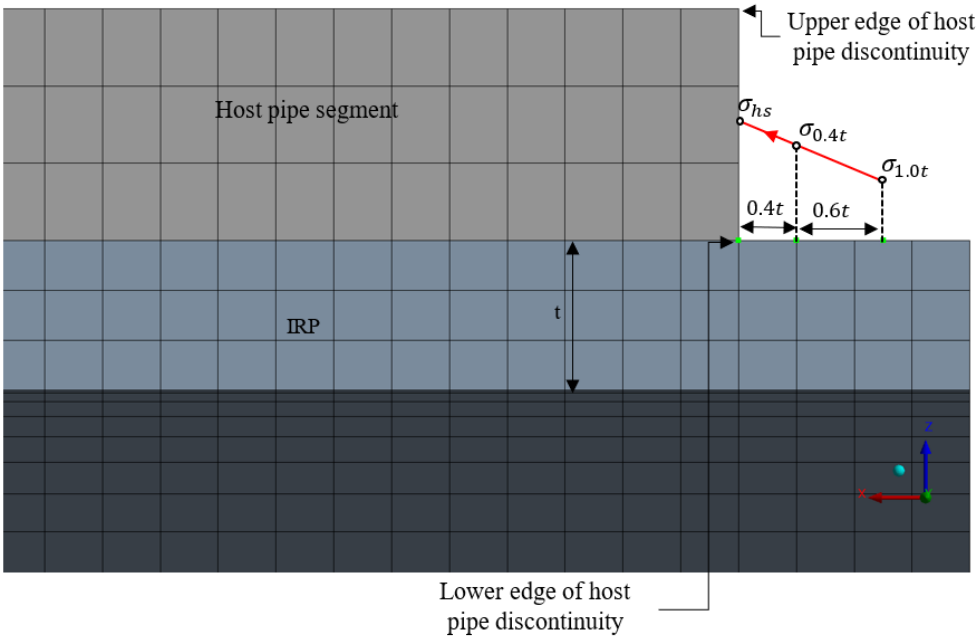

Fig. 8. Linear extrapolation method for obtaining HSS from the FE model

$$\sigma_{hs} = 1.67\sigma_{0.4t} - 0.67\sigma_{1.0t} \quad (2)$$

Fig. 9 presents a comparative analysis of HSS and localised stress in IRP at the edge of host pipe discontinuity on the tension side subjected to a traffic load of 14.8 kN (3.3 kips) under internal pressure levels of zero, 206.8 kPa (30.0 psi), 413.7 kPa (60.0 psi) and 620.5 kPa (90.0 psi). Based on the data shown in the figure, both HSS and localised stress at the discontinuity edge exhibit a comparable trend as the internal pressure is increased. The maximum discrepancy between the HSS and localised stress is approximately 8%, which is considered negligible for this type of problem. Although the process of assessing fatigue life through the HSS approach is relatively efficient when dealing with a small number of FE models, it becomes more challenging and time-consuming when confronted with a substantial number of different scenarios in parametric studies. The reason for this is that the HSS approach in the current study necessitates manual calculation of alternating stress and the corresponding fatigue life. In contrast, the ANSYS fatigue tool can provide a direct measurement of fatigue life by employing the local stress approach, thereby excluding the necessity for manual calculations.

While the local stress may exhibit a sight over-conservative tendency, typically within an 8% range of HSS values, it can still be regarded as a reasonable estimate. Therefore, the local stress approach has been chosen over the HSS method for fatigue life analysis in this study due to its ability to achieve a balance of practicality and accuracy while effectively meeting the requirements of the analysis.

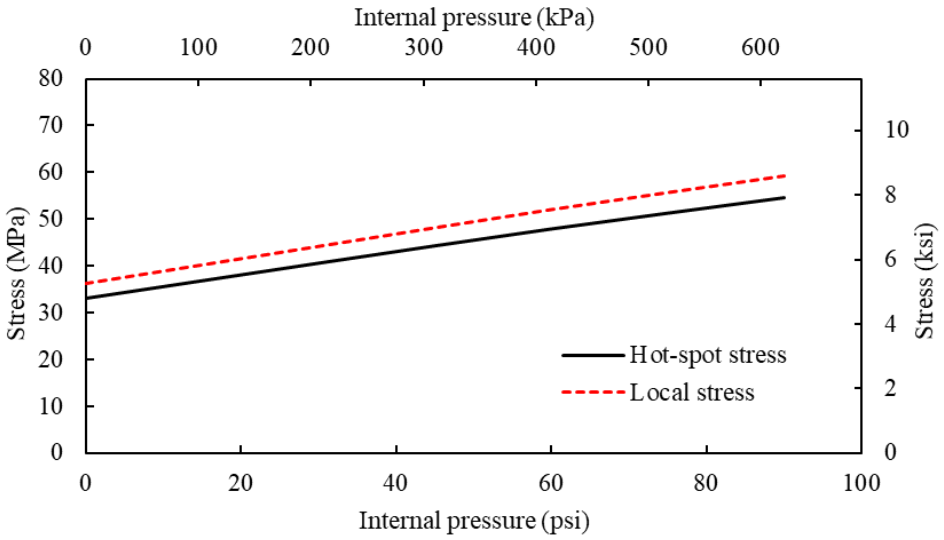

Fig. 9. A comparison of HSS and local stress in IRP at the crack edge of the host pipe on the tension side

2.4 Validating the numerical model

The accuracy of the FEA results is ensured through validation with laboratory experimental results from CUB. The present study consists of a comparison between the load-strain (Fig. 10) and load-deflection (Fig. 11) behaviours of a GFRP-1 IRP installed in a steel host pipe with a discontinuity width of 12.7 mm (0.5 in) under a cyclic bending load of 14.3 kN (3.2 kips) obtained from FEA and laboratory experiments. The results are extracted from multiple locations at the crown and invert of both the left and right halves of the IRP. The distances to each location in both Fig. 10 and Fig. 11 are measured from the midspan. The load-strain and load-deflection behaviours obtained from FEA are in good agreement with experimental results, as depicted in Fig. 10 and Fig. 11, respectively.

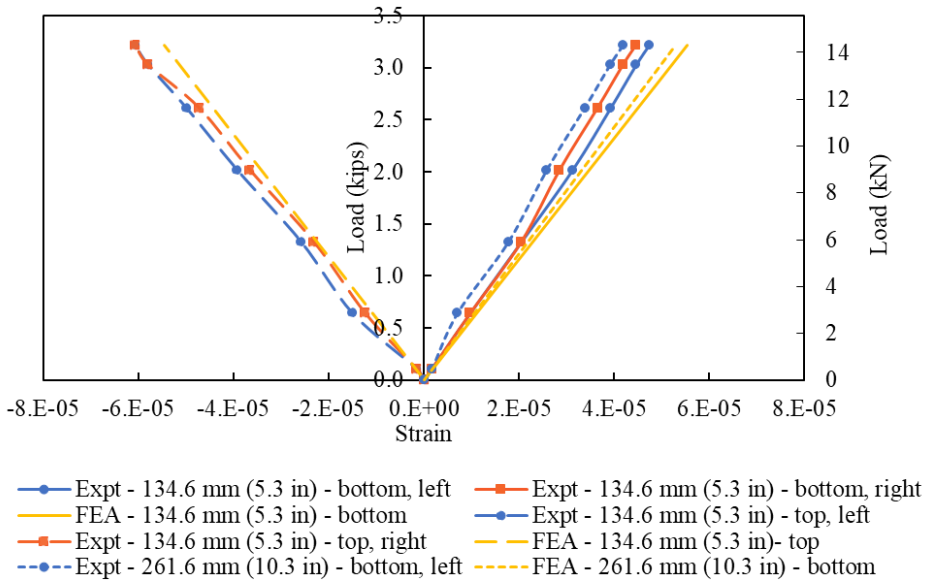

Fig. 10. Comparison of load-strain behaviours of IRP from FEA and laboratory experiments

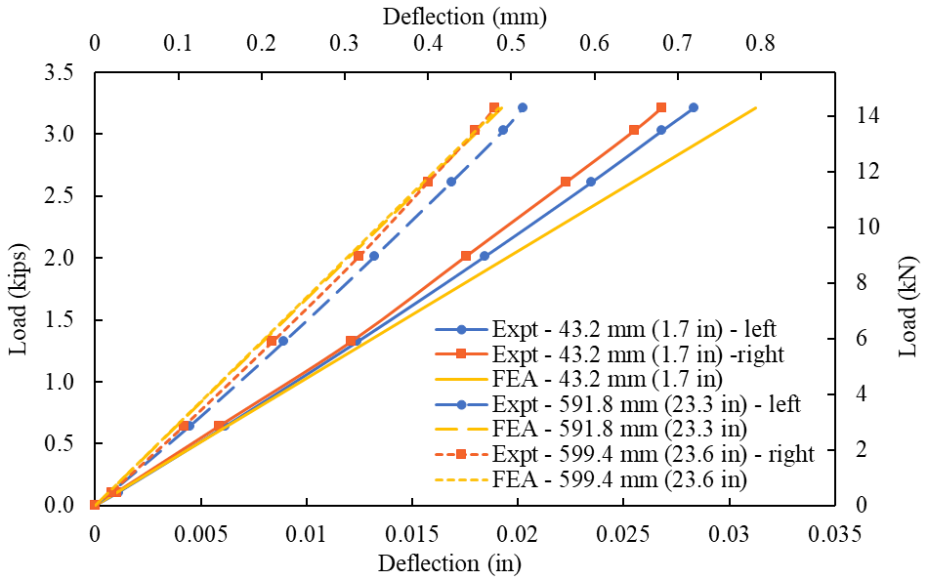

Fig. 11. Comparison of load-deflection behaviours of IRP from FEA and laboratory experiments

3 Results and discussion

3.1 Longitudinal stresses, hoop stresses and fatigue lives

When an IRP repair system that is under internal pressure is exposed to cyclic bending, it undergoes a combination of bending stress caused by bending moment and hoop stress resulting from the internal pressure. The longitudinal and hoop stress at the discontinuity edge and the midspan of the IRP, as the internal pressure increases, are demonstrated in Fig. 12. GFRP-1 repair material is utilized to conduct this analysis with a repair thickness of 4.1 mm

(0.2 in) while the internal pressure is varied between zero and 620.5 kPa (90.0 psi) under a traffic loading of 14.8 kN (3.3 kips). It can be seen from the figure that the level of longitudinal and hoop stresses in the IRP at both the discontinuity edge and the midspan of the bottom are in tension and increase almost linearly, while those at the top of the IRPs are in compression and decrease linearly.

The reason for such behaviour is that when internal pressure is present, it creates forces along the length of the host pipe that cause the IRP to elongate in the axial direction, inducing longitudinal stresses. In the tensile region (bottom) of the IRP, the additional longitudinal stress induced by internal pressure combined with the bending stress resulted in a relatively higher tensile stress compared to that of the system with no internal pressure. In the compression region (top) of IRP, the bending stresses reduce the longitudinal stresses induced by internal pressure resulting in relatively lower compressive stress compared to the system with no internal pressure. Since the magnitude of the longitudinal stress induced is proportional to the internal pressure applied, an increasing internal pressure under the same level of traffic load leads to a rise in longitudinal stresses, which ultimately results in an overall increase in tensile stress while a decrease in compressive stress in IRP.

Under all internal pressure levels, longitudinal stresses are higher than the corresponding hoop stresses at each of the locations on IRP being considered. At all the internal pressure levels, longitudinal tensile stress at the bottom of IRP at the discontinuity edge is the dominant stress during bending fatigue when the system is fully bonded, which is similar to that without internal pressure (Fig. 13). Without internal pressure, the lower portion of IRP at midspan exhibits a slight bulging effect between the discontinuity edges of the host pipe, while the upper portion undergoes a minor inward bending as depicted in Fig. 13. As the internal pressure increases, the bulge at the bottom of IRP becomes more pronounced due to the increase in longitudinal tensile stress while the inward bending at top diminishes because of the decrease in longitudinal compressive stress (Fig. 14). The overall increase in the critical stress at the discontinuity edge at the bottom as the internal pressure rises from zero to 620.5 kPa (90.0 psi) is around 72%. According to Tien et al [26], it is possible to reduce the stress concentration due to internal pressure at the discontinuity edge by not bonding the IRP to the host pipe up to a certain length. This approach allows the unbonded length of the IRP to slide relatively within the host pipe, enabling more effective formation around the discontinuity edge compared to the fully bonded scenario. Additionally, rounding the edges of the host pipe can reduce potential stress concentration in bonded IRP systems.

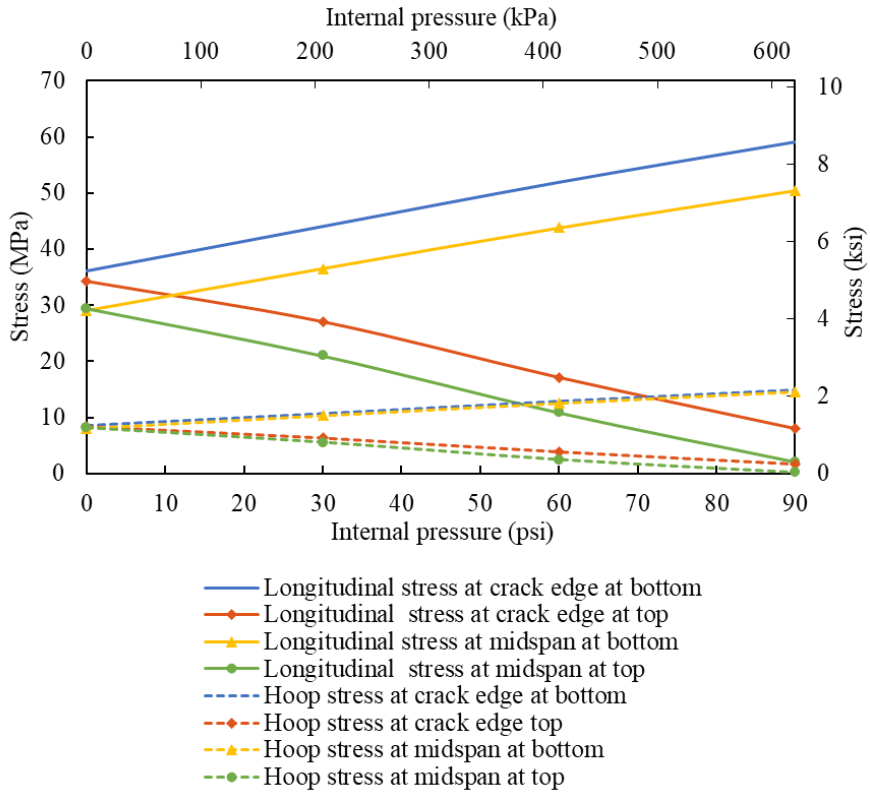

Fig. 12. Comparison between longitudinal stresses and circumferential stresses in IRP system with different internal pressures after undergoing cyclic bending

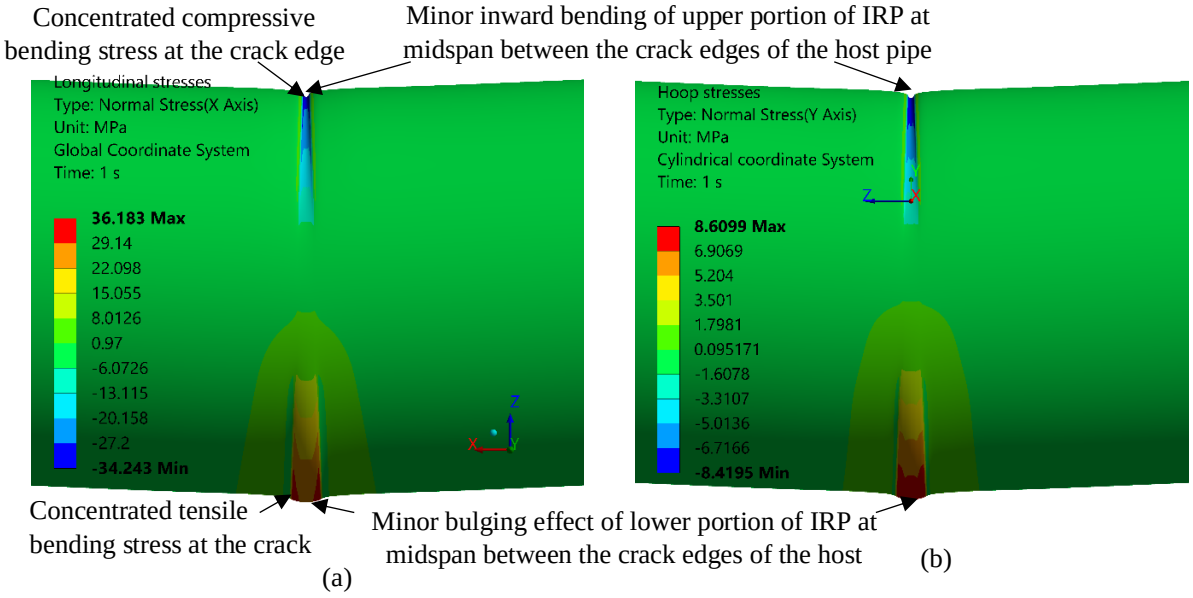

Fig. 13. (a) Longitudinal and (b) hoop stress distribution on the outer surface of non-pressurised IRP (To facilitate clear visualisation, host pipe segments are hidden)

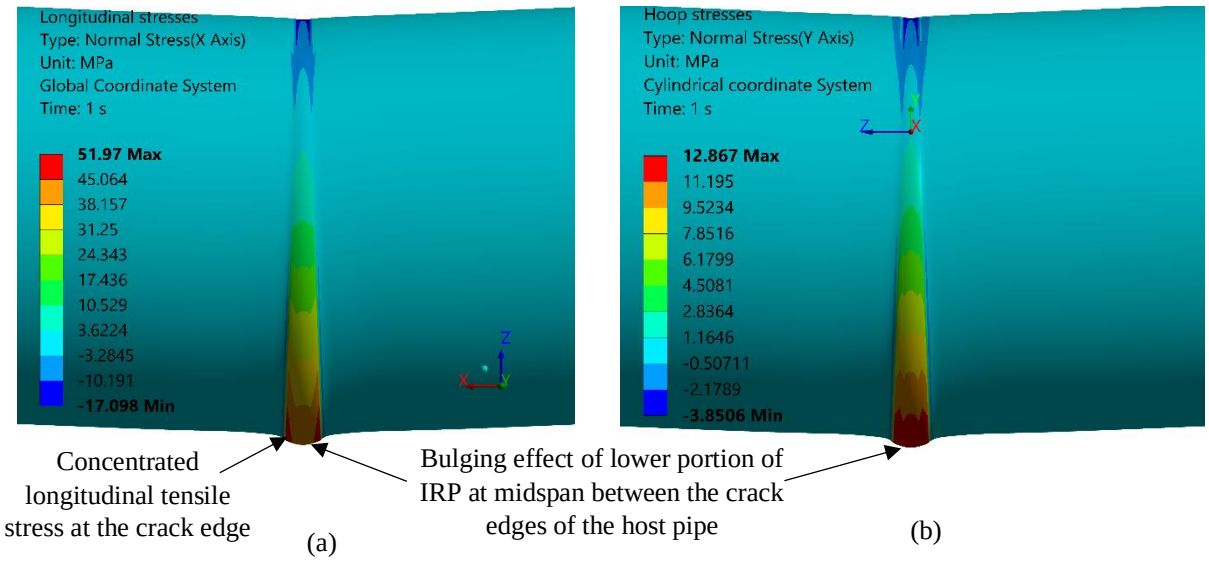

Fig. 14. (a) Longitudinal and (b) circumferential stress distribution on the outer surface of IRP between the discontinuity edges of host pipes with an internal pressure of 413.7 kPa (60.0 psi) (To facilitate clear visualisation, host pipe segments are hidden)

Table 2. Fatigue life comparison between the circumferential and longitudinal stresses

Internal pressure	Fatigue life (cycles)	
	Based on maximum alternating stress in longitudinal direction and corresponding S-N behaviour (MOE of 3.7 GPa or 536.6 ksi)	Based on maximum alternating stress in circumferential direction and corresponding S-N behaviour (MOE of 9.7 GPa or 1406.9 ksi)
zero	2.7E+06	>>1.0E+09
206.8 kPa (30.0 psi)	1.2E+05	>>1.0E+09
413.7 kPa (60.0 psi)	8492	>>1.0E+09
620.5 kPa (90.0 psi)	869	>>1.0E+09

Table 2 presents a comparison of fatigue life between the circumferential and longitudinal stresses for a 4.1 mm (0.2 in) thick GFRP-1 IRP subjected to a traffic load of 14.8 kN (3.3 kips) under different levels of internal pressure. The fatigue life of IRP, based on maximum alternating stress in the longitudinal direction and corresponding S-N behaviour at an internal pressure of zero, 206.8 kPa (30.0 psi), 413.7 kPa (60.0 psi) and 620.5 kPa (90.0 psi) are determined to be 2.7E+06, 1.2E+05, 8492 and 869 cycles, respectively. In contrast, even when exposed to an internal pressure of 620.5 kPa (90.0 psi), the fatigue life of IRP, determined based on the maximum alternating stress in the circumferential direction and corresponding S-N behaviour, exceeds one billion cycles. This is because the circumferential stresses that arise in an IRP system during bending are significantly lower than the axial stresses, as previously explained. The reason for this is that most IRP systems are designed to be stiffer and stronger

in the circumferential than in the longitudinal directions. Hence, it is considered acceptable to neglect the analysis of fatigue life during bending based on the circumferential stresses. In subsequent analysis, the estimation of fatigue life is therefore based solely on the longitudinal stresses.

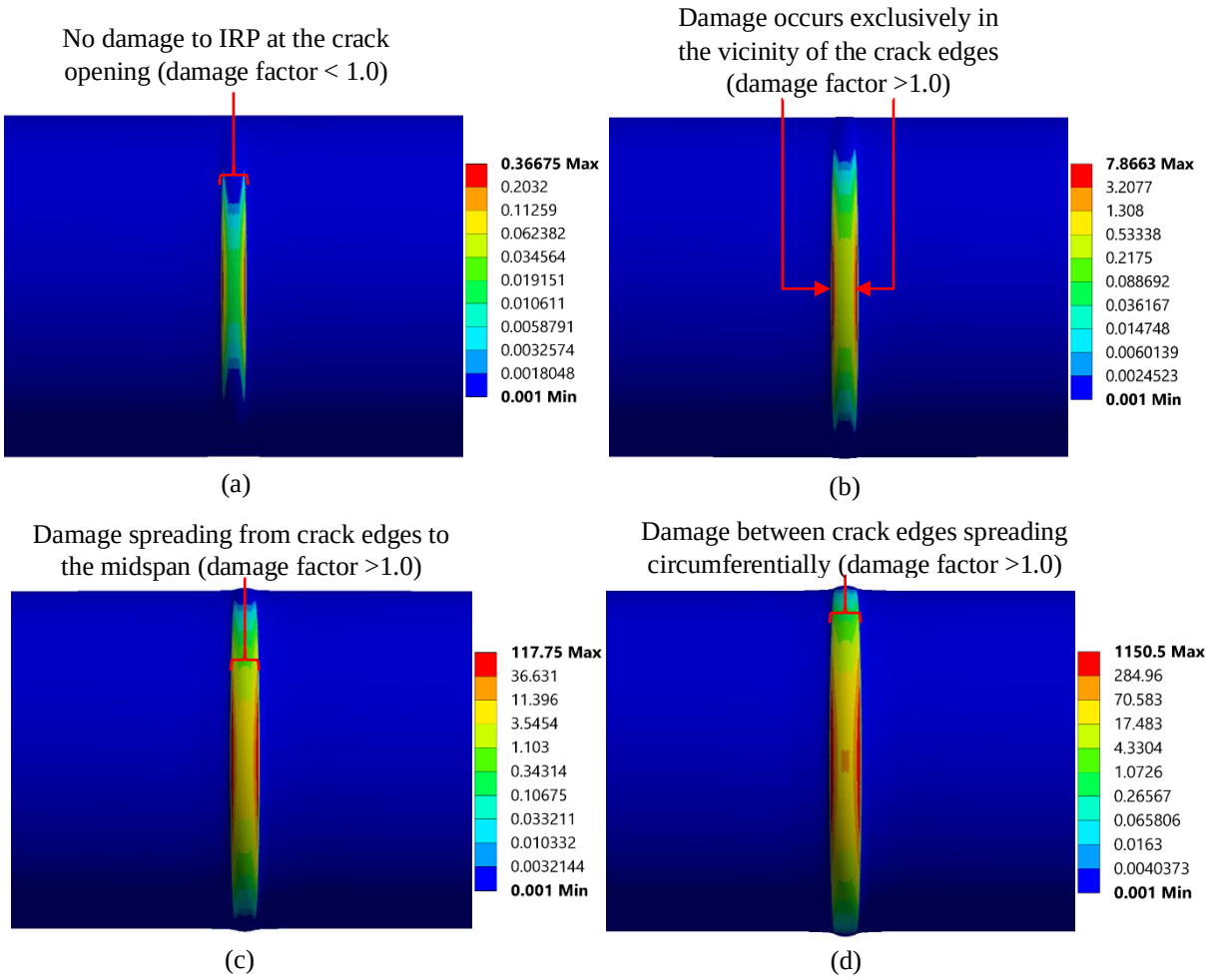

Fig. 15. Fatigue damage at the bottom midspan GFRP-1 with an internal pressure of (a) zero, (b) 30 psi, (c) 60 psi and (d) 90 psi during the service life (To facilitate clear visualisation, host pipe segments are hidden)

According to the observed minimum fatigue lives, only the non-pressurized GFRP-1 out of four different scenarios examined, seems to be capable of meeting the design life requirement of one million loading cycles, while the systems with 206.8 kPa (30.0 psi) or higher are susceptible to failure well before reaching the intended service life. The contour plots in Fig. 15 show the amount of fatigue damage experienced by GFRP-1 IRP systems over their intended design life, quantified as a damage factor. It is important to note that the damage factor represents the ratio of the fatigue life of the IRP system to its intended design life of one

million cycles. The fatigue damage contour plots reveal that, throughout its service life, the bottom of GFRP-1 IRP will undergo fatigue damage, with a damage factor greater than 1.0, exclusively at the discontinuity edges of host pipe segments when subjected to an internal pressure of 206.8 kPa (30.0 psi) as depicted in Fig. 15b. However, when exposed to an internal pressure of 413.7 kPa (60.0 psi) and 620.5 kPa (90.0 psi), even bottom midspan GFRP-1 will be susceptible to damage as shown in Fig. 15c and d. As the internal pressure rises, the damage to the lower portion of the IRP expands in its circumferential direction. Linear interpolation reveals that the GFRP-1 with thicknesses of 4.1 mm (0.2 in) and exposed to a traffic load of 14.8 kN (3.3 kips) will satisfy the design fatigue life if the internal pressure does not surpass 121.3 kPa (17.6 psi).

3.2 Effect of internal pressure with different repair thickness

The effect of internal pressure on critical stress (i.e. longitudinal tensile stress) and fatigue life for different repair thicknesses of GFRP-1 ranging from 3.2 mm (0.1 in) to 9.5 mm (0.4 in) under a traffic load of 14.8 kN (3.3 kips) is shown in Fig. 16a and b, respectively. According to Fig. 16a, under the same level of traffic loading, the critical stress in IRP with repair thicknesses of 3.2 mm (0.1 in), 6.4 mm (0.3 in) and 9.5 mm (0.4 in) increases linearly as the internal pressure rises, similar to that of IRP with 4.1 mm (0.2 in). This is because an increase in the internal pressure amplifies the force that causes IRP to elongate in the longitudinal direction. This results in an increase in internal pressure-induced longitudinal stress, which combines with the bending stress to produce the overall tensile stress in the longitudinal direction.

Additionally, with an internal pressure of 620.5 kPa (90.0 psi), the maximal tensile stress generated in the IRP with thicknesses of 3.2 mm (0.1 in) and 9.5 mm (0.4 in) are respectively 62.3% and 60.3% higher than corresponding repair systems with no internal pressure. On the other hand, as the internal pressure rises, fatigue life exhibits a nonlinear decrease for all IRP thicknesses considered, even on a semi-log scale (Fig. 16b). Furthermore, while the 9.5 mm (0.4 in) thick IRP achieves the design life of one million cycles even with an internal pressure of 620.5 kPa (90.0 ksi), the 3.2 mm (0.1 in) thick IRP is unable to meet the design requirement even without internal pressure. The IRP with thicknesses of 6.4 mm (0.3 in), on the other hand, cannot achieve one million cycles when the internal pressure exceeds 385.4 kPa (55.9 psi).

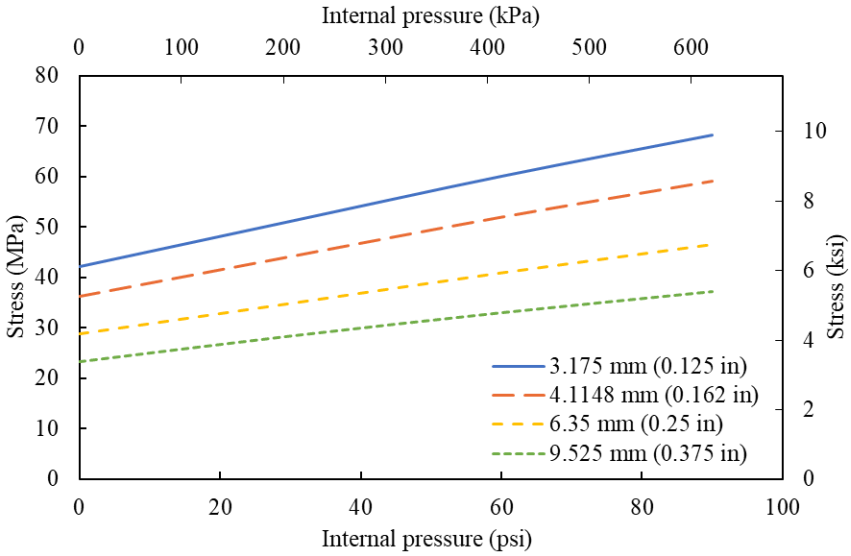

(a)

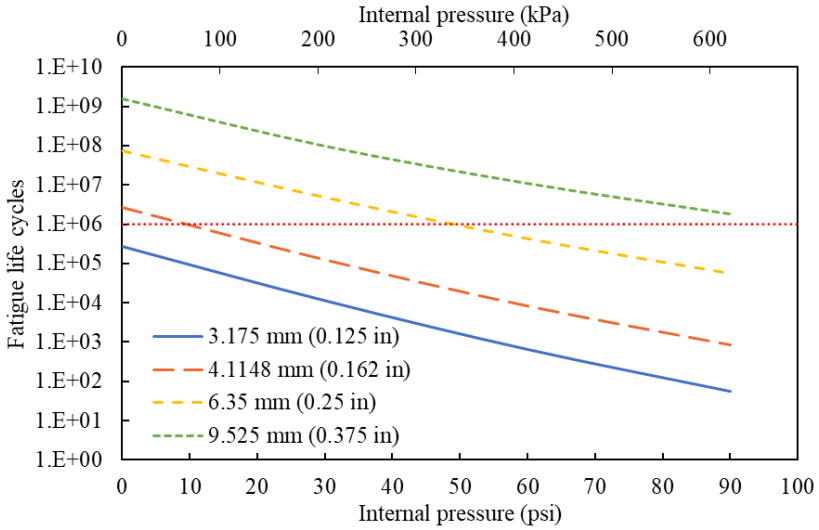

(b)

Fig. 16. Effect of internal pressure on (a) critical tensile stress and (b) minimum fatigue life of IRP repair systems with different repair thickness

The influence of IRP thickness on the critical tensile stress in GFRP-1 under 14.8 kN (3.3 kips) of traffic load with multiple levels of internal pressure varying from zero to 620.5 kPa (90.0 psi) is depicted in Fig. 17a and b, respectively. As can be seen from Fig. 17a, the critical tensile stress decreases nonlinearly as the IRP thickness increases from 3.2 mm (0.1 in) to 9.5 mm (0.4 in) for all the internal pressures considered. This is because the increasing IRP thickness can distribute the combined forces induced by both bending and internal pressure more evenly across the cross-section. Additionally, thicker IRP also has greater bending and

axial stiffness, which enables it to resist deformation and strain under combined loading. This also results in lower stress concentration at the discontinuity edge, as thicker IRP can better withstand the loading condition without experiencing excessive deformation. The greatest stress reduction (45.5%) occurs when the repair thickness increases under the highest internal pressure (620.5 kPa or 90.0 psi), while the lowest reduction (44.9%) is observed when there is no internal pressure in the system.

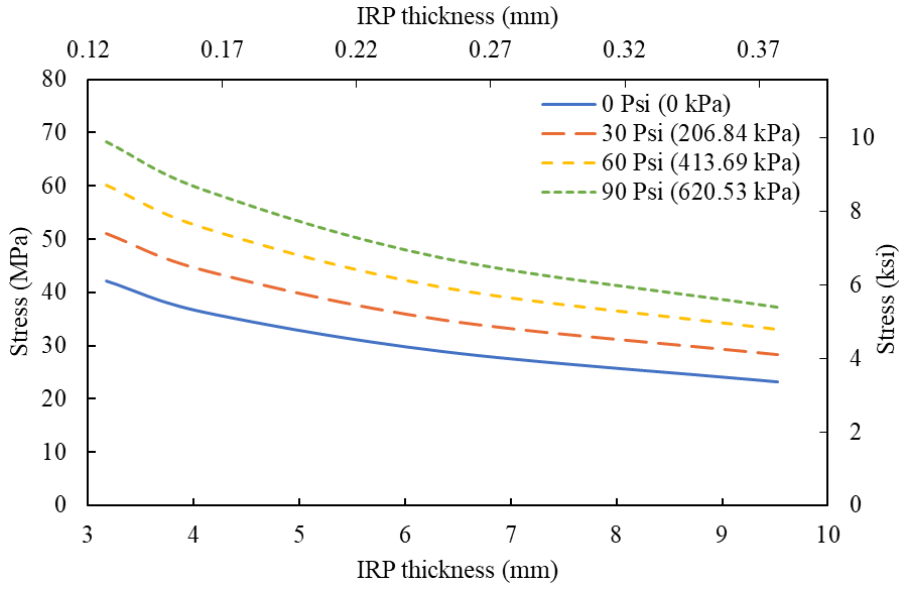

(a)

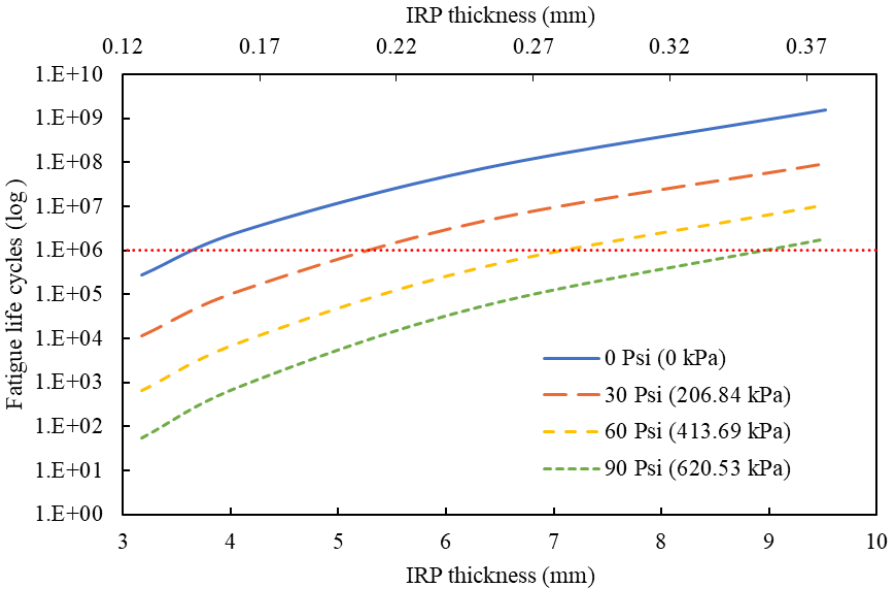

(b)

Fig. 17. Effect of IRP thickness on (a) critical tensile stress and (b) minimum fatigue life of IRP systems with different internal pressure

3.3 Effect of internal pressure with different MOE of IRP materials

Fig. 18 compares the effect of MOE on the critical tensile strain of 4.1 mm (0.2 in) thick IRP for different levels of internal pressure under the traffic load of 14.8 kN (3.3 kips). Regardless of the level of internal pressure, the strain undergoes a dramatic nonlinear decrease when the MOE increases from 1.7 GPa (246.6 ksi) to 7.9 GPa (1145.8 ksi), followed by a gradual reduction until it reaches a MOE of 38.6 GPa (5598.5 ksi). The reduction in strain with increasing MOE is consistent across all the internal pressure levels, with an overall reduction of 96.7%. When the MOE of IRP is at or below 2.4 GPa (348.1 ksi), 2.9 GPa (420.6 ksi) and 3.2 GPa (464.1 ksi), respectively, the critical strain surpasses the design strain limitation of 0.02 at internal pressures of 206.8 kPa (30.0 psi), 413.7 kPa (60.0 psi) and 620.5 kPa (90.0 psi).

Fig. 19 displays the response of critical stress of IRP with different levels of internal pressure as the MOE increases under a traffic loading of 14.8 kN (3.3 kips). The graph indicates that the critical stress remains almost constant at all internal pressures as the MOE of IRP increases from 1.7 GPa (246.6 ksi) to around 15.0 GPa (2175.6 ksi). However, from 15.0 GPa (2175.6 ksi) up to 30 GPa (4351.1 ksi) of MOE, the critical stress produced in the IRP without internal pressure and internal pressures of 206.8 kPa (30.0 psi) and 413.7 kPa (60.0 psi) nonlinearly decreases in a concave up manner, after which it remains stable until MOE of 38.6 GPa (5598.5 ksi). On the other hand, the critical stress generated in the IRP with the internal pressure of 620.5 kPa (90.0 psi) decreases nonlinearly in a concave-down manner as MOE increases from 15.0 GPa (2175.6 ksi) to 38.6 GPa (5598.5 ksi). The decrease in stress is because the MOE is directly related to the stiffness or its ability to resist deformation under stress. When a stiffer IRP is used, it can more effectively distribute the load and resist deformation under the combined effect of internal pressure and traffic load than a more flexible IRP. As a result, the concentration of stress at the discontinuity edge diminishes, resulting in a reduction of maximum tensile stress.

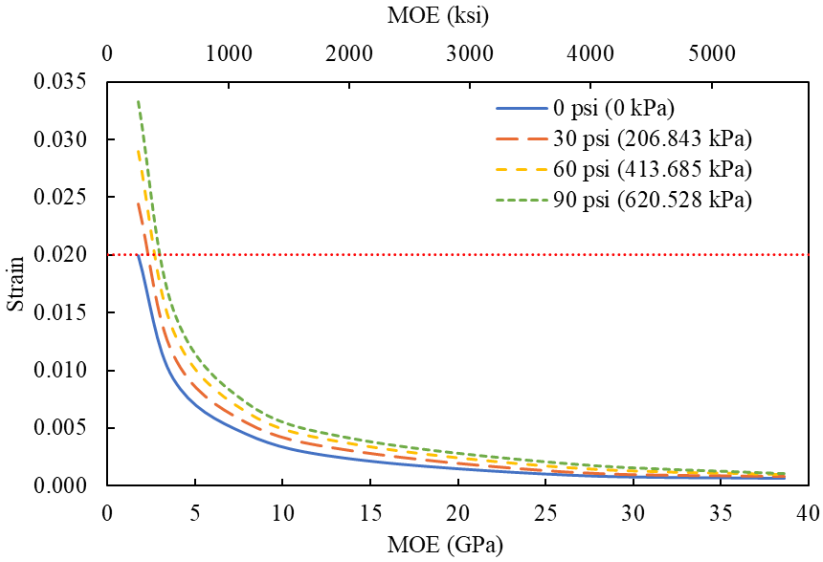

Fig. 18. Effect of MOE on the critical tensile strain of IRP with different internal pressure

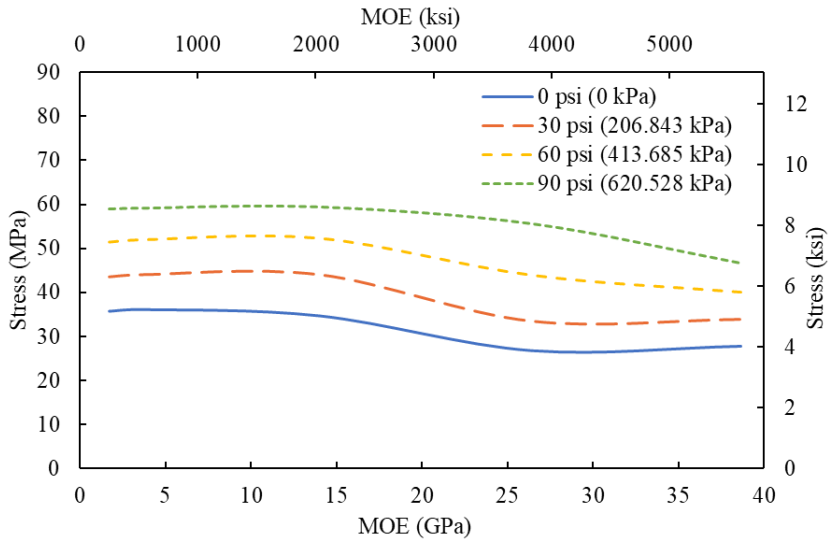

Fig. 19. Effect of MOE on critical stress in 4.1 mm (0.2 in) thick IRP with different internal pressure

Table 3 illustrates the fatigue life of IRP with different levels of internal pressures subjected to a traffic loading of 14.8 kN (3.3 kips) with varying MOE. It is evident that the IRP with MOE of 1.7 GPa (246.6 ksi), 3.7 GPa (536.6 ksi), and 7.9 GPa (1145.8 ksi) exhibits a significant increase in fatigue life as the internal pressure is raised from zero to 620.5 kPa (90.0 psi). Among all the material systems evaluated, the polymeric IRP, which has the lowest MOE demonstrates the shortest fatigue life across all the internal pressure levels. The polymeric IRP lasts only 130 cycles and one cycle under conditions of zero internal pressure and internal

pressure of 206.8 kPa (30.0 psi), respectively. However, when the polymeric IRPs are exposed to an internal pressure of 413.7 kPa (60.0 psi) or above, they fail before even completing a single cycle because the alternating stress levels are too high compared to the maximum limit specified in the S-N curve. When the MOE of IRP is 7.9 GPa (1145.8 ksi) or higher, the design life requirement is met even at the highest internal pressure under consideration. Furthermore, to satisfy the design life criterion under internal pressures of zero, 206.8 kPa (30.0 psi), 413.7 kPa (60.0 psi) and 620.5 kPa (90.0 psi), it is necessary for MOE of IRP with a thickness of 4.1 mm (0.2 in) to be 3.5 GPa (507.6 ksi), 4.2 GPa (609.2 ksi), 4.8 GPa (696.2 ksi) and 5.3 GPa (768.7 ksi), correspondingly (using liner interpolation).

Table 3. Minimum fatigue life of 4.1 mm (0.2 in) thick IRP with different MOE and levels of internal pressure

Internal pressure	Fatigue life cycles					
	1.7 GPa (246.6 ksi) [Polymer]	3.7 GPa (536.6 ksi) [GFRP-1]	7.9 GPa (1145.8 ksi) [GFRP-2]	14.0 GPa (2030.5 ksi) [GFRP-3]	26.4 GPa (3829.0 ksi) [GFRP-4]	38.6 GPa (5598.5 ksi) [GFRP-5]
zero	130	2.7E+06	3.0E+11	>>1E+12	>>1E+12	>>1E+12
206.8 kPa (30.0 psi)	1	1.2E+05	5.2E+10	>>1E+12	>>1E+12	>>1E+12
413.7 kPa (60.0 psi)	0	8492	1.3E+10	>>1E+12	>>1E+12	>>1E+12
620.5 kPa (90.0 psi)	0	869	4.13E+09	>>1E+12	>>1E+12	>>1E+12

3.4 Effect of internal pressure with different traffic loading levels

The influence of internal pressure on critical tensile stress and fatigue life of GFRP-1 with a repair thickness of 4.1 mm (0.2 in) under different levels of traffic loads is shown in Fig. 20a and b, respectively. As per Fig. 20a, critical stress in IRP increases linearly with the rise in internal pressure for traffic loads of 10.0 kN (2.2 kips), 20.0 kN (4.5 kips) and 25.0 kN (5.6 kips), similar to the behaviour observed under the traffic load of 14.8 kN. It should be noted, however, that the design strain limit of 0.02 is exceeded by the repair system with the internal pressure of 620.5 kPa (90.0 psi) when subjected to a traffic load of 25.0 kN (5.6 kips). In

comparison to the non-pressurized system, the overall increase in maximal tensile stresses in IRP at 620.5 kPa (90.0 psi) under traffic loads of 10.0 kN (2.2 kips), 14.8 kN (3.3 kips), 20.0 kN (4.5 kips) and 25.0 kN (5.6 kips) are 88.63%, 62.08, 47.8% and 38.7%, respectively. This suggests that an increase in internal pressure leads to a more pronounced impact on repair systems that are exposed to comparably lower traffic loads. This is due to the significant contribution of the longitudinal stress component produced by internal pressure in the resultant longitudinal tensile stress relative to the contribution of the bending stress induced by the traffic load. As illustrated in Fig. 20b, the fatigue life of IRP subjected to the traffic load of 10.0 kN (2.2 kips) decreases nonlinearly with increasing internal pressure from zero to 620.5 kPa (90.0 psi), which is similar to the behaviour when subjected to a load of 14.8 kN, whereas those under 20.0 kN (4.5 kips) or higher decrease almost linearly. The IRP subjected to traffic loads of 10.0 kN (2.2 kips) exceeds one million cycles when the internal pressure is lower than 389.6 kPa (56.5 psi). However, IRPs exposed to traffic loads of 20.0 kN (4.5 kips) or greater are unable to meet the design life requirement, even in the absence of internal pressure.

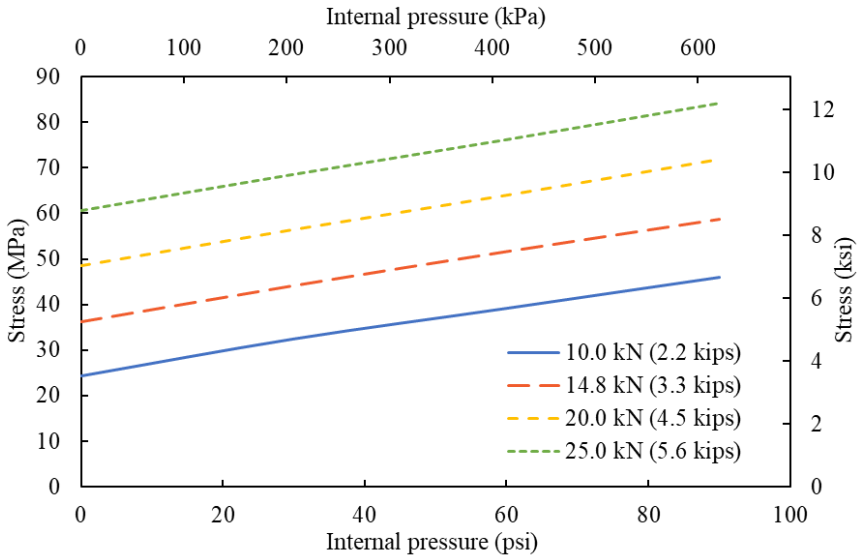

(a)

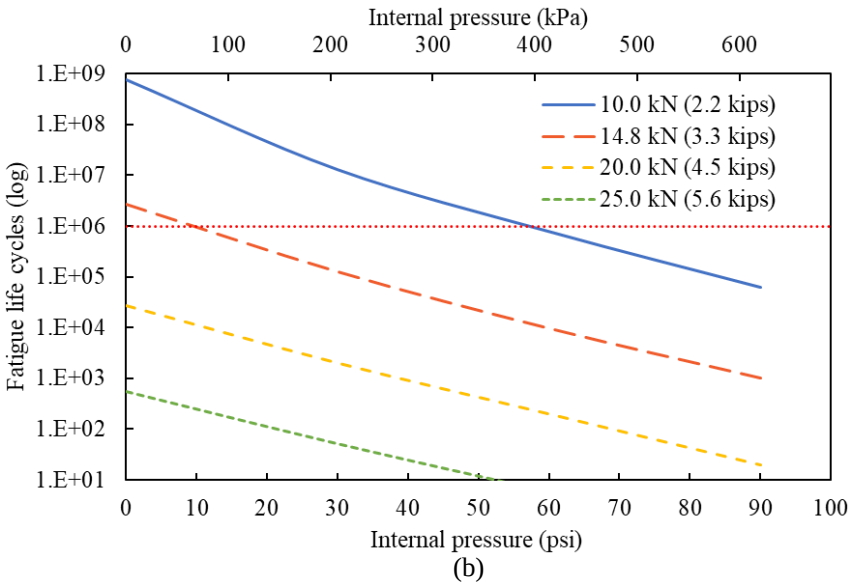

(b)

Fig. 20. Effect of internal pressure on (a) critical tensile stress and (b) minimum fatigue life of IRP systems exposed to different levels of traffic loads

Fig. 21a and b show the effect of traffic load on the critical tensile stress and service life of GFRP-1IRP with a thickness of 4.1 mm (0.2 in) under various levels of internal pressure ranging from zero to 620.5 kPa (90.0 psi). As can be seen from Fig. 21a, the critical tensile stresses experienced by non-pressurized, and all pressurized IRPs increase almost linearly as the traffic load rises from 5.0 kN (1.1 kips) to 25.0 kN (5.6 kips). The corresponding percentage increases in critical tensile stresses at an internal pressure of zero, 206.8 kPa (30.0 psi), 413.7 kPa (60.0 psi) and 620.5 kPa (90.0 psi) are 523.1%, 244.9%, 189.9% and 149.8%, respectively. This is because an increasing traffic load causes a greater deformation of the IRP, which leads to a more pronounced change in stress distribution and a greater concentration of stress at the discontinuity edge. Additionally, compared to the system without internal pressure, the presence of internal pressure causes the IRP to expand, which can further change stress distribution and increase stress concentration at the discontinuity edge.

Fig. 21b demonstrates that the fatigue lives of IRP, both with and without internal pressure, exhibit a slight nonlinear decrease as the traffic load is increased, even when represented on a semi-log scale. The IRP with a thickness of 4.1 mm (0.2 in) operating at zero, 206.8 kPa (30.0 psi), 413.7 kPa (60.0 psi) and 620.5 kPa (90.0 psi) internal pressure can only satisfy the design fatigue life criteria if the traffic load level remains below 15.8 kN (3.6 kips), 12.4 kN (2.8 kips), 9.7 kN (2.2 kips) and 6.7 kN (1.5 kips), respectively.

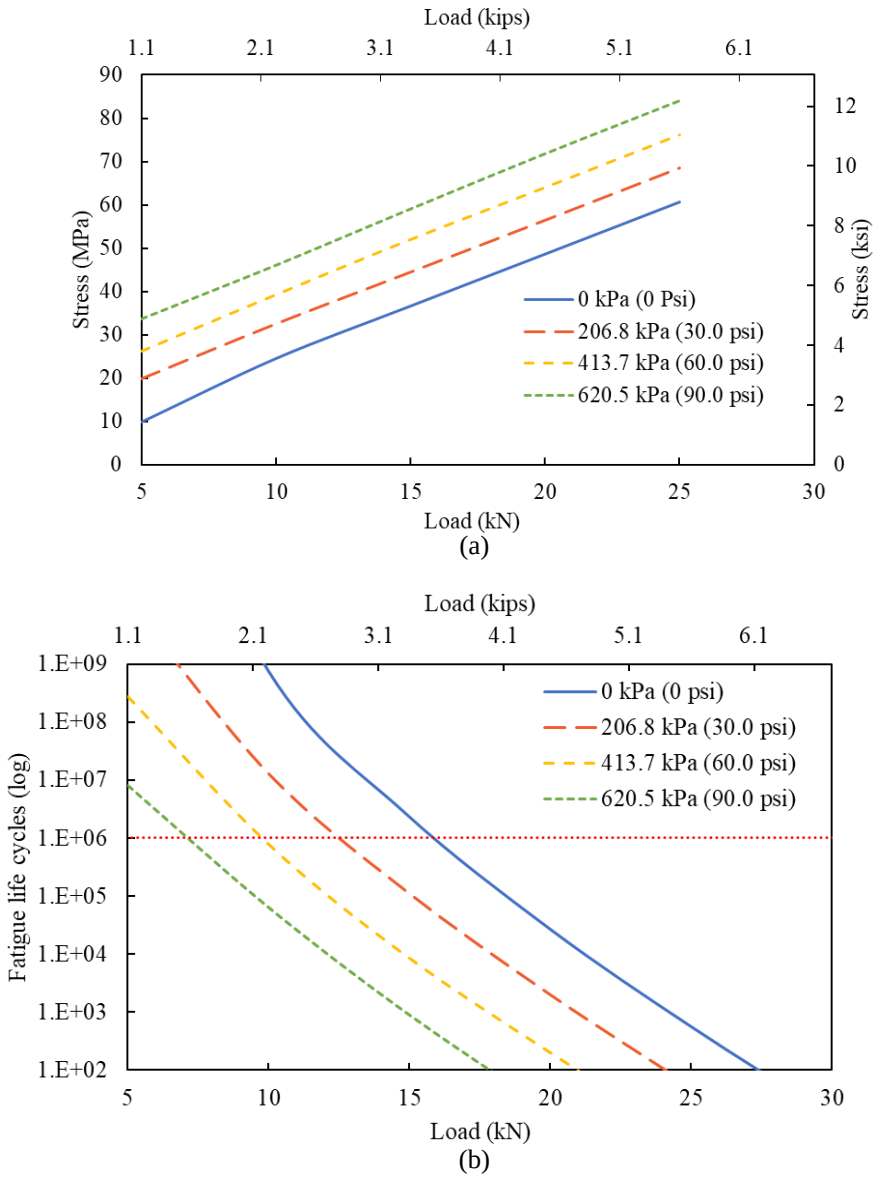

Fig. 21. Effect of traffic load level on (a) critical tensile stress and (b) minimum fatigue life of IRP with different levels of internal pressure

3.5 Mathematical expressions for fatigue life prediction of IRP systems

Two mathematical formulae were developed to predict the fatigue life and strain of an IRP under the combined effect of internal pressure and traffic load. The formulae are established based on the FEA results obtained from a comprehensive parametric study, with the aim of facilitating efficient design practice. The purpose of formulating an equation for estimating strain is to ensure that the IRP system is within the designated strain limit of 0.02 prior to conducting predictions of fatigue life, which will be elaborated on subsequently. Both equations contain four independent variables, namely, MOE and thickness of IRP, traffic load, and internal pressure. The selection of the MOE range, from 1.7 GPa (246.6 ksi) to 7.9 GPa, is

based on finite fatigue life observation obtained from the parametric study. The repair thicknesses and internal pressures employed are in accordance with the ones detailed in section 2.1. However, the scope of the traffic load, as described in section 2.1, has been expanded to cover a wide range of data. The expanded traffic load ranges from 5.0 kN (1.1 kips) to 40.0 kN (9.0 kips).

Nonlinear regression analysis is adopted to fit the FEA dataset into nonlinear models and derive mathematical expressions. To ensure consistent and standardised comparison across different scales and to facilitate meaningful analysis and interpretation of data, the effect of distinct scales or units presented in variables is eliminated. This is accomplished by dividing both independent and dependent variables by their respective referenced values while ensuring consistency in units before model fitting and equation derivation. Through this process, dimensionless quantities are obtained, thereby ensuring normalisation and enhancing the validity of the derived equations. Eq. (3) and Eq. (4) present the model equations utilised in nonlinear regression analysis for fatigue life cycles (N) and strain (ε), respectively, where E is the MOE of repair material in MPa, t is the repair thickness in mm, F is the traffic load in N, and p is the internal pressure in MPa. The referenced values for MOE, repair thickness, traffic load, internal pressure, fatigue life cycles, and strain are denoted by E_{ref}, t_{ref}, F_{ref}, p_{ref}, N_{ref}, and ε_{ref}, respectively. The model equations for fatigue life cycles and strain are characterized by eight unknown dimensionless coefficients, denoted as $\alpha_1 - \alpha_8$ for the former, and as $\beta_1 - \beta_8$ for the latter.

$$\frac{\log_{10}(N)}{\log_{10}(N_{ref})} = \alpha_1 \left(\frac{E}{E_{ref}}\right)^{\alpha_2} + \alpha_3 \left(\frac{t}{t_{ref}}\right)^{\alpha_4} + \alpha_5 \left(\frac{F}{F_{ref}}\right)^{\alpha_6} + \alpha_7 \left(\frac{p}{p_{ref}}\right)^{\alpha_8} \quad (3)$$

$$\frac{\varepsilon}{\varepsilon_{ref}} = \beta_1 \left(\frac{E}{E_{ref}}\right)^{\beta_2} + \beta_3 \left(\frac{t}{t_{ref}}\right)^{\beta_4} + \beta_5 \left(\frac{F}{F_{ref}}\right)^{\beta_6} + \beta_7 \left(\frac{p}{p_{ref}}\right)^{\beta_8} \quad (4)$$

where,

- $E_{ref} = 3700$ MPa (MOE of GFRP-1 IRP material)
- $t_{ref} = 4.1$ mm
- $F_{ref} = 14800$ N (Traffic load)
- $p_{ref} = 0.4$ MPa (Operating internal pressure)
- $N_{ref} = 10^6$ (Design life)
- $\varepsilon_{ref} = 0.02$ (Design strain limit)

The mathematical formulation obtained through the nonlinear regression analyses for predicting the fatigue life of the IRP in a logarithmic scale is presented in Eq. (5). Additionally, the formula for predicting the strain is given in Eq. (6). In order to assess the validity of the predictive capabilities of the derived Eqs. (5) and (6), a comparison was conducted between the predicted fatigue life and strain responses and corresponding FEA counterparts, as illustrated in Fig. 22 and Fig. 23, respectively. The comparisons indicate a favourable level of agreement between the FE responses and predicted responses for both fatigue life and strain, with only minor deviations, confirming the robustness of the proposed equations. The R-squared values of Eqs. (5) and (6) are determined to be 0.96 and 0.95, respectively, demonstrating a strong correlation between predicted and FE responses for both fatigue life and strain. In addition, the root means square error (RMSE) and mean absolute error (MAE) of Eq. (5) are both found to be 0.4, whereas those of Eq. (6) are computed to be 0.001, showing a relatively close fit between the predicted and FEA responses. Overall, according to the comparison of FE and predicted responses and evaluated metrics, the generated Eq. (5) and (6) can be considered to have satisfactory accuracy and predictive capabilities.

$$\log_{10}(N) = 6\left(0.79 \quad \left(\frac{E}{3700}\right)^{1.15} + 5.07\left(\frac{t}{4.1}\right)^{0.09} - 5.01\left(\frac{F}{14800}\right)^{0.13} - 0.2\left(\frac{p}{0.4}\right)^{1.1}\right) \tag{5}$$

$$\varepsilon = 0.02\left(-7.6\left(\frac{E}{3700}\right)^{0.07} + 7.22\left(\frac{t}{4.1}\right)^{-0.04} + 0.95\left(\frac{F}{14800}\right)^{0.35} + 0.12\left(\frac{p}{0.4}\right)^{1.06}\right) \tag{6}$$

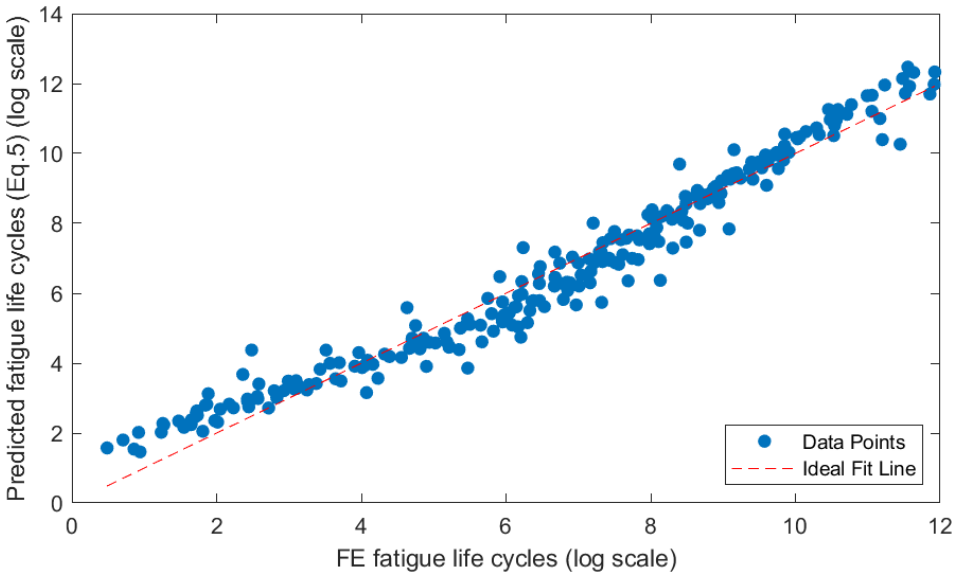

Fig. 22. A comparison between FE and predicted fatigue life cycles on a logarithmic scale

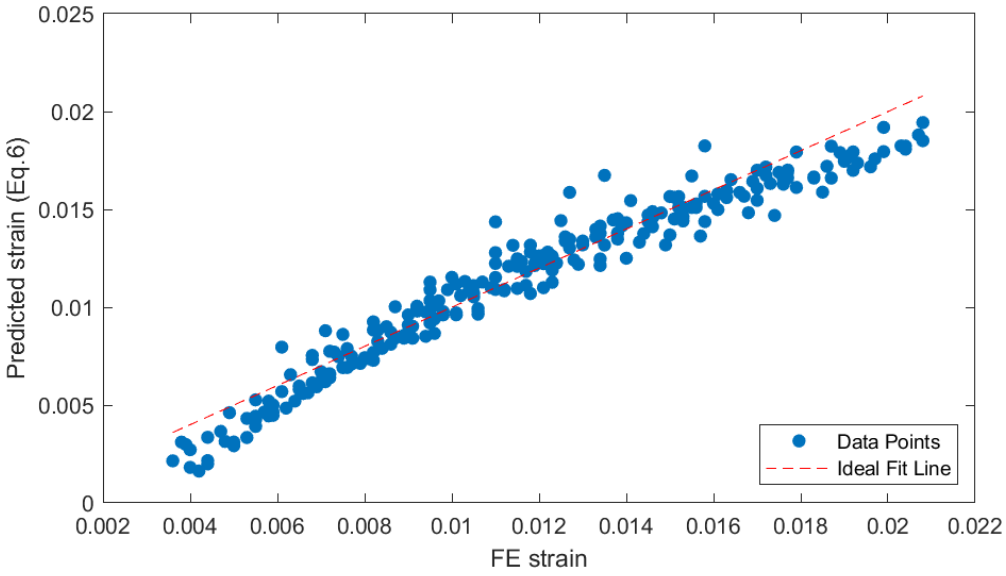

Fig. 23. A comparison between FE and predicted strain

To facilitate the application of the derived formulations for generating design charts for the fatigue life of IRP systems, a MATLAB function was developed. The function enables the user to input the desired traffic load and internal pressure. It then calculates the maximum strain of the IRP system by utilizing Eq. (6) over a specified range of MOEs and thicknesses of the repair materials. Eq. (6) is constrained to ensure that it predicts the strain values within the design strain limit of 0.02. The function then extracts all possible combinations of MOE of IRP materials and IRP thickness that satisfy the design strain criteria, given a user-defined traffic load and internal pressure. The extracted parameters are subsequently applied to Eq. (7) to estimate the corresponding fatigue life cycles and generate a graphical representation of fatigue lives in the form of a contour plot for various combinations of MOE and IRP thicknesses.

The predicted fatigue lives shown on the contour plots are limited to a minimum of 1000 cycles and a maximum of 100 million cycles. This function enables users to input relevant parameters interactively and generate fatigue life plots, thereby exploring various combinations of MOE and IRP thicknesses that meet the desired service life. This feature facilitates engineers and designers to make informed decisions for selecting design parameters that meet the intended design life requirement. Employing the developed function, the obtained fatigue life contour plots for varying MOE and thickness exposed to a traffic load of 14.8 kN (3.3 kips) under internal pressures of zero, 206.8 kPa (30.0 psi), 413.7 kPa (60.0 psi) and 620.5 kPa (90.0 psi) are shown in Fig. 24- Fig. 27, respectively.

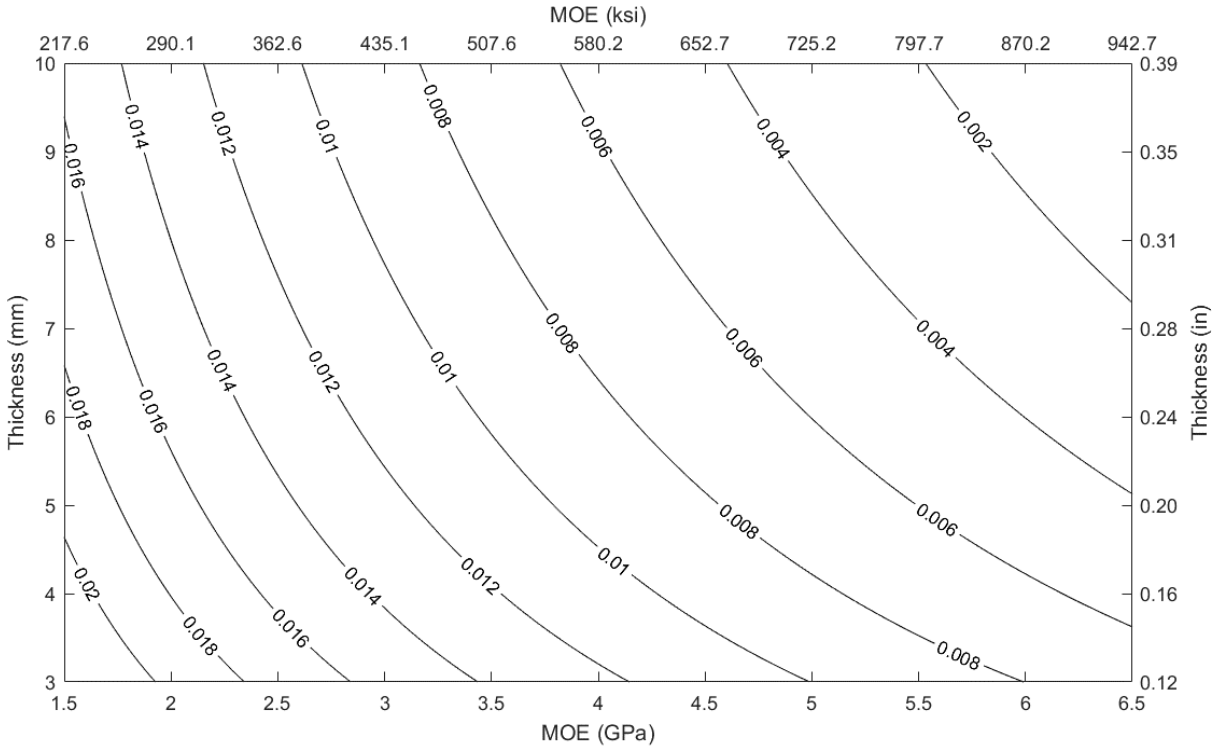

(a)

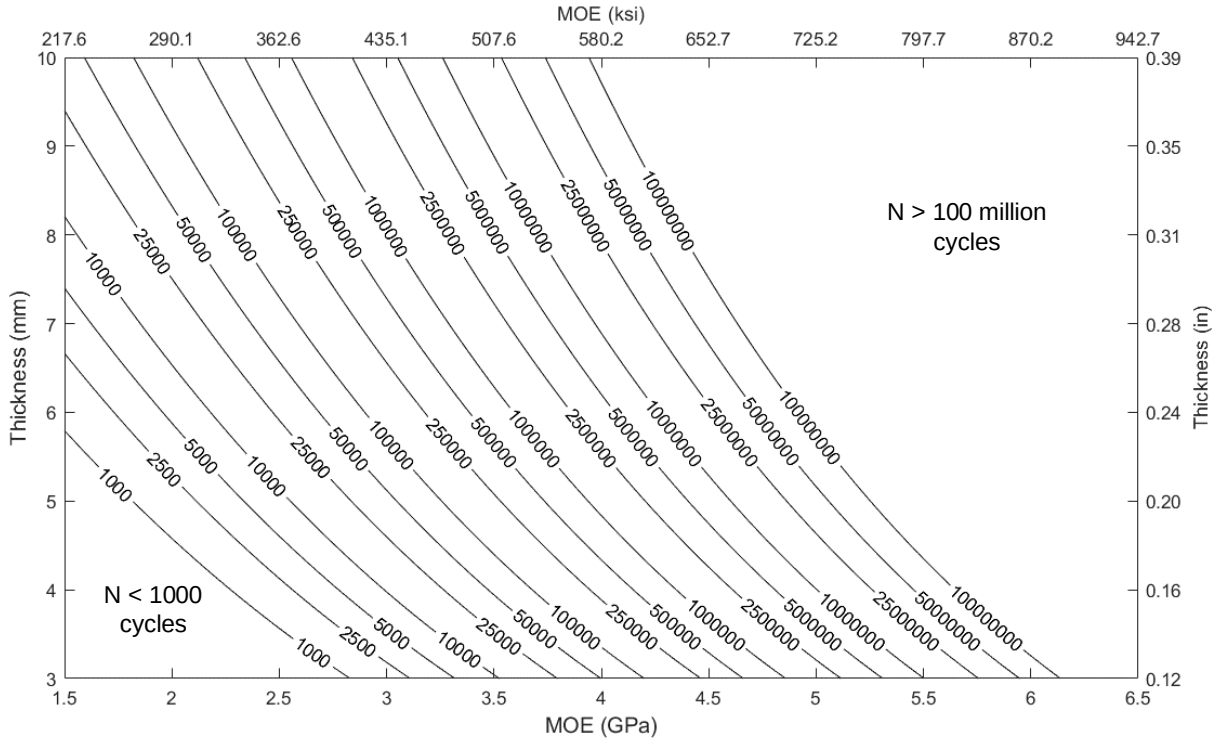

(b)

Fig. 24. (a) Strain and (b) fatigue life responses for varying MOE and thickness subjected to traffic load of 14.8 kN (3.3 kips) under zero internal pressure

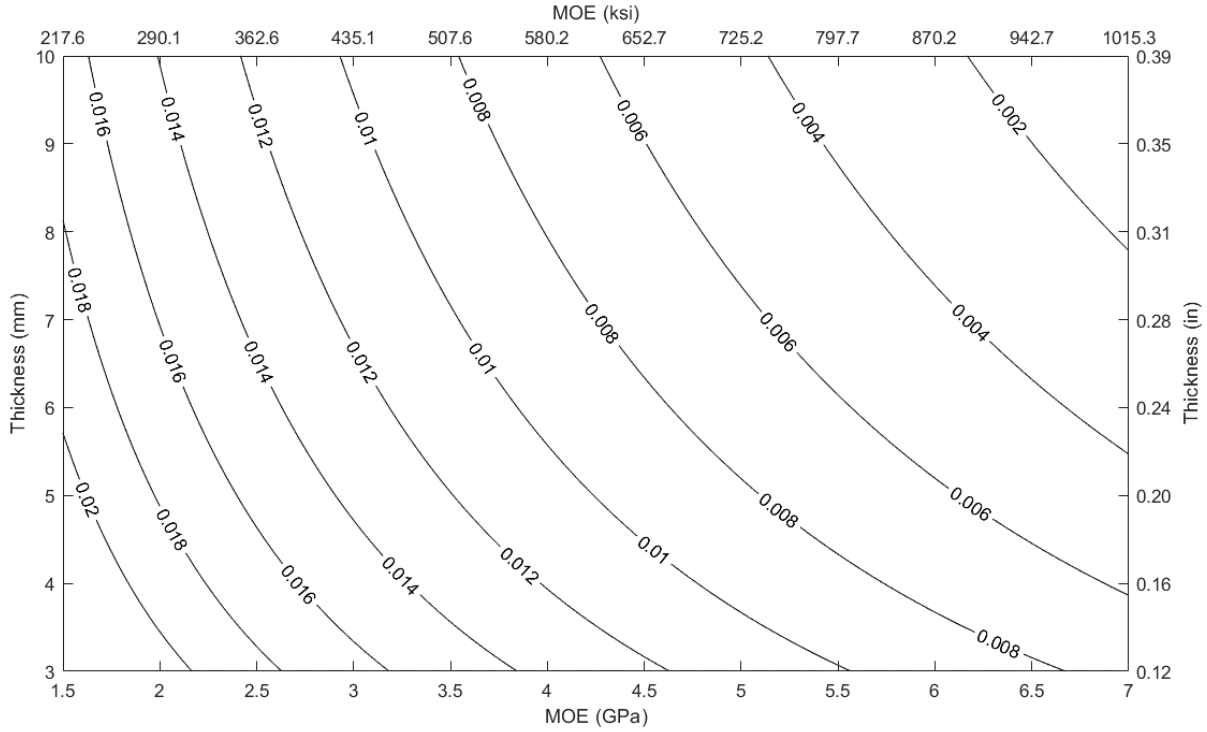

(a)

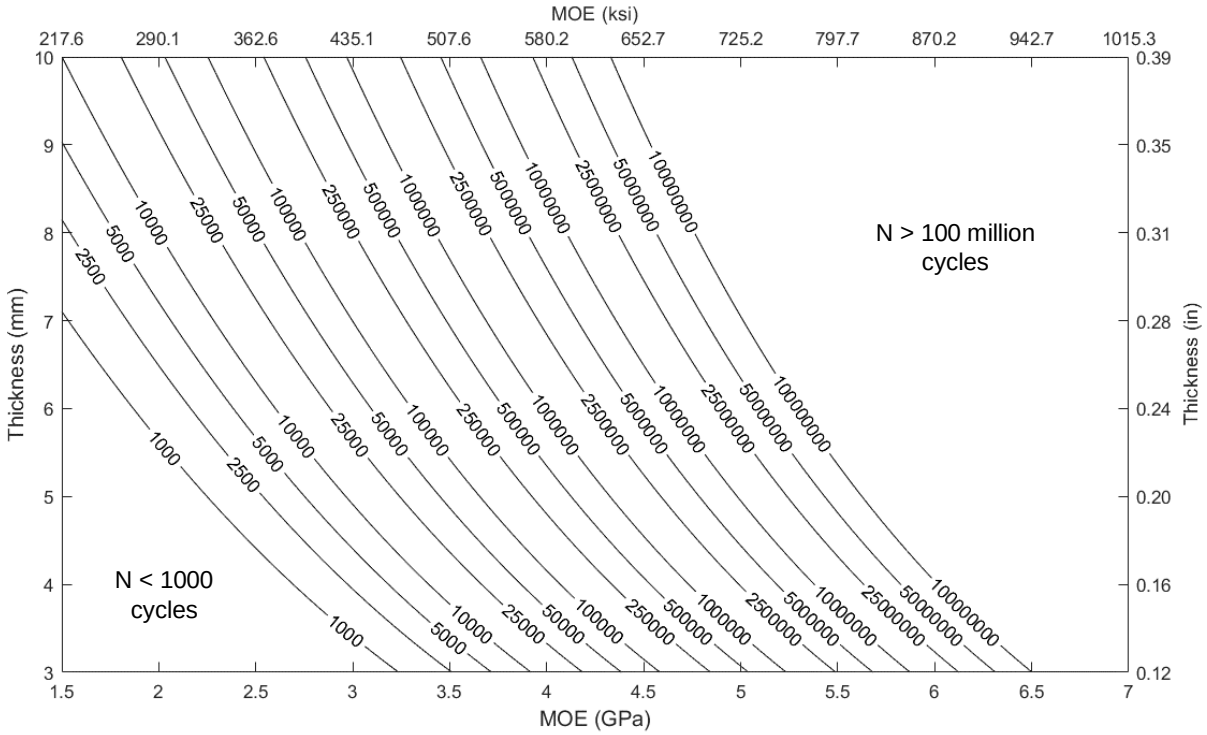

(b)

Fig. 25. (a) Strain and (b) fatigue life responses for varying MOE and thickness subjected to a traffic load of 14.8 kN (3.3 kips) under internal pressure of 206.8 kPa (30.0 psi)

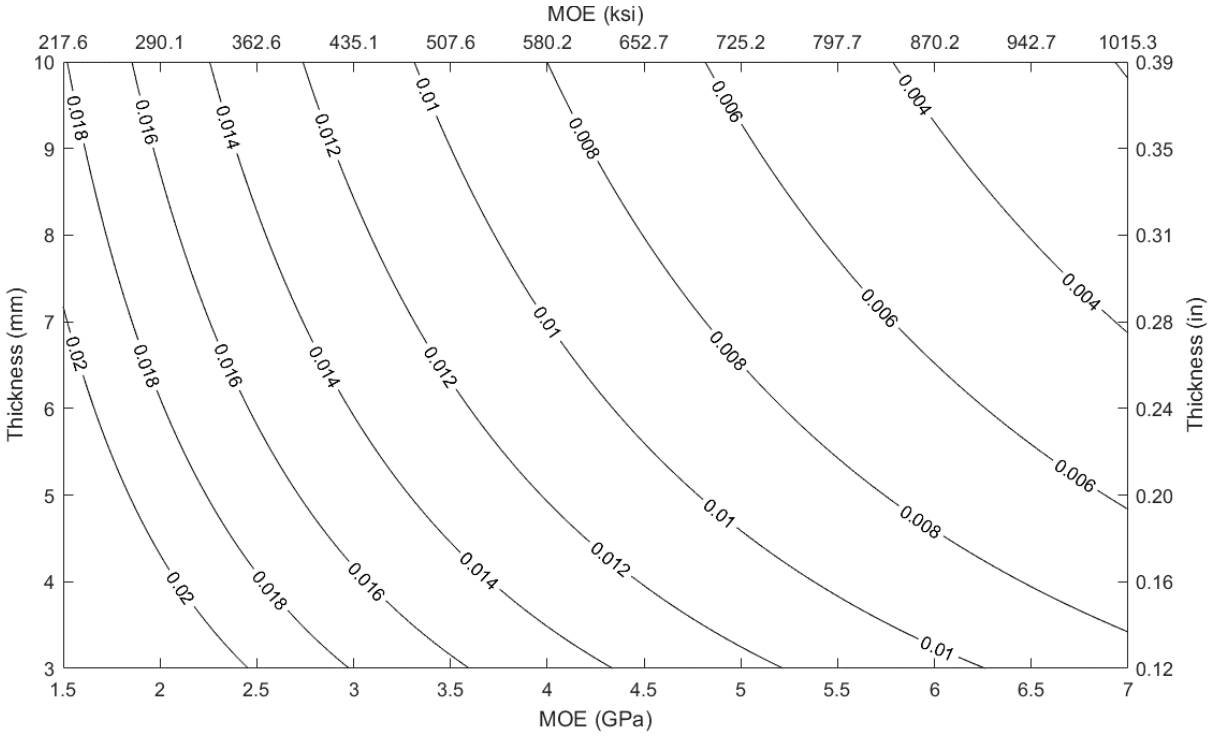

(a)

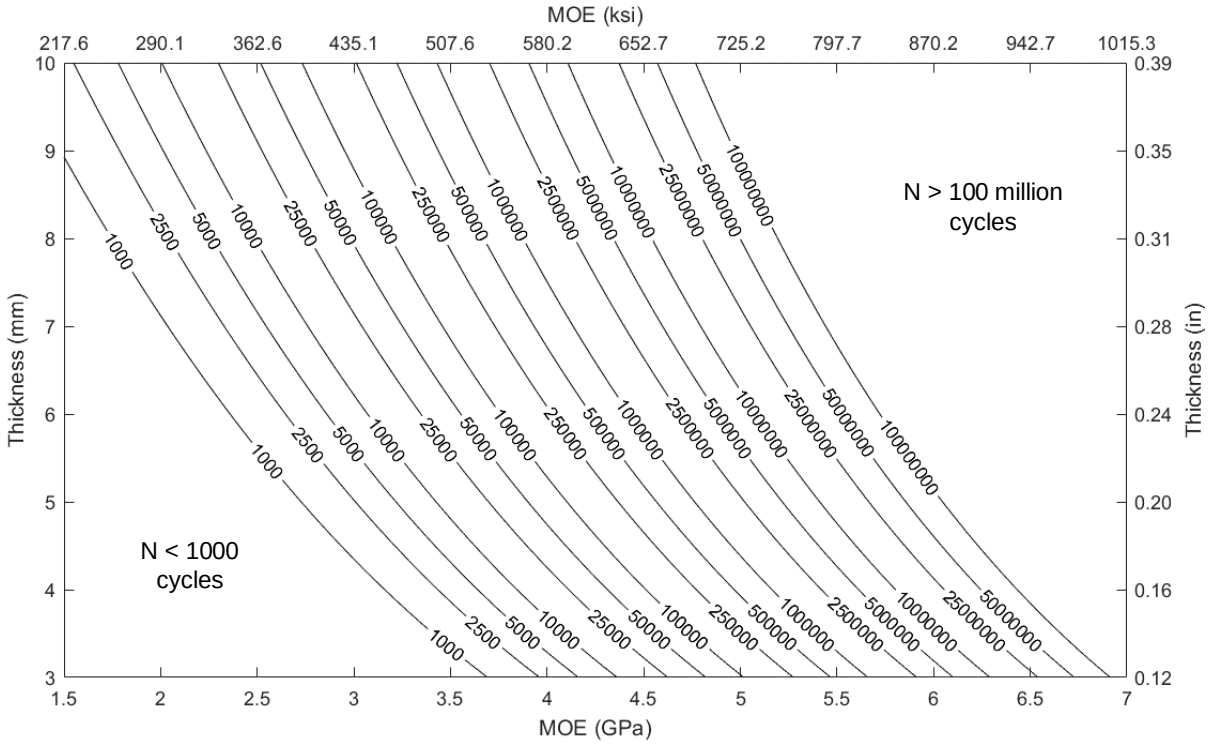

(b)

Fig. 26. (a) Strain and (b) fatigue life responses for varying MOE and thickness subjected to traffic load of 14.8 kN (3.3 kips) under internal pressure of 413.7 kPa (60.0 psi)

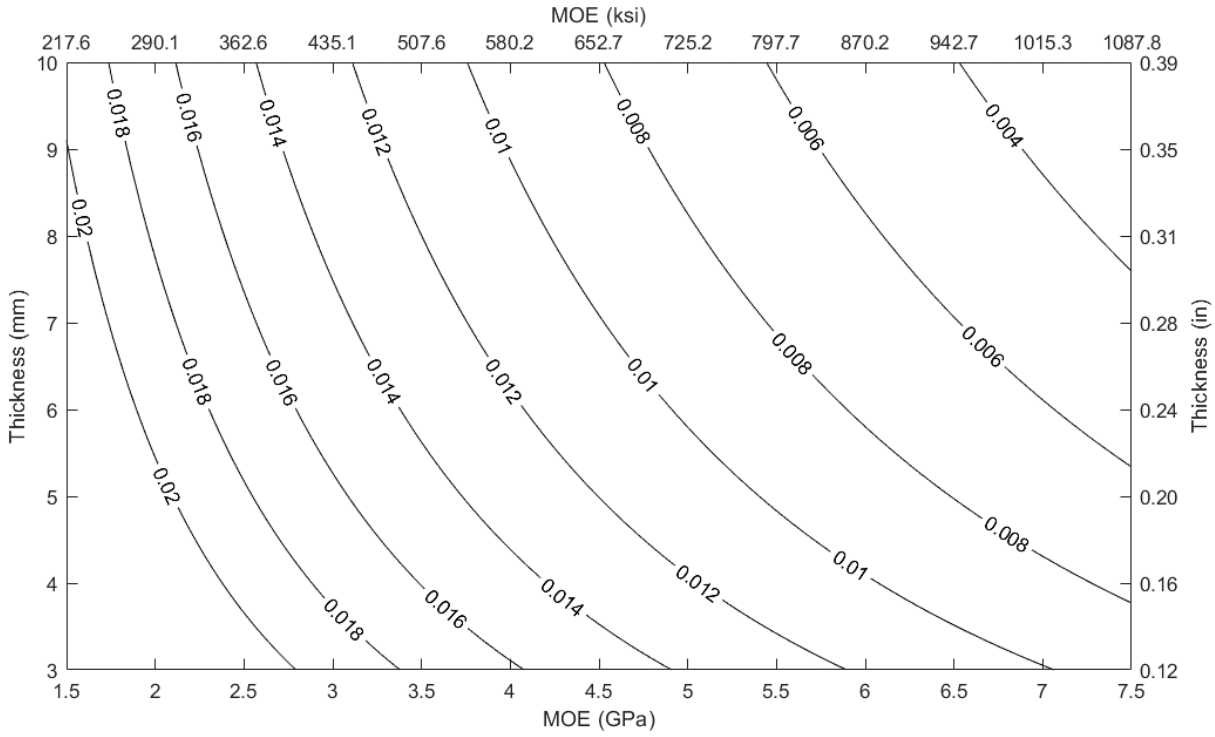

(a)

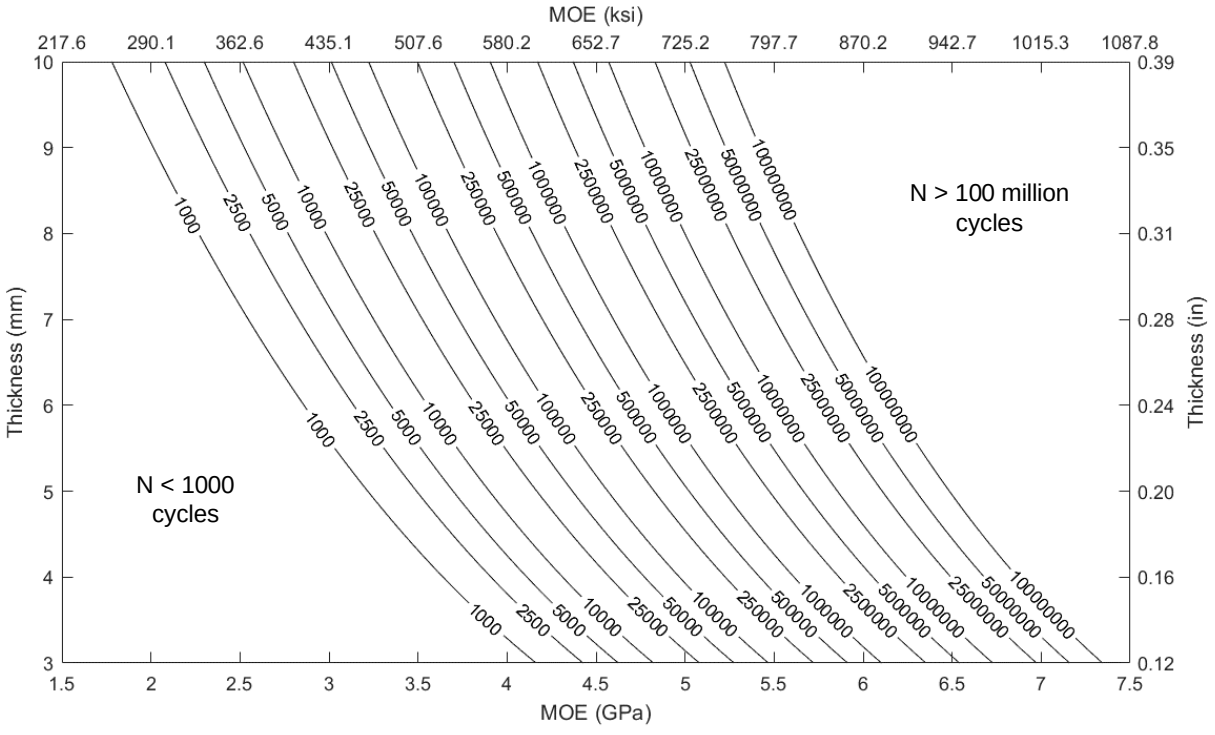

(b)

Fig. 27. (a) Strain and (b) fatigue life responses for varying MOE and thickness subjected to traffic load of 14.8 kN (3.3 kips) under internal pressure of 620.5 kPa (90.0 psi)

4 Conclusion

This study presents a process to numerically investigate the fatigue performance of internal replacement pipe (IRP) systems used for the rehabilitation of discontinuous legacy pipelines under the combined effect of traffic loading and internal pressure. The influence of repair thickness, modulus of elasticity (MOE) of the repair material, the magnitude of traffic load and the level of internal pressure on the fatigue performance was also analysed. The present study required simplifications for effective fatigue analysis under a variety of internal pressures and external load levels. This work assumed that the IRP remained fully bonded to the host pipe throughout fatigue loading, which is an important simplification but one that represents a worst-case scenario for the induced stress levels. The material assumptions included: linear elastic isotropic materials, failure strains of 0.02, and S-N curves developed from literature and limited experimental data. The use of the local stress opposed to the more rigorous HSS is justified. Future work to investigate these various aspects and expand on the presented methodology is encouraged. Considering these aforementioned simplifications, the following conclusions can be drawn from the outcomes of this study:

- The rise in the internal pressure increases the longitudinal and hoop stresses in the invert of IRP, which is under tension due to bending but decreases the stresses in the crown of IRP, which is under compression.
- Longitudinal stresses during bending are significantly greater than hoop stress at any location along IRP, regardless of the magnitude of internal pressure.
- The most critical stress during the bending of a fully bonded IRP system with any level of internal pressure is the longitudinal tensile stress at the bottom of IRP at the discontinuity edge.
- The increased concentration of longitudinal tensile stresses at the discontinuity edges caused by the rise in internal pressure during bending can significantly shorten the fatigue life of the IRP.
- The level of internal pressure changes the failure behaviour of IRP under bending fatigue. Bulging in the middle of the bottom portion of IRP between the discontinuity edges of the host pipe and bending slightly inward at the top is the failure of the repair system without internal pressure. However, as the internal pressure increases, the bulge at the bottom of IRP becomes more pronounced, while the inward bending at the top disappears.
- The fatigue life of IRP exhibits a slight nonlinear decline with increasing internal pressure under constant traffic loading. GFRP-1 IRP system having a thickness of 4.1 mm (0.2 in)

and being subjected to a traffic load of 14.8 kN (3.3 kips) can last one million cycles of fatigue loading if the internal pressure remains below 121.3 kPa (17.6 psi).

- The critical tensile stress of IRP systems, whether pressurised or non-pressurized, exhibits a nonlinear decline with increasing repair thickness. The most significant decrease in stress is observed when the repair thickness is increased under the highest internal pressure, whereas the least reduction is noted in the absence of internal pressure.
- The fatigue life of both pressurised and non-pressurized IRP systems increases nonlinearly with respect to repair thickness. To satisfy the design fatigue life criteria at an internal pressure level of zero, 206.8 kPa (30.0 psi), 413.7 kPa (60.0 psi) and 620.5 kPa (90.0 psi), the minimum repair thicknesses required for a traffic load of 14.8 kN (3.3 kips) are 3.7 mm (0.1 in), 5.3 mm (0.2 in), 7.1 mm (0.3 in) and 8.9 mm (0.4 in), respectively.
- Polymeric IRP has low resistance under fatigue loading even without internal pressure. To achieve a design fatigue life of one million cycles when exposed to a traffic load of 14.8 kN (3.3 kips) under internal pressures of zero, 206.8 kPa (30.0 psi), 413.7 kPa (60.0 psi) and 620.5 kPa (90.0 psi), it is necessary for the MOE of IRP with a thickness of 4.1 mm (0.2 in) be at least 3.5 GPa (507.6 ksi), 4.2 GPa (609.2 ksi), 4.8 GPa (696.2 ksi) and 5.3 GPa (768.7 ksi), respectively.
- Internal repair pipe systems subjected to relatively lower traffic loads are severely affected by a rise in internal pressure. When tested with a traffic load of 10.0 kN (2.2 kips), the GFRP-1 IRP system could satisfy the design life requirement under an internal pressure of no more than 389.6 kPa (56.5 psi). Without internal pressure, GFRP-1 IRP systems subjected to traffic loads of 20.0 kN (4.5 kips) or higher fail to continue functioning up to their intended service life.
- Fatigue lives of IRP systems, regardless of the magnitude of internal pressure, demonstrate a slight nonlinear reduction with an increase in traffic load. GFRP-1 IRP system with a repair thickness of 4.1 mm (0.2 in) operating at internal pressure levels of zero, 206.8 kPa (30.0 psi), 413.7 kPa (60.0 psi) and 620.5 kPa (90.0 psi), can only achieve the expected fatigue life if the traffic load level does not exceed 15.8 kN (3.6 kips), 12.4 kN (2.8 kips), 9.7 kN (2.2 kips) and 6.7 kN (1.5 kips), respectively.
- The developed simplified mathematical formulations and design charts for predicting the fatigue life of IRP systems can assist engineers and designers to make informed decisions for selecting design parameters that meet the desired design life requirement, as well as to achieve more efficient and optimised designs while reducing costs and time.

Acknowledgement

The information, data, or work presented herein was funded in part by the Advanced Research Projects Agency-Energy (ARPA-E), US Department of Energy, under Award Number DE-AR0001327. The views and opinions of authors expressed herein do not necessarily state or reflect those of the United States Government or any agency thereof.

5 References

1. Deng, M.L., C. Bao, A.T.S. Hung, N. Md Noor, and K.S. Lim, *Effect of defect geometries upon burst capacity of composite repaired pipe.* Physics and Chemistry of the Earth, Parts A/B/C, 2022. **128**: p. 103274.
2. El-Abbasy, M.S., A. Senouci, T. Zayed, and F. Mosleh, *A condition assessment model for oil and gas pipelines using integrated simulation and analytic network process.* Structure and Infrastructure Engineering, 2015. **11**(3): p. 263-281.
3. Shamsuddoha, M. Islam, T. Aravinthan, A. Manalo, and K.-t.A. Lau, *Effectiveness of using fibre-reinforced polymer composites for underwater steel pipeline repairs.* Composite Structures, 2013. **100**: p. 40-54.
4. Alabtah, F.G., E. Mahdi, and F.F. Eliyan, *The use of fiber reinforced polymeric composites in pipelines: A review.* Composite Structures, 2021. **276**: p. 114595.
5. Rohem, N.R.F., L.J. Pacheco, S. Budhe, M.D. Banea, E.M. Sampaio, and S.d. Barros, *Development and qualification of a new polymeric matrix laminated composite for pipe repair.* Composite Structures, 2016. **152**: p. 737-745.
6. Velázquez, J.C., N.E. González-Arévalo, M. Díaz-Cruz, A. Cervantes-Tobón, H. Herrera-Hernández, and E. Hernández-Sánchez, *Failure pressure estimation for an aged and corroded oil and gas pipeline: A finite element study.* Journal of Natural Gas Science and Engineering, 2022. **101**: p. 104532.
7. Kraidi, L., R. Shah, W. Matipa, and F. Borthwick, *Analyzing the critical risk factors associated with oil and gas pipeline projects in Iraq.* International Journal of Critical Infrastructure Protection, 2019. **24**: p. 14-22.
8. Xu, D., L. Chen, C. Yu, S. Zhang, X. Zhao, and X. Lai, *Failure analysis and control of natural gas pipelines under excavation impact based on machine learning scheme.* International Journal of Pressure Vessels and Piping, 2023. **201**: p. 104870.
9. Chen, X., Z. Wu, W. Chen, R. Kang, X. He, and Y. Miao, *Selection of key indicators for reputation loss in oil and gas pipeline failure event.* Engineering Failure Analysis, 2019. **99**: p. 69-84.
10. Chin, W.S. and D.G. Lee, *Development of the trenchless rehabilitation process for underground pipes based on RTM.* Composite Structures, 2005. **68**(3): p. 267-283.
11. Abd-Elhady, A.A., H.E.-D.M. Sallam, I.M. Alarifi, R.A. Malik, and T.M.A.A. EL-Bagory, *Investigation of fatigue crack propagation in steel pipeline repaired by glass fiber reinforced polymer.* Composite Structures, 2020. **242**: p. 112189.
12. Makar, J.M., R. Desnoyers, and S.E. McDonald, *Failure modes and mechanisms in gray cast iron pipe*. 1 ed. 2001, Ottawa, Ontario, Canada: Institute for Research in Construction, National Research Council Canada. 10.
13. Jeon, S.-S., T.D. O'Rourke, and A.N. Neravali, *Repetitive loading effects on cast iron pipelines with cast-in-place pipe lining system.* Journal of Transportation Engineering, 2004. **130**(6): p. 692-705.

14. Akhi, A.H. and A.S. Dhar, *Fracture parameters for buried cast iron pipes subjected to internal surface corrosions and cracks.* Journal of Pipeline Science and Engineering, 2021. **1**(2): p. 187-197.
15. Shirazi, H., R.L. Eadie, and W. Chen, *A review on current understanding of pipeline circumferential stress corrosion cracking in near-neutral PH environment.* Engineering Failure Analysis, 2023. **148**.
16. Dixon, P.G., T. Tafsirojjaman, J. Klingaman, M.H. Hubler, S. Dashti, T.D. O'rourke, K.A. Farrag, A. Manalo, and B.P. Wham, *State-of-the-Art Review of Performance Objectives for Legacy Gas Pipelines with Pipe-in-Pipe Rehabilitation Technologies.* Journal of Pipeline Systems Engineering and Practice, 2023. **14**(2).
17. Fu, G., B. Shannon, R.M. Azoor, J. Ji, R.N. Deo, and J.K. Kodikara, *Reliability based failure assessment of deteriorated cast iron pipes lined with polymeric liners.* Structure and Infrastructure Engineering, 2022. **19**(11): p. 1516–1529.
18. Allouche, E.N., S. Alam, J. Simicevic, R. Sterling, W. Condit, J.C. Matthews, and A. Selvakumar, *A pilot study for retrospective evaluation of cured-in-place pipe (CIPP) rehabilitation of municipal gravity sewers.* Tunnelling and Underground Space Technology, 2014. **39**: p. 82-93.
19. Lu, H., S. Behbahani, M. Azimi, J.C. Matthews, S. Han, and T. Iseley, *Trenchless Construction Technologies for Oil and Gas Pipelines: State-of-the-Art Review.* Journal of Construction Engineering and Management-asce, 2020. **146**(6): p. 03120001.
20. Li, B., W.J. Yu, Y.-p. Xie, H. Fang, X. Du, N. Wang, K. Zhai, D. Wang, X. Chen, M. Du, M. Sun, and X. Zhao, *Trenchless rehabilitation of sewage pipelines from the perspective of the whole technology chain: A state-of-the-art review.* Tunnelling and Underground Space Technology, 2023. **134**.
21. Fuselli, F., S.S. Huber, and S. Mambretti, *Environmental aspects of trenchless pipe rehabilitation methods.* Urban Water Journal, 2022. **19**: p. 879 - 887.
22. Yahong, Z., H. Sheng, M. Baosong, Z. Cong, Y. Xuefeng, T. Zhongsen, L. Han, and D. Caiying, *Experiment and evaluation model of liner design for renewal of deteriorated reinforced concrete pipes utilizing cured-in-place-pipe technology.* Tunnelling and Underground Space Technology, 2023. **132**.
23. Wang, R., F. Wang, J.-g. Xu, Y.-h. Zhong, and L. Shikun, *Full-scale experimental study of the dynamic performance of buried drainage pipes under polymer grouting trenchless rehabilitation.* Ocean Engineering, 2019. **181**: p. 121-133.
24. Ha, S.K., H.K. Lee, and I.S. Kang, *Structural behavior and performance of water pipes rehabilitated with a fast-setting polyurea–urethane lining.* Tunnelling and Underground Space Technology, 2016. **52**: p. 192-201.
25. Stewart, H.E., A.N. Netravali, and T.D. O'Rourke, *Performance Testing of Field-Aged Cured-in-Place Liners (CIPL) for Cast Iron Piping* 2015: School of Civil and Environmental Engineering, Cornell University p. 1-128.
26. Tien, C.M.T., A. Manalo, P. Dixon, T. Tafsirojjaman, W. Karunasena, W.W. Flood, H. Ahmadi, S.H. Kiriella, A.M. Salah, and B.P. Wham, *Effects of the legacy pipe ends on the behaviour of pipe-in-pipe repair systems under internal pressure.* Engineering Failure Analysis, 2023. **144**.
27. Brown, M.J.P., I.D. Moore, and A. Fam, *Performance of a cured-in-place pressure pipe liner passing through a pipe section without structural integrity.* Tunnelling and Underground Space Technology, 2014. **42**: p. 87-95.
28. Shou, K.J. and B.C. Chen, *Numerical analysis of the mechanical behaviors of pressurized underground pipelines rehabilitated by cured-in-place-pipe method.* Tunnelling and Underground Space Technology, 2018. **71**: p. 544-554.

29. Shou, K.J. and C.C. Huang, *Numerical analysis of straight and curved underground pipeline performance after rehabilitation by cured-in-place method.* Underground Space, 2020. **5**(1): p. 30-42.
30. Tafsirojjaman, T., A. Manalo, C.M.T. Tien, B. Wham, A. Salah, S. Kiriella, W. Karunasena, and P. Dixons, *Analysis of failure modes in pipe-in-pipe repair systems for water and gas pipelines.* Engineering Failure Analysis, 2022. **140**.
31. Huang, Z.-y., W. Zhang, X. Qian, Z. Su, D.C. Pham, and N. Sridhar, *Fatigue behaviour and life prediction of filament wound CFRP pipes based on coupon tests.* Marine Structures, 2020. **72**: p. 102756.
32. Ansys, *Finite Element Analysis (FEA) Software for Structuaral Engineering*. 2021, ANSYS, Inc.
33. Kiriella, S., A. Manalo, C.M.T. Tien, H. Ahmadi, B.P. Wham, A. Salah, T. Tafsirojjaman, W. Karunasena, P. Dixon, and T.D. O'Rourke, *Lateral deformation behaviour of structural internal replacement pipe repair systems.* Composite Structures, 2023. **319**.
34. Kiriella, S., A. Manalo, C.M.T. Tien, H. Ahmadi, P.G. Dixon, W. Karunasena, A. Salah, and B.P. Wham, *Bending fatigue behaviour of internal replacement pipe systems.* Composite Structures, 2024. **331**: p. 117910.
35. Klingaman, J., P.G. Dixon, B.P. Wham, S. Dashti, and M.H. Hubler. *Traffic Loading Effects on Rehabilitated Cast Iron Distribution Pipelines*. in *Pipelines 2022*. 2022. Indianapolis, Indiana.
36. Mellott, S.R. and A. Fatemi, *Fatigue behavior and modeling of thermoplastics including temperature and mean stress effects.* Polymer Engineering and Science, 2014. **54**(3): p. 725-738.
37. Zakaria, K.A., R.H. Jimit, S.N.R. Ramli, A.A. Aziz, O. Bapokutty, and M.B. Ali, *Study On Fatigue Life And Fracture Behaviour Of Fibreglass Reinforced Composites.* Journal of Mechanical Engineering and Sciences, 2016. **10**(3): p. 2300-2310.
38. Huh, Y.H., J.H. Lee, D. Kim, and Y.-S. Lee, *Effect of stress ratio on fatigue life of GFRP composites for WT blade.* Journal of Mechanical Science and Technology, 2012. **26**: p. 2117-2120.
39. ASTM, *ASTM D3479/D3479M-19*, in *Standard Test Method for Tension-Tension Fatigue of Polymer Matrix Composite Materials*. 2019, ASTM International. p. 1-6.
40. Puigoriol-Forcada, J.M., A. Alsina, A.G. Salazar-Martín, G. Gómez-Gras, and M.A. Pérez, *Flexural fatigue properties of polycarbonate fused-deposition modelling specimens.* Materials & Design, 2018. **155**: p. 414-421.
41. Ferdous, W., A. Manalo, J. Peauril, C. Salih, K. Raghava Reddy, P. Yu, P. Schubel, and T. Heyer, *Testing and modelling the fatigue behaviour of GFRP composites@ Effect of stress level, stress concentration and frequency.* Engineering Science and Technology, an International Journal, 2020. **23**(5): p. 1223-1232.
42. Fajri, A., A.R. Prabowo, E. Surojo, F. Imaduddin, J.M. Sohn, and R. Adiputra, *Validation and Verification of Fatigue Assessment using FE Analysis: A Study Case on the Notched Cantilever Beam.* Procedia Structural Integrity, 2021. **33**: p. 11-18.
43. Zhang, C., H. Chen, and T.-l. Huang, *Fatigue damage assessment of wind turbine composite blades using corrected blade element momentum theory.* Measurement, 2018. **129**: p. 102-111.
44. Susmel, L., R. Tovo, and P. Lazzarin, *The mean stress effect on the high-cycle fatigue strength from a multiaxial fatigue point of view.* International Journal of Fatigue, 2005. **27**: p. 928-943.

45. Preedawiphat, P., N. Mahayotsanun, K. Sa-ngoen, M. Noipitak, P. Tuengsook, S. Sucharitpwatskul, and K. Dohda, *Mechanical Investigations of ASTM A36 Welded Steels with Stainless Steel Cladding.* Coatings, 2020. **10**(9): p. 844.
46. Mecséri, B.J. and B. Kövesdi, *Discussion on the Hot-Spot and Notch Stress Based Fatigue Assessment Methods Based on Test Results.* International Journal of Steel Structures, 2020: p. 1-15.
47. Haghpanahi, M. and H. Pirali, *Hot Spot Stress Determination for a Tubular T-Joint under Combined Axial and Bending Loading.* International Journal of Industrial Engineering & Production Research, 2006. **17**: p. 21-28.
48. Hobbacher, A.F., *The new IIW recommendations for fatigue assessment of welded joints and components – A comprehensive code recently updated.* International Journal of Fatigue, 2009. **31**: p. 50-58.

5.3. Links and implications

The investigation conducted in Chapter 5 showed that the level of operating internal pressure changes the failure behaviour of IRP systems under bending. The increase in internal pressure causes a rise in longitudinal and hoop stresses in the invert of IRP, while simultaneously reducing the stresses in the crown of IRP. Regardless of the level of operating internal pressure applied, longitudinal stresses during bending fatigue are larger than the hoop stresses at any location along the IRP. During the bending of a fully bonded IRP system with any level of internal pressure, the most critical stress is the longitudinal tensile stress at the edges of the host pipe discontinuity. Additionally, the concentration of longitudinal tensile stress in fully bonded systems caused by the rise in internal pressure may significantly reduce the fatigue life of IRP. Consequently, the potential for mitigating high stress that develops at the discontinuity edges and enhancing the fatigue life of IRP systems by implementing various bonding levels at the interface between the host pipe and IRP was investigated in Chapter 6.

CHAPTER 6: PAPER 4 – INFLUENCE OF THE BONDING LEVEL ON THE BENDING FATIGUE BEHAVIOUR OF INTERNAL REPLACEMENT PIPE SYSTEMS

6.1. Introduction

Chapter 5 demonstrated that when IRP is fully bonded to the discontinuous host pipe segments, the operating internal pressure can cause a substantial increase in the concentration of longitudinal stress in IRP at the discontinuity edges under bending, resulting in premature fatigue failure. As discussed in Chapter 2, the existing research on IRP-repaired legacy gas pipeline systems subjected to internal pressure alone has shown that unbonded repair systems offer advantages over fully bonded systems in terms of reducing stress concentration at the damaged area of the host pipe and improving the structural capacity of the repair pipe. However, there is no research investigating the potential impact of varying bonding levels on the bending fatigue performance of IRP-repaired discontinuous legacy gas pipes.

This chapter addressed Objective 4 by numerically investigating the impact of bonding level, specifically characterised by the unbonded length of IRP to the host pipe, on the flexural fatigue performance of IRP systems in both pressurised and non-pressurised scenarios. The analyses considered a wide range of unbonded lengths for each segment of discontinuous host pipe ranging from zero, signifying a fully bonded state, to 1518.9 mm (59.8 in), representing a completely unbonded state. This evaluation was conducted by considering various design parameters such as repair thickness, repair material, internal pressure levels and traffic loading, which were selected based on the findings of Chapter 5. An extensive discussion of the analysis and findings can be found in Section 6.2.

6.2. Publication

Influence of bonding level on the bending fatigue behaviour of internal replacement pipe systems

Shanika M. Kiriella[1a], Allan C. Manalo[1b], Cam M. T. Tien[1c], Hamid Ahmadi*[1], Warna Karunasena[1d], Patrick G. Dixon[2e], Ahmad Salah[1f], Brad P. Wham[2g]

[1] Center for Future Materials, University of Southern Queensland, Toowoomba, Queensland 4350, Australia.

[2]Center for Infrastructure, Energy, and Space Testing, University of Colorado, Boulder, CO 80309, US.

Abstract. Internal replacement pipe (IRP) is a novel trenchless repair technology for rehabilitating legacy gas and oil pipelines. The current knowledge of the behaviour of IRP systems under repetitive traffic loading is limited due to insufficient research work. This study aimed to examine how the bonding level between the host pipe and IRP affects the flexural fatigue performance of IRP used for repairing legacy gas pipelines with circumferential discontinuities. The investigation was conducted using numerical four-point bending simulations under both pressurised and non-pressurised conditions. The influence of the thickness and material properties of IRP and the magnitude of traffic loads are also explored. The results of the analyses showed that the minimum fatigue life of all pressurised systems with any bonding level is primarily controlled by the tensile failure of the bottom outer surface of IRP. Based on a loading configuration of 762-1016-762 mm (30-40-30 in), it has been determined that unbonding 311.2 mm (12.3 in) diameter IRP from the host pipe to a length at least equal to the diameter of the IRP from the discontinuity edge provides the longest service life for non-pressurised repair systems. Similarly, for all pressurised systems, the longest fatigue life can be achieved by unbonding them to a length of at least twice the diameter of the IRP from the discontinuity edge.

Keywords. Internal replacement pipe (IRP); Host pipes; Traffic loading; Internal pressure; Flexural fatigue behaviour; Finite element analysis (FEA); Fully bonded; Unbonded; Stress concentration

* Corresponding Author, PhD., E-mail: hamid.ahmadi@unisq.edu.au
[a] PhD. Student, E-mail: shanika.kiriella@unisq.edu.au
[b] PhD., E-mail: allan.manalo@unisq.edu.au
[c] PhD., E-mail: camminhtri.tien@unisq.edu.au
[d] PhD., E-mail: karu karunasena@unisq.edu.au
[e] PhD., E-mail: padi9036@colorado.edu
[f] PhD. Student, E-mail: ahmad.salah@unisq.edu.au
[g] PhD., E-mail: brad.wham@colorado.edu

1 Introduction

Pipelines are widely regarded as the most cost-effective method for transporting natural gas and crude oil over long distances (Bubbico 2018, Chen *et al.* 2022, Mao *et al.* 2022, Singh and Markeset 2009, Toh *et al.* 2018). During the transportation process, pipelines may experience failure due to various factors such as ageing, corrosion, third-party excavation, construction defects, and operational errors (Akram *et al.* 2020, Cao *et al.* 2019, Chen *et al.* 2019, Su *et al.* 2021, Zhou *et al.* 2016). Such failures can result in loss of life, serious personal injuries, significant financial losses, and irreversible environmental damage (Cunha 2016, Shahriar *et al.* 2012, Shehata and El-Shamy 2023) and therefore require effective repair solutions. The aged underground pipelines are commonly located below busy roads, and the traditional method of replacing them can cause significant disruption to traffic flow and nearby businesses (Brown *et al.* 2008, Hsu and Shou 2022a, Yang *et al.* 2022). As a result, trenchless technologies have become increasingly popular for pipeline rehabilitation, as they allow for the installation of repair systems without the need for extensive excavation (Hsu and Shou 2022a, Lu *et al.* 2020). Other advantages of trenchless rehabilitation include lower comprehensive cost, shorter construction time, low construction noise, and less pollution (Li *et al.* 2023, Tetreault *et al.* 2018, Xia *et al.* 2022). Trenchless repair techniques have undergone significant advancement recently, specifically with the introduction of a novel pipeline rehabilitation approach known as internal replacement pipe (IRP) systems (Dixon *et al.* 2023, Tafsirojjaman *et al.* 2022, Wang *et al.* 2016). The utilisation of IRP systems enhances the performance and longevity of existing legacy pipelines.

Fatigue failure induced by the ground vibration resulting from vehicle movement over road surfaces has been identified as a potential failure mode associated with host pipe and IRP systems, as stated in Ha *et al.* (2016), Wang *et al.* (2019), Tafsirojjaman *et al.* (2022), Zhang *et al.* (2022) and Dixon *et al.* (2023). Fatigue is a phenomenon that can cause a reduction in the strength of the material, potentially resulting in the fracture of the pipe walls and subsequently compromising pipeline integrity (Bajcar *et al.* 2012). Currently, there is a limited number of studies available in the open literature that have examined the fatigue behaviour of host pipes with circumferential discontinuities repaired using either cured-in-place pipe (CIPP) liners or spray-applied pipe liners (SAPL) under repetitive traffic loading (Ha *et al.* 2016, Jeon *et al.* 2004, Stewart *et al.* 2015). A few studies under internal pressure and static bending have demonstrated that the presence of circumferential discontinuities in the host pipe can have a detrimental effect on the IRP primarily due to the high stress concentration that arises at the

interface between the two pipes (Brown *et al.* 2014, Kiriella *et al.* 2023, Tien *et al.* 2023). The occurrence of such stress concentration during cyclic bending might potentially cause a decrease in fatigue life and lead to premature fatigue failure before reaching the intended service life.

In an experimental investigation of the fatigue behaviour of cast iron host pipe with circumferential discontinuity repaired with CIPP liner, Jeon *et al.* (2004) observed that some level of debonding between the host pipe and the liner occurs, leading to a reduction in stress concentration at the crack edge. In this study, however, the level of debonding and the extent to which the stress concentration decreases, and fatigue life increases are not clearly demonstrated. When repairing damaged host pipes, IRP can be either partially bonded or completely unbonded to host pipes (Hsu and Shou 2022b, Kozman 2020, Zhong *et al.* 2018). Kozman (2020) and Hsu and Shou (2022b) demonstrated that the utilisation of an unbonded length could potentially mitigate stress concentrations and enhance the structural capacity of the IRP under internal pressure alone and static bending. However, research into how the bonding level might affect the bending fatigue behaviour of the pressurised and non-pressurised IRP-repaired damaged host pipes remains unexplored. As a result, pipeline developers and designers are currently facing a knowledge gap regarding the optimal bonding level that should be implemented between the host pipe and the IRP to enhance the service life (Knight and Bontus 2018).

Under a maximum allowable internal pressure of 1379 kPa (200 psi), Tien *et al.* (2023) used finite element analysis (FEA) to study the behaviour of 3.2 mm (0.1 in) thick IRP made from different materials with MOE ranging from 1.0 GPa (145.0 ksi) to 200.0 GPa (29,007.5 ksi) installed in 323.9 mm (12.8 in) diameter host pipes with circumferential discontinuities in both fully bonded and unbonded conditions at their ends. The results of the study indicated that when IRP is fully bonded, the discontinuity edge of the host pipe can cause a significant concentration of longitudinal stresses in IRP. In unbonded systems, the portion of the unbonded IRP can slide relative to the host pipe, thereby decreasing the internal pressure-induced stress concentration in IRP at the discontinuity edges by up to 15%. The influence of the unbonded length on the behaviour of the repair system and the optimal unbonded length required to minimise stress concentrations and improve the service life may vary greatly depending on the loading type. For instance, an unbonded length which can increase the capacity of IRP under internal pressure or static bending alone may not be suitable for flexural fatigue. Since the internal pressure also has a detrimental effect on the longitudinal stress of the repair pipe,

particularly when the discontinuous host pipe segments are present, the optimum unbonded length that should be implemented into the repair systems to enhance the fatigue life during cyclic bending may also be affected by the level of internal pressure. This highlights the necessity of investigating the influence of bonding level on the flexural fatigue behaviour of IRP repair systems with varying levels of internal pressure.

Studies have shown that the fatigue life of repaired pipes can be substantially influenced by their wall thickness, MOE, and the magnitude of the traffic load. In their numerical investigation of the fatigue behaviour of repair pipes made of various materials with MOE ranging from 1 GPa (145.0 ksi) to 200 GPa (29,007.5 ksi) and wall thicknesses varying from 3.2 mm (0.1 in) to 25.4 mm (1.0 in) exposed to a repetitive traffic load of 17.4 kN (3.9 kips), Tafsirojjaman *et al.* (2022), demonstrated that increasing MOE and thickness can significantly extend the service life. Huang *et al.* (2020) demonstrated that carbon fibre polymer pipes with thicknesses of 5.0 mm (0.2 in) and 11.2 mm (0.4 in) subjected to 43.6 kN (9.8 kips) exhibited no failure even after one million cycles, whereas those subjected to relatively higher loads (87.0 kN or 19.6 kips) failed before meeting their anticipated design life of one million cycles. These findings highlight the importance of conducting investigations on the influence of bonding level on flexural fatigue, considering different repair thicknesses, repair materials and traffic load levels. Therefore, the present study examines numerically the influence of bonding level, which is defined by the unbonded length of the IRP to the host pipe, on the flexural fatigue behaviour of IRP. The investigation was carried out by varying thickness and MOE of the IRP and the traffic loads. The findings of this study will provide significant new information and practical guidance in the development, design, and implementation of safe, reliable and cost-effective IRP systems for the repair of damaged pipelines.

2 Methodology

2.1 Modelling and analysis of IRP systems

Three-dimensional finite element (FE) four-point bending simulations are performed using ANSYS mechanical software (Ansys 2021) to examine the fatigue behaviour of IRP systems installed in host pipes with full circumferential discontinuities at the midspan. The simulations are performed under repetitive traffic loading conditions over a service life of 50 years, which is equivalent to one million loading cycles. The simulation employs a loading configuration of 762-1016-762 mm (30-40-30 in), which is identical to the one utilised by Kiriella *et al.* (2023). In order to optimise computational efficiency, only one-quarter of the

system is modelled, taking advantage of symmetry. Appropriate boundary conditions in both longitudinal and transverse directions are applied accordingly.

Throughout the investigation, it was ensured that the outer diameter and the thickness of the host pipe remained constant at 325.9 mm (12.8 in) and 6.4 mm (0.3 in), respectively. The outer diameter of the IRP is determined by the inner diameter of the host pipe, which measures 311.2 mm (12.3 in). The selection of these parameters is based on a prior investigation carried out by Tafsirojjaman *et al.* (2022). The current investigation uses a narrow discontinuity width of 12.7 mm (0.5 in), which is determined to be critical during an analysis of IRP under static bending, as stated in Kiriella *et al.* (2023). The width of this discontinuity represents the existence of a joint that has been pulled out but is still functioning in legacy pipes. A pinned support with a frictionless connection between the host pipe and clamps is employed to ensure an accurate representation of the experimental setup and to minimise convergence issues. The loading head is connected to a separate clamp by means of a pin-lug mechanism. All the components of the systems are modelled using standard SOLID186, higher-order 3D solid elements, each of which consists of 20 nodes. Steel is utilised for the host pipe as well as loading head, clamps, pins and lugs.

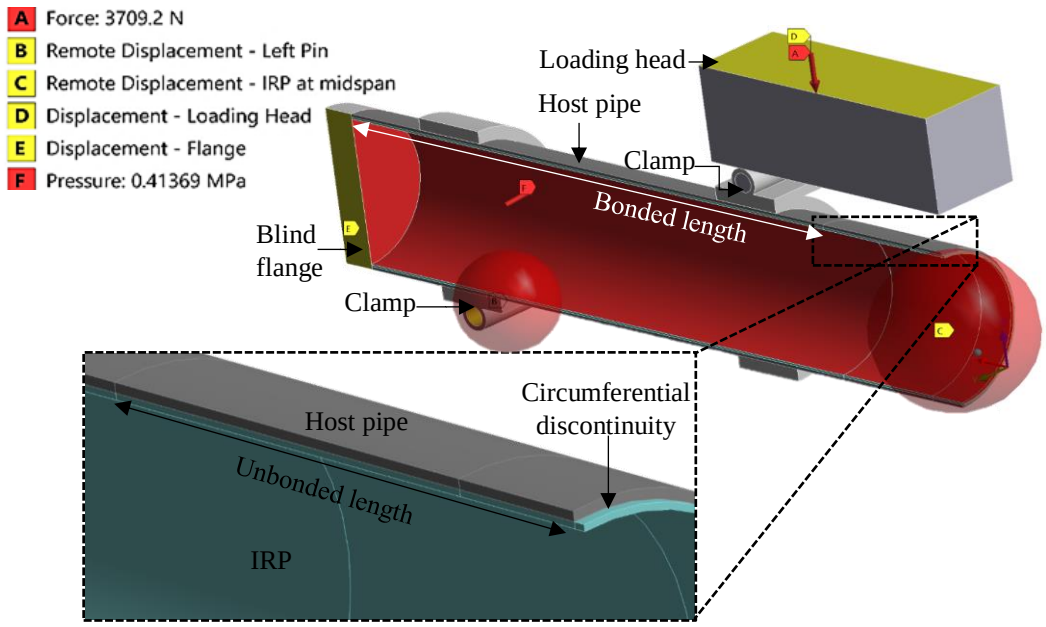

Fig. 1. One-quarter of the FE model of an IRP installed in a host pipe with circumferential discontinuity at the midspan

The study investigates the effect of varying bonding levels in the IRP system by utilizing predefined unbonded regions in both the host pipe segment and IRP. The analysis

considers a wide range of lengths for the unbonded region (unbonded lengths), ranging from zero, which represents the fully bonded condition to 1518.9 mm (59.8 in), which represents the completely unbonded condition. A fully bonded connection involves adhering the IRP and the discontinuous host pipe segments along their entire interface. The unbonded length is applied uniformly throughout the entire circumference of both the host pipe and IRP. Additionally, it is important to note that the specified unbonded lengths are applied to each segment of the discontinuous host pipe. The bonded portion of the IRP and the host pipe segments are connected using the bonded connection type in ANSYS mechanical. On the other hand, a frictionless connection type is employed at the interface between the unbonded portion of the host pipe segments and IRP. Internal pressure levels utilised include 206.8 kPa (30.0 psi), 413.7 kPa (60.0 psi) and 620.5 kPa (90.0 psi). These levels of internal pressure are selected to cover the highest operating internal pressure of the legacy steel pipe, which has been reported to be 413.7 kPa (60.0 psi) by the Advanced Research Project Agency-Energy (Tien *et al.* 2023), as well as internal pressure levels above and below this limit by 206.8 kPa (30 psi), in addition to zero internal pressure condition.

The investigation was carried out by varying thicknesses and materials of the IRP and traffic loadings. The repair thicknesses considered are 3.2 mm (0.1 in), 4.1 mm (0.2 in) and 6.4 mm (0.3 in). The repair materials employed consist of a polymer, and two types of glass fibre-reinforced polymer composite, i.e. GFRP-1 and GFRP 2 with MOE values of 1.7 GPa (246.6 ksi), 3.7 GPa (536.6 ksi) and 7.9 GPa (1145.8 ksi), respectively. The different levels of traffic loading are 14.8 kN (3.3 kips), 20.0 kN (4.5 kips), 25.0 kN (5.6 kips) and 30 kN (6.7 kips), with a constant amplitude and a loading ratio of zero. These parameters are based on Kiriella *et al.* (2023). The analysis is conducted under the assumption that both polymeric and composites possess design strain limits of 0.02 (Tafsirojjaman *et al.* 2022). The study employs the stress-life (S-N) approach to estimate fatigue life, considering a design life of one million loading cycles. The stress-life data for polymeric and GFRP-2 materials were obtained from the studies conducted by Mellott and Fatemi (2014) and Zakaria *et al.* (2016), respectively. Additionally, the S-N curve for GFRP-1, as shown in Fig. 2, was established through tension-tension fatigue testing conducted following the ASTM D 3479/D D3479M standards (ASTM 2019).

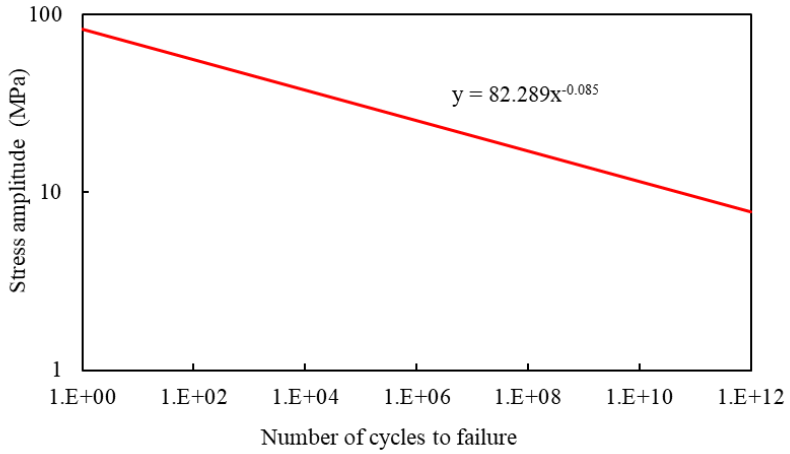

Fig. 2. S-N curve of GFRP-1 repair material

2.2 Mesh convergence study

A mesh convergence study is performed in order to determine the ideal mesh size for generating accurate FEA outcomes. The reliability of the numerical results is evaluated by comparing the maximum normal stress obtained through FEA with the maximum theoretical stress of 18.8 MPa (2.7 ksi) calculated using the bending stress formula. To achieve this, an IRP alone with a MOE of 3.7 GPa (536.6 ksi) and dimensions as outlined in section 2.1 is subjected to a traffic load of 14.8 kN (3.3 kips). The number of elements in the direction of thickness is specified as three, while the surface element size of the pipe ranges from 25×25 mm (1.0×1.0 in) to 2.0×2.0 mm (0.08×0.08 in). Fig. 3a illustrates the correlation between the maximum normal stress and the number of elements within the FE model. It is found that the FE result closely approximates the theoretical result of 18.8 MPa (2.7 ksi), with a deviation of only 1.6% when utilising an element size of 5.0×5.0 mm (0.2×0.2 in). To ensure the proper representation of potential stress concentration, a mesh refinement was implemented in the vicinity of the host pipe discontinuity. The determination of the ideal surface element size for the refined mesh was achieved by conducting a mesh sensitivity analysis, as shown in Fig. 3b. This was accomplished by analysing a steel host pipe with a 12.7 mm (0.5 in) wide circumferential discontinuity that has been repaired under a traffic loading of 14.8 kN (3.3 kips). The IRP utilised in this analysis is identical to the one described in the mesh convergence study.

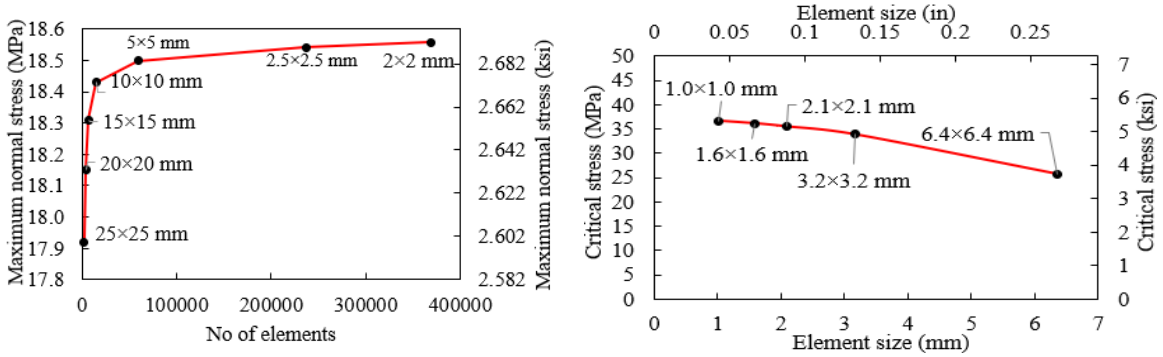

(a) (b)

Fig. 3. (a) Mesh convergence and (b) Mesh sensitivity analysis

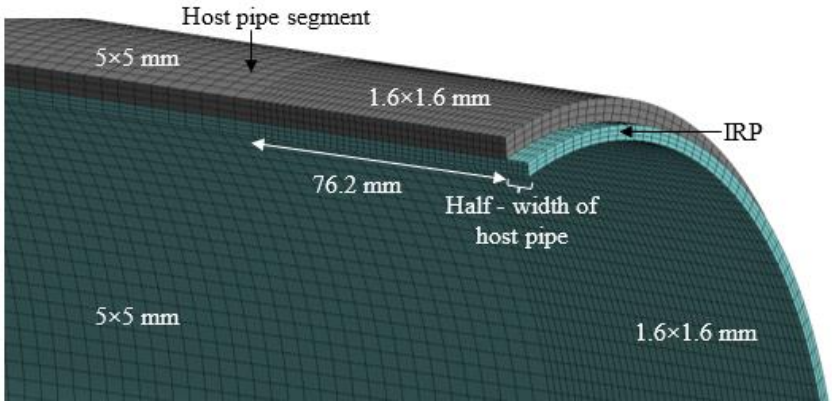

Fig. 4. Mesh refinement in the vicinity of the host pipe discontinuity

To optimise computational efficiency, the mesh refinement is conducted over a length that corresponds to the discontinuity width, along with an additional 76.2 mm (3.0 in) beyond the discontinuity edge. The surface element size of the refined mesh is varied during the sensitivity analysis between 6.4×6.4 mm (0.3×0.3 in) and 1.0×1.0 mm (0.04×0.04 in). Outside of this zone, the surface element size is set to 5.0×5.0 mm (0.2×0.2 in). The influence of different element sizes used for mesh refinement on the stress concentrated in IRP at the discontinuity edge is shown in Fig. 3b According to the figure, the localised stress begins to approach a finite value once the surface element size is decreased to 2.1×2.1 mm (0.08×0.08 in). Based on the consideration of computational cost and the observation that the discrepancy in local stress at the discontinuity edge between the element sizes of 1.0×1.0 mm (0.04×0.04 in) and 1.6×1.6 mm (0.06×0.06 in) is below 2.0%, the latter is selected for the mesh refinement. Fig. 4 depicts the mesh refinement of a quarter symmetry model of an IRP installed in a host pipe with a discontinuity width of 12.7 mm (0.5 in).

2.3 Validating the FE model of an IRP system

The accuracy of the FE model is ensured by validating the results with the outcomes obtained from a laboratory test conducted by the University of Colorado Boulder (CUB). The validation process includes a comparison of load-deflection behaviours and load-strain behaviours between FEA and physical testing. The comparison is conducted at various locations, both at the bottom and top of GFRP-1 IRP installed within a steel host pipe. The discontinuity width of the host pipe is 12.7 mm (0.5 in), and the cyclic lateral load applied is 14.3 kN (3.2 kips) (Klingaman *et al.* 2022). Fig. 5a shows a strong correlation between the load-deflection behaviours obtained from FEA and experimental testing. The load-strain behaviours obtained from FEA also exhibit a good agreement with the corresponding experimental outcomes, as depicted in Fig. 5b.

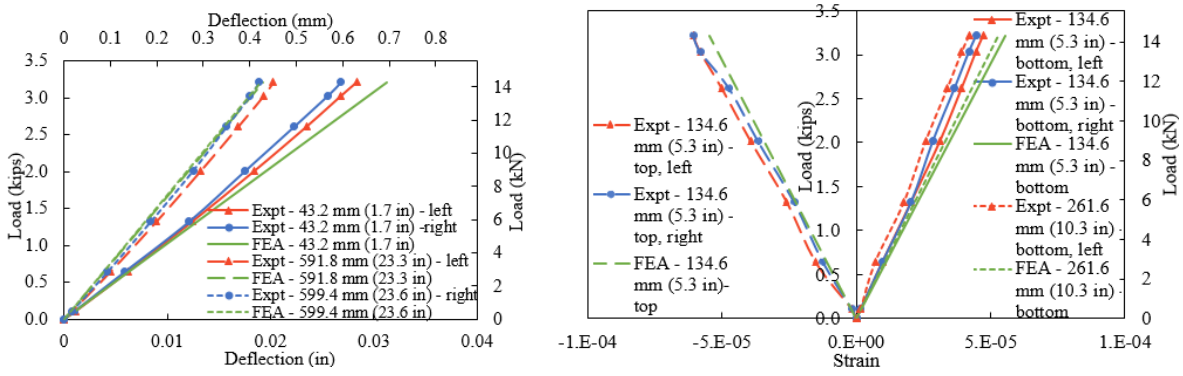

(a) Load-deflection behaviour (b) Load-strain behaviour

Fig. 5. Comparison between FEA and experimental behaviours of IRP under cyclic traffic loading

3 Results and discussion

3.1 Longitudinal stress, hoop stresses and fatigue lives

Under different levels of bonding, Fig. 6a, b, c and d show comparisons between the maximum longitudinal and hoop stresses in the GFRP-1 IRP with internal pressures of zero, 206.8 kPa (30.0 psi), 413.7 kPa (60.0 psi) and 620.5 kPa (90.0 psi), respectively when subjected to a traffic load of 14.8 kN (3.3 kips). In this analysis, the unbonded length varies from zero (fully bonded connection) to 1518.9 in (59.8 in) (totally unbonded state), while the repair thickness is kept at 4.1 mm (0.2 in). During the bending process, the top portion of the IRP system undergoes compression, while the bottom portion experiences tension. As shown in Fig. 6a-d, increasing the unbonded length from 0 to 579. 1 mm (22.8 in), the maximum

longitudinal tensile stresses in both pressurised and non-pressurised IRP decrease nonlinearly and gradually and then remain stable until the systems are completely unbonded. Based on the results, it is evident that increasing the unbonded length from 0 to 579. 1 mm (22.8 in) results in a more significant reduction in maximum longitudinal tensile stress when the internal pressure is lower. Regardless of the magnitude of the internal pressure, the greatest longitudinal tensile stress in a fully bonded IRP occurs at the discontinuity edge at the bottom (Fig. 7a). The amplification of longitudinal tensile stress at the discontinuity edge is caused by the sudden reduction in cross-sectional area, which creates stress concentration.

When the unbonded length is within the load span, i.e., the distance between the centre of the load clamps, the maximum longitudinal tensile stress in GFRP-1 arises at the bottom, where the bonded and unbonded regions are separated (Fig. 7b, c and d). This is true for both non-pressurised and pressurised IRP systems. With increasing unbonded lengths, the maximum longitudinal tensile stress of a partially bonded repair system can be explained by the load transfer mechanism and concept of stress distribution. In a partially bonded system, the bonded region of the host pipe and IRP acts as a fixed boundary condition, while the unbonded section of IRP can slide relative to the host pipe. This creates a stress concentration point at the location where the bonded and unbonded regions meet.

Additionally, the difference in stiffness also contributes to a higher stress level at the interface between the unbonded and bonded regions. As the unbonded length increases, the load transfer decreases, and the stresses generated at the bonded and unbonded interfaces become more evenly distributed along the length of IRP. The portion of IRP that is unbonded to the host pipe undergoes relatively greater deformation and strain compared to the bonded portion due to the lack of constraints. This increase in deformation experienced by IRP, as depicted in Fig. 8a, leads to the redistribution of the stresses away from the bonded and unbonded interfaces toward the midspan, resulting in a decrease in the longitudinal tensile stress that can be localised at the bonded and unbonded interface at the bottom of IRP (Fig. 7d, e and f). In partially bonded systems, the IRP that is not bonded has the ability to slide relative to the host pipe leading to a reduction in stress concentration at the discontinuity edges caused by both traffic load and internal pressure. Similar results were found by Tien *et al.* (2023) for the behaviour of longitudinal stress concentration at the discontinuity edge in bonded and unbonded systems when subjected to internal pressure alone.

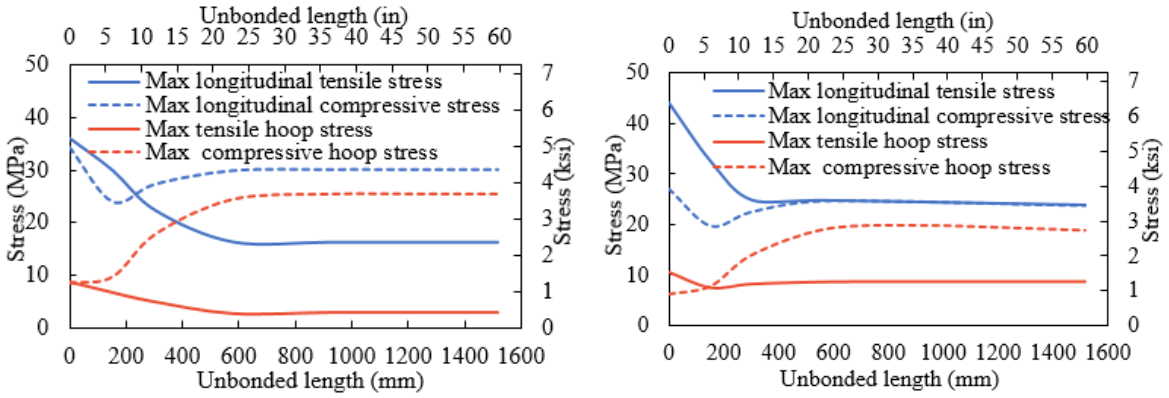

(a) No internal pressure

(b) Internal pressure of 206.8 kPa (30.0 psi)

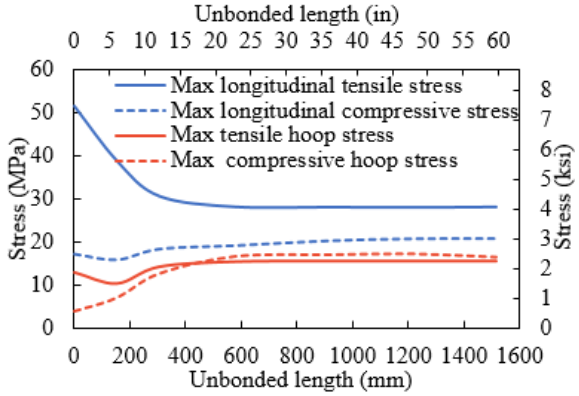

(c) Internal pressure of 413.7 kPa (60.0 psi)

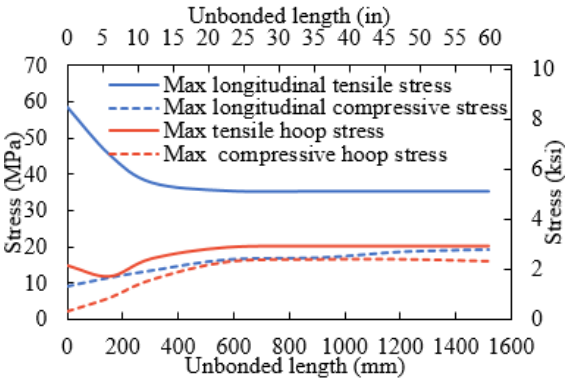

(d) Internal pressure of 620.5 kPa (90.0 psi)

Fig. 6. Behaviours of maximum longitudinal and hoop stresses in GFRP-1 IRP with increasing unbonded under a 14.8 kN (3.3 kips) traffic load at different internal pressures

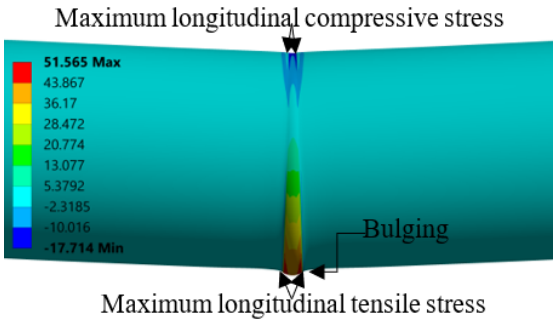

(a) Fully bonded

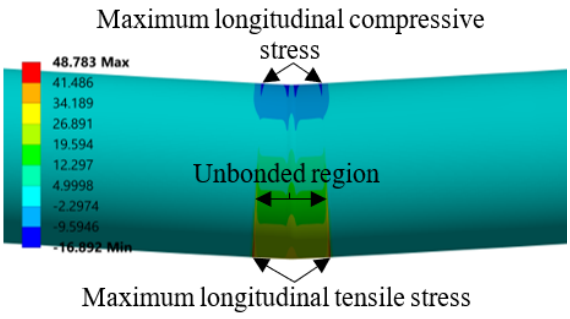

(b) Unbonded length of 50.8 mm (2.0 in)

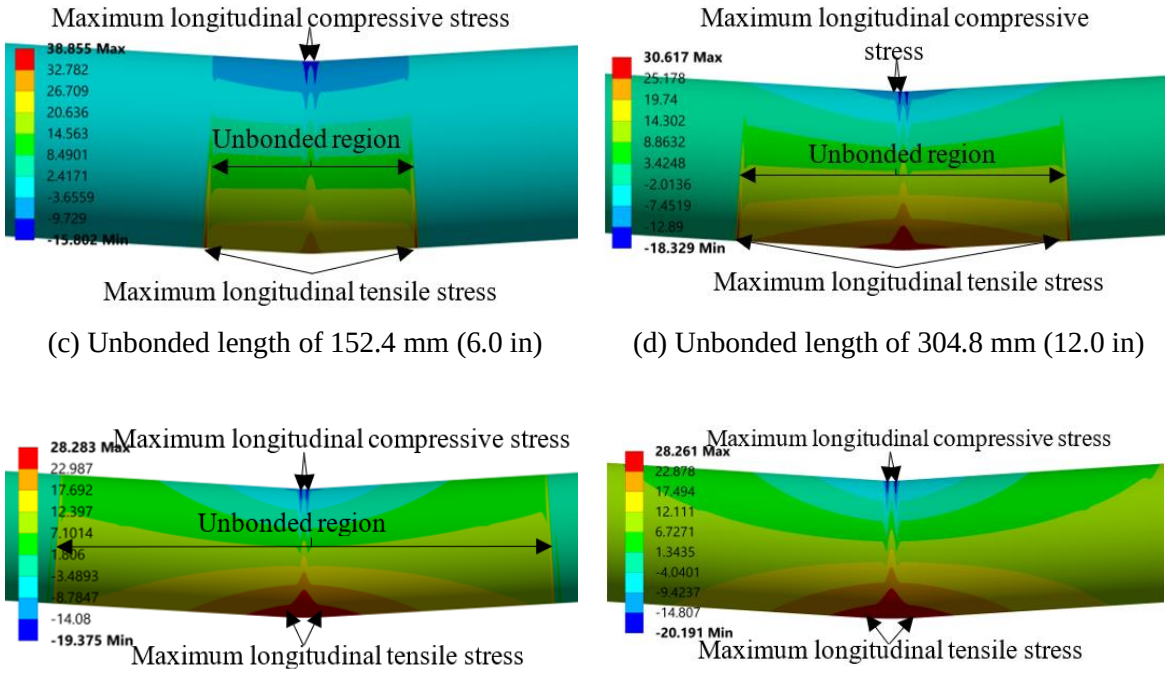

(c) Unbonded length of 152.4 mm (6.0 in)

(d) Unbonded length of 304.8 mm (12.0 in)

(e) Unbonded length of 579.1 mm (22.8 in)

(f) Completely unbonded condition

Fig. 7. Longitudinal stress distribution in IRP with internal of 413.7 kPa (60.0 psi) subjected to traffic load of 14.8 kN (3.3 kips) at different unbonded length (host pipe segments are hidden) [Units: MPa]

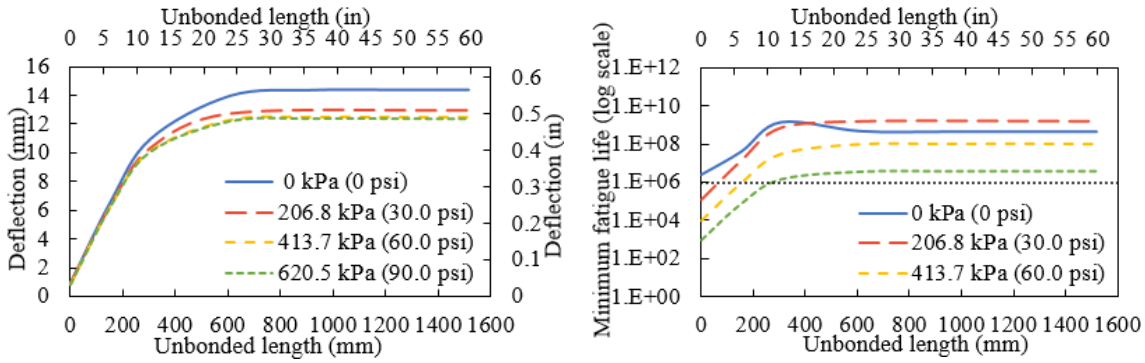

(a)

(b)

Fig. 8. Comparison of the behaviours of (a) maximum deflections and (b) fatigue lives of GFRP-1 with increasing unbonded length at different internal pressures under a 14.8 kN (3.3 kips) traffic load

At zero internal pressure, when the interface between the bonded and unbonded region is located outside the load span, the location where the maximum longitudinal tensile stress arises shifts to the inner surface of IRP at the bottom midspan. This is because the load transfer

from the host pipe to IRP is negligible at this point; thus, there is no concentration of longitudinal tensile stress at the interface between bonded and unbonded regions. Therefore, IRP behaves more independently, and the maximum longitudinal tensile in IRP is primarily due to the bending stress induced by external loading. This can be explained by IRP acting as a cantilever beam, and the maximum longitudinal tensile stress occurs at the free end, which is the invert at the midspan due to the bending moment created by external loading. This leads to a consistent peak longitudinal tensile stress when the location where the bonded and unbonded region meets is beyond the loading span. Unlike the non-pressurised systems, the location of the maximum longitudinal tensile stress in the pressurised systems with this bonding condition varies depending on the levels of internal pressure present. At internal pressures of 206.8 kPa (30.0 psi), 413.7 kPa (60.0 psi) and 620.5 kPa (90.0 psi), these locations are 107.0 mm (4.2 in) from the outer surface of the bottom midspan, 35.0 mm (1.4 in) from the outer surface of the bottom midspan, and the bottom midspan, respectively.

The maximum longitudinal compressive stresses in the crown of IRP at internal pressures of zero, 206.8 kPa (30.0 psi) and 413.7 kPa (60.0 psi) gradually reduce when the unbonded length is extended from zero to 152.4 mm (6.0 in). Consequently, the reduction in maximum longitudinal compressive stress becomes less significant as the internal pressure rises. Under an internal pressure of 620.5 kPa (90.0 psi), the crown of IRP no longer experiences a decrease in maximum longitudinal compressive stress with an increase in unbonded length (Fig. 6d). The observed phenomenon can be attributed to the significant reduction in longitudinal compressive stress concentration in the crown of fully bonded IRPs at the discontinuity edges, as internal pressure rises. Under an internal pressure of 413.7 kPa (60.0 psi) or lower, the maximum longitudinal compressive stress experienced by IRP is observed at the interfaces between the bonded and unbonded regions at the top, for unbonded length between 0.25 in (the shortest unbonded length under consideration) and 152.4 mm (6.0 in), similar to the tension side (Fig. 7b). This is due to the abrupt change in stiffness at the interface between bonded and unbonded regions at the top of IRP, which concentrates compressive stress at that location. This compressive stress concentration, however, diminishes as the unbonded length is extended, leading to a more uniform distribution of compressive stresses along the length of IRP.

Once the unbonded length exceeds 152.4 mm (6.0 in), the maximum longitudinal compressive stresses under internal pressures of zero and 206.8 kPa (30.0 psi) experience a sudden and nonlinear increase that continues until the unbonded length reaches the boundary

of the loading clamp outside the load span. The reason for the change in the trend at an unbonded length of 152.4 mm (6.0 in) is attributed to the changing of the location where the maximum longitudinal compressive stress arises. At or beyond 152.4 mm (6.0 in), the concentration of longitudinal compressive stress at the top of IRP where the bonded and unbonded regions meet experiences a further reduction, while the concentration of stress at the top of IRP at the discontinuity edge of the host pipe becomes higher again. This causes the location of the highest longitudinal compressive stress in the crown of IRP to shift from the interface between bonded and unbonded regions to the discontinuity edge (Fig. 7b and c). However, once the unbonded length is increased beyond the load span, the maximum longitudinal compressive stress in IRP under internal pressure of 206.8 kPa (30.0 psi) or below remains constant until the system is completely unbonded, which is similar to the behaviour of maximum longitudinal tensile stress. In this case, the longitudinal compressive stress in IRP remains concentrated at the discontinuity edge, while there is no concentration of longitudinal compressive stress in IRP at the bonded and unbonded interface (Fig. 7d, e and f).

Non-pressurised GFRP-1 experiences a gradual decrease in its maximum tensile hoop stress as the unbonded length is extended from 0 to 579. 1 mm (22.8 in), followed by a stable state until the system is completely unbonded (Fig. 6a). The observed behaviour in maximum tensile hoop stress is similar to that of the maximum longitudinal tensile stress. However, in the cases where the pressure within IRP is 206.8 kPa (30.0 psi) or above, the highest tensile hoop stress reduces only to an unbonded length of approximately 152.4 mm (6.0 in). Upon exceeding this limit, the maximum tensile hoop stress observed in IRP subjected to an internal pressure of 206.8 kPa (30.0 psi) remains relatively constant, while that in IRP exposed to an internal pressure of 413.7 kPa (60.0 psi) and 620.5 kPa (90.0 psi) displays a minor nonlinear increase until an unbonded length of roughly 254.0 mm (10.0 in) and 579.1 mm (22.8 in), respectively, before stabilising. Regardless of any internal pressure level, it can be observed that all the partially bonded IRPs experience the greatest amount of tensile hoop stress at the bottom, where the interface between the bonded and unbonded regions is located, while in the case of completely unbonded IRP, it is observed at the bottom midspan. The maximum compressive hoop stresses experienced by both pressurised and non-pressurised systems demonstrate a nonlinear increase as the unbonded length is extended from 0 to 579. 1 mm (22.8 in), after which they stabilise until the systems are completely detached. Unlike tensile hoop stress, the compressive hoop stress in IRPs that are fully bonded, partially bonded or

completely unbonded, and with or without internal pressure, always reaches its peak at the crown, where the discontinuity edges of host pipe segments are located.

In non-pressurised IRPs, the longitudinal tensile stress is the highest when the unbonded length is less than 254.0 mm (10.0 in). In the cases where the unbonded length exceeds 254.0 mm (10.0 in), the maximum longitudinal compressive stress surpasses the longitudinal tensile stress and remains critical until the system is completely unbonded (Fig. 6a). Additionally, the maximum compressive hoop stress exceeds the longitudinal tensile stress when the unbonded length reaches approximately 381.0 mm (15.0 in) while remaining below the maximum longitudinal compressive stress. The observed behaviours can be attributed to the fact that, in the absence of internal pressure, when the ratio of the unbonded length to the host pipe length within the load span exceeds 0.5, the deformation in the unbonded section becomes more pronounced at the crown of IRP than at its bottom. This is because the bottom of IRP is more constrained by support, which limits its deformation and reduces maximum tensile stress. The increased deformation at the crown resulted in a higher concentration of both longitudinal and hoop compressive stress at the discontinuity edge compared to longitudinal tensile stress. Under an internal pressure of 206.8 kPa (30.0 psi), the maximum longitudinal compressive in IRP approaches the corresponding maximum tensile stress after an unbonded length of 579. 1 mm (22.8 in), while the maximum compressive hoop stress remains below the longitudinal stresses at any unbonded length.

With an internal pressure of 413.7 kPa (60.0 psi) or above, the maximum longitudinal tensile stress at any unbonded length is much greater than both maximum longitudinal and hoop compressive stresses (Fig. 6c and d). Both maximum longitudinal and hoop compressive stresses stay even below the corresponding maximum tensile hoop stress for any unbonded length at the highest internal pressure under consideration. Therefore, the presence of internal pressure greater than 206.8 kPa (30.0 psi) causes the maximum longitudinal tensile stress in IRP to become dominant across all the unbonded lengths. This is because, at higher internal pressure, a relatively larger proportion of the resultant longitudinal stress is contributed by internal pressure. Unlike non-pressurised systems, pressurised IRPs exhibit the highest difference between the maximum longitudinal tensile and compressive stresses when they are fully bonded. Although the bottom of IRP in a fully bonded state results in the formation of bulging between the discontinuity edges of the host pipe (Fig. 7a), this bulging disappears once an unbonded length is implemented, due to the reduction in tensile stresses, as illustrated in Fig. 7b-f.

Fig. 8b shows a comparison of the minimum fatigue life of a 4.1 mm (0.2 in) thick GFRP-1 with varying unbonded lengths under a traffic load of 14.8 kN (3.3 kips) with different internal pressures. Even on a semi-log plot, the minimum fatigue lives of both pressurised and non-pressurised GFRP-1 exhibit a significant increase as the unbonded length is extended from 0 to 304.8 mm (12.0 in). The location where the bonded and unbonded regions meet at the bottom span of IRP, which experiences the highest stress, controls the minimum fatigue life of the non-pressurised system from the shortest unbonded length up to approximately 254.0 mm (10.0 in) (Fig. 9b, c and d). Thus, the reduction in maximum longitudinal tensile stress amplitude at this particular location within the given range of unbonded length is directly correlated with the increase in fatigue life. Subsequently, until an unbonded length of 579.1 mm (22.8 in) is reached, the fatigue life of the non-pressurised system declines nonlinearly by 64.9%, while that of all the pressurised systems continues to increase gradually.

Additionally, implementation of an unbonded length of 304.8 mm (12.0 in) or greater drops the service life of non-pressurised IRP below that of pressurised IRP operating at 206.8 kPa (30.0 psi). When the unbonded length reaches 304.8 mm (12.0 in) or more, the service life of non-pressurised repair systems is primarily determined by the crown of IRP (compressive side) at the discontinuity edge, where the stress concentration becomes critical. In the absence of internal pressure, the rise in longitudinal compressive stress amplitude at this specific location, with an unbonded length between 304.8 mm (12.0 in) and 579.1 mm (22.8 in), is directly correlated with the reduction in fatigue life. Interestingly, these unbonded lengths are almost equal to one time and two times, respectively the external diameter of the IRP. In contrast, the fatigue life of IRP with internal pressure at any unbonded length is determined by the tension side (bottom span) (Fig. 9).

Increasing the unbonded length from 579.1 mm (22.8 in) until the repair systems are completely detached from their host pipes, the service lives of both pressurised and non-pressurised systems remain nearly constant. This is due to the relatively constant maximum longitudinal stresses in IRP. The longest fatigue life of non-pressurised GFRP-1 is 1.3E+09 cycles with an unbonded length of at least 304.8 mm (12.0 in), nearly 500 times larger than that of the fully bonded case. On the other hand, the longest fatigue life of a pressurised IRP with an unbonded up to a length of 579.1 mm (22.8 in) is greater than that of corresponding fully bonded systems. While GFRP-1 system without internal pressure satisfies the design life requirement even with a fully bonded connection, those operating at internal pressures of 206.8 kPa (30.0 psi), 413.7 kPa (60.0 psi) and 620.5 kPa (90.0 psi) necessitate unbonded lengths of

at least 94.0 mm (3.7 in), 154.9 mm (6.1 in) and 279.4 mm (11.0 in), respectively, to achieve the design life of 1 million cycles. As the internal pressure to which the system is exposed during cyclic bending rises, it leads to an increase in the minimum unbonded length required to meet the design life.

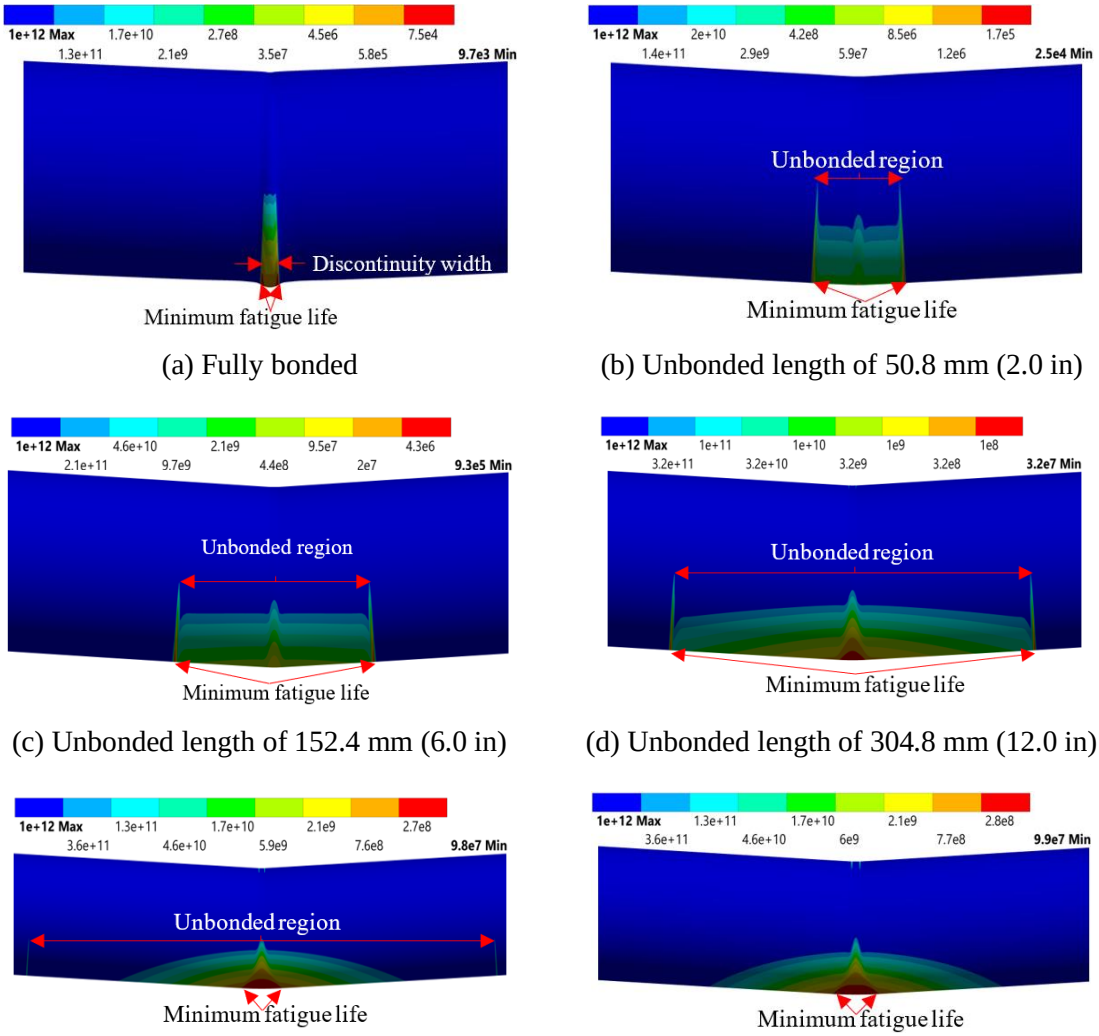

Fig. 9. Minimum fatigue life of IRP with internal pressure of 413.7 kPa (60.0 psi) subjected to traffic load of 14.8 kN (3.3 kips) with different bonding levels (host pipe segments are hidden)

3.2 Effect of unbonded length with different repair thickness

Fig. 10a, b, c and d compare the behaviour of the maximum longitudinal tensile stress (σt_max) and maximum compressive stress (σc_max) generated in the GFRP-1 with different

thicknesses (t) under varying levels of bonding and internal pressure. This analysis is conducted under a traffic load of 14.8 kN (3.3 kips) with repair thicknesses of 3.2 mm (0.1 in), 4.1 mm (0.2 in) and 6.4 mm (0.3 in). With increasing unbonded length, the maximum longitudinal tensile stresses in both pressurised and non-pressurised IRP systems with repair thicknesses of 3.2 mm (0.1 in) and 6.4 mm (0.3 in) display comparable trends to those observed in IRP with a thickness of 4.1 mm (0.2 in) under the same internal pressure conditions. An increase in the unbonded length of both pressurized and non-pressurised systems from 0 to 579.1 mm (22.8 in) leads to a more pronounced reduction in the maximum longitudinal tensile stress when the repair thickness is relatively higher. The findings of this analysis confirm that, under four points bending with all repair thicknesses considered, longitudinal tensile stress concentration in a partially bonded system, whether pressurised or non-pressurised, occurs exclusively at the bonded and unbonded interfaces, as long as it is located within the loading span. However, extending the unbonded length beyond the boundary of the loading clamp does not yield a noticeable effect on the maximum longitudinal tensile stress generated in either pressurised or non-pressurised IRP systems with any repair thickness.

With increasing repair thickness, there is a corresponding rise in the reduction of maximum longitudinal compressive stress at an internal pressure of 413.7 kPa (60.0 psi) or lower. At all repair thicknesses, the rise in maximum longitudinal compressive stress beyond 152.4 mm (6.0 in) of unbonded length is comparatively more pronounced for IRPs that are not pressurised, indicating that the increase in the maximum longitudinal compressive stress becomes less significant as the repair thickness increases. At an internal pressure of 206.8 kPa (30.0 psi), the maximum longitudinal compressive in IRP with a repair thickness of 6.4 mm (0.3 in) exceeds the corresponding maximum longitudinal tensile stress at an unbonded length of approximately 381.0 mm (15.0 in). At this level of internal pressure, maximum longitudinal compressive in IRP with a repair thickness of 3.2 mm (0.1 in) only reaches, but never exceeds, the magnitude of corresponding maximum tensile stress after an unbonded length of 579.1 mm (22.8 in), which is consistent with the findings for repair thickness of 4.1 mm (0.2 in).

Maximum longitudinal compressive stresses in IRP with thicknesses of 3.2 mm (0.1 in) and 6.4 mm (0.3 in) under internal pressures of 413.7 kPa (60.0 psi) and 620.5 kPa (90.0 psi) remain well below the corresponding maximum longitudinal tensile stress at any unbonded length (Fig. 10c and d), as observed for repair thickness of 4.1 mm (0.2 in). Therefore, the presence of internal pressure greater than 206.8 kPa (30.0 psi) causes the maximum longitudinal tensile stress in IRP to become dominant across all the unbonded lengths for all

repair thicknesses. Interestingly, Fig. 10a, b, c and d demonstrate that as the unbonded length is increased, the maximum stresses in IRP with varying repair thicknesses at the same internal pressure level follow a similar trend, regardless of their magnitudes. This could possibly be attributed to the similar ratios of the unbonded length to the host pipe length within the load span.

The fatigue lives of the GFRP-1 with varying unbonded lengths for different repair thicknesses under internal pressures of zero, 206.8 kPa (30.0 psi), 413.7 kPa (60.0 psi) and 620.5 kPa (90.0 psi) and subjected to a traffic load of 14.8 kN (3.3 kips), are compared in Fig. 11a, b, c and d, respectively. The service life of non-pressurised systems exhibits a consistent trend across different repair thicknesses wherein the unbonded length increases, as shown in Fig. 11a. The fatigue lives of pressurised systems against unbonded length also follow a similar trend. Based on these results, it can be concluded that an increase in unbonded length results in a greater improvement in fatigue life for the thicker IRP than it does for the thinner IRP. This observation indicated that, in the absence of internal pressure, an increase in unbonded length from 304.8 mm (12.0 in) to 579.1 mm (22.8 in) causes a comparatively greater decline in fatigue lives of thinner IRPs as opposed to thicker IRPs.

Based on Fig. 11a, when no internal pressure exists, the GFRP-1 IRP, with a thickness of 3.2 mm (0.1 in), can only satisfy the design life requirement if an unbonded length of at least 109.8 mm (4.3 in) is employed. Under an internal pressure of 206.8 kPa (30.0 psi), while IRP with a thickness of 6.4 mm (0.3 in) can fulfil the design life requirement even with a fully bonded connection, repair thicknesses of 3.2 mm (0.1 in) need at least an unbonded length of 154.9 mm (6.1 in) to achieve one million loading cycles. To satisfy the anticipated service life under an internal pressure of 413.7 kPa (60.0 psi), IRP with thicknesses of 3.2 mm (0.1 in) and 6.4 mm (0.3 in) requires a minimum unbonded length of 271.8 mm (10.7 in) and 50.8 mm (2.0 in), respectively. Under an internal pressure of 620.5 kPa (90.0 psi), although the IRP with a thickness of 6.4 mm (0.3 in) is capable of meeting the design life requirement when it is unbonded from the host pipe for at least 81.3 mm (3.2 in) length, a repair thickness of 3.2 mm (0.1 in) will never meet the design life requirement even if the unbonded length is extended beyond the load span. Therefore under the same internal pressure level, lowering the IRP thickness increases the minimum unbonded length required for achieving the design life cycles. Further, the minimum unbonded length that must be implemented at each repair thickness increases as the internal pressure to which the system is exposed rises.

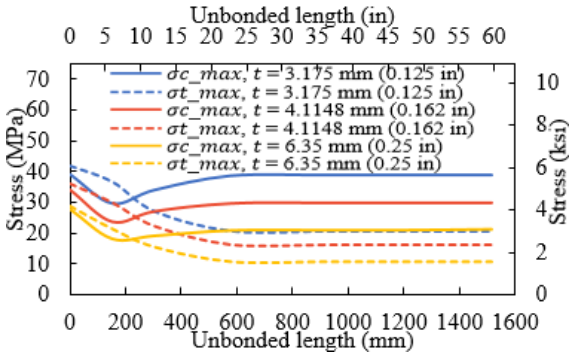

(a) No internal pressure

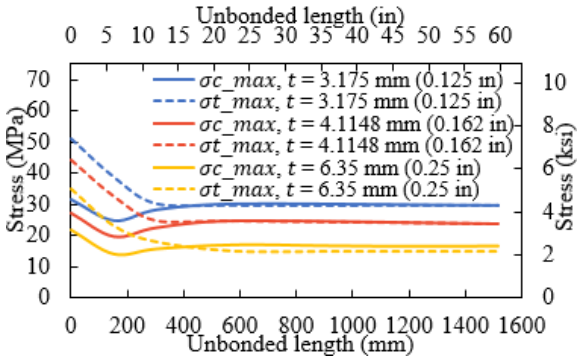

(b) Internal pressure of 206.8 kPa (30.0 psi)

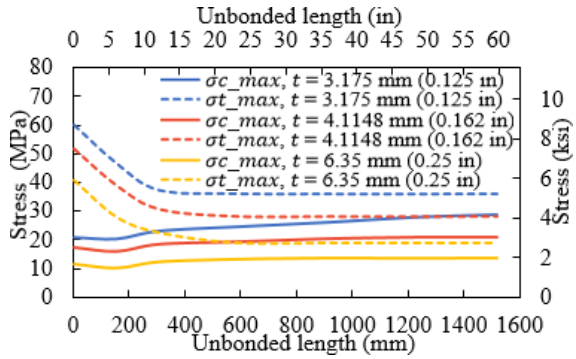

(c) Internal pressure of 413.7 kPa (60.0 psi)

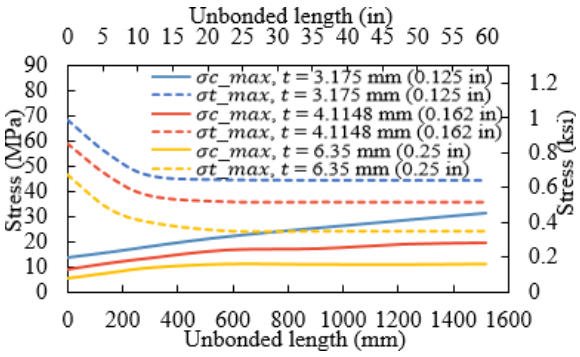

(d) Internal pressure of 620.5 kPa (90.0 psi)

Fig. 10: Comparison of the maximum tensile and compressive stress behaviour of GFRP-1 with different thicknesses as the unbonded length increases at different internal pressures

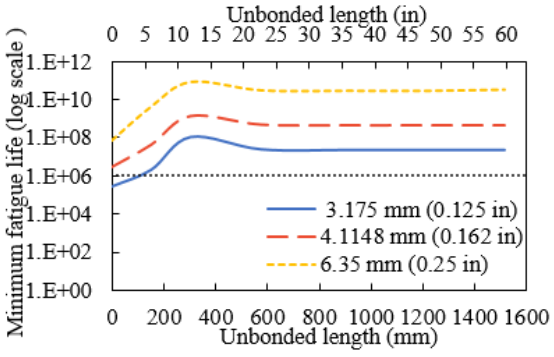

(a) No internal pressure

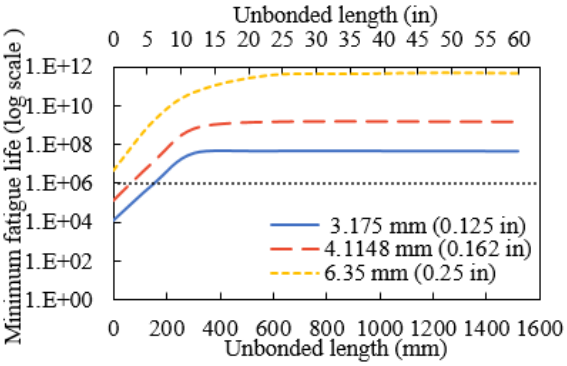

(b) Internal pressure of 206.8 kPa (30.0 psi)

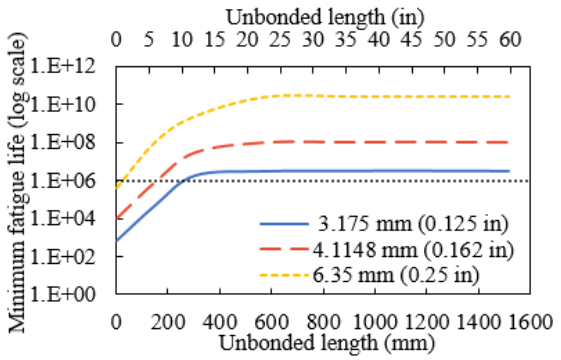

(c) Internal pressure of 413.7 kPa (60.0 psi)

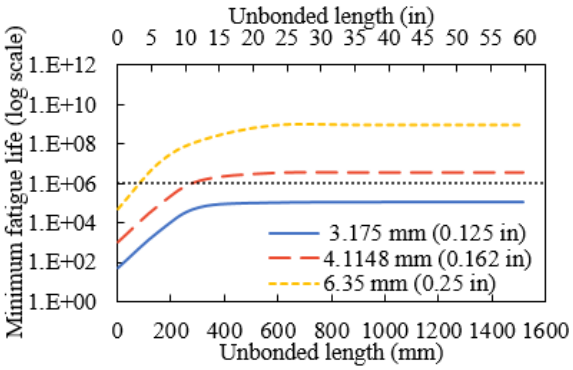

(d) Internal pressure of 620.5 kPa (90.0 psi)

Fig. 11 Comparison of the behaviour of minimum fatigue life of GFRP-1 with different thicknesses as unbonded length increases at different internal pressures

3.3 Effect of unbonded length with different repair materials

In Fig. 12a, b, c and d, comparisons are made between the behaviours of IRPs with different materials in terms of their minimum fatigue life as the unbonded length increases under bending, considering different levels of internal pressure. This investigation employs a thickness of 4.1 mm (0.2 in) and IRP made from polymer, GFRP-1 and GFRP-2 composites, along with a traffic load of 14.8 kN (3.3 kips). Due to polymeric material exceeding the design strain limit of 0.02 for all the unbonded lengths at an internal pressure of 413.7 kPa (60.0 psi) or above, only GFRP-2 is compared with GFRP-1 in Fig. 12c and d. According to Fig. 12a, in the absence of internal pressure, the fatigue lives of polymeric and GFRP-2 with MOE of 1.7 GPa (246.6 ksi) and 7.9 GPa (1145.8 ksi), respectively, exhibit a trend similar to that of GFRP-1 with a MOE of 3.7 GPa (536.6 ksi), as the unbonded length is increased. The potential reason for this could be associated with the identical proportions between the unbonded length and the length of the host pipe within the load span. Extending the unbonded length from zero to 304.8 mm (12.0 in) increases the minimum fatigue lives of non-pressurised IRP with MOE of 1.7 GPa (246.6 ksi), 3.7 GPa (536.6 ksi) and 7.9 GPa (1145.8 ksi), by factors of 2031, 505 and 25, respectively, relative to fully bonded systems.

The reason why IRP with lower MOE experiences a relatively greater improvement in minimum fatigue life with an increase in unbonded length from 0 to 304.8 mm (12.0 in) compared to IRP with higher MOE is because of their higher ability to redistribute the stress along repair pipe. IRPs with lower MOE are more flexible and can deform more easily than stiffer IRPs, which allows them to better redistribute the stress concentration caused by the unbonded length. This ability of better redistribution of stress ultimately leads to a greater

improvement in minimum fatigue life. Conversely, stiffer IRPs have a limited ability to redistribute stress, resulting in a lower improvement in minimum fatigue life with an increase in unbonded length. Extending the unbonded length from 304.8 mm (12.0 in) to 579.1 mm (22.8 in) reduces the minimum fatigue life of non-pressurised IRP.

The findings suggest that an increase in unbonded length from 304.8 mm (12.0 in) to 579.1 mm (22.8 in) results in a relatively greater reduction in minimum fatigue life of non-pressurised IRPs having lower MOE compared to systems having higher MOE. This is because once the unbonded length exceeds a certain threshold, i.e. the ratio of the unbonded length to the host pipe length is greater than 0.5, the stress at the crown at the discontinuity edge becomes excessive for IRP to handle, even if they possess greater flexibility. In this situation, IRP may be able to better resist the stresses due to their higher stiffness, resulting in a smaller reduction in minimum fatigue life compared to repair materials with lower MOE.

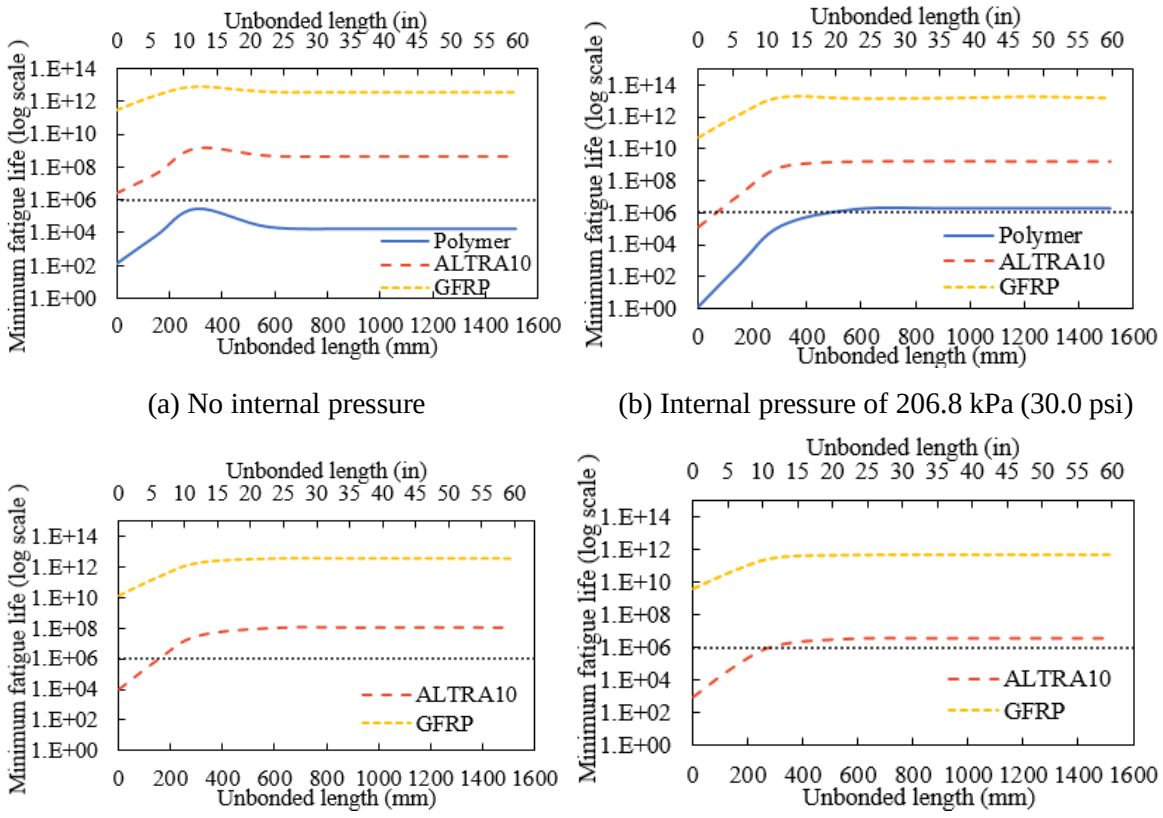

(a) No internal pressure

(b) Internal pressure of 206.8 kPa (30.0 psi)

(c) Internal pressure of 413.7 kPa (60.0 psi)

(d) Internal pressure of 620.5 kPa (90.0 psi)

Fig. 12. Comparison of the behaviour of minimum fatigue life of IRP with different MOE with increasing unbonded length at different internal pressures

Fig. 12b, c and d show that at internal pressures of 206.8 kPa (30.0 psi), 413.7 kPa (60.0 psi) and 620.5 kPa (90.0 psi), the fatigue life of GFRP-2 increases considerably from an unbonded length of zero to approximately 304.8 mm (12.0 in) before remaining stable, which is quite similar to the behaviour of GFRP-1 at the same level of internal pressure. At an internal pressure of 206.8 kPa (30.0 psi), the improvement in the service life of a polymeric system that has the lowest MOE, on the other hand, continues until an unbonded length of 579.1 mm (22.8 in) is reached before it becomes stable. In comparison to the fully bonded state, the fatigue lives of IRPs improved upon extending the unbonded length from zero to 579.1 mm (22.8 in). Similar to the GFRP-1, the maximum compressive stresses in IRP made from polymeric and GFRP-2 materials in the presence of internal pressure do not exceed their respective maximum longitudinal tensile stresses, and the minimum fatigue life of all IRPs at any unbonded length is governed by the tension side. This is why, unlike non-pressurised materials systems, there is no reduction in fatigue life for pressurised IRP with any repair materials with an unbonded length from 304.8 mm (12.0 in) to 579.1 mm (22.8 in).

Fig. 12a also shows that the longest service life attainable by the non-pressurised polymeric system, with a thickness of 4.1 mm (0.2 in) and under a traffic load of 14.8 kN (3.3 kips), is only 2.6E+05 cycles at an unbonded length of 304.8 mm (12.0 in). This indicates that unlike GFRP-1 and GFRP-2, implementing even the optimum unbonded length into a non-pressurised polymeric system does not meet the design life requirement. On the other hand, a polymeric system that is subjected to an internal pressure of 206.8 kPa (30.0 psi) has the capability of satisfying the design life requirement by unbonding IRP to the host pipe by at least 490.2 mm (19.3 in). This is because, in contrast to scenarios where internal pressure is absent, the maximum longitudinal compressive stress does not surpass the corresponding maximum longitudinal tensile stress when internal pressure is present, resulting in no reduction in service life after an unbonded length of 304.8 mm (12.0 in).

3.4 Effect of unbonded length with different lateral loading levels

Fig. 13a, b, c and d compare the variation of maximum longitudinal tensile and compressive stresses in the GFRP-1 IRP, with a repair thickness of 4.1 mm (0.2 in), with increasing unbonded length under different levels of traffic load and internal pressure. As increasing unbonded length, the maximum longitudinal tensile stresses in both pressurised and non-pressurised IRP under 20.0 kN (4.5 kips), 25.0 kN (5.6 kips) and 30.0 kN (6.7 kips) exhibit trends similar to that seen under 14.8 kN (3.3 kips) with the same internal pressure condition.

When the bonding condition is altered from a fully bonded state to an unbonded length of 579.1 mm (22.8 in), the maximum longitudinal tensile stresses at the bottom span decrease. As unbonded length is increased, it appears that the ultimate reduction in maximum longitudinal tensile stress in non-pressurised IRP remains relatively consistent across different levels of applied load while it increases with increasing traffic load in pressurised repair systems.

As the unbonded length is increased from zero to 152.4 mm (6.0 in), there is a nearly identical overall percentage reduction in compressive stress in non-pressurised IRP under different loading levels. However, when the unbonded length is increased from 152.4 mm (6.0 in) to 579.1 mm (22.8 in), the percentage increase in maximum compressive stresses in non-pressurised IRP systems becomes more prominent with higher loading magnitude. This is because, beyond 152.4 mm (6.0 in), the bending stress induced by external loading becomes the primary factor in determining the maximum longitudinal compressive stresses that occur at the crown of non-pressurised IRP at the discontinuity edge. Additionally, when subjected to traffic load levels of 20.0 kN (4.5 kips), 25.0 kN (5.6 kips) and 30.0 kN (6.7 kips), the maximum longitudinal tensile stress in non-pressurised IRP systems is critical only when the system is fully bonded or has an unbonded length of less than 254.0 mm (10.0 in); beyond this limit, the maximum longitudinal compressive stress becomes dominant as observed under the load of 14.8 kN (3.3 kips).

In the presence of internal pressure of 206.8 kPa (30.0 psi) (Fig. 13b), the maximum longitudinal compressive stress in IRP under a traffic load of 14.8 kN (3.3 kips) never exceeds the corresponding maximum tensile stress values at any unbonded length. It does however exceed the longitudinal tensile stress and becomes the dominant stress type at unbonded lengths of 304.8 mm (12.0 in), 254.0 mm (10.0 in) and 203.2 mm (8.0 in) under traffic loads of 20.0 kN (4.5 kips), 25.0 kN (5.6 kips) and 30.0 kN (6.7 kips), respectively. This is because increasing the traffic load under the same internal pressure reduces the effect of internal pressure on the resultant longitudinal stress distribution in IRP by a significant amount. With internal pressure of 413.7 kPa (60.0 psi), the maximum compressive stress experienced by IRP under a traffic load of 20.0 kN (4.5 kips) stays below the corresponding maximum longitudinal tensile stress at any unbonded length, similar to that experienced under a traffic load of 14.8 kN. Under the same internal pressure, increasing the traffic load to 25.0 kN (5.6 kips) leads to maximum longitudinal compressive stress approaching the corresponding maximum longitudinal tensile stress after an unbonded length of 579.1 mm (22.8 in).

Under the condition of an internal pressure of 413.7 kPa (60.0 psi), a traffic load of 30.0 kN (6.7 kips) results in the maximum compressive stress exceeding the corresponding maximum tensile stress at an unbonded length of 381.0 mm (15.0 in). In the presence of an internal pressure of 620.5 kPa (90.0 psi), the dominant stress experienced by IRP at any unbonded length, even when exposed to a traffic load of 25.0 kN (5.6 kips), is longitudinal tensile stress. This phenomenon occurs due to the potential of high internal pressure becoming the significant factor in the distribution of resultant longitudinal stress at any unbonded length, despite the existence of a relatively high traffic load. It is important to note that when subjected to a traffic load of 30.0 kN (6.7 kips) along with an internal pressure of 413.7 kPa (60.0 psi) and 25.0 kN (5.6 kips) along with an internal pressure of 620.5 kPa (90.0 psi), the maximum longitudinal tensile strain in systems with unbonded lengths less than 73.7 mm (2.9 in) and 43.2 mm (1.7 in), respectively exceed the design strain limit of 0.02.

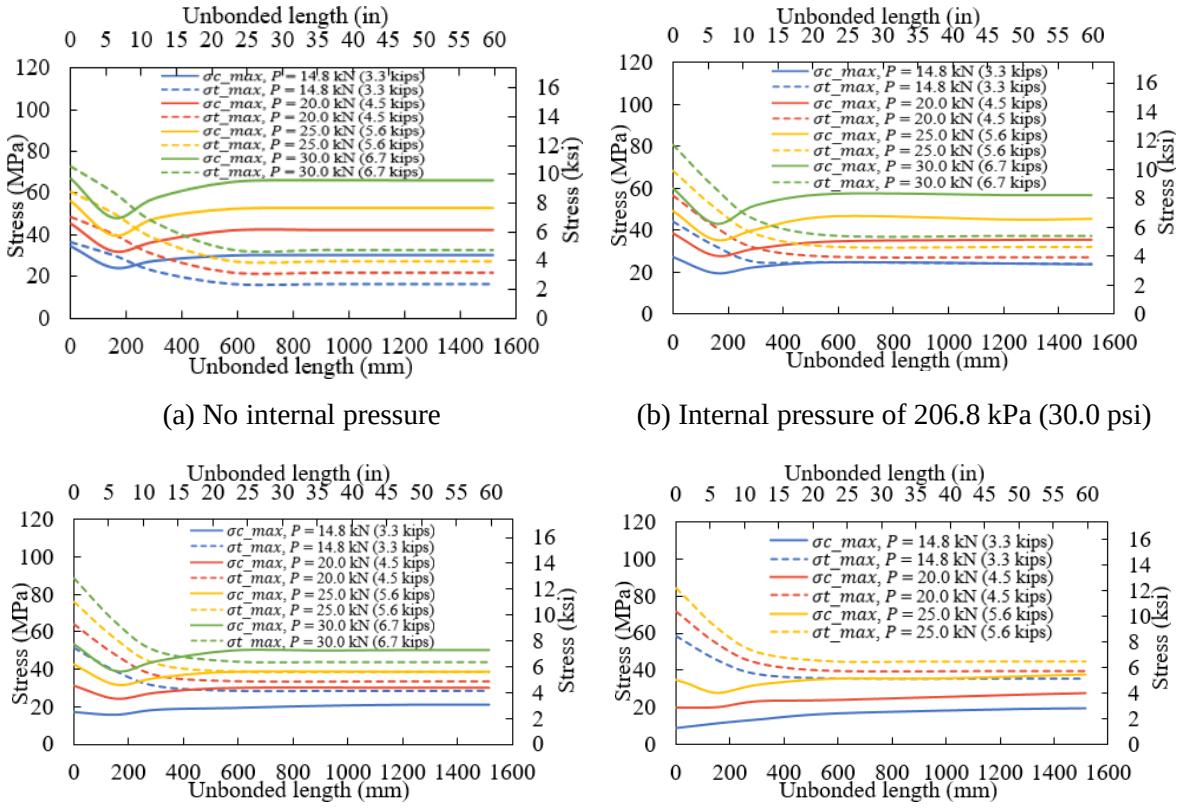

(a) No internal pressure

(b) Internal pressure of 206.8 kPa (30.0 psi)

(c) Internal pressure of 413.7 kPa (60.0 psi)

(d) Internal pressure of 620.5 kPa (90.0 psi)

Fig. 13. Maximum tensile and compressive stress behaviour in GFRP-1 under different levels of traffic loads with increasing unbonded length at different internal pressures

The fatigue lives of 4.1 mm (0.2 in) thick GFRP-1 with increasing unbonded length are compared in Fig. 14a, b, c and d at internal pressures of zero, 206.8 kPa (30.0 psi), 413.7 kPa (60.0 psi) and 620.5 kPa (90.0 psi), respectively. The service life of non-pressurised IRP exhibits a consistent trend across all the traffic loads as unbonded length increases, as shown in Fig. 14a. The fatigue life of pressurised systems against unbonded length across all the traffic loads also shows a similar trend. Similar to the system under the traffic of 14.8 kN (3.3 kips), these service lives are observed when the non-pressurised repair systems are unbonded up to a length of 304.8 mm (12.0 in) and are greater than those of corresponding fully bonded non-pressurised systems. On the other hand, the longest fatigue lives of pressurised IRP can be observed when the repair system is unbonded up to a length of 579.1 mm (22.8 in). Also, IRP demonstrates a relatively greater improvement in fatigue life under higher loads at each internal pressure level. This can be attributed to the fact that when subjected to higher traffic loads, stress amplitude is already relatively high, and therefore even a minor reduction in stress range can lead to a relatively substantial rise in the number of cycles required to induce fatigue failure.

The effect of reduction in stress range is more pronounced for higher loads, leading to a comparatively greater enhancement in service as opposed to lower loads, where the stress range is narrower, and the material may be subjected to more cycles of loading before it fails. The results also suggest that pressurised IRP under each traffic load exposed to relatively lower internal pressure levels experience a relatively more significant increase in minimum fatigue life when increasing unbonded length from 0 to 579.1 mm (22.8 in). On the other hand, increasing the unbonded length from 304.8 mm (12.0 in) to 579.1 mm (22.8 in) reduces the minimum fatigue life of non-pressurised IRP.

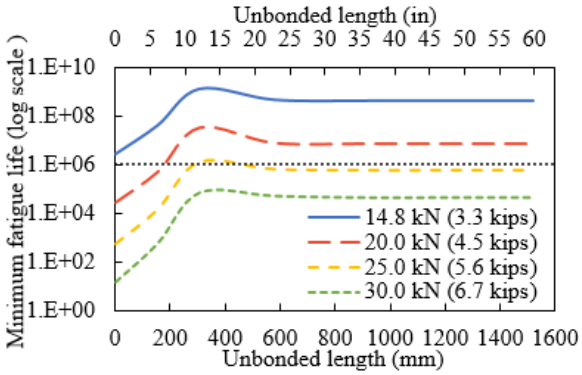

(a) No internal pressure

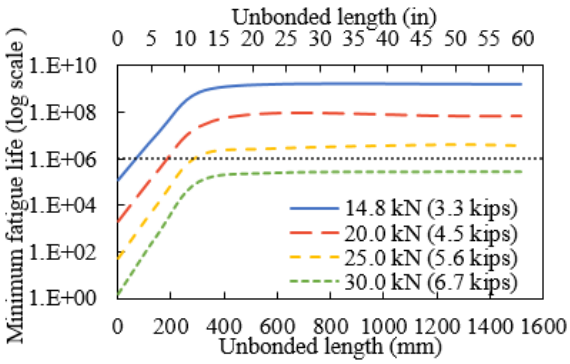

(b) Internal pressure of 206.8 kPa (30.0 psi)

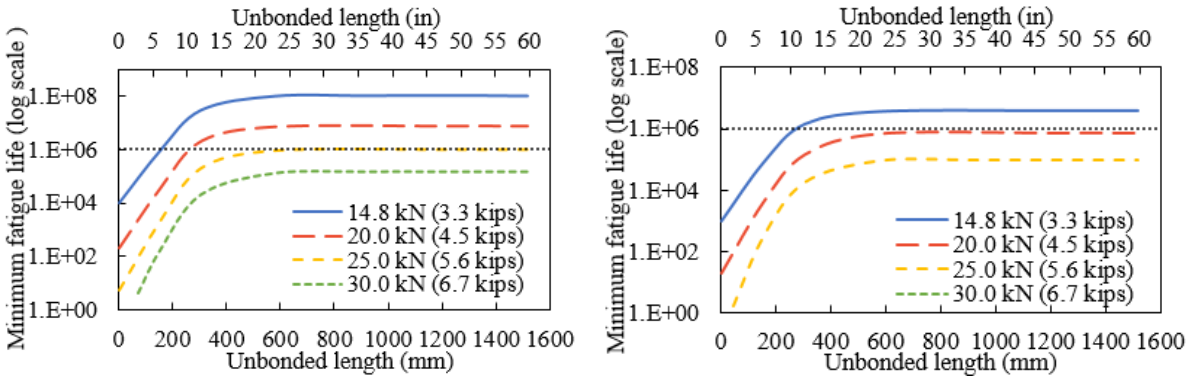

(c) Internal pressure of 413.7 kPa (60.0 psi)

(d) Internal pressure of 620.5 kPa (90.0 psi)

Fig. 14. Comparison of the behaviour of minimum fatigue life of GFRP-1 under different levels of traffic loads with increasing unbonded length at different internal pressures

The findings in Fig. 14a suggest that to reach one million cycles in the absence of internal pressure, the GFRP-1 exposed to a traffic load of 20.0 kN (4.5 kips) necessitates an unbonded length of no less than 170.2 mm (6.7 in), whereas that under 25.0 kN (5.6 kips) should range between 294.6 mm (11.6 in) – 381.0 mm (15.0 in). In contrast, the non-pressurised IRP which undergoes a 30.0 kN (6.7 kips) load is unable to withstand one million loading cycles even if the optimal unbonded length of 304.8 mm (12.0 in) is utilised. Under an internal pressure of 206.8 kPa (30.0 psi), IRP subjected to 20.0 kN (4.5 kips) and 25.0 kN (5.6 kips) are capable of enduring one million loading cycles with an unbonded length of at least 182.9 mm (7.2 in) and 292.1 mm (11.5 in), respectively, but those subjected to 30.0 kN (6.7 kips) are incapable of withstanding such condition with any unbonded length. On the other hand, with an internal pressure of 413.7 kPa (60.0 psi), the IRP system exposed to 20.0 kN (4.5 kips) can complete one million cycles with an unbonded length of at least 10.6 in, while those exposed to 25.0 kN (5.6 kips) or higher fail to meet this criterion. At an internal pressure of 620.5 kPa (90.0 psi), it is observed that any system exposed to a traffic load exceeding 14.8 kN (3.3 kips) is unable to complete one million loading cycles, even if the unbonded length is extended beyond the load span.

4 Conclusions

This study investigated numerically the influence of bonding level, represented by unbonded length, on the flexural fatigue performance of internal replacement pipe (IRP) for repairing steel pipelines with circumferential discontinuities. The effect of thickness and

modulus of elasticity (MOE) of IRP, magnitude of traffic loads, and internal pressure are investigated. The following conclusions can be drawn from the outcomes of this study.

- IRP systems with a diameter of 311.2 mm (12.3 in), whether pressurised or non-pressurised will have improved fatigue lives when the unbonded length is extended from 0 to 304.8 mm (12.0 in) due to a reduction in maximum longitudinal tensile stress.
- The minimum fatigue life is directly correlated to the maximum tensile stress of partially bonded pressurised and non-pressurised IRPs with unbonded lengths less than 304.8 mm (12.0 in), which occurs at the bonded and unbonded regions on the bottom outer surface of IRP.
- As the unbonded length is extended beyond 304.8 mm (12.0 in), the fatigue life of the non-pressurised system experiences a nonlinear decrease, whereas the fatigue lives of all the pressurised systems increase continuously. When the unbonded length is between this range, the service life of non-pressurised repair systems is predominately influenced by the discontinuity edge at the crown of IRP (compressive side). The increase in longitudinal compressive stress at the discontinuity edge located at the crown of IRP, as unbonded length is extended up to the boundary of the loading clamp outside the load span, is directly correlated with a decrease in the fatigue life in the absence of internal pressure.
- The minimum fatigue life of all pressurised IRP systems with any unbonded length is governed by the tensile failure of the bottom outer surface of IRP.
- Unbonding to a length of 304.8 mm (12.0 in) or at least one IRP diameter provides the longest service lives for non-pressurised repair systems, whereas unbonding at least up to the boundary of the loading clamp beyond the load span results in the longest fatigue lives for all pressurised systems. The relative improvement in fatigue due to an increase in unbonded length is greater for the thicker IRP than it is for the thinner IRP at any internal pressure level.
- The minimum fatigue life of flexible IRP material systems without internal pressure demonstrates a more significant improvement when the unbonded length is increased from 0 to 304.8 mm (12.0 in), compared to stiffer IRP material systems. This statement holds true for any pressurised systems that undergo an increase in their unbonded length from 0 to 579.1 mm (22.8 in), which is equal to twice the diameter of the IRP.
- When the unbonded length is increased, pressurised IRPs subjected to relatively lower internal pressure levels tend to exhibit a more substantial improvement in their fatigue lives.

- Even if the unbonded length is increased beyond the load span, any IRP subjected to a traffic load greater than 14.8 kN (3.3 kips) at an internal pressure of 620.5 kPa (90.0 psi) is unable to complete one million loading cycles.

Acknowledgement

The information, data, or work presented herein was funded in part by the Advanced Research Projects Agency-Energy (ARPA-E), US Department of Energy, under Award Number DE-AR0001327 The views and opinions of authors expressed herein do not necessarily state or reflect those of the United States Government or any agency thereof.

References

Akram, A., Mustaffa, Z. b. and Albarody, T. M. B. (2020), "Burst capacity of pipe under corrosion defects and repaired with thermosetting liner", *Steel and Composite Structures,* **35**, 171-186. https://doi.org/10.12989/scs.2020.35.2.17.

Ansys. (2021). Finite Element Analysis (FEA) Software for Structuaral Engineering: ANSYS, Inc.

ASTM. (2019). ASTM D3479/D3479M-19. In *Standard Test Method for Tension-Tension Fatigue of Polymer Matrix Composite Materials* (pp. 1-6): ASTM International.

Bajcar, T., Cimerman, F., Širok, B. and Ameršek, M. (2012), "Impact assessment of traffic-induced vibration on natural gas transmission pipeline", *Journal of Loss Prevention in The Process Industries,* **25**(6), 1055-1068. https://doi.org/10.1016/j.jlp.2012.07.021.

Brown, M. J., Fam, A. and Moore, I. D. (2008), "Material characterization of components and assembled behavior of a composite liner for rehabilitation of cast iron pressure pipes", *Polymer Engineering and Science,* **48**(7), 1231-1239. https://doi.org/10.1002/pen.20975.

Brown, M. J. P., Moore, I. D. and Fam, A. (2014), "Performance of a cured-in-place pressure pipe liner passing through a pipe section without structural integrity", *Tunnelling and Underground Space Technology,* **42**, 87-95. https://doi.org/10.1016/j.tust.2014.01.005.

Bubbico, R. (2018), "A statistical analysis of causes and consequences of the release of hazardous materials from pipelines. The influence of layout", *Journal of Loss Prevention in The Process Industries,* **56**, 458-466. https://doi.org/10.1016/j.jlp.2018.10.006.

Cao, J., Zhang, Z., Guo, Y. and Gong, T. (2019), "Inhomogeneous bonding state modeling for vibration analysis of explosive clad pipe", *Steel and Composite Structures,* **31**(3), 233-242. https://doi.org/10.12989/scs.2019.31.3.233.

Chen, X., Wu, Z., Chen, W., Kang, R., He, X. and Miao, Y. (2019), "Selection of key indicators for reputation loss in oil and gas pipeline failure event", *Engineering Failure Analysis,* **99**, 69-84. https://doi.org/10.1016/j.engfailanal.2019.01.071.

Chen, X., Zhao, J., She, G.-L., Jing, Y., Pu, H. and luojun. (2022), "Nonlinear free vibration analysis of functionally graded carbon nanotube reinforced fluid-conveying pipe in thermal environment", *Steel and Composite Structures,* **45**(5), 641-652. https://doi.org/10.12989/scs.2022.45.5.641.

Cunha, S. d. (2016), “A review of quantitative risk assessment of onshore pipelines”, *Journal of Loss Prevention in The Process Industries,* **44**, 282-298. https://doi.org/10.1016/j.jlp.2016.09.016.

Dixon, P. G., Tafsirojjaman, T., Klingaman, J., Hubler, M. H., Dashti, S., O'rourke, T. D., Farrag, K. A., Manalo, A. and Wham, B. P. (2023), “State-of-the-Art Review of Performance Objectives for Legacy Gas Pipelines with Pipe-in-Pipe Rehabilitation Technologies”, *Journal of Pipeline Systems Engineering and Practice,* **14**(2). https://doi.org/10.1061/JPSEA2.PSENG-1371.

Ha, S. K., Lee, H. K. and Kang, I. S. (2016), “Structural behavior and performance of water pipes rehabilitated with a fast-setting polyurea–urethane lining”, *Tunnelling and Underground Space Technology,* **52**, 192-201. https://doi.org/10.1016/j.tust.2015.12.003.

Hsu, J.-M. and Shou, K. J. (2022a), “Experimental study of the separated joint of an underground pipeline rehabilitated by cured-in-place pipe”, *Underground Space,* **7**(4), 543-563. https://doi.org/10.1016/j.undsp.2021.11.005.

Hsu, J.-M. and Shou, K. J. (2022b), “Numerical analysis of the mechanical behavior of separated joints in underground pipelines rehabilitated by cured-in-place pipes”, *Tunnelling and Underground Space Technology,* **125**. https://doi.org/10.1016/j.tust.2022.104520.

Huang, Z.-y., Zhang, W., Qian, X., Su, Z., Pham, D. C. and Sridhar, N. (2020), “Fatigue behaviour and life prediction of filament wound CFRP pipes based on coupon tests”, *Marine Structures,* **72**, 102756. https://doi.org/10.1016/j.marstruc.2020.102756.

Jeon, S.-S., O’Rourke, T. D. and Neravali, A. N. (2004), “Repetitive loading effects on cast iron pipelines with cast-in-place pipe lining system”, *Journal of Transportation Engineering,* **130**(6), 692-705.

Kiriella, S., Manalo, A., Tien, C. M. T., Ahmadi, H., Wham, B. P., Salah, A., Tafsirojjaman, T., Karunasena, W., Dixon, P. and O'Rourke, T. D. (2023), “Lateral deformation behaviour of structural internal replacement pipe repair systems”, *Composite Structures,* **319**. https://doi.org/10.1016/j.compstruct.2023.117144.

Klingaman, J., Dixon, P. G., Wham, B. P., Dashti, S. and Hubler, M. H. (2022), “Traffic Loading Effects on Rehabilitated Cast Iron Distribution Pipelines”, *Pipelines 2022,* Indianapolis, Indiana, August.

Knight, M. A. and Bontus, G. J. (2018), “Pressure Testing of CIPP Liners to Failure”, *Pipelines 2018,* Toronto, Canada, July.

Kozman, D. P. (2020), “Bonded or Unbonded Liners? How Longitudinal Bending Impacts Pipe Lining Design and Performance”, *Pipelines 2020,* San Antonio, Texas, August.

Li, B., Yu, W. J., Xie, Y.-p., Fang, H., Du, X., Wang, N., Zhai, K., Wang, D., Chen, X., Du, M., Sun, M. and Zhao, X. (2023), “Trenchless rehabilitation of sewage pipelines from the perspective of the whole technology chain: A state-of-the-art review”, *Tunnelling and Underground Space Technology,* **134**. https://doi.org/10.1016/j.tust.2023.105022.

Lu, H., Matthews, J. C. and Iseley, T. (2020), “How does trenchless technology make pipeline construction greener? A comprehensive carbon footprint and energy consumption analysis”, *Journal of Cleaner Production,* **261**. https://doi.org/10.1016/j.jclepro.2020.121215.

Mao, L., Gan, L., Li, W. and Zhang, P. (2022), “Failure analysis on weld joint of centrifugal pump diffuser for oil and gas pipeline transportation”, *Engineering Failure Analysis,* **140**. https://doi.org/10.1016/j.engfailanal.2022.106620.

Mellott, S. R. and Fatemi, A. (2014), "Fatigue behavior and modeling of thermoplastics including temperature and mean stress effects", *Polymer Engineering and Science,* **54**(3), 725-738. https://doi.org/10.1002/pen.23591.

Shahriar, A., Sadiq, R. and Tesfamariam, S. (2012), "Risk analysis for oil & gas pipelines: A sustainability assessment approach using fuzzy based bow-tie analysis", *Journal of Loss Prevention in The Process Industries,* **25**(3), 505-523. https://doi.org/10.1016/j.jlp.2011.12.007.

Shehata, M. and El-Shamy, A. M. (2023), "Hydrogen-based failure in oil and gas pipelines a review", *Gas Science and Engineering,* **115**. https://doi.org/10.1016/j.jgsce.2023.204994.

Singh, M. and Markeset, T. (2009), "A methodology for risk-based inspection planning of oil and gas pipes based on fuzzy logic framework", *Engineering Failure Analysis,* **16**(7), 2098-2113. https://doi.org/10.1016/j.engfailanal.2009.02.003.

Stewart, H. E., Netravali, A. N. and O'Rourke, T. D. (2015), "Performance Testing of Field-Aged Cured-in-Place Liners (CIPL) for Cast Iron Piping ", Research Report No. 151215; School of Civil and Environmental Engineering, Cornell University

Su, Y., Li, J., Yu, B., Zhao, Y. and Yao, J. (2021), "Fast and accurate prediction of failure pressure of oil and gas defective pipelines using the deep learning model", *Reliability Engineering & System Safety,* **216**. https://doi.org/10.1016/j.ress.2021.108016.

Tafsirojjaman, T., Manalo, A., Tien, C. M. T., Wham, B., Salah, A., Kiriella, S., Karunasena, W. and Dixons, P. (2022), "Analysis of failure modes in pipe-in-pipe repair systems for water and gas pipelines", *Engineering Failure Analysis,* **140**. https://doi.org/10.1016/j.engfailanal.2022.106510.

Tetreault, J., Moore, I. D., Hoult, N. A., Tanzil, D. and Maher, M. L. J. (2018), "Development of a Sustainability Evaluation System for Culvert Replacement and Rehabilitation Projects", *Journal of Pipeline Systems Engineering and Practice,* **9**(2). https://doi.org/10.1061/(ASCE)PS.1949-1204.0000315.

Tien, C. M. T., Manalo, A., Dixon, P., Tafsirojjaman, T., Karunasena, W., Flood, W. W., Ahmadi, H., Kiriella, S. H., Salah, A. M. and Wham, B. P. (2023), "Effects of the legacy pipe ends on the behaviour of pipe-in-pipe repair systems under internal pressure", *Engineering Failure Analysis,* **144**. https://doi.org/10.1016/j.engfailanal.2022.106957.

Toh, W., Tan, L. B., Tse, K. M., Raju, K., Lee, H. P. and Tan, V. B. C. (2018), "Numerical evaluation of buried composite and steel pipe structures under the effects of gravity", *Steel and Composite Structures,* **26**(1), 55-66. https://doi.org/10.12989/scs.2018.26.1.055.

Wang, R., Wang, F., Xu, J.-g., Zhong, Y.-h. and Shikun, L. (2019), "Full-scale experimental study of the dynamic performance of buried drainage pipes under polymer grouting trenchless rehabilitation", *Ocean Engineering,* **181**, 121-133. https://doi.org/10.1016/j.oceaneng.2019.04.009.

Wang, Y., Qian, X., Liew, J. Y. R. and Zhang, M.-h. (2016), "A numerical and theoretical investigation on composite pipe-in-pipe structure under impact", *Steel and Composite Structures,* **22**(5), 1085-1114. https://doi.org/10.12989/scs.2016.22.5.1085.

Xia, Y., Shi, M., Zhang, C., Wang, C., Sang, X., Liu, R., Zhao, P., An, G. and Fang, H. (2022), "Analysis of flexural failure mechanism of ultraviolet cured-in-place-pipe materials for buried pipelines rehabilitation based on curing temperature monitoring", *Engineering Failure Analysis,* **142**. https://doi.org/10.1016/j.engfailanal.2022.106763.

Yang, K., Fang, H., Zhang, X., Li, B. and Hu, Q. (2022), "Investigation of mechanical properties of corroded concrete pipes after cured-in-place-pipe (CIPP) rehabilitation under multi-field coupling", *Tunnelling and Underground Space Technology,* **128**. https://doi.org/10.1016/j.tust.2022.104656.

Zakaria, K. A., Jimit, R. H., Ramli, S. N. R., Aziz, A. A., Bapokutty, O. and Ali, M. B. (2016), "Study On Fatigue Life And Fracture Behaviour Of Fibreglass Reinforced Composites", *Journal of Mechanical Engineering and Sciences,* **10**(3), 2300-2310. https://doi.org/10.15282/jmes.10.3.2016.8.0214.

Zhang, D., Liu, X., Yang, Y., Shi, N., Jiang, J., Chen, P., Wu, X., Gao, H. and Zhang, H. (2022), "Field experiment and numerical investigation on the mechanical response of buried pipeline under traffic load", *Engineering Failure Analysis,* **142**. https://doi.org/10.1016/j.engfailanal.2022.106734.

Zhong, Z., Wang, S., Zhao, M., Du, X.-l. and Li, L. (2018), "Performance of ductile iron push-on joints rehabilitated with CIPP liner under repetitive and seismic loadings", *Soil Dynamics and Earthquake Engineering,* **115**(776-786). https://doi.org/10.1016/j.soildyn.2018.09.031.

Zhou, Q., Wu, W., Liu, D., Li, K. and Qiao, Q. (2016), "Estimation of corrosion failure likelihood of oil and gas pipeline based on fuzzy logic approach", *Engineering Failure Analysis,* **70**, 48-55. https://doi.org/10.1016/j.engfailanal.2016.07.014.

6.3. Links and implications

The study conducted in Chapter 6 found that the IRP systems with unbonded conditions, whether they are pressurised or not, exhibit significantly longer fatigue life compared to their fully bonded state due to a substantial reduction in concentration of longitudinal stresses at the discontinuity edges. The minimum fatigue life of all pressurised systems, regardless of the bonding level, is governed by the tensile failure of the outer bottom surface of IRP. The longest service life for non-pressurized IRP systems is achieved by unbonding IRP from the host pipe segments to a length on each side, measured from the discontinuity edge that is at least equal to the diameter of the IRP. On the other hand, unbonding the pressurised systems to a distance from the discontinuity edge that is at least twice the diameter of the IRP will maximize their fatigue life. The significant findings in Chapter 6 and other studies presented in previous chapters are highlighted in the Conclusion section.

CHAPTER 7: CONCLUSION AND RECOMMENDATION

Trenchless rehabilitation technology has advanced significantly in recent years, particularly with the introduction of internal replacement pipe (IRP) systems that use a range of materials including polymers, fibre-reinforced composites and metals. Despite the great potential of IRP systems as a viable trenchless solution for rehabilitating legacy gas and oil pipelines with full circumferential cracks or discontinuities, their implementation has still been limited by the lack of established design procedures and standards. This thesis conducted a comprehensive investigation into the lateral deformation and fatigue behaviour of IRP systems installed in discontinuous host pipes under static and repetitive traffic loading, respectively. These loading conditions have been identified as the most critical for both IRPs and host pipes, as per the existing literature. Due to the high cost and time constraints associated with full-scale laboratory experiments, this study employs numerical and analytical approaches for the investigations. Additionally, the influence of various design parameters was also systematically evaluated. The primary outcomes of this study are provided in the following sections.

7.1. State-of-the-art review of bending behaviour of pipe repair systems

Internal replacement pipe systems have emerged as an innovative trenchless technique, gathering significant attention for the rehabilitation of legacy gas and oil pipelines with full circumferential cracks or discontinuities. Based on the available literature, lateral deformation and fatigue failure caused by vehicular traffic loading have been identified as the most detrimental conditions for host pipes and IRP systems. However, the knowledge of the static and fatigue behaviour of IRP systems installed in discontinuous host pipes under traffic loading is currently limited due to a lack of studies in this area. Based on the comprehensive review conducted, the subsequent findings have been derived.

- The static and cyclic surface loads encountered by pipelines are often attributed to overhead vehicular traffic. The worst possible damage that can occur in the host pipe is a full circumferential crack or discontinuity resulting from excessive deterioration or joint pull-out failure.
- The available simplified analytical model for assessing the maximum deformation of the repaired legacy pipes with circumferential cracks under the traffic loading does not consider any structural contribution of the repair system. This oversimplification is no longer applicable in structural repair systems due to the novel IRP materials having relatively higher stiffness than CIPP liners.

- Available studies on the repair systems of legacy pipes with circumferential cracks or discontinuities focused solely on low-modulus liners. New and emerging IRP systems are now under development, employing a variety of repair materials such as polymeric coating, thermoplastics, FRP composites and metals. Numerous studies have shown that the static and fatigue performance of these materials exhibit significant variations because of differences in their strength, stiffness, toughness, and resistance to cracking and fracture. Consequently, an in-depth understanding of the static and fatigue behaviour of legacy pipes rehabilitated utilizing IRP made from a variety of materials is important.
- Several studies on different pipe repair systems have demonstrated that static and fatigue behaviour of pipes can be affected by factors such as defect size, wall thickness and level of applied load. However, most of these studies focused either on single pipes or continuous host pipe systems with surface corrosion defects. Therefore, the potential impact of these design parameters on the performance of IRP systems in the presence of discontinuous host pipe segments has yet to be investigated.
- Internal pressure can lead to a concentration of stresses at the damaged location of the pipes with repair systems. However, no research has explicitly demonstrated how varying operating internal pressure levels might impact the bending fatigue behaviour of IRP systems in discontinuous host pipe segments.
- Detaching the repair pipe from the host pipe to a particular distance from the damaged area can reduce the stress concentration and enhance the capacity of the repair pipe. However, investigations into how the varied bonding levels might affect the bending fatigue behaviour of IRP-repaired discontinuous host pipes have not been studied.

The literature review reveals a growing interest in the utilisation of IRP systems for rehabilitating legacy gas and oil pipelines primarily composed of cast iron and bare steel. However, there remains an insufficient understanding regarding their performance under various loading conditions, including the static and fatigue behaviour induced by vehicular traffic. Furthermore, there is a lack of established design procedures and standards for this specific trenchless technology. Therefore performing in-depth investigations of the static and fatigue behaviour of IRP systems is necessary to ensure their safe and reliable design and development.

7.2. Lateral deformation behaviour of structural internal replacement pipe repair systems

This study focused on the numerical investigation of the flexural behaviour of IRP systems installed in legacy pipes with full circumferential cracks or discontinuities caused by excessive deterioration and joint pull-out failure under vehicular traffic loading. A systematic evaluation was conducted to assess the impact of the discontinuity width of the host pipe, repair thickness, repair material and magnitude of traffic load on the bending behaviour of IRP-repaired damaged host pipe systems. Additionally, a simplified and robust analytical model which can accurately replicate the lateral deformation behaviour of different IRP systems including host pipe with circumferential discontinuity repaired with IRP, continuous host pipe with IRP and standalone IRP was developed. The established analytical model was subsequently employed to predict the performance of various IRP systems and compared against the outcomes obtained from both FE simulations and full-scale laboratory testing. Based on the findings obtained from the investigations, the following conclusions can be made.

- The host pipe has the greatest effect on the lateral deformation behaviour of a continuous steel pipe with IRP. The failure of the system is initiated by the yielding of the host pipe, which is then followed by the occurrence of local compressive buckling of the IRP. Although the incorporation of the IRP does not enhance the load at the yielding of the host pipe, it does result in an 11% increase in ultimate load and a 23% increase in the maximum deflection capacity of the system.
- The lateral deformation behaviour of an IRP installed in a host pipe with a narrow discontinuity width is predominantly influenced by the host pipe, whereas in a system with a wider discontinuity width, it is primarily governed by the IRP. The repair system experiences a reduction in strength and stiffness as the width of the host pipe discontinuity increases. Regardless of the discontinuity width, the failure mode is attributed to the localised outward buckling of the crown of IRP between the edges of discontinuity.
- The mechanical contribution of the IRP systems was found to be an important factor in the analysis of their bending behaviour. As a result, the existing analytical models, which disregard the structural contribution of the repair pipe, are no longer considered valid.
- The flexural capacity of the system is enhanced by increasing the thickness of the IRP, exhibiting a nonlinear increase for the systems with wide discontinuity widths and a

linear increase for the systems with narrow discontinuity widths. The thickness of the IRP has a greater influence on the lateral deformation behaviour of systems with wider discontinuity widths compared to the systems with narrower discontinuity widths.

- The midspan deflection of an IRP system experiences a significant decrease when the MOE of IRP is increased from 1 GPa (145 ksi) to 24.5 GPa (3,553 ksi). The variation in MOE of IRP has a more pronounced impact on the lateral deformation of the systems when the discontinuities are relatively wider.

- The simplified FMA demonstrated a consistent ability to accurately forecast the lateral deformation behaviour of the IRP system within host pipes that contain wider circumferential discontinuities. The use of factored FMA, which considers the ratio of average normal FEA stresses along the discontinuity width to that of the corresponding average FMA stresses, provides an accurate prediction of the load midspan deformation behaviour of systems with narrow discontinuities.

The aforementioned outcomes have demonstrated that the structural performance of IRP installed in legacy pipes with narrow and wider discontinuities varies during static bending tests. However, given the cyclic nature of traffic load, understanding the fatigue behaviour of these systems is essential to ensure their long-term performance.

7.3. Bending fatigue behaviour of internal replacement pipe systems

The bending fatigue behaviour of IRP-repaired discontinuous legacy pipe systems under the influence of the repeated nature of vehicular traffic loading was studied using FE numerical simulations. In the FE models, the IRP and the host pipe segments are adhered together along their entire interface. Several important design parameters, such as discontinuity width of the host pipe, repair thickness, repair material and level of traffic load were examined in detail regarding fatigue performance The evaluated parameters were subsequently ranked based on their relative contribution to the fatigue strength using multiple regression analysis. The following conclusions can be made based on the findings of this study.

- Discontinuous legacy pipe segments that are repaired using IRP with a fully bonded connection between their interface can pose a critical issue in bending fatigue. This is because the presence of these discontinuities induces a high stress concentration in IRP at the discontinuity edges leading to a decrease in fatigue life or an increased risk of failure before achieving the intended design life.

- The stresses that arise in IRP during bending are stabilized by the continuity of the host pipe, thereby significantly extending its fatigue life.
- The stress and the fatigue life experienced by the midspan of the IRP system in host pipes with wide discontinuities tend to align more closely with those of standalone IRPs.
- The level of stress concentration in the IRP at the edge of the host pipe discontinuity is not significantly affected by the discontinuity width. This suggests that the fully bonded IRP systems with different discontinuity widths may experience fatigue failure at approximately the same service life.
- An increase in repair thickness and MOE of repair material are shown to significantly extend the fatigue lives of IRP systems installed in discontinuous host pipe by reducing the potential stress concentration at the discontinuity edges of host pipe segments.
- The level of traffic load is found to be the most influential factor in determining the maximum stress produced in IRP during bending fatigue, followed by repair thickness, MOE of repair material and discontinuity width. However, the contribution to the fatigue life by MOE of IRP is identified as the highest, followed by the level of load repair thickness and the discontinuity width.

In contrast to static bending, the fatigue performance of IRP installed in a legacy pipe under repeated traffic loading is independent of the width of the host pipe discontinuity. Understanding the long-term performance of IRP systems under the concurrent application of repetitive action of traffic loading and internal pressure, on the other hand, is critical for effectively integrating them into the rehabilitation process of legacy pipelines.

7.4. Effect of internal pressure on the flexural fatigue behaviour of internal replacement pipe systems

This study focused on investigating the bending fatigue performance of IRP-repaired discontinuous host pipes by analysing the combined effect of operating internal pressure and repetitive traffic loading. This was achieved by changing the critical design parameters identified in the previous investigation. Additionally, a bonded condition along the entire interface between IRP and host pipe was also employed. Using the data collected from in-depth parametric studies, mathematical expressions that accurately predict the fatigue life of IRP systems under the combined influence of internal pressure and recurrent traffic loading were established. The derived equations were subsequently employed to generate design charts

encompassing a range of internal pressure and traffic load combinations. The outcomes of this study yield the following conclusions.

- An increase in internal pressure during the process of bending leads to an elevation in tensile stress in both the longitudinal and circumferential directions at the invert of IRP, while a reduction in the compressive stresses in both the longitudinal and circumferential directions at the crown of IRP.
- Regardless of the level of internal pressure, the longitudinal stresses experienced during bending fatigue surpass the hoop stress anywhere along the IRP.
- Under any internal pressure level, the longitudinal tensile stress that develops at the discontinuity edge is the dominating stress during the bending of a fully bonded IRP system.
- As internal pressure rises during bending, the fatigue life of an IRP is significantly decreased due to the amplification of the longitudinal tensile stress concentration at the discontinuity edges. It is essential that longitudinal tensile stress concentration at the discontinuity edge be kept to a minimum to avoid premature fatigue failure when designing an IRP system for installation in host pipes with a full circumferential discontinuity.
- The failure behaviour of IRP during bending fatigue is influenced by the magnitude of internal pressure. In the absence of internal pressure, the failure of the IRP repair system is characterised by a bulging of invert and a minor inward bending of the crown of IRP between discontinuity edges. As internal pressure increases, the bulge of the invert of IRP becomes more prominent, whereas the inward bending of the crown of IRP diminishes.
- Similar to the non-pressurised systems, the concentration of tensile stress in pressurised IRP at the discontinuity edge of the host pipe demonstrated a nonlinear reduction as the repair thickness increased, leading to a nonlinear increase in the fatigue life of IRP. The increase in repair thickness under the highest operating internal pressure under consideration resulted in the most significant reduction in stress concentration, whereas the reduction is least pronounced in the absence of internal pressure.
- Under the combined effect of traffic load and internal pressure, polymeric IRP has much lower resistance to fatigue failure than GFRP systems with higher MOE.
- The rise in internal pressure severely affected the fatigue life of IRP under relatively lower traffic loading.

- The simplified mathematical formulations and design charts to predict the fatigue life of IRP systems can provide valuable assistance to engineers and designers in making informed decisions regarding the selection of optimal design parameters that meet the desired design life requirement.

The above findings indicate that when complete bonding is present at the interface between IRP and host pipe, simultaneous application of repetitive traffic load and internal pressure can significantly accelerate longitudinal tensile stress concentrations at the discontinuity edge and thereby induce premature fatigue failure of IRP. Therefore, research into the effectiveness of varying bonding levels at the interface between the IRP and the host pipe in reducing potential stress concentrations and increasing the fatigue life of IRP was subsequently carried out.

7.5. Influence of bonding level on the bending fatigue behaviour of internal replacement pipe systems

The impact of the bonding level, defined by the unbonded length of IRP to the host pipe, on the bending fatigue performance of IRP-repaired legacy steel pipes with circumferential discontinuities subjected to repetitive traffic loading under both pressurised and non-pressurised conditions was numerically examined. The analysis encompassed a wide range of unbonded length which is applied to each segment of the host pipe. These lengths varied from zero indicating a fully bonded state, to 1518.9 mm (59.8 in), which represents a completely unbonded state. The evaluation was performed by considering the different design parameters, which were chosen according to the outcome of the prior investigation. The findings of this investigation lead to the following conclusions.

- The fatigue life of IRP systems regardless of their level of internal pressure, improves significantly when unbonded length is increased from zero to one pipe diameter owing to a decrease in the maximal longitudinal stresses.
- The minimum fatigue life of partially bonded pressurised and non-pressurized IRPs with any unbonded length shorter than one pipe diameter is directly proportional to the maximum tensile stress that develops on the bottom outer surface of IRP where the bonded and unbonded regions meet.
- When the unbonded length exceeds one pipe diameter, the fatigue life of the non-pressurised system exhibits a nonlinear decrease, while all pressurised systems demonstrate a continuous increase. When the unbonded length falls within this range,

the service life of non-pressurised repair systems is primarily determined by the crown of the IRP at the discontinuity edge. In the absence of internal pressure, the reduction in fatigue life as unbonded length is increased toward the boundary of the loading clamp beyond the load span is directly proportional to the rise in the compressive stress in the crown of IRP at the discontinuity edges.

- The fatigue life of pressurised IRP systems with any bonding level is determined by the tensile failure of the bottom outer surface of the IRP.
- In the case of non-pressurised repair systems, the fatigue life is maximised when the unbonded length is equivalent to the diameter of the IRP. However, for pressurised systems, a minimum unbonded length of twice the diameter of the IRP is required to achieve the longest fatigue life.
- Regardless of the level of operating pressure, the fatigue life improvement resulting from an increase in unbonded length is more pronounced for relatively thicker IRPs.
- The fatigue life of flexible non-pressurised IRP material systems shows a greater improvement when the unbonded length is extended from zero to one pipe diameter, as compared to stiff IRP material systems. This statement holds true for any pressurised system in which the unbonded length is increased from zero to twice the pipe diameter.
- An increase in the unbonded length results in a more significant enhancement in fatigue life for pressurised systems experiencing relatively lower internal pressure levels.

7.6. New opportunities and future research

- The research findings presented in this study were derived from a standard in-service legacy steel natural gas pipeline system located in the United States. Therefore, consideration of legacy pipes with other possible dimensions and other materials such as cast iron can yield supplementary enhancement to the reliability of these findings.

- The FMA analytical model was originally developed to accurately capture the lateral deformation behaviour of fully bonded IRP systems in response to surface load until the material reaches its ultimate strain. However, the scope of this model can be broadened to include predictions of the capacity of the IRP systems against local failure modes. Additionally, it can also be extended to account for complex scenarios involving the influence of combined loading and the effect of different bonding levels.

- The fatigue behaviour of partially and completely unbonded systems in this study was investigated under the assumption of frictionless contact along the unbonded interface between the host pipe and IRP. However, further analysis can be implemented to explore how different levels of friction at the unbonded interface can affect the overall fatigue performance of the repair pipe.

- In order to address the issue of concentration of stresses during bending fatigue, this research examined the effect of incorporating varying levels of bonding between the host pipe and IRP. Therefore, it is recommended that future research attempts explore alternating approaches that may effectively tackle this issue, such as investigating the impact of roundness of the end of host pipe segments.

- This study assumed that there is no progressive debonding between the IRP and the host pipe during bending fatigue, which represents the worst-case scenario. However, it is encouraged that future studies incorporate the effect of progressive debonding between IRP and host pipe in both static and fatigue loading scenarios.

- Due to the challenges posed by the complexities associated with conducting experiments on IRP systems that are debonded from the host pipe, the FE model used in the analysis in Chapter 6 was validated using an experiment involving a fully bonded configuration. As a result, it is recommended that future studies should evaluate the findings from Chapter 6 by conducting laboratory experiments involving debonded configurations.

REFERENCES

Adebola, T., Moore, I. & Hoult, N. 2021, 'Use of Optical Fibers to Investigate Strength Limit States for Pressure Pipe Liners Spanning across Circular Perforations', *Journal of Pipeline Systems Engineering and Practice*, vol. 12, no. 2, p. 04021006, <https://ascelibrary.org/doi/abs/10.1061/%28ASCE%29PS.1949-1204.0000523>.

Akhi, A.H. & Dhar, A.S. 2021, 'Fracture parameters for buried cast iron pipes subjected to internal surface corrosions and cracks', *Journal of Pipeline Science and Engineering*, vol. 1, no. 2, pp. 187-97, <https://www.sciencedirect.com/science/article/pii/S2667143321000329>.

Al-Sabaeei, A.M., Alhussian, H., Abdulkadir, S.J. & Jagadeesh, A. 2023, 'Prediction of oil and gas pipeline failures through machine learning approaches: A systematic review', *Energy Reports*, vol. 10, pp. 1313-38, <https://www.sciencedirect.com/science/article/pii/S2352484723011502>.

Alam, P., Mamalis, D., Robert, C., Floreani, C. & Ó Brádaigh, C.M. 2019, 'The fatigue of carbon fibre reinforced plastics - A review', *Composites Part B: Engineering*, vol. 166, no. 1, pp. 555-79, <https://www.sciencedirect.com/science/article/pii/S1359836818321784>.

Alam, S., Sterling, R.L., Allouche, E., Condit, W., Matthews, J., Selvakumar, A. & Simicevic, J. 2015, 'A retrospective evaluation of the performance of liner systems used to rehabilitate municipal gravity sewers', *Tunnelling and Underground Space Technology*, vol. 50, pp. 451-64, <https://www.sciencedirect.com/science/article/pii/S0886779815300353>.

Albouy, W., Vieille, B. & Taleb, L. 2014, 'Influence of matrix ductility on the high-temperature fatigue behaviour of quasi-isotropic woven-ply thermoplastic and thermoset laminates', *Composites Part A-applied Science and Manufacturing*, vol. 67, pp. 22-36, <https://www.sciencedirect.com/science/article/pii/S1359835X14002103>.

Allouche, E., Bainbridge, K. & Moore, I. 2005, 'Laboratory examination of a cured in place pressure pipe liner for potable water distribution system', *North American Society for Trenchless Technology (NASTT) NO-DIG 2005*, Orlando, Florida.

Allouche, E.N., Alam, S., Al-Masud, M. & Dulam, R. 2012, 'Experimental Examination of Selected Limit States of Structural Liners at Locations of Ring Fracture', *Pipelines Conference 2012*: *Proceedings of the Pipelines Conference 2012* pp. 783-94.

Almahakeri, M., Fam, A. & Moore, I.D. 2013, 'Longitudinal Bending and Failure of GFRP Pipes Buried in Dense Sand under Relative Ground Movement', *Journal of Composites for Construction*, vol. 17, no. 5, pp. 702-10, <https://ascelibrary.org/doi/10.1061/%28ASCE%29CC.1943-5614.0000340>.

Alzabeebee, S., Chapman, D.N. & Faramarzi, A. 2018, 'A comparative study of the response of buried pipes under static and moving loads', *Transportation Geotechnics*, vol. 15, pp. 39-46, <https://www.sciencedirect.com/science/article/pii/S2214391217302106>.

Amiri, A. 2012, 'Experimental Investigation Of Fatigue Behavior Of Carbon Fiber Composites Using Fully-Reversed Four-Point Bending Test', University of North Dakota, Grand Forks, North Dakota.

Ansari, M.T.A., Singh, K.K. & Azam, M.S. 2018, 'Fatigue damage analysis of fiber-reinforced polymer composites A review', *Journal of Reinforced Plastics and Composites*, vol. 37, pp. 636 - 54, <https://journals.sagepub.com/doi/pdf/10.1177/0731684418754713>.

Argyrou, C., Bouziou, D., O'Rourke, T.D. & Stewart, H.E. 2018, 'Retrofitting pipelines with cured-in-place linings for earthquake-induced ground deformations', *Soil Dynamics*

and Earthquake Engineering, vol. 115, pp. 156-68, <https://www.sciencedirect.com/science/article/pii/S0267726117309028>.
Argyrou, C., O'rourke, T.D., Stewart, H.E. & Wham, B.P. 2019, 'Large-Scale Fault Rupture Tests on Pipelines Reinforced with Cured-in-Place Linings', *Journal of Geotechnical and Geoenvironmental Engineering*, vol. 145, no. 3, <https://ascelibrary.org/doi/10.1061/%28ASCE%29GT.1943-5606.0002018>.
Arifin, H.H., Zardasti, L., Lim, K.S., Md. Noor, N., Yahaya, N., Mazlan, A.N. & Mohd. Sam, A.R. 2021, 'Stress distribution analysis of composite repair with Carbon Nanotubes reinforced putty for damaged steel pipeline', *International Journal of Pressure Vessels and Piping*, vol. 194, p. 104537, <https://www.sciencedirect.com/science/article/pii/S0308016121002325>.
ARPA-E 2020, *Rapid Encapsulation of Pipelines Avoiding Intensive Replacement (REPAIR)* Advanced Research Project Agency - Energy, U.S. Department of Energy
Becerril García, D. & Moore, I.D. 2015, 'Performance of deteriorated corrugated steel culverts rehabilitated with sprayed-on cementitious liners subjected to surface loads', *Tunnelling and Underground Space Technology*, vol. 47, pp. 222-32, <https://www.sciencedirect.com/science/article/pii/S0886779815000061>.
Belmonte, E., Monte, M.d., Hoffmann, C. & Quaresimin, M. 2017, 'Damage initiation and evolution in short fiber reinforced polyamide under fatigue loading: Influence of fiber volume fraction', *Composites Part B-engineering*, vol. 113, pp. 331-41, <https://www.sciencedirect.com/science/article/pii/S1359836817302056>.
Belvederesi, C., Thompson, M.S. & Komers, P.E. 2018, 'Statistical analysis of environmental consequences of hazardous liquid pipeline accidents', *Heliyon*, vol. 4, no. 11, <https://www.sciencedirect.com/science/article/pii/S2405844018356020>.
Biezma, M.V., Andrés, M., Agudo, D. & Briz, E. 2020, 'Most fatal oil & gas pipeline accidents through history: A lessons learned approach', *Engineering Failure Analysis*, vol. 110, <https://www.sciencedirect.com/science/article/pii/S1350630719312324>.
Bokaian, A. 2004, 'Thermal expansion of pipe-in-pipe systems', *Marine Structures*, vol. 17, no. 6, pp. 475-500, <https://www.sciencedirect.com/science/article/pii/S0951833904000929>.
Brown, M.J.P., Moore, I.D. & Fam, A. 2014, 'Performance of a cured-in-place pressure pipe liner passing through a pipe section without structural integrity', *Tunnelling and Underground Space Technology*, vol. 42, pp. 87-95, <https://www.sciencedirect.com/science/article/pii/S0886779814000091>.
Brown, M.J.P., Moore, I.D. & Fam, A. 2020, 'Analysis of a cured-in-place pressure pipe liner spanning circular voids', *Tunnelling and Underground Space Technology*, vol. 101, p. 103424, <https://www.sciencedirect.com/science/article/pii/S0886779820303783>.
Budhe, S., Banea, M.D. & De Barros, S. 2020, 'Composite repair system for corroded metallic pipelines: an overview of recent developments and modelling', *Journal of Marine Science and Technology*, vol. 25, pp. 1308–23, <https://link.springer.com/article/10.1007/s00773-019-00696-3>.
Chandran, K.S.R. 2016, 'Mechanical fatigue of polymers: A new approach to characterize the SN behavior on the basis of macroscopic crack growth mechanism', *Polymer*, vol. 91, pp. 222-38, <https://www.sciencedirect.com/science/article/pii/S003238611630204X>.
Chegeni, B., Jayasuriya, S. & Das, S. 2019, 'Effect of corrosion on thin-walled pipes under combined internal pressure and bending', *Thin-walled Structures*, vol. 143, <https://www.sciencedirect.com/science/article/pii/S0263823119301818>.
Chen, A.S., Almond, D.P. & Harris, B. 2002, 'Impact damage growth in composites under fatigue conditions monitored by acoustography', *International Journal of Fatigue*,

vol. 24, no. 2-4, pp. 257-61, <https://www.sciencedirect.com/science/article/pii/S0142112301000809>.
Chen, J., Wang, H., Salemi, M. & Balaguru, P.N. 2021, 'Finite Element Analysis of Composite Repair for Damaged Steel Pipeline', *THE Coatings*, vol. 11, p. 301.
Chen, Q.H., Ni, P. & Qin, X. 2023, 'Numerical investigation on failure modes of bell-spigot jointed ductile iron pipelines subjected to dip-slip faults with different dip angles', *Tunnelling and Underground Space Technology*, vol. 133, <https://www.sciencedirect.com/science/article/pii/S0886779823000020>.
Chen, X., Wu, Z., Chen, W., Kang, R., He, X. & Miao, Y. 2019, 'Selection of key indicators for reputation loss in oil and gas pipeline failure event', *Engineering Failure Analysis*, vol. 99, pp. 69-84, <https://www.sciencedirect.com/science/article/pii/S1350630718302802>.
Chin, W.S. & Lee, D.G. 2005, 'Development of the trenchless rehabilitation process for underground pipes based on RTM', *Composite Structures*, vol. 68, no. 3, pp. 267-83, <https://www.sciencedirect.com/science/article/pii/S0263822304000765>.
Colombi, P. & Fava, G. 2012, 'Fatigue behaviour of tensile steel/CFRP joints', *Composite Structures*, vol. 94, no. 8, pp. 2407-17, <https://www.sciencedirect.com/science/article/pii/S0263822312000979>.
Crawford, R.J. & Benham, P.P. 1974, 'Cyclic stress fatigue and thermal softening failure of a thermoplastic', *Journal of Materials Science*, vol. 9, pp. 18-28, <https://link.springer.com/article/10.1007/BF00554752>.
Cunha, S.d. 2016, 'A review of quantitative risk assessment of onshore pipelines', *Journal of Loss Prevention in The Process Industries*, vol. 44, pp. 282-98, <https://www.sciencedirect.com/science/article/pii/S0950423016302601>.
Danninger, H. & Weiss, B. 2003, 'The influence of defects on high cycle fatigue of metallic materials', *Journal of Materials Processing Technology*, vol. 143, pp. 179-84, <https://www.sciencedirect.com/science/article/pii/S0924013603004096>.
Deng, M.L., Bao, C., Hung, A.T.S., Md Noor, N. & Lim, K.S. 2022, 'Effect of defect geometries upon burst capacity of composite repaired pipe', *Physics and Chemistry of the Earth, Parts A/B/C*, vol. 128, p. 103274, <https://www.sciencedirect.com/science/article/pii/S147470652200167X>.
Dixon, P.G., Tafsirojjaman, T., Klingaman, J., Hubler, M.H., Dashti, S., O'rourke, T.D., Farrag, K.A., Manalo, A. & Wham, B.P. 2023, 'State-of-the-Art Review of Performance Objectives for Legacy Gas Pipelines with Pipe-in-Pipe Rehabilitation Technologies', *Journal of Pipeline Systems Engineering and Practice*, vol. 14, no. 2, <https://ascelibrary.org/doi/10.1061/JPSEA2.PSENG-1371>.
Elhady, A.A., Sallam, H.E.-D.M., Alarifi, I.M., Malik, R.A. & EL-Bagory, T.M.A.A. 2020, 'Investigation of fatigue crack propagation in steel pipeline repaired by glass fiber reinforced polymer', *Composite Structures*, vol. 242, p. 112189, <https://www.sciencedirect.com/science/article/pii/S0263822319337110>.
Ferdous, W., Manalo, A., Peauril, J., Salih, C., Raghava Reddy, K., Yu, P., Schubel, P. & Heyer, T. 2020, 'Testing and modelling the fatigue behaviour of GFRP composites@ Effect of stress level, stress concentration and frequency', *Engineering Science and Technology, an International Journal*, vol. 23, no. 5, pp. 1223-32, <https://www.sciencedirect.com/science/article/pii/S2215098619321135>.
Fu, G., Shannon, B., Azoor, R., Deo, R.N. & Kodikara, J. 2022a, 'Equations for gap-spanning design of underground cast iron pipes lined with thermosetting polymeric liners', *Tunnelling and Underground Space Technology*, vol. 119, <https://www.sciencedirect.com/science/article/pii/S0886779821004259>.

Fu, G., Shannon, B., Azoor, R.M., Ji, J., Deo, R.N. & Kodikara, J.K. 2022b, 'Reliability based failure assessment of deteriorated cast iron pipes lined with polymeric liners', *Structure and Infrastructure Engineering*, vol. 19, no. 11, pp. 1516–29, <https://www.tandfonline.com/doi/full/10.1080/15732479.2022.2035404>.

Gao, X., Shao, Y., Chen, C., Zhu, H. & Li, K. 2022, 'Experimental and numerical investigation on transverse impact resistance behaviour of pipe-in-pipe submarine pipelines after service time', *Ocean Engineering*, vol. 248, p. 110868, <https://www.sciencedirect.com/science/article/pii/S0029801822003080>.

Ghaffari, M.A. & Hosseini, T.H. 2013, 'Fatigue Crack Propagation Analysis of Repaired Pipes With Composite Patch Under Cyclic Pressure', *Journal of Pressure Vessel Technology-transactions of The Asme*, vol. 135, no. 3, pp. 1-9.

Gras-Travesset, F., Andreu-Torras, A. & Pérez, M.A. 2023, 'A novel test procedure for evaluating the performance of composite cured-in-place-pipe liners in water pressure pipe rehabilitation', *Case Studies in Construction Materials*, vol. 19, p. e02381, <https://www.sciencedirect.com/science/article/pii/S2214509523005612>.

Günaydın, B., Dağhan, B. & Avc, A. 2013, 'Fatigue behavior of surface-notched composite pipes repaired by composite patches', *International Journal of Damage Mechanics*, vol. 22, no. 4, pp. 490 - 8, <https://journals.sagepub.com/doi/10.1177/1056789512450596>.

Guo, B., Song, S., Chacko, J. & Ghalambor, A. 2005, *Offshore Pipelines*, 1 edn, Elsevier, Burlington, MA.

Ha, S.K., Lee, H.K. & Kang, I.S. 2016, 'Structural behavior and performance of water pipes rehabilitated with a fast-setting polyurea–urethane lining', *Tunnelling and Underground Space Technology*, vol. 52, pp. 192-201, <https://www.sciencedirect.com/science/article/pii/S0886779815303357>.

Hilberink, A., Gresnigt, A.M. & Sluys, L.J. 2011, 'Mechanical Behaviour of Lined Pipe During Bending: Numerical and Experimental Results Compared', *ASME 2011 30th International Conference on Ocean, Offshore and Arctic Engineering*, pp. 401-12.

Howarth, R.W. 2014, 'A bridge to nowhere: methane emissions and the greenhouse gas footprint of natural gas', *Energy Science & Engineering*, vol. 2, no. 2, pp. 47 - 60, <https://onlinelibrary.wiley.com/doi/epdf/10.1002/ese3.35>.

Hsu, J.-M. & Shou, K.J. 2022, 'Numerical analysis of the mechanical behavior of separated joints in underground pipelines rehabilitated by cured-in-place pipes', *Tunnelling and Underground Space Technology*, vol. 125, <https://www.sciencedirect.com/science/article/pii/S0886779822001602>.

Huang, Z., Zhang, W., Qian, X., Su, Z., Pham, D.C. & Sridhar, N. 2020, 'Fatigue behaviour and life prediction of filament wound CFRP pipes based on coupon tests', *Marine Structures*, vol. 72, <https://www.sciencedirect.com/science/article/pii/S0951833920300502>.

IEA 2021, *Key World Energy Statistics 2021*, Statistics report, International Energy Agency, https://www.iea.org/reports/key-world-energy-statistics-2021>.

Jaganathan, A., Allouche, E. & Baumert, M. 2007, 'Experimental and numerical evaluation of the impact of folds on the pressure rating of CIPP liners', *Tunnelling and Underground Space Technology*, vol. 22, no. 5-6, pp. 666-78, <https://www.sciencedirect.com/science/article/pii/S0886779806001246>.

Jeon, S.-S., O'Rourke, T.D. & Neravali, A.N. 2004, 'Repetitive loading effects on cast iron pipelines with cast-in-place pipe lining system', *Journal of Transportation Engineering*, vol. 130, no. 6, pp. 692-705, <https://ascelibrary.org/doi/10.1061/%28ASCE%290733-947X%282004%29130%3A6%28692%29>.

Ji, H.W., Koo, D.D. & Kang, J.-H. 2020, 'Short- and Long-Term Structural Characterization of Cured-in-Place Pipe Liner with Reinforced Glass Fiber Material', *International Journal of Environmental Research and Public Health*, vol. 17, no. 6, p. 2073, <https://www.mdpi.com/1660-4601/17/6/2073>.

Jing, M., Zhang, S., Fu, L., Cao, G. & Wang, R. 2023, 'Reducing heat losses from aging district heating pipes by using cured-in-place pipe liners', *Energy*, vol. 273, p. 127260, <https://www.sciencedirect.com/science/article/pii/S0360544223006540>.

Jo, N.J., Takahara, A. & Kajiyama, T. 1993, 'Analysis of Fatigue Behavior of High-Density Polyethylene Based on Nonlinear Viscoelastic Measurement under Cyclic Fatigue', *Polymer Journal*, vol. 25, pp. 721-9, <https://www.nature.com/articles/pj199391>.

Jollivet, T., Peyrac, C. & Lefebvre, F. 2013, 'Damage of Composite Materials', *5th Fatigue Design Conference, Fatigue Design 2013*, pp. 746-58, <https://www.sciencedirect.com/science/article/pii/S1877705813019619>.

Karbhari, V.M. 2014, Rehabilitation of Pipelines Using Fiber-reinforced Polymer (FRP) Composites, Elsevier Science, 2015, Cambridge, United Kingdom.

Kishawy, H.A. & Gabbar, H.A. 2010, 'Review of pipeline integrity management practices', *International Journal of Pressure Vessels and Piping*, vol. 87, no. 7, pp. 373-80, <https://www.sciencedirect.com/science/article/pii/S0308016110000827>.

Klingaman, J., Dixon, P.G., Wham, B.P., Dashti, S.and Hubler, M.H. 2022, 'Traffic Loading Effects on Rehabilitated Cast Iron Distribution Pipelines', Pipelines 2022, Indianapolis, Indiana, pp. 313-23, <https://ascelibrary.org/doi/epdf/10.1061/9780784484296.037>.

Kohankar Kouchesfehani, Z., Darabnoush Tehrani, A., Najafi, M. & Syar, J. 2020, 'Laboratory testing of invert-cut corrugated metal pipes renewed with polymeric spray applied pipe lining', *Transportation Geotechnics*, vol. 25, p. 100413, <https://www.sciencedirect.com/science/article/pii/S2214391220303019>.

Kozman, D.P. 2020, 'Bonded or Unbonded Liners? How Longitudinal Bending Impacts Pipe Lining Design and Performance', *Pipelines 2020*, American Society of Civil Engineers, San Antonio, Texas, pp. 263-70, <https://ascelibrary.org/doi/10.1061/9780784483190.030>.

Kumar, S.S., Abraham, D.M., Behbahani, S.S., Matthews, J.C. & Iseley, T. 2020, 'Comparison of Technologies for Condition Assessment of Small-Diameter Ductile Iron Water Pipes', *Journal of Pipeline Systems Engineering and Practice*, vol. 11, no. 4, p. 04020039, <https://ascelibrary.org/doi/10.1061/%28ASCE%29PS.1949-1204.0000456>.

Li, B.-j., Zhu, L.-s. & Fu, X.-s. 2020, 'Influence of Grout Strength and Residual Deformation on Performance of Rehabilitated RC Pipes', *Journal of Pipeline Systems Engineering and Practice*, vol. 11, no. 2, p. 04020003, <https://ascelibrary.org/doi/abs/10.1061/%28ASCE%29PS.1949-1204.0000448>.

Li, B., Yu, W.J., Xie, Y.-p., Fang, H., Du, X., Wang, N., Zhai, K., Wang, D., Chen, X., Du, M., Sun, M. & Zhao, X. 2023a, 'Trenchless rehabilitation of sewage pipelines from the perspective of the whole technology chain: A state-of-the-art review', *Tunnelling and Underground Space Technology*, vol. 134, <https://www.sciencedirect.com/science/article/pii/S0886779823000421>.

Li, C., Yang, F., Jia, W., Liu, C., Zeng, J., Song, S. & Zhang, Y. 2023b, 'Pipelines Reliability Assessment Considering Corrosion-related Failure Modes and Probability Distributions Characteristic using Subset Simulation', *Process Safety and Environmental Protection*, vol. 178, pp. 226-39, <https://www.sciencedirect.com/science/article/pii/S0957582023007140>.

Li, Z., Jiang, X. & Hopman, H. 2019, 'Numerical analysis on the SIF of internal surface cracks in steel pipes reinforced with CRS subjected to bending', *Ships and Offshore Structures*, vol. 15, no. 10, pp. 1070 - 83, <https://www.tandfonline.com/doi/full/10.1080/17445302.2019.1702769>.

Lian, W. & Yao, W. 2010, 'Fatigue life prediction of composite laminates by FEA simulation method', *International Journal of Fatigue*, vol. 32, no. 1, pp. 123-33, <https://www.sciencedirect.com/science/article/pii/S0142112309000292>.

Lim, K.S., Azraai, S.N.A., Noor, N.M. & Yahaya, N. 2015, 'An Overview of Corroded Pipe Repair Techniques Using Composite Materials', *World Academy of Science, Engineering and Technology, International Journal of Chemical, Molecular, Nuclear, Materials and Metallurgical Engineering*, vol. 10, no. 1, pp. 19-25, <https://publications.waset.org/10003226/an-overview-of-corroded-pipe-repair-techniques-using-composite-materials>.

Liu, W., Guo, Q., Qiao, C. & Hou, W. 2019, 'Strain design method of buried pipeline crossing fault', *Engineering Failure Analysis*, vol. 105, pp. 659-71, <https://www.sciencedirect.com/science/article/pii/S1350630718308112>.

Lu, H., Xi, D. & Qin, G. 2023, 'Environmental risk of oil pipeline accidents', *The Science of the total environment*, vol. 874, p. 162386, <https://www.sciencedirect.com/science/article/pii/S0048969723010021>.

Lu, H., Wu, X., Ni, H., Azimi, M., Yan, X. & Niu, Y. 2020a, 'Stress analysis of urban gas pipeline repaired by inserted hose lining method', *Composites Part B: Engineering*, vol. 183, p. 107657, <https://www.sciencedirect.com/science/article/pii/S1359836819314027>.

Lu, H., Behbahani, S., Azimi, M., Matthews, J.C., Han, S. & Iseley, T. 2020b, 'Trenchless Construction Technologies for Oil and Gas Pipelines: State-of-the-Art Review', *Journal of Construction Engineering and Management-asce*, vol. 146, no. 6, p. 03120001, <https://ascelibrary.org/doi/10.1061/%28ASCE%29CO.1943-7862.0001819>.

Makar, J.M., Desnoyers, R. & McDonald, S.E. 2001, *Failure modes and mechanisms in gray cast iron pipe*, 1 edn, Institute for Research in Construction, National Research Council Canada, Ottawa, Ontario, Canada.

Malpot, A., Touchard, F. & Bergamo, S. 2015, 'Fatigue Behaviour of a Thermoplastic Composite Reinforced with Woven Glass Fibres for Automotive Application', *6th Fatigue Design conference, Fatigue Design 2015*, pp. 136-47, <https://www.sciencedirect.com/science/article/pii/S1877705815045609>.

Manan, A., Kamal, K., Ratlamwala, T.A.H., Sheikh, M.F., Abro, A.G. & Zafar, T. 2021, 'Failure classification in natural gas pipe-lines using artificial intelligence: A case study', *Energy Reports*, vol. 7, pp. 7640-7, <https://www.sciencedirect.com/science/article/pii/S2352484721011112>.

Mao, L., Gan, L., Li, W. & Zhang, P. 2022, 'Failure analysis on weld joint of centrifugal pump diffuser for oil and gas pipeline transportation', *Engineering Failure Analysis*, vol. 140, <https://www.sciencedirect.com/science/article/pii/S1350630722005933>.

Matthews, J.C., Selvakumar, A. & Condit, W. 2013, 'Current and Emerging Water Main Renewal Technologies', *Journal of Infrastructure Systems*, vol. 19, no. 2, pp. 231-41, <https://ascelibrary.org/doi/abs/10.1061/%28ASCE%29IS.1943-555X.0000121>.

Matthews, J.C., Allouche, E.N. & Sterling, R.L. 2015, 'Social cost impact assessment of pipeline infrastructure projects', *Environmental Impact Assessment Review*, vol. 50, pp. 196-202, <https://www.sciencedirect.com/science/article/pii/S0195925514001036>.

Mattos, H.d.C., Reis, J.M.L., Paim, L.M., Silva, M.L.d., Junior, R.L. & Perrut, V.A. 2016, 'Failure analysis of corroded pipelines reinforced with composite repair systems', *Engineering Failure Analysis*, vol. 59, pp. 223-36, <https://www.sciencedirect.com/science/article/pii/S1350630715301072>.

Melissianos, V.E., Vamvatsikos, D. & Gantes, C.J. 2017, 'Performance-based assessment of protection measures for buried pipes at strike-slip fault crossings', *Soil Dynamics and Earthquake Engineering*, vol. 101, pp. 1-11, <https://www.sciencedirect.com/science/article/pii/S0267726117301124>.

Mellott, S.R. 2012, 'Tensile, Creep, and Fatigue Behaviors of Thermoplastics Including Thickness, Mold Flow Direction, Mean Stress, Temperature, and Loading Rate Effects', The University of Toledo.

Mellott, S.R. & Fatemi, A. 2014, 'Fatigue behavior and modeling of thermoplastics including temperature and mean stress effects', *Polymer Engineering and Science*, vol. 54, no. 3, pp. 725-38.

Mini, K.M., Lakshmanan, M., Mathew, L. & Mukundan, M. 2012, 'Effect of fibre volume fraction on fatigue behaviour of glass fibre reinforced composite', *Fatigue & Fracture of Engineering Materials & Structures*, vol. 35, pp. 1160-6, <https://onlinelibrary.wiley.com/doi/full/10.1111/j.1460-2695.2012.01709.x>.

Moeini, R., Zare, M.R. & karimian, F. 2021, 'Reduce repair cost of wastewater pipelines for using trenchless and open cut technology', *Ain Shams Engineering Journal*, vol. 12, no. 1, pp. 423-35, <https://www.sciencedirect.com/science/article/pii/S2090447920301003>.

Mogielski, K.A., Kuliczkowski, A. & Kuliczkowska, E. 2017, 'Change in Toughness Parameters of Sewer Pipes Rehabilitated with Two Types of Epoxy CIPP Liners', *Journal of Pipeline Systems Engineering and Practice*, vol. 8, no. 4, p. 04017015, <https://ascelibrary.org/doi/abs/10.1061/%28ASCE%29PS.1949-1204.0000278>.

Mortazavian, S., Fatemi, A., Mellott, S.R. & Khosrovaneh, A. 2015, 'Effect of cycling frequency and self-heating on fatigue behavior of reinforced and unreinforced thermoplastic polymers', *Polymer Engineering and Science*, vol. 55, no. 10, pp. 2355-67, <https://4spepublications.onlinelibrary.wiley.com/doi/10.1002/pen.24124>.

Muc, A. 2000, 'Design of composite structures under cyclic loads', *Computers & Structures*, vol. 76, no. 1-3, pp. 211-8, <https://www.sciencedirect.com/science/article/pii/S0045794999001595>.

Mughrabi, H. 2015, 'Microstructural mechanisms of cyclic deformation, fatigue crack initiation and early crack growth', *Philosophical Transactions of the Royal Society A: Mathematical, Physical and Engineering Sciences*, vol. 373, pp. 1-21.

Najafi, M. 2016, Pipeline Infrastructure Renewal and Asset Management, McGraw-Hill Education, New York.

Netravali, A., O'Rourke, T., Gerretisen, K., Singh, Y., Jeon, S. & Zhao, D. 2000, Advanced pipeline support and stabilized backfill for gas mains affected by excavations—Part 2: Cast-in-place pipe lining systems for cast iron and steel gas mains, Fiber Science Program, Cornell University

Ithaca, NY.

Neya, B.N., Ardeshir, M.A., Delavar, A.A., Zaman, M. & Bakhsh, R. 2017, 'Three-Dimensional Analysis of Buried Steel Pipes under Moving Loads', *Open Journal of Geology*, vol. 7, no. 1, pp. 1-11, <https://www.scirp.org/journal/paperinformation?paperid=73407>.

Ng, P.C.F. 1994, 'Behaviour of buried pipelines subjected to external loading', University of Sheffield.

Nguyen, T., Tang, H., Chuang, T.-j., Chin, J., Wu, F. & Lesko, J. 2000, *A Fatigue Model for Fiber-Reinforced Polymeric Composites for Offshore Applications*, National Institute of Standards and Technology, United states.

Nuruddin, M., DeCocker, K., Sendesi, S.M.T., Whelton, A.J., Youngblood, J.P. & Howarter, J.A. 2020, 'Influence of aggressive environmental aging on mechanical and thermo-mechanical properties of Ultra Violet (UV) Cured in Place Pipe liners', *Journal of Composite Materials*, vol. 54, no. 23, pp. 3365-79, <https://journals.sagepub.com/doi/abs/10.1177/0021998320913988>.

O'Rourke, T.D., Strait, J.E., Mottl, N., Berger, B., Wham, B., Stewart, H.E. & Price, D. 2021, *Performance Evaluation of Aqua-Pipe under Earthquake-Induced*
Ground Deformation, Cornell University, Ithaca, NY.

Orowan, E. 1939, 'Theory of the Fatigue of Metals', Proceedings of The Royal Society A: Mathematical, Physical and Engineering Sciences, vol. 171, pp. 79-106.

Paepegem, W.V., Degrieck, J. & Baets, P.D. 2001, 'Finite element approach for modelling fatigue damage in fibre-reinforced composite materials', *Composites Part B-engineering*, vol. 32, no. 7, pp. 575-88, <https://www.sciencedirect.com/science/article/pii/S1359836801000385>.

Pang, J.C., Li, S.X., Wang, Z.G. & Zhang, Z.F. 2014, 'Relations between fatigue strength and other mechanical properties of metallic materials', *Fatigue & Fracture of Engineering Materials & Structures*, vol. 37, no. 9, pp. 945-1054, <https://onlinelibrary.wiley.com/doi/epdf/10.1111/ffe.12158>.

Parka, A., Kuliczkowska, E., Kuliczkowski, A. & Zwierzchowska, A. 2020, 'Selection of pressure linings used for trenchless renovation of water pipelines', *Tunnelling and Underground Space Technology*, vol. 98, p. 103218, <https://www.sciencedirect.com/science/article/pii/S0886779818306989>.

Pedersen, M.M. 2018, *Introduction to Metal Fatigue*, Technical report DoEM Engineering, Aarhus University.

Petersen, D.L., Nelson, C.R., Li, G., McGrath, T.J. & Kitane, Y. 2010, *Recommended Design Specifications for Live Load Distribution to Buried Structures*, National Research Cooperative Highway Program, Washington, D.C.

Pruitt, L.A. 2000, 'Fatigue Testing and Behavior of Plastics', in H Kuhn & D Medlin (eds), *ASM Handbook*, ASM International, vol. 8.

Qin, X. & Wang, Y. 2022, 'Different failure modes assessment of bell-spigot jointed ductile iron pipes under abrupt transverse ground movements', *Soil Dynamics and Earthquake Engineering*, vol. 163, <https://www.sciencedirect.com/science/article/pii/S0267726122004031>.

Risicato, J.-V., Kelly, F.M., Soulat, D., Legrand, X., Trümper, W., Cochrane, C. & Koncar, V. 2014, 'A Complex Shaped Reinforced Thermoplastic Composite Part Made of Commingled Yarns With Integrated Sensor', *Applied Composite Materials*, vol. 22, pp. 81-98.

Robert, D.J., Rajeev, P., Kodikara, J. & Rajani, B. 2016, 'Equation to predict maximum pipe stress incorporating internal and external loadings on buried pipes', *Canadian Geotechnical Journal*, vol. 53, no. 8, pp. 1315-31, <https://cdnsciencepub.com/doi/abs/10.1139/cgj-2015-0500>.

Saeed, N., Kang, W.-H. & Samali, B. 2022, 'Composite overwrap repair of pipelines-reliability based design framework', *Structures*, vol. 40, pp. 448-59, <https://www.sciencedirect.com/science/article/pii/S2352012422002909>.

Samanci, A., Tarakcioglu, N. & Akdemir, A. 2012, 'Fatigue failure analysis of surface-cracked (±45°)3 filament-wound GRP pipes under internal pressure', *Journal of*

Composite Materials, vol. 46, no. 9, pp. 1041 - 50, <https://journals.sagepub.com/doi/10.1177/0021998311414945>.
Samanci, A., Avci, A., Tarakcioglu, N. & Şahin, Ö.S. 2008, 'Fatigue crack growth of filament wound GRP pipes with a surface crack under cyclic internal pressure', *Journal of Materials Science*, vol. 43, pp. 5569-73, <https://link.springer.com/article/10.1007/s10853-008-2820-x>.
Selvakumar, A., Clark, R.M. & Sivaganesan, M. 2002, 'Costs for Water Supply Distribution System Rehabilitation', *Journal of Water Resources Planning and Management*, vol. 128, no. 4, pp. 303-6, <https://ascelibrary.org/doi/abs/10.1061/%28ASCE%290733-9496%282002%29128%3A4%28303%29>.
Selvakumar, A., Tafuri, A.N., Morrison, R. & Sterling, R. 2011, 'State of technology for renewal of sewer force mains', *Urban Water Journal*, vol. 8, no. 5, pp. 279-92, <https://www.tandfonline.com/doi/full/10.1080/1573062X.2011.598171>.
Selvakumar, A., Morrison, R., Sangster, T., Downey, D., Matthews, J. & Condit, W. 2013, *State of Technology for Rehabilitation of Water Distribution Systems*, EPA Office of Research and Development, Washington, DC.
Senouci, A., El-Abbasy, M.S. & Zayed, T. 2014, 'Fuzzy-Based Model for Predicting Failure of Oil Pipelines', *Journal of Infrastructure Systems*, vol. 20, no. 4, p. 04014018, <https://ascelibrary.org/doi/abs/10.1061/%28ASCE%29IS.1943-555X.0000181>.
Shanmugam, V., Das, O., Babu, K., Marimuthu, U., Veerasimman, A., Johnson, D.J., Neisiany, R.E., Hedenqvist, M.S., Ramakrishna, S. & Berto, F. 2021, 'Fatigue behaviour of FDM-3D printed polymers, polymeric composites and architected cellular materials', *International Journal of Fatigue*, vol. 143, pp. 1-15, <https://www.sciencedirect.com/science/article/pii/S0142112320305399>.
Shehata, M. & El-Shamy, A.M. 2023, 'Hydrogen-based failure in oil and gas pipelines a review', *Gas Science and Engineering*, vol. 115, <https://www.sciencedirect.com/science/article/pii/S294990892300122X>.
Sheldon, T., Sezen, H. & Moore, I.D. 2015, 'Joint Response of Existing Pipe Culverts under Surface Live Loads', *Journal of Performance of Constructed Facilities*, vol. 29, no. 1, p. 04014037, <https://ascelibrary.org/doi/abs/10.1061/%28ASCE%29CF.1943-5509.0000494>.
Shi, P. 2015, 'Surface wave propagation effects on buried segmented pipelines', *Journal of rock mechanics and geotechnical engineering*, vol. 7, no. 4, pp. 440-51, <https://www.sciencedirect.com/science/article/pii/S1674775515000633>.
Shirazi, H., Eadie, R.L. & Chen, W. 2023, 'A review on current understanding of pipeline circumferential stress corrosion cracking in near-neutral PH environment', *Engineering Failure Analysis*, vol. 148, <https://www.sciencedirect.com/science/article/pii/S1350630723001693>.
Shou, K.J. & Chen, B.C. 2018, 'Numerical analysis of the mechanical behaviors of pressurized underground pipelines rehabilitated by cured-in-place-pipe method', *Tunnelling and Underground Space Technology*, vol. 71, pp. 544-54, <https://www.sciencedirect.com/science/article/pii/S0886779816308926>.
Shou, K.J. & Huang, C.C. 2020, 'Numerical analysis of straight and curved underground pipeline performance after rehabilitation by cured-in-place method', *Underground Space*, vol. 5, no. 1, pp. 30-42, <https://www.sciencedirect.com/science/article/pii/S2467967418300850>.
Shuai, Y., Wang, X. & Cheng, Y.F. 2021, 'Buckling resistance of an X80 steel pipeline at corrosion defect under bending moment', *Journal of Natural Gas Science and Engineering*, vol. 93, p. 104016, <https://www.sciencedirect.com/science/article/pii/S1875510021002225>.

Skibo, M.D., Hertzberg, R.W. & Manson, J.A. 1978, The Effect of Temperature on the Frequency Sensitivity of Fatigue Crack Propagation in Polymers.
Song, C.L., Liu, X.B., Pan, X., Chen, Q.G., Wang, P. & Fang, Y. 2021, 'Failure Analysis of the Leakage and Ignition of an Oil–Gas Mixture Transportation Pipeline', *Journal of Failure Analysis and Prevention*, vol. 22, pp. 259-66, <https://link.springer.com/article/10.1007/s11668-021-01279-4>.
Song, S., Hua, W., Luo, X. & Maria Cruz, A. 2023, 'Methodology for assessing pipeline failure probability due to a debris flow in the near field', *Heliyon*, vol. 9, no. 5, <https://www.sciencedirect.com/science/article/pii/S2405844023031638>.
Soomro, A.A., Mokhtar, A.A., Kurnia, J.C., Lashari, N.u.R., Sarwar, U., Jameel, S.M., Inayat, M. & Oladosu, T.L. 2022, 'A review on Bayesian modeling approach to quantify failure risk assessment of oil and gas pipelines due to corrosion', *International Journal of Pressure Vessels and Piping*, vol. 200, <https://www.sciencedirect.com/science/article/pii/S0308016122002265>.
Sousa, R., Sousa, H. & Guedes, J.P.M. 2013, 'Diagonal compressive strength of masonry sample“ experimental and numerical approach', *Materials and Structures*, vol. 46, pp. 765-86, <https://link.springer.com/article/10.1617/s11527-012-9933-z>.
Stewart, H.E., Netravali, A.N. & O'Rourke, T.D. 2015, *Performance Testing of Field-Aged Cured-in-Place Liners (CIPL) for Cast Iron Piping* 151215, School of Civil and Environmental Engineering, Cornell University
Tafsirojjaman, T., Manalo, A., Tien, C.M.T., Wham, B., Salah, A., Kiriella, S., Karunasena, W. & Dixons, P. 2022, 'Analysis of failure modes in pipe-in-pipe repair systems for water and gas pipelines', *Engineering Failure Analysis*, vol. 140, <https://www.sciencedirect.com/science/article/pii/S1350630722004848>.
Tarar, W. 2008, 'A New Finite Element Procedure For Fatigue Life Prediction And High Strain Rate Assessment Of Cold Worked Advanced High Strength Steel', The Ohio State University.
Tetreault, J., Moore, I.D., Hoult, N.A., Tanzil, D. & Maher, M.L.J. 2018, 'Development of a Sustainability Evaluation System for Culvert Replacement and Rehabilitation Projects', *Journal of Pipeline Systems Engineering and Practice*, vol. 9, no. 2, <https://ascelibrary.org/doi/10.1061/%28ASCE%29PS.1949-1204.0000315>.
Tien, C.M.T., Manalo, A., Dixon, P., Tafsirojjaman, T., Karunasena, W., Flood, W.W., Ahmadi, H., Kiriella, S.H., Salah, A.M. & Wham, B.P. 2023, 'Effects of the legacy pipe ends on the behaviour of pipe-in-pipe repair systems under internal pressure', *Engineering Failure Analysis*, vol. 144, <https://www.sciencedirect.com/science/article/pii/S1350630722009244>.
Trickey, S.A., Moore, I.D. & Balkaya, M. 2016, 'Parametric study of frost-induced bending moments in buried cast iron water pipes', *Tunnelling and Underground Space Technology*, vol. 51, pp. 291-300, <https://www.sciencedirect.com/science/article/pii/S0886779815302029>.
Uslu, A., Ulke, A. & Beden, N. 2015, 'Review of Pipe Deterioration Failure Condition Assessment Techniques in WDS', European Water Resources Association, 9th World Congress, Water Resources Management in a Changing World: Challenges and Opportunities.
Valadi, Z., Bayesteh, H. & Mohammadi, S. 2018, 'XFEM fracture analysis of cracked pipeline with and without FRP composite repairs', *Mechanics of Advanced Materials and Structures*, vol. 27, no. 22, pp. 1888 - 99, <https://www.tandfonline.com/doi/full/10.1080/15376494.2018.1529844>.

Vasilikis, D. & Karamanos, S.A. 2012, 'Mechanical behavior and wrinkling of lined pipes', *International Journal of Solids and Structures*, vol. 49, no. 23-24, pp. 3432-46, <https://www.sciencedirect.com/science/article/pii/S0020768312003241>.

Vasseghi, A., Haghshenas, E., Soroushian, A. & Rakhshandeh, M. 2021, 'Failure analysis of a natural gas pipeline subjected to landslide', *Engineering Failure Analysis*, vol. 119, <https://www.sciencedirect.com/science/article/pii/S1350630720315338>.

Vazouras, P., Karamanos, S.A. & Dakoulas, P.C. 2012, 'Mechanical behavior of buried steel pipes crossing active strike-slip faults', *Soil Dynamics and Earthquake Engineering*, vol. 41, pp. 164-80, <https://www.sciencedirect.com/science/article/pii/S0267726112001078>.

Wang, D., Tan, Q., Yang, J. & Huang, D. 2022, 'New type of high-strength flexible cover plate to prevent engineering failure in oil and gas pipeline engineering', *Engineering Failure Analysis*, vol. 139, p. 106477, <https://www.sciencedirect.com/science/article/pii/S1350630722004514>.

Wang, R., Wang, F., Xu, J.-g., Zhong, Y.-h. & Shikun, L. 2019, 'Full-scale experimental study of the dynamic performance of buried drainage pipes under polymer grouting trenchless rehabilitation', *Ocean Engineering*, vol. 181, pp. 121-33, <https://www.sciencedirect.com/science/article/pii/S002980181930160X>.

Wasim, M. & Djukic, M.B. 2022, 'External corrosion of oil and gas pipelines: A review of failure mechanisms and predictive preventions', *Journal of Natural Gas Science and Engineering*, vol. 100, <https://www.sciencedirect.com/science/article/pii/S1875510022000580>.

Wham, B.P. & O'rourke, T.D. 2016, 'Jointed Pipeline Response to Large Ground Deformation', *Journal of Pipeline Systems Engineering and Practice*, vol. 7, no. 1, p. 04015009, <https://ascelibrary.org/doi/10.1061/%28ASCE%29PS.1949-1204.0000207>.

Woldesellasse, H. & Tesfamariam, S. 2023, 'Failure assessment of oil and gas transmission pipelines using an integrated Bayesian belief network and GIS model', *International Journal of Pressure Vessels and Piping*, vol. 205, <https://www.sciencedirect.com/science/article/pii/S0308016123001011>.

Yang, K., Xue, B., Fang, H., Du, X., Bin, L. & Chen, J. 2021, 'Mechanical sensitivity analysis of pipe-liner composite structure under multi-field coupling', *Structures*, vol. 29, pp. 484-93, <https://www.sciencedirect.com/science/article/pii/S2352012420306779>.

Yao, J., Liang, W. & Xiong, J. 2022, 'Novel intelligent diagnosis method of oil and gas pipeline defects with transfer deep learning and feature fusion', *International Journal of Pressure Vessels and Piping*, vol. 200, <https://www.sciencedirect.com/science/article/pii/S0308016122001673>.

Yu, H.N., Kim, S.S., Hwang, I.U. & Lee, D.G. 2008, 'Application of natural fiber reinforced composites to trenchless rehabilitation of underground pipes', *Composite Structures*, vol. 86, no. 1-3, pp. 285-90, <https://www.sciencedirect.com/science/article/pii/S0263822308000913>.

Zakikhani, K., Nasiri, F. & Zayed, T.M. 2020a, 'A Review of Failure Prediction Models for Oil and Gas Pipelines', *Journal of Pipeline Systems Engineering and Practice*, vol. 11, no. 1, p. 03119001, <https://ascelibrary.org/doi/full/10.1061/%28ASCE%29PS.1949-1204.0000407>.

Zakikhani, K., Zayed, T., Abdrabou, B. & Senouci, A. 2020b, 'Modeling Failure of Oil Pipelines', *Journal of Performance of Constructed Facilities*, vol. 34, no. 1, p. 04019088, <https://ascelibrary.org/doi/abs/10.1061/%28ASCE%29CF.1943-5509.0001368>.

Zang, X., Xu, Z., Lu, H., Zhu, C. & Zhang, Z. 2023, 'Ultrasonic guided wave techniques and applications in pipeline defect detection: A review', *International Journal of Pressure Vessels and Piping*, vol. 206, <https://www.sciencedirect.com/science/article/pii/S0308016123001503>.

Zhai, K. & Moore, I. 2023, 'Axial stresses in pressure pipe liners spanning joints with initial gap, opening as a result of differential ground movements', *Tunnelling and Underground Space Technology*, vol. 133, <https://www.sciencedirect.com/science/article/pii/S088677982200606X>.

Zhang, Z., Wang, L., Yan, X. & Wang, H. 2022, 'Numerical study on automatic repair inside the pipeline for the small leakage gas pipeline by using fibrous particles', *Powder Technology*, vol. 407, <https://www.sciencedirect.com/science/article/pii/S0032591022005009>.

Zhao, X., Wang, X., Wu, Z. & Zhu, Z. 2016, 'Fatigue behavior and failure mechanism of basalt FRP composites under long-term cyclic loads', *International Journal of Fatigue*, vol. 88, pp. 58-67, <https://www.sciencedirect.com/science/article/pii/S0142112316300093>.

Zhong, Z., Wang, S., Zhao, M., Du, X.-l. & Li, L. 2018, 'Performance of ductile iron push-on joints rehabilitated with CIPP liner under repetitive and seismic loadings', *Soil Dynamics and Earthquake Engineering*, vol. 115, no. 776-786, <https://www.sciencedirect.com/science/article/pii/S0267726117306425>.

Zhong, Z., Bouziou, D., Wham, B., Filiatrault, A., Aref, A., O'Rourke & Stewart 2014, 'Seismic Testing of Critical Lifelines Rehabilitated with Cured in Place Pipeline Lining Technology', *Journal of Earthquake Engineering*, vol. 18, no. 6, pp. 964–85, <https://www.tandfonline.com/doi/full/10.1080/13632469.2014.916632>.

Zhu, H., Wang, T., Wang, Y. & Li, V.C. 2021, 'Trenchless rehabilitation for concrete pipelines of water infrastructure: A review from the structural perspective', *Cement & Concrete Composites*, vol. 123, p. 104193, <https://www.sciencedirect.com/science/article/pii/S0958946521002614>.

APPENDIX A: CONFERENCE PAPER

A simplified theoretical prediction of vertical bending behaviour of structural pipe repair systems

Shanika Kiriella [1], Allan Manalo [1], Cam Minh Tri Tien [1], Warna Karunasena [1], Hamid Ahmadi [1], Ahmad Salah [1], Patrick Dixon [2], Brad P. Wham [2], Thomas D. O'Rourke [3]

[1] Centre for Future Materials (CFM), University of Southern Queensland (UniSQ), Toowoomba, QLD 4350, Australia.
[2] Center for Infrastructure, Energy, and Space Testing, University of Colorado Boulder, Boulder, CO 80309, US.
[3] School of Civil and Environmental Engineering, Cornell University, Ithaca, NY 14853, US

ABSTRACT: Internal replacement pipe (IRP) system is an emerging trenchless pipeline repair technology. Vertical bending caused by surface loads from vehicular traffic is considered to be the worst condition for IRP systems, particularly for host pipes with circumferential discontinuities. However, available studies on the flexural behaviour of IRP systems installed host pipes with discontinuities are limited. Moreover, a simplified and robust analytical model that can reliably predict the behaviour of discontinuous host pipes repaired with IRP systems subject to bending is not available. Consequently, a simplified analytical model based on fibre model analysis (FMA) was developed to examine the load-deflection behaviour of IRP systems in host pipes with circumferential discontinuities. Finite element analysis (FEA) was also performed to simulate the bending behaviour of the IRP system and to validate the FMA results. FMA showed a good correlation between the linear and non-linear load-deflection behaviours of the IRP in a host pipe with different discontinuity widths. The findings of this study will give the research community and construction specialities a better knowledge of the bending behaviour of IRP systems installed in gas pipelines with discontinuities resulting from circumferential cracking to scenarios where longitudinal sections are effectively missing. The FMA analytical model, which was calibrated and validated with experimental, and FEA numerical results, will be a very reliable and simple tool for predicting the flexural behaviour of IRP systems for trenchless repair, in contrast to expensive and time-consuming laboratory experiments and extensive FEA.

1. INTRODUCTION

Corrosion of oil and gas pipelines, often made from legacy cast iron and bare steel presents a major issue for the energy industry (Zhang and Zhou 2014; Ossai et al. 2015). Failure of these pipelines can result in catastrophic damage to people and property due to the highly combustible materials contained within (Yang et al. 2016; Biezma et al. 2020). Consequently, oil and gas pipeline systems that have either reached or approaching their intended service life are in need of economical repair methods to restore their originally designed operational capacity,

maintain their structural integrity, and prolong their operational life. These circumstances have led to the investigation of various pipe repairing techniques that are appropriate for either conventional open trench or trenchless installations (Wu et al. 2021). The trenchless approach has gained popularity as the main choice for repairing pipes in many countries due to its ability to minimise damage to the environment and excavation procedures, resulting in greater reliability and cost efficiency (Jung and Sinha 2007; Yu et al. 2008). This repair technique has advanced significantly in recent years, employing a novel approach called internal replacement pipe (IRP) (Tafsirojjaman et al. 2022; Tien et al. 2022; Dixon et al. 2023).

Failure mechanisms of both host pipes and IRP systems are significantly influenced by loading conditions. The bending deformation caused by surface load from vehicular traffic is regarded as the most severe loading condition for both host pipes and IRP systems, among various other loading conditions (Jeon et al. 2004; Tafsirojjaman et al. 2022). The worst type of discontinuity that can occur along a host pipe is a complete circumferential cracking or a pipe joint (Stewart et al. 2015). In the presence of circumferential discontinuities on the host pipe, the IRP may be at risk from stresses, displacements and rotations resulting from traffic loading. The existing research related to vertical bending behaviours of discontinuous host pipes repaired by IRP systems is very limited (Jeon et al. 2004; Allouche et al. 2012; Stewart et al. 2015; Shou and Chen 2018). Importantly, there is a lack of a simplified and reliable analytical model that can accurately predict the bending behaviour of discontinuous host pipes repaired by IRP systems under surface loading. Insufficient research has led to a limited understanding of the bending behaviour of IRP systems in host pipes that have undergone damage. In addition, the majority of existing models have been developed specifically for individual materials or continuous IRP systems (Tafsirojjaman et al. 2022). In practical scenarios, pipes requiring repair systems typically exhibit pre-existing damages such as circumferential discontinuities resulting from the presence of joints. Due to the potential impact of discontinuities in the host pipe on the functionality of the IRP system, it is essential to conduct in-depth investigations to address this issue appropriately.

The comprehensive evaluation of different design parameters of IRP repair systems subjected to loading such as traffic is challenging to accomplish exclusively through full-scale laboratory testing due to their high cost and time demands. Numerical simulations through finite element analysis (FEA) on the other hand are cost and time-effective but need to be validated by physical experiments. However, FEA is a complex and extensive process that necessitates specialised expertise. This may pose a constraint for professionals involved in material development within the industry who desire to gain a better understanding of how their IRP material systems respond when subjected to loads. Therefore, the development of a simplified analytical model that can still accurately capture the bending behaviour of IRP systems would be highly advantageous since it would require less execution time and expertise in comparison to advanced FEA. The present study utilised simple fibre model analysis (FMA) as described by Manalo et al. (2010) to investigate analytically the performance of IRP systems that span between discontinuities in the host pipes when subjected to bending deformations generated by traffic loads. In addition, analytical predictions are verified through experimentation and compared to outcomes from finite element analysis (FEA) to facilitate an in-depth understanding of the actual bending behaviour of IRP systems. The findings of this study provide construction professionals with enhanced insight into the bending deformation behaviour of discontinuous gas pipelines that have been repaired with IRP systems. Unlike expensive and time-consuming laboratory experiments and extensive FEA, the FMA analytical model, which was calibrated and validated with experimental, and FEA results, will be a highly reliable tool for predicting the bending behaviour of IRP systems under surface loading.

2. FIBRE MODEL ANALYSIS (FMA)

A simplified theoretical prediction of the load-deflection behaviour of the IRP system under bending was performed using FMA (Manalo 2011), considering the stress-strain behaviour of IRP and host pipe materials in tension and compression. The current study has implemented the analysis using MATLAB, although it is possible to develop this computational method in a Microsoft Excel spreadsheet. The bending behaviour of IRP systems in steel host pipes with circumferential discontinuity widths ranging from 12.7 mm (0.5 in) – 152.4 mm (6.0 in)

is assessed using FMA. The experimental setup utilised for this purpose is a four-point bending test, developed at the University of Colorado Boulder (CUB) (Figure 1a) following wheel load configuration as suggested in AASHTO (Klingaman et al. 2022). The dimensions of the test setup are 762-1016-762 mm (30 -40 -30 in) (Figure 1b). The outer diameter and the thickness of the host pipe are 324.0 mm (12.8 in.) and 6.4 mm (0.3 in) respectively. The outer diameter of IRP was established as 311.2 mm (12.3 in) in accordance with the inner diameter of the host pipe. The thickness of the IRP ranges between 3.2 mm (0.1 in) and 9.5 mm (0.4 in) and the modulus of elasticity (MOE) varies between 1.0 (145.0 ksi) and 200.0 GPa (29,0007.5 ksi). The parametric investigation considered multiple materials for IRP covering polymers, thermoplastics, glass fibre-reinforced polymer (GFRP) composites, and metallic (cast iron and steel) materials. The selection of these parameters was influenced by a prior investigation conducted by Tafsirojjaman et al. (2022) in the context of IRP systems. It is important to note that the analysis is conducted under the condition of zero internal pressure, which can be considered as the worst-case scenario, particularly when the system is subjected to bending.

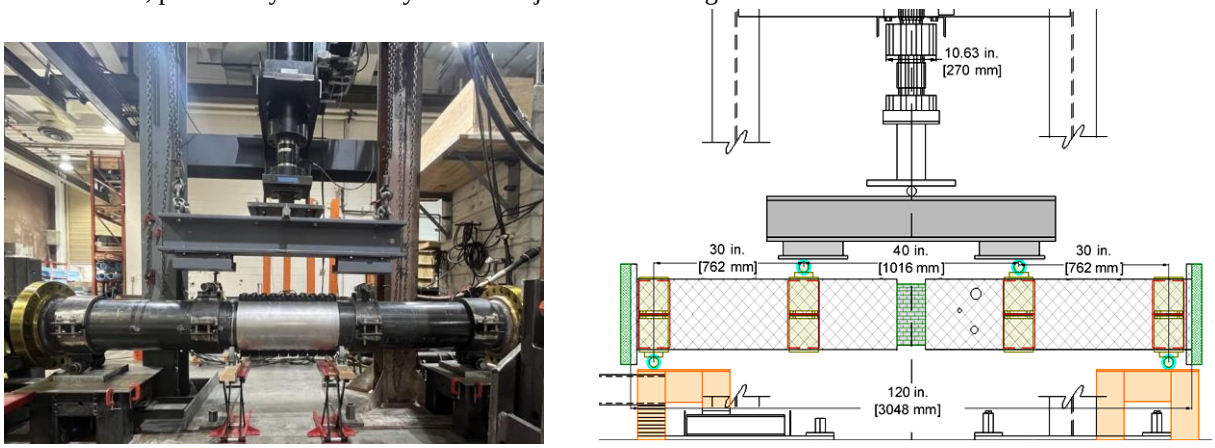

(a) (b)

Figure 1. (a) Actual set-up and (b) schematic view of four-point bending test of IRP systems (Kiriella et al. 2023)

The nonlinear load-deflection behaviour of the IRP system is determined by dividing its cross-section and loading length into small segments. The basic assumptions of FMA are illustrated in Figure 2. In the diagram, the outer diameter of IRP is denoted as $D_{p(out)}$, and the inner diameter of IRP as $D_{p(in)}$. The tensile stress and tensile strain of the host pipe material are represented by $\sigma_{h(t)}$ and $\varepsilon_{h(t)}$, respectively, while the compressive stress and compressive strain of the host pipe materials are represented by $\sigma_{h(c)}$ and $\varepsilon_{h(c)}$, respectively. The tensile failure strength and strain of IRP material are denoted by $\sigma_{p(t)}$ and $\varepsilon_{p(t)}$, respectively, whereas the compressive failure strength and strain of IRP material are indicated by $\sigma_{p(c)}$ and $\varepsilon_{p(c)}$, respectively. A detail description of the analysis can be found in a journal article by the authors of this paper, Kiriella et al. (2023). Figure 3 presents a schematic diagram of IRP within a host pipe that contains a discontinuity at the midspan. The diagram illustrates the following variables: $\Delta_{\max}$ is maximum deflection; L is the length of the IRP between supports; $\frac{(L-l)}{2}$ is the length of the host pipe half; l is the discontinuity width; P is half of the applied load; a is the loading length; n is the total number of segments into which the loading length is subdivided, w_i is the length to the right boundary of each segment from the left support, $(EI)_{eff_i}$ is the equivalent effective secant stiffness of the cross-section of each segment of IRP with host pipe over the loading length measured from the left support to the left loading point and b is the length measured from the left support to the point where the deflection requires to be computed. The FMA model employs Equation [11 to determine the maximum midspan deflection of IRPs in host pipes with circumferential discontinuities. The deflection along its length, $0 \leq b \leq a$, a$\leq b \leq \frac{(L-l)}{2}$ and $\frac{(L-l)}{2} \leq b \leq \frac{L}{2}$ is determined by Equation 2, 3and 4, respectively.

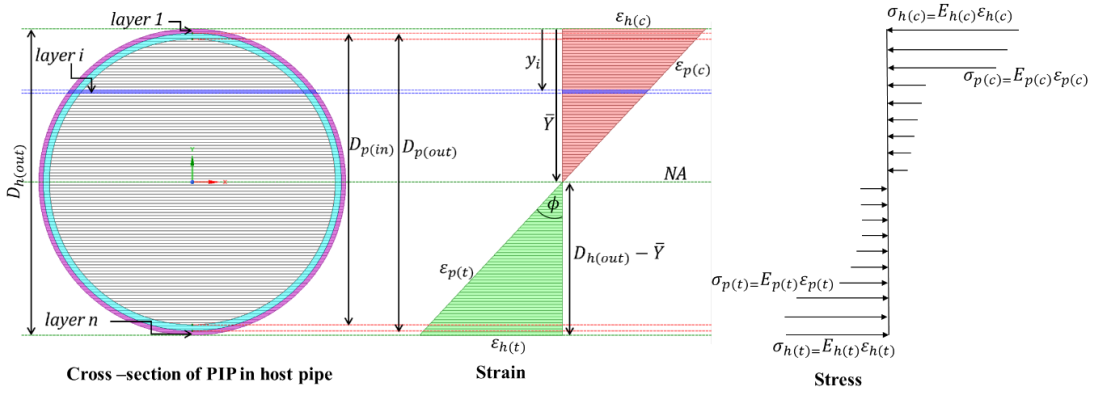

Figure 2. Fundamental assumptions of FMA (Kiriella et al. 2023)

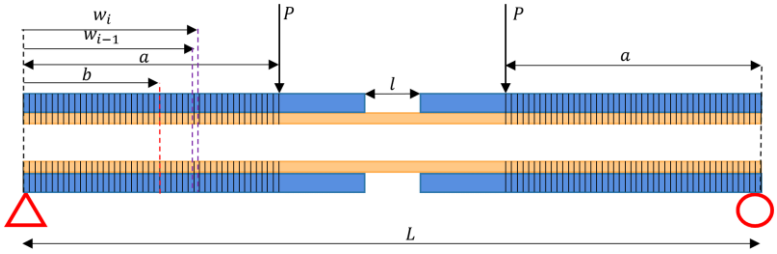

Figure 3. Schematic illustration of IRP in host pipe with a central discontinuity

$$\Delta_{\max} = 2\left\{\sum_{i=1}^{n}\left[\frac{P({w_i}^3 - {w_{i-1}}^3)}{6(EI)_{eff_i}}\right] + \frac{Pa}{16(EI)_{EFF}}((L-l)^2 - 4a^2) + \frac{Pa}{16(EI)_{SIRP}}(2Ll - l^2)\right\} \quad [1]$$

$$\begin{aligned}\Delta_{(0 \le b \le a)} = &\sum_{i=1}^{n_b}\left\{\frac{P\left(1-\frac{b}{L}\right)({w_i}^3 - {w_{i-1}}^3)}{3(EI)_{eff_i}}\right\} + \sum_{i=1}^{(n-n_b)}\left\{\frac{Pb}{(EI)_{eff_{(a-b)_i}}}\left[\left(\frac{{w_i}^2 - {w_{i-1}}^2}{2}\right) - \left(\frac{{w_i}^3 - {w_{i-1}}^3}{3L}\right)\right]\right\} \\ &+ \frac{Pab}{(EI)_{EFF}}\left\{\frac{L-l}{2} - a - \frac{(L-l)^2}{8L} + \frac{a^2}{2L}\right\} + \frac{Pabl}{2(EI)_{PIP}} \\ &+ \frac{Pab}{(EI)_{EFF}}\left\{\left(\frac{L}{2} - a - \frac{l}{2}\right) - \frac{1}{2L}\left[(L-a)^2 - \frac{(L+l)^2}{4}\right]\right\} \\ &+ \sum_{i=1}^{n}\left\{\frac{Pb}{\left((EI)_{eff}\right)'_i}\left[L(w_i - w_{i-1}) - ({w_i}^2 - {w_{i-1}}^2) + \frac{1}{3L}({w_i}^3 - {w_{i-1}}^3)\right]\right\}\end{aligned} \quad [2]$$

$$\begin{aligned}\Delta_{\left(a \le b \le \frac{L-l}{2}\right)} = &\sum_{i=1}^{n}\left\{\frac{P\left(1-\frac{b}{L}\right)({w_i}^3 - {w_{i-1}}^3)}{3(EI)_{eff_i}}\right\} + \frac{Pa\left(1-\frac{b}{L}\right)(b^2 - a^2)}{2(EI)_{EFF}} + \frac{Pab}{8L(EI)_{EFF}}(3L^2 - 2Ll - 8bL - l^2 + 4b^2) \\ &+ \frac{Pabl}{2(EI)_{SIRP}} + \frac{Pab}{(EI)_{EFF}}\left\{\left(\frac{L}{2} - a - \frac{l}{2}\right) - \frac{1}{2L}\left[(L-a)^2 - \frac{(L+l)^2}{4}\right]\right\} \\ &+ \sum_{i=1}^{n}\left\{\frac{Pb}{\left((EI)_{eff}\right)'_i}\left[L(w_i - w_{i-1}) - ({w_i}^2 - {w_{i-1}}^2) + \frac{1}{3L}({w_i}^3 - {w_{i-1}}^3)\right]\right\}\end{aligned} \quad [3]$$

$$\Delta_{\left(\frac{L-l}{2} \le b \le \frac{L}{2}\right)} = \sum_{i=1}^{n}\left\{\frac{P\left(1-\frac{b}{L}\right)\left({w_i}^3-{w_{i-1}}^3\right)}{3(EI)_{eff_i}}\right\} + \frac{Pa}{8(EI)_{EFF}}[(L-l)^2-4a^2] + \frac{Pa\left(1-\frac{b}{L}\right)[4b^2-(L-l)^2]}{8(EI)_{SIRP}}$$
$$+ \frac{Pab\left\{\frac{L+l}{2}-b-\frac{(L+l)^2}{8L}+\frac{b^2}{2L}\right\}}{(EI)_{PIP}} + \frac{Pab}{(EI)_{EFF}}\left\{\left(\frac{L}{2}-a-\frac{l}{2}\right)-\frac{1}{2L}\left[(L-a)^2-\frac{(L+l)^2}{4}\right]\right\} \quad [4]$$
$$+ \sum_{i=1}^{n}\left\{\frac{Pb}{\left((EI)_{eff}\right)'_i}\left[L(w_i-w_{i-1})-({w_i}^2-{w_{i-1}}^2)+\frac{1}{3L}({w_i}^3-{w_{i-1}}^3)\right]\right\}$$

where $\Delta_{(0 \le b \le a)}$, $\Delta_{\left(a \le b \le \frac{L-l}{2}\right)}$ and $\Delta_{\left(\frac{L-l}{2} \le b \le \frac{L}{2}\right)}$ are the deflection at any point along $0 \le b \le a$, $a \le b \le \frac{(L-l)}{2}$ and $\frac{(L-l)}{2} \le b \le \frac{L}{2}$ of IRP, respectively, n_b and $(n-n_b)$ are the number of segments over length b and length $(a-b)$, respectively, $(EI)_{eff_{(a-b)_i}}$ is the equivalent effective secant stiffness of the cross-section of each IRP with host pipe segment over length $(a-b)$ from length b to the loading point and $\left((EI)_{eff}\right)'_i$ is the equivalent effective secant stiffness of the cross-section of each IRP with host pipe segment over the length a (on the right side half of the system) from the loading point to support.

3. FINITE ELEMENT ANALYSIS

The primary purpose of utilising FEA in this study is to compare the outcomes obtained from the FMA analytical model with those produced by FEA models. FEA models are generated by employing ANSYS/Mechanical software.

Figure **4** illustrates a typical repair scenario where an IRP is used to repair a steel host pipe with 152.4 mm (6.0 in) wide discontinuity at the midspan. To simplify the analysis, a quarter model is used, which involves applying quarter symmetric boundary conditions in both longitudinal and transverse directions. The system is modelled using the standard SOLID 186. The ends of the system are enclosed by blind flanges made of steel. The experimental setup is represented by pinned supports and connecting the loading head with the pipe clamps through the pin-lug system, as displayed in

Figure **4**. The host pipe and IRP systems are fully bonded. The contacts between the host pipe and the supports are established using a frictionless connection type. The contact pairs comprise clamp-pipe and lug-pin. A force equivalent to one-fourth of the total force is exerted vertically downward on the loading head of the setup.

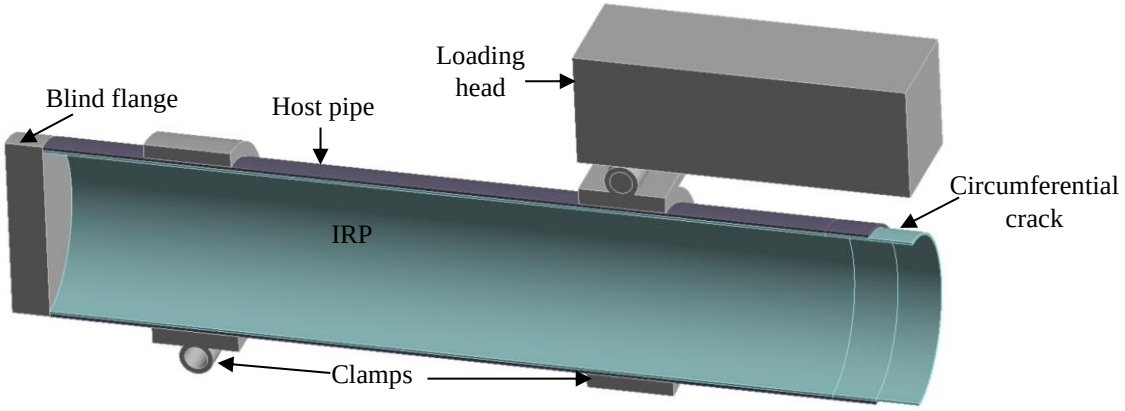

Figure 4. Geometry and boundary conditions of quarter FE model of IRP in host pipe with 152.4 mm (6.0 in) wide discontinuity

4. RESULTS AND DISCUSSION

4.1 FMA for IRP systems with wider crack widths

The behaviour of IRP repair systems in host pipes with wider discontinuities is evaluated by comparing the load and midspan deflection from the FMA and FEA prediction. Figure 5a compares FMA and FEA predictions of the load-midspan deflection behaviour of IRP in a host pipe with discontinuity widths of 101.6 mm (4.0 in), 152.4 mm (6.0 in) and 203.2 mm (8.0 in) under the applied loading. The load-deflection relationship for discontinuity widths of 101.6 mm (4.0 in), 152.4 mm (6.0 in) and 203.2 mm (8.0 in), is found to be linear in FMA results up to loadings of 16.8 kN (3.8 kips),16.6 kN (3.7 kips) and 16.2 kN (3.6 kips), respectively. After that, there is a slight nonlinear decrease in stiffness until the point of failure which occurred at loadings of 28.9 kN (6.5 kips), 27.7 kN (6.2 kips) and 27.0 kN (6.1 kips) for the respective discontinuity widths. This overall behaviour of FMA corresponds well with FEA, exhibiting a maximum discrepancy of under 6%. Also, the findings suggest that an increase in discontinuity width in the host pipe leads to a decrease in the ultimate loading capacity of the IRP, while simultaneously causing a corresponding increase in maximum deflection. Additionally, as per FEA, the ultimate failure of an IRP in a host pipe with a wider discontinuity subjected to bending is governed by buckling at the crown of the IRP between the edges of the discontinuity (Figure 6). This failure mechanism is identical to the ultimate failure of IRP alone as reported in Tafsirojjaman et al. (2022). Consequently, it is evident that the load-carrying capacity and failure of the IRP in a host pipe with wider discontinuities are primarily controlled by the IRP. The deflection along the left half lengths of IRPs installed in host pipes with previous discontinuity widths, under a load of 15.0 kN (3.4 kips) is shown in Figure 5b. According to the results, when the discontinuity widens, the IRP repair experiences an increase in deformation even under the same loading level. Both FMA and FEA results demonstrate a nearly linear deflection response over the length of the pipe up to the edge of the discontinuity. However, as one moves from support to the discontinuity edge, the difference between the predictions of the two methods increases gradually. This difference can reach up to 9.3% at the edge of a 101.6 mm (4.0 in) wide discontinuity. The discrepancy observed between the outcomes obtained from FMA and FEA of the IRP system with 101.6 mm (4.0 in) wide discontinuity is over double the variation identified at the midspan (4.4%) under the same load. The difference between FMA and FEA is due to the change in geometry of IRP induced by local buckling, which is not captured by the current FMA model.

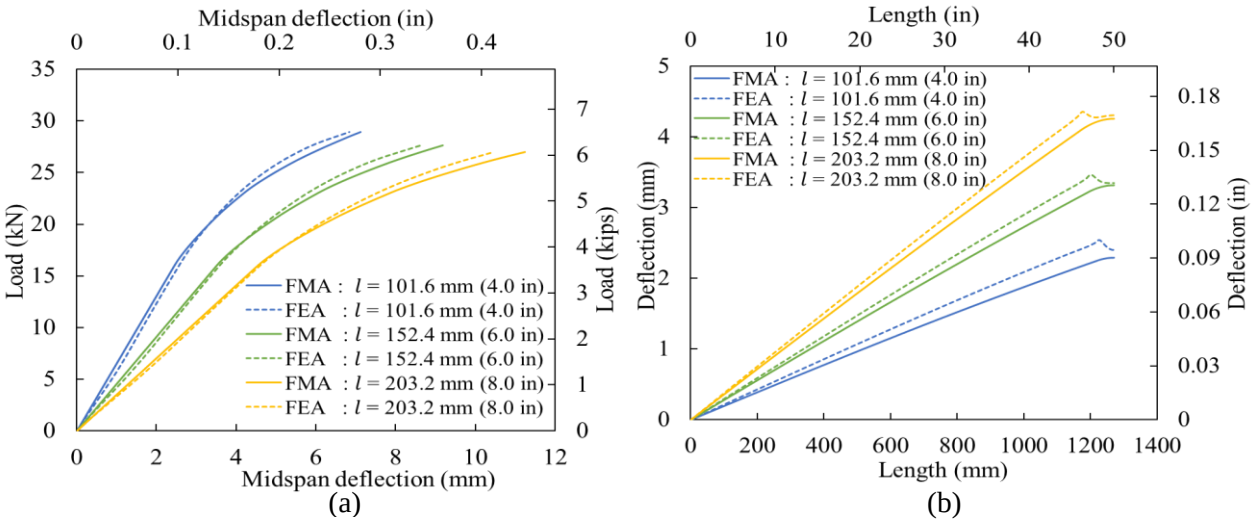

Figure 5. (a) Load-midspan deflection behaviour (b) deflection from left support to midspan of IRP in host pipe with 101.6, 152.4 mm (6.0 in) and 203.2 mm (8.0 in) discontinuity widths

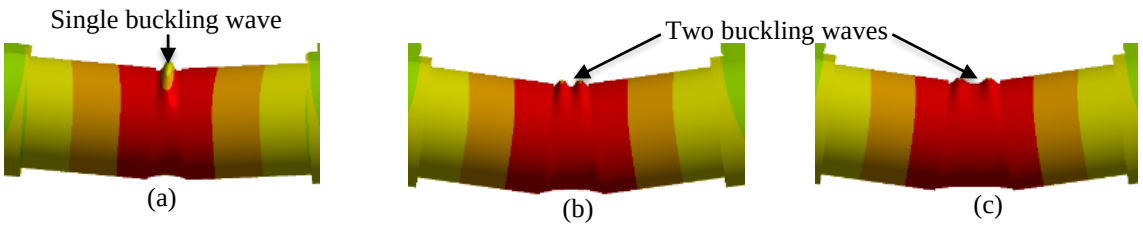

Figure 6. Failure modes of IRP installed in a host pipe with wider discontinuity widths, i.e. (a) 101.6 mm (4.0 in), (b) 152.4 mm (6.0 in) and (c) 203.2 mm (8.0 in)

The effect of the repair thickness on the midspan deflection of ALTRA10 IRP installed in the host pipe with a 152.4 mm (6.0 in) wide discontinuity under an applied loading of 15.0 kN (3.4 kips) as estimated by both FMA and FEA are presented in

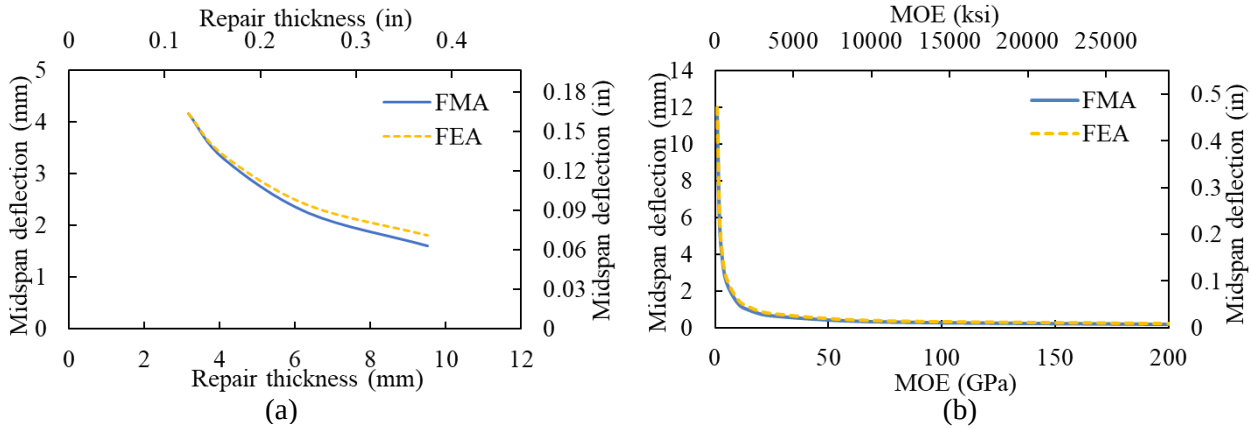

Figure **7**a. The findings indicate that, under the same loading conditions, the deformation of ALTRA10 IRP repair systems, as predicted by both FMA and FEA models, exhibits a nonlinear reduction as the repair thickness decreases. This is attributed to the increased stiffness of IRP. Overall, an increase in repair thickness from 3.2 mm (0.1 in) to 9.5 mm (0.4 in) yielded a decrease in midspan deflection by 61% and 57%, as determined by FMA and FEA, correspondingly. On the other hand, under an applied loading of 15.0 kN (3.4 kips),

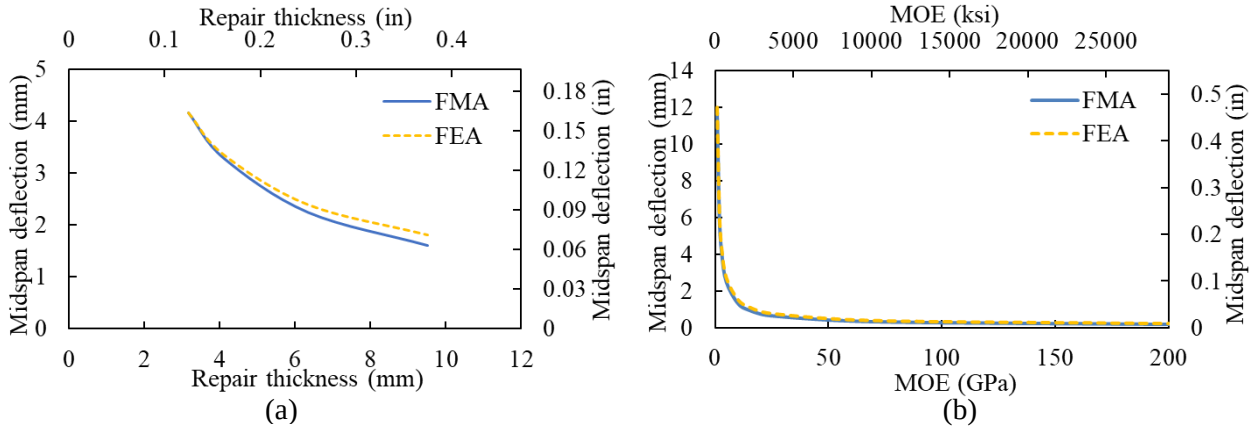

Figure **7**b shows the anticipated midspan deflection of a host pipe with a 152.4 mm (6.0 in) wide discontinuity that has been repaired using a 4.1 mm (0.2 in) thick IRP with MOE ranging from 1.0 GPa (145.0 ksi) to 200 GPa (29,007.5 ksi). The results suggest that an increase in the MOE of IRP from 1.0 GPa (145.0 ksi) to 24.5 GPa (3,553.4 ksi) leads to a reduction in midspan deflection by 94%, as observed from both FMA and FEA. With an increase in the MOE of the IRP from 24.5 GPa (3,553.4 ksi) to 200 GPa (29,007.5 ksi), the midspan deflection is reduced by 71% and 72%, as per FMA and FEA calculations, respectively. As a result, the alteration in the MOE

of repair material has a significant effect on the vertical bending of the IRP system when the host pipe discontinuities are wider.

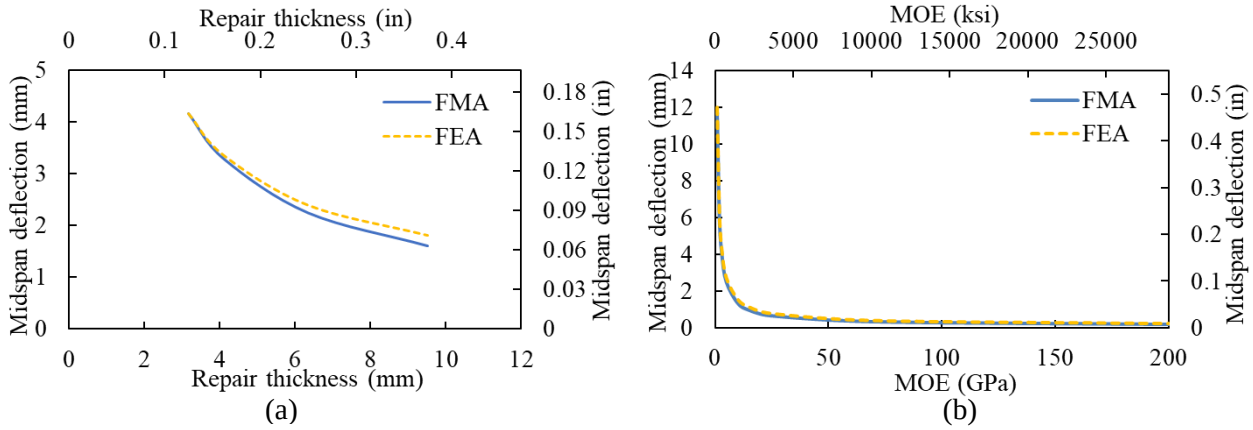

Figure 7. Effect of (a) repair thickness and (b) MOE of repair material on the midspan deflection of a 4.1 mm (0.2 in) thick IRP installed in a host pipe with 152.4 mm (6.0 in) gap width under 15.0 kN (3.4 kips) load

4.2 Factored FMA for IRP systems with very narrow crack widths

While FMA is capable of accurately predicting non-linear load-deflection behaviours of IRP in host pipe with wider discontinuities, high average stresses over very narrow discontinuities resulting from stress concentrations at the discontinuity edges of host pipe segments lead to a significant discrepancy between initial FMA and FEA/experimental outcomes. In order to address this issue, an average stress factor (ASF) was formulated and integrated into the original FMA. The ASF was determined by dividing the average normal stress along the bottom of IRP between discontinuity edges of host pipes, as obtained from FEA by the corresponding average stress obtained by FMA. Parametric studies were conducted to develop an equation for predicting ASF. The study considered different repair thicknesses ranging from 3.2 mm (0.1 in) to 12.7 mm (0.5 in), discontinuity widths ranging from 12.7 mm (0.5 in) to 152.4 mm (6.0 in) and MOE of repair material ranging from 1.0 GPa (145.0 ksi) to 200 GPa (29,007.5 ksi). The results of the parametric investigation indicate that the ASF is primarily influenced by the geometry of the discontinuity, specifically the width of the discontinuity and the thickness of IRP. Conversely, the MOE of repair material does not significantly affect the ASF. Thus, by considering the ASFs as a function of two governing dimensionless parameters, namely the ratio of discontinuity widths (l) to IRP wall thicknesses and the ratio of total wall thicknesses (IRP and host pipe thickness) to IRP thickness, a mathematical formulation for the ASF was derived through nonlinear regression analysis as shown in Equation 5, where t_{total} is the total wall thickness of the host pipe plus the repair and t_{repair} is the repair thickness. The factored FMA deflection, which takes into account the influence of stress concentration on average stresses across discontinuity width, was then obtained through the multiplication of the initially predicted FMA deflection by the ASF.

$$ASF = 1.097e^{-0.015\left(\frac{t_{total}}{t_{repair}}\right)} + 1.461e^{-0.337\left(\frac{l}{t_{repair}}\right)} \quad [5]$$

The validation of the factored FMA results for very narrow discontinuities is carried out by utilizing the outcomes from both FEA and full-scale laboratory tests conducted by CUB, as illustrated in Figure 8. The load-deflection behaviours of an IRP system with a 12.7 mm (0.5 in) discontinuity width, as predicted by factored FMA, are consistent with those observed in both FEA and experimental results. The graph demonstrates a linear relationship between deflection and applied load on the IRP systems across all scenarios. Based on Figure 8, the discrepancies between factored FMA and FEA results for the deflection of IRP at the discontinuity edge and loading point, when subjected to a load of 14.8 kN (3.3 kips) are roughly 1.9% and 2.2%, respectively. Moreover, for the same load,

the maximum differences between the factored FMA and the experimental outcomes for the deflection at the discontinuity edge and point load are 4.7% and 10.8%, respectively.

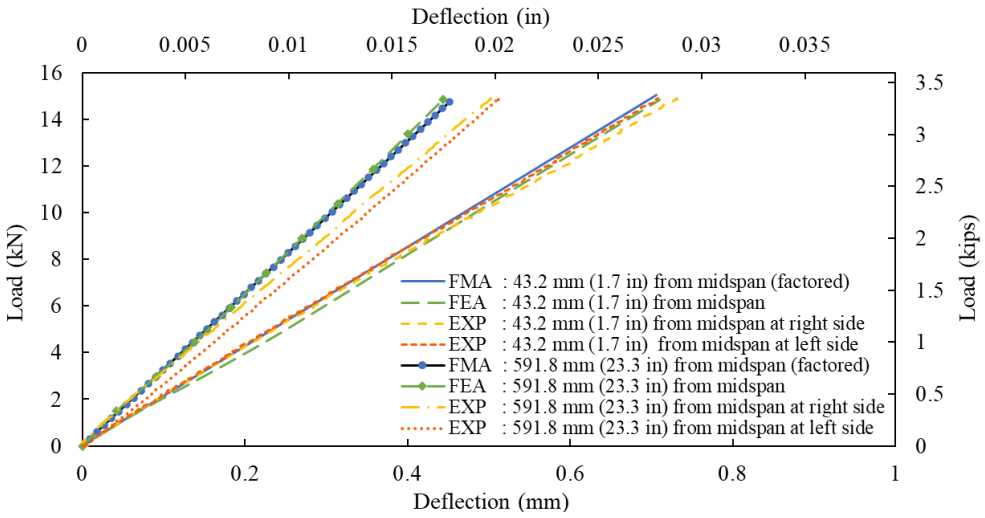

Figure 8. Comparison of FMA, FEA and experimental load-displacement behaviours of ALTRA10 IRP in host pipe with 12.7 mm (0.5 in) opening

The graphical representation in Figure 9 illustrates the correlation between discontinuity widths, ranging from 12.7 mm (0.5 in) to 203.2 mm (8.0 in), and the midspan deflection of IRP obtained from factored FMA and FEA under loading of 15.0 kN (3.4 kips). Under the same loading condition, the midspan deflection of the IRP repair system determined by factored FMA exhibits a nearly linear increase as the discontinuity width of the host pipe widens, which is very similar to the behaviour predicted by FEA. According to the results of both factored FMA and FEA, increasing the discontinuity width from 12.7 mm (0.5 in) to 203.2 mm (8.0 in) resulted in an 81% increase in midspan deflection This is due to the fact that, unlike IRP in host pipe systems with wider discontinuity widths, the overall load-deflection behaviour of IRP systems with narrow discontinuity widths is primarily controlled by the host pipe, which has a higher stiffness than IRP and hence results in significantly lower deformations.

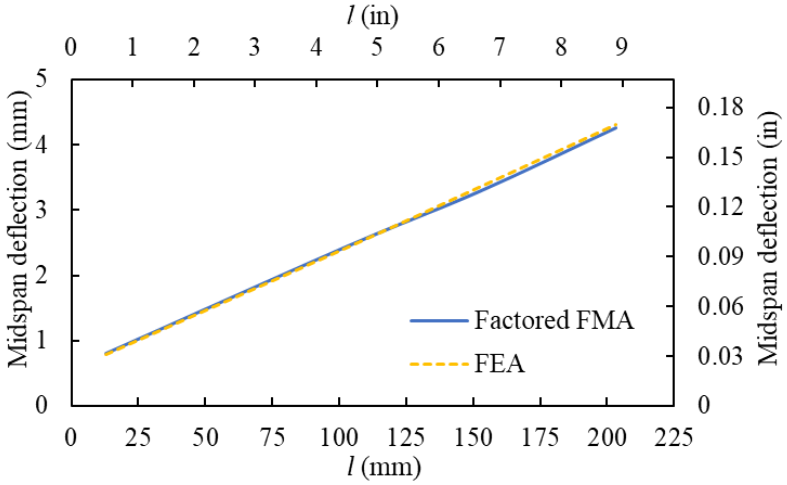

Figure 9. Effect of discontinuity width of host pipe on maximum midspan deflection of ALTRA10 IRP system under loading of 15.0 kN (3.4 kips) load

5. CONCLUSION

This study investigated analytically the bending behaviour of IRP in a host pipe with narrow and wider discontinuity widths and compared it with FEA outcomes. From the results of these analyses and investigations, the following conclusions can be drawn:

- The vertical bending of the IRP in host pipe with a wider discontinuity width is higher than one with a narrower discontinuity width indicating that IRPs with wider discontinuity widths have a higher tendency to fail due to buckling of the crown of the IRP at the midspan.
- The load-deflection behaviour of IRP systems with wider discontinuity widths is primarily controlled by the IRP, while that of narrow discontinuity widths is mainly governed by the host pipe.
- IRP repair system in a host pipe with a very narrow discontinuity width similar to a circumferential crack experiences significant average stress over the discontinuity width caused by stress concentration at the discontinuity edge compared with a wider discontinuity width.
- The MOE and the thickness of the IRP have a significant influence on the vertical bending of the IRP systems.
- The comparisons between FEA and FMA reveal that FMA is capable of providing a similar understanding of the flexural behaviour of different IRP systems to FEA up to the ultimate loading in a considerably shorter time and agrees well with the FEA outcomes.
- The factored FMA prediction of load-midspan deflection behaviour and the deflection along the pipe length using the mechanical properties of the constitutive materials established from coupon tests is also found to be in good agreement with the experimental results, giving confidence in the validity of the underlying assumptions.

6. REFERENCES

Allouche, EN, Alam, S, Al-Masud, M & Dulam, R 2012, 'Experimental Examination of Selected Limit States of Structural Liners at Locations of Ring Fracture', *Pipelines Conference 2012*: *Proceedings of the Pipelines Conference 2012* pp. 783-94.

Biezma, MV, Andrés, M, Agudo, D & Briz, E 2020, 'Most fatal oil & gas pipeline accidents through history: A lessons learned approach', *Engineering Failure Analysis*, vol. 110.

Dixon, PG, Tafsirojjaman, T, Klingaman, J, Hubler, MH, Dashti, S, O'rourke, TD, Farrag, KA, Manalo, A & Wham, BP 2023, 'State-of-the-Art Review of Performance Objectives for Legacy Gas Pipelines with Pipe-in-Pipe Rehabilitation Technologies', *Journal of Pipeline Systems Engineering and Practice*.

Jeon, S-S, O'Rourke, TD & Neravali, AN 2004, 'Repetitive loading effects on cast iron pipelines with cast-in-place pipe lining system', *Journal of Transportation Engineering-asce*, vol. 130, pp. 692-705.

Jung, YJ & Sinha, SK 2007, 'Evaluation of Trenchless Technology Methods for Municipal Infrastructure System', *Journal of Infrastructure Systems*, vol. 13, pp. 144-56.

Kiriella, S, Manalo, AC, Minh Tri Tien, C, Ahmadi, HR, Wham, BP, Salah, AM, Tafsirojjaman, T, Karunasena, W, Dixon, P & D.O'Rourke, T 2023, 'Lateral deformation behaviour of structural internal replacement pipe repair systems', *Composite Structures*, vol. 319.

Klingaman, J, Dixon, PG, Wham, BP, Dashti, S & Hubler, MH 2022, 'Traffic Loading Effects on Rehabilitated Cast Iron Distribution Pipelines', *Pipelines 2022*.

Manalo, A 2011, 'Behaviour of Fibre Composite Sandwich Structures: A case study on railway sleeper application', University of Southern Queensland.

Manalo, A, Aravinthan, T, Karunasena, W & Islam, M 2010, 'Flexural behaviour of structural fibre composite sandwich beams in flatwise and edgewise positions', *Composite Structures*, vol. 92, pp. 984-95.

Ossai, CI, Boswell, B & Davies, IJ 2015, 'Pipeline failures in corrosive environments A conceptual analysis of trends and effects', *Engineering Failure Analysis*, vol. 53, pp. 36-58.

Shou, KJ & Chen, BC 2018, 'Numerical analysis of the mechanical behaviors of pressurized underground pipelines rehabilitated by cured-in-place-pipe method', *Tunnelling and Underground Space Technology*, vol. 71, pp. 544-54.

Stewart, HE, Netravali, AN & O'Rourke, TD 2015, *Performance Testing of Field-Aged Cured-in-Place Liners (CIPL) for Cast Iron Piping* School of Civil and Environmental Engineering, Cornell University
Tafsirojjaman, T, Manalo, A, Tien, CMT, Wham, B, Salah, A, Kiriella, S, Karunasena, W & Dixons, P 2022, 'Analysis of failure modes in pipe-in-pipe repair systems for water and gas pipelines', *Engineering Failure Analysis*, vol. 140.
Tien, CMT, Manalo, A, Dixon, P, Tafsirojjaman, T, Karunasena, W, Flood, WW, Ahmadi, H, Kiriella, SH, Salah, AM & Wham, BP 2022, 'Effects of the legacy pipe ends on the behaviour of pipe-in-pipe repair systems under internal pressure', *Engineering Failure Analysis*.
Wu, Y, Kang, C, Nojumi, MM, Bayat, A & Bontus, GJ 2021, 'Current water main rehabilitation practice using trenchless technology', *Water Practice and Technology*, vol. 6, no. 3, pp. 707-23.
Yang, H, Chen, J-h, Chiu, H-j, Ting-Jia, K, Tsai, H-Y & Chen, JR 2016, 'Confined vapor explosion in Kaohsiung City – A detailed analysis of the tragedy in the harbor city', *Journal of Loss Prevention in The Process Industries*, vol. 41, pp. 107-20.
Yu, H, Kim, SS, Hwang, IUB & Lee, DG 2008, 'Application of natural fiber reinforced composites to trenchless rehabilitation of underground pipes', *Composite Structures*, vol. 86, pp. 285-90.
Zhang, S & Zhou, W 2014, 'Cost-based optimal maintenance decisions for corroding natural gas pipelines based on stochastic degradation models', *Engineering Structures*, vol. 74, pp. 74-85.

APPENDIX B: ADDITIONAL CONTRIBUTION

The following is a list of published journal papers resulting from the REPAIR project where additional contributions in the numerical simulations, data analysis and reviewing the manuscripts are provided by the PhD student.

1. Tafsirojjaman, T., Manalo, A., Tien, C.M.T., Wham, B., Salah, A., **Kiriella, S.**, Karunasena, W. and Dixons, P. (2022), "Analysis of failure modes in pipe-in-pipe repair systems for water and gas pipelines", *Engineering Failure Analysis*, vol. 140 (Impact factor: 4; Cite score: 6.3)

2. Tien, C.M.T., Manalo, A., Dixon, P., Tafsirojjaman, T., Karunasena, W., Flood, W.W., Ahmadi, H., **Kiriella, S**., Salah, A.M. and Wham, B.P. (2023), "'Effects of the legacy pipe ends on the behaviour of pipe-in-pipe repair systems under internal pressure", Engineering Failure Analysis, vol. 144 (Impact factor: 4; Cite score: 6.3)

APPENDIX C: RANKING OF THE PERFORMANCE OBJECTIVES AND ASSOCIATED FAILURE MECHANISMS OF IRP SYSTEMS

The project employed an analytical hierarchy process to rank the performance objectives and associated failure mechanisms of IRP systems. The results of this ranking can be found in Table 1 to Table 3. Accordingly, the lateral deformation is identified as the most critical performance objective on global priority, in addition to being determined by the thickness and MOE criteria of the IRP system, for all three design pressures under consideration, i.e., 60 psi (413.7 kPa), 100 psi (689.5 kPa) and 200 psi (1379.0 kPa). When the design pressure is set to 60 psi (413.7 kPa), the global ranking for the remaining critical performance objectives is impact loading, repetitive surface loading, axial deformation, hoop stress, and cross-section ovalization, respectively. On the other hand, when the design pressure is considered to be 100 psi (689.5 kPa), the global ranking for the remaining critical performance objectives for the IRP system is impact loading, hoop stress, repetitive surface loading, axial deformation and cross-section ovalization, respectively. However, if the design pressure is increased to 200 psi (1379.0 kPa), the global ranking switches to hoop stress, impact loading, repetitive surface loading, axial deformation and cross-section ovalization, respectively. However, it is important to note that the analysis conducted to assess the ranking of the critical performance objectives in this study did not consider the potential impact of damaged host pipe segments. Comprehensive information regarding this ranking is available in Tafsirojjaman et al. (2022).

Table 1. Ranking of critical performance objectives of IRP for design internal pressure of 60 psi (413.7 kPa)

Criteria						Global priority		
Thickness			MOE					
Rank	Performance objective	Priority (%)	Rank	Performance objective	Priority (%)	Rank	Performance objective	Priority (%)
1	Lateral deformation	21.3	1	Lateral deformation	20.8	1	Lateral deformation	21.1
2	Puncture	19.1	2	Puncture	16.7	2	Puncture	18.9
3	Repetitive surface loads	19.1	3	Repetitive surface loads	18.8	3	Repetitive surface loads	17.9
4	Axial deformation	14.9	4	Hoop stress	14.6	4	Axial deformation	14.7
5	Hoop stress	12.8	5	Axial deformation	14.6	5	Hoop stress	13.7
6	Cross-section ovalization	12.8	6	Cross-section ovalization	14.6	6	Cross-section ovalization	13.7

Table 2. Ranking of critical performance objectives of IRP for design internal pressure of 100 psi (689.5 kPa)

Criteria						Global priority		
Thickness			MOE					
Rank	Performance objective	Priority (%)	Rank	Performance objective	Priority (%)	Rank	Performance objective	Priority (%)
1	Lateral deformation	20.4	1	Lateral deformation	21.7	1	Lateral deformation	21.1
2	Puncture	18.4	2	Puncture	19.6	2	Puncture	19.0
3	Repetitive surface loads	18.4	3	Hoop stress	17.4	3	Hoop stress	16.9
4	Hoop stress	16.3	4	Repetitive surface loads	15.2	4	Repetitive surface loads	16.8
5	Axial deformation	14.3	5	Axial deformation	13.0	5	Axial deformation	13.7
6	Cross-section ovalization	12.2	6	Cross-section ovalization	13.0	6	Cross-section ovalization	12.6

Table 3. Ranking of critical performance objectives of IRP for design internal pressure of 200 psi (1379.0 kPa)

Criteria						Global priority		
Thickness			MOE					
Rank	Performance objective	Priority (%)	Rank	Performance objective	Priority (%)	Rank	Performance objective	Priority (%)
1	Lateral deformation	20.8	1	Lateral deformation	0.2	1	Lateral deformation	20.4
2	Hoop stress	18.8	2	Hoop stress	0.18	2	Hoop stress	18.4
3	Puncture	16.7	3	Puncture	0.18	3	Puncture	17.3
4	Repetitive surface loads	16.7	4	Repetitive surface loads	0.16	4	Repetitive surface loads	16.3
5	Axial deformation	16.6	5	Axial deformation	0.14	5	Axial deformation	14.3
6	Cross-section ovalization	12.5	6	Cross-section ovalization	0.14	6	Cross-section ovalization	13.3

APPENDIX D: FATIGUE BEHAVIOUR OF DIFFERENT IRP MATERIALS

The following is a discussion of the fatigue properties of potential IRP materials.

Fatigue behaviour of polymer coating

Polymer coatings (generally epoxy systems, polyurethanes, or polyureas) are one of the primary IRP material types used in SAPL (Selvakumar et al. 2013; Najafi 2016). Also, the fatigue life of polymeric materials is influenced by a variety of parameters. Unlike metals, the fatigue behaviour of polymers is governed by the viscoelastic effect (Chandran 2016). Other factors include stress/strain amplitude, mean stress, frequency, presence of stress concentration or initial defects in the component, temperature, test environment, and molecular characteristics (Pruitt 2000). Softening and melting occur at higher frequencies, and fatigue failure is primarily determined by the test frequency (Pruitt 2000). Fatigue failure becomes less sensitive to test frequency at lower frequencies, and failure occurs as a result of fracture initiation and propagation (Crawford et al. 1974; Skibo et al. 1978). These characteristics of the polymer come from the production of hysteresis energy during fatigue. Some of this energy is released as heat, a portion of which is dissipated, but the majority is absorbed by the sample, raising its temperature (Crawford et al. 1974; Pruitt 2000; Chandran 2016). The increase in temperature causes material degradation and a reduction in the fatigue life of polymer materials (Crawford et al. 1974; Pruitt 2000; Chandran 2016).

Fatigue behaviour of thermoplastics

Thermoplastic materials have some unfavourable properties, including a lower modulus of elasticity, lower tensile strength, narrow operating temperature range, and a tendency to soften due to self-heating (Mellott 2012). In the condition that ultimately leads to fatigue failure, the nonlinear viscoelastic behaviour becomes predominant, since thermoplastics which is a class of polymeric materials are subjected to a large amplitude of imposed strain that is greater than that of the linear viscoelastic limit (Jo et al. 1993; Mellott 2012). As a result, it is reasonable to consider that the mechanism of fatigue failure of thermoplastics is related to their nonlinear viscoelastic behaviour (Jo et al. 1993; Mellott 2012). When a thermoplastic material is subjected to cyclic load/stress, its temperature rises, resulting in failure by one of the two fundamentally distinct processes (Crawford et al. 1974). In the first type of failure, the temperature rises for a short period of time before stabilising and allowing a conventional crack

initiation and propagation process to occur, whereas, in the second type of failure, the temperature continues to rise, resulting in a thermal softening failure of the material (Crawford et al. 1974). Due to self-heating, high frequency cycles may play a significant role in the fatigue behaviour of thermoplastics, leading to softening of the materials and premature failure (Mellott 2012; Mellott et al. 2014; Mortazavian et al. 2015). Fatigue of the thermoplastic material with mean tensile stress results in a shorter fatigue life as compared to the tests performed under fully reversed conditions (Mellott 2012; Mellott et al. 2014).

Fatigue behaviour of FRP composites

Due to the anisotropic nature of FRP composite, their fatigue behaviour is more complicated than homogenous and isotropic materials such as plastics and metals (Amiri 2012). The most typical failure mechanisms generated by the fatigue of FRP composite materials are matrix cracking, fibre debonding, delamination, and fibre fracture in addition to crack initiation and crack propagation (Nguyen et al. 2000; Samanci et al. 2008; Samanci et al. 2012; Malpot et al. 2015; Shanmugam et al. 2021). The damage grows in small increments during the first stage of fatigue, then maintains a constant growth rate before accelerating in the final stage (Muc 2000; Paepegem et al. 2001; Chen et al. 2002). Unlike metal fatigue, the stiffness loss of the composite is visible from the early stage of the fatigue loading and may lead to significant stiffness degradation over the subsequent fatigue process (Lian et al. 2010; Colombi et al. 2012). Most composites do not have an endurance limit (Amiri 2012).

The fatigue life of composite material is influenced by several main factors, material properties (including matrix material and fibre material), fibre orientation, fibre volume fraction, applied maximum stress, stress amplitude, stress ratio, and loading frequency (Albouy et al. 2014; Ferdous et al. 2020; Huang et al. 2020). Because of their brittle nature, polymer-based composite fails at low strains, making it difficult to study stress-controlled fatigue. In the case of glass fibres, S-glass has greater strength and stiffness than other glass fibres (Ansari et al. 2018). The fatigue performance of high-modulus carbon fibre-reinforced polymer (CFRP) is better compared to that of low-modulus CFRP. Carbon fibres with relatively high modulus retain large stress along their lengths, causing longitudinal matrix cracking (Zhao et al. 2016). The matrix properties have a major impact on the fatigue strength of the GFRP composite. In most cases, fatigue damage initiates as a crack in the matrix. In comparison to thermosetting resin, thermoplastic resin has a much longer fatigue life (Ansari et al. 2018). The fibre volume fraction has a significant impact on the crack path. The fatigue performance of the composite improves as the fibre volume fraction increases (Mini et al. 2012; Belmonte et al. 2017).

Fatigue behaviour of the metallic systems

The fatigue damage of metallic material systems begins with crack initiation, followed by crack propagation, and ends in ultimate failure. A predominant single crack is the most typical failure mechanism of metals, as a significant portion of the fatigue process is spent on propagating a single crack (Risicato et al. 2014). The tensile/yield strength of the metal has a strong influence on the fatigue strength in the crack initiation phase, but not in the crack propagation phase (Pedersen 2018). Conversely, it has been shown that the crack propagation rate is more dependent on the elastic modulus (Pedersen 2018). The crack propagation phase is longer due to the strain hardening of the metals. As a crack attempts to propagate through the metal, plasticity occurs at the crack tip, resulting in crack blunting and strain hardening. The crack blunting, strain hardening, and crack propagation process can be repeated for several thousands of cycles (Jollivet et al. 2013; Risicato et al. 2014; Mughrabi 2015). A metallic material, no matter how ductile, might fail in a fatigue test with no visible external deformation, similar to a brittle material (Orowan 1939). Under high cycle fatigue loading, void defects and microstructural irregularities can adversely affect metallic materials and significantly reduce their fatigue life (Danninger et al. 2003). Some low-strength ferrous alloys can exhibit a horizontal asymptote in the S-N curve, indicating a fatigue limit below which there appear to be infinite cycles that would never cause failure (Pang et al. 2014). Other metallic materials, such as high-strength ferrous alloys and non-ferrous metals, do not have a distinct horizontal asymptote and will fail as the number of cycles increases (Pang et al. 2014). This different behaviour of IRP material systems is important in understanding the fatigue behaviour of repaired pipelines.

APPENDIX E: INSTRUMENTATION OF BENDING TEST SETUP

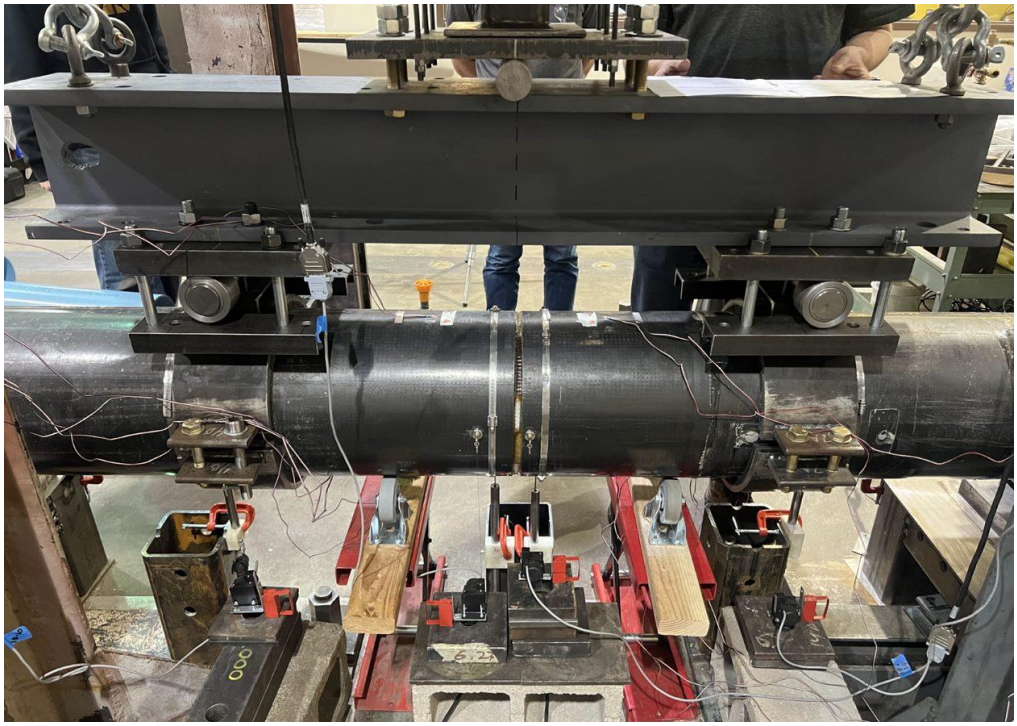

Fig. 16. Actual bending test setup, showing the positions of Linear Variable Differential Transformers (LVDTs) and strain gauges (CUB)

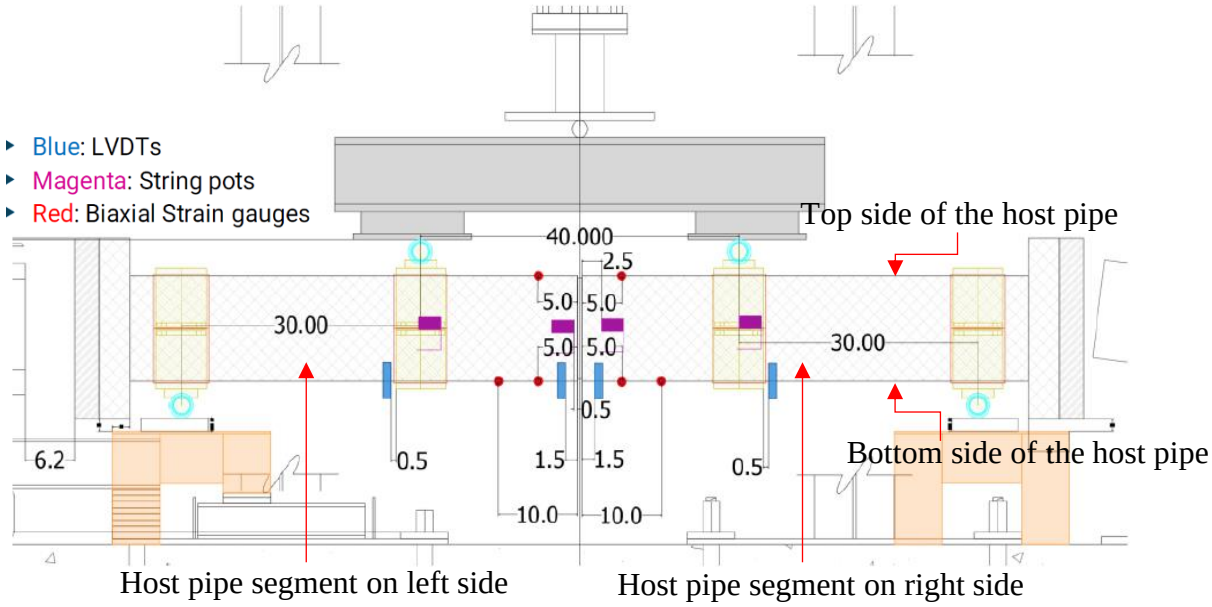

Fig. 17. Schematic diagram of the bending test setup, showing the positions of LVDTs and strain gauges (CUB) [Units: in]